The Atmospheric Dynamics of Pulsar Companions

Adam S. Jermyn

Thesis Mentor: E. S. Phinney
Option Representative: Lynne Hillenbrand

Division of Physics, Mathematics, and Astronomy
California Institute of Technology
June 10, 2015

Curiosity demands that we ask questions, that we try to put things together and try to understand this multitude of aspects as perhaps resulting from the action of a relatively small number of elemental things and forces acting in an infinite variety of combinations.

– Richard P. Feynman

Acknowledgements

Except where otherwise noted, and to the best of my knowledge, all work presented here is my own. Getting to this point, however, is something for which I am deeply indebted to those around me. Professor Sterl Phinney, my thesis mentor, taught me that intuition is more useful than precision, and patiently introduced me to the art of astronomy. Dr. Ravishankar Sundaraman, my collaborator and co-conspirator, showed me that numerical methods can be elegant as well as useful. Professor Jason Alicea, my adviser, introduced me to the subtle world of statistical physics, and gave me an appreciation for the many mysteries therein. Dr. Milo Lin, my friend and colleague, brought me into the fold of proteins and biophysics, and in so doing gave me my first taste of emergence. Dr. Frank Rice, my laboratory instructor, impressed upon me the importance of always being grounded in experiment and observation. Professor Gil Refael, the leader of nights of free-wheeling physics and Thai food, gave me the firm belief that any problem in Nature may be solved with enough of both. My friend Nicholas Schiefer gave me a little nudge towards astronomy in just the right way, and lent me an ear at all of the right times, and for that I will always be grateful. Of my professors and friends at Caltech, Tom Tombrello is the one I'll never truly be able to thank. My adviser and advocate till the day he passed away, he believed in me even when I didn't, and helped me find my way by gently pointing out the doors he had opened all around me. The other person I cannot thank properly is my grandfather Robert Katz, who passed away in May of 2014. He told me stories about the world through science and art and history, and in doing so piqued my curiosity. Finally, I would like to thank Mom and Dad. You set me on my way in this adventure.

Abstract

Pulsars emit radiation over an extremely wide frequency range, from radio through gamma[1]. Recently, systems in which this radiation significantly alters the atmospheres of low-mass pulsar companions have been discovered[2]. These systems, ranging from ones with highly anisotropic heating to those with transient X-ray emissions, represent an exciting opportunity to investigate pulsars through the changes they induce in their companions. In this work, we present both analytic and numerical work investigating these phenomena, with a particular focus on atmospheric heat transport, transient phenomena, and the possibility of deep heating via gamma rays. We find that certain classes of binary systems may explain decadal-timescale X-ray transient phenomena[3], as well as the formation of so-called redback companion systems[4]. We also posit an explanation for the formation of high-eccentricity millisecond pulsars with white dwarf companions[5]. In addition, we examine the temperature anisotropy induced by the

[1]A. Smith David. "Gamma Ray Pulsars with the Fermi LAT". in: 3rd Fermi Symposium. May 2011. URL: `http://fermi.gsfc.nasa.gov/science/mtgs/symposia/2011/program/session14/Smith_FermiPSRs.pdf`; H. et al Anderhub. "Search for Very High Energy Gamma-ray Emission from Pulsar-Pulsar Wind Nebula Systems with the MAGIC Telescope". In: *The Astrophysical Journal* 710.1 (2010), p. 828. URL: `http://stacks.iop.org/0004-637X/710/i=1/a=828`; T. Padmanabhan. *Theoretical Astrophysics*. Vol. 2. ISBN: 978-0521566315. Cambridge University Press, 2001. Chap. 6.

[2]Mallory S. E. Roberts. *Surrounded by Spiders! New Black Widows and Redbacks in the Galactic Field*. 2012. eprint: `arXiv:1210.6903`. URL: `http://arxiv.org/abs/1210.6903`; M. T. Reynolds et al. "The light curve of the companion to PSR B1957+20". In: *Monthly Notices of the Royal Astronomical Society* 379.3 (2007), pp. 1117–1122. DOI: `10.1111/j.1365-2966.2007.11991.x`. eprint: `http://arxiv.org/abs/0705.2514`. URL: `http://mnras.oxfordjournals.org/content/379/3/1117.abstract`.

[3]M. Linares. "X-Ray States of Redback Millisecond Pulsars". In: *The Astrophysical Journal* 795, 72 (Nov. 2014), p. 72. DOI: `10.1088/0004-637X/795/1/72`. arXiv: `1406.2384 [astro-ph.HE]`.

[4]P. Podsiadlowski, S. Rappaport, and E. D. Pfahl. "Evolutionary Sequences for Low- and Intermediate-Mass X-Ray Binaries". In: *The Astrophysical Journal* 565 (Feb. 2002), pp. 1107–1133. DOI: `10.1086/324686`. eprint: `astro-ph/0107261`; P. Podsiadlowski. "Irradiation-driven mass transfer low-mass X-ray binaries". In: *Nature* 350 (Mar. 1991), pp. 136–138. DOI: `10.1038/350136a0`.

[5]B. Knispel et al. "Einstein@Home Discovery of a PALFA Millisecond Pulsar in an Eccentric Binary Orbit". In: *ArXiv e-prints* (Apr. 2015). arXiv: `1504.03684 [astro-ph.HE]`.

Pulsar in its companion, and demonstrate that this may be used to infer properties of both the companion and the Pulsar wind. Finally, we explore the possibility of spontaneously generated banded winds in rapidly rotating convecting objects.

Contents

Acknowledgements **i**

Abstract **ii**

Definition of Symbols **ix**

List of Figures **xvii**

Motivation **1**

I Physics 5

1 Geometry and Optical Depth **6**

2 One-Dimensional Model **14**
2.1 Equations of Stellar Structure 14
2.2 Simulations 18
2.3 Luminosity and Radial Variation 28

3 Higher Dimensional Models **36**
3.1 Zero-Wind Analytic Model 39
3.1.1 Iterative Method 40
3.1.2 Eigenfunction Expansion 42
3.2 Zero-Divergence Wind Model 46

4 Review of Fluid Mechanics **49**
4.1 Microscopic Viscosity 49
4.2 Reynolds Number 54
4.3 Rayleigh Number 57

4.4 Richardson Number . . . 59
4.5 Rossby Number . . . 61
4.6 Mach Number . . . 62

5 Stability and Turbulence 65
5.1 Sheared Convection . . . 66
5.1.1 Shear-dominated flow . . . 69
5.1.2 Convection-dominated flow . . . 72
5.1.3 Mixed shear-convective flow . . . 73
5.2 Non-Convective Shear . . . 75

6 Global Wind Patterns 79
6.1 Turbulent Zonal Flow . . . 79
6.2 Alternative Patterns . . . 82
6.2.1 Large Rossby Number . . . 83
6.2.2 Small Rossby Number . . . 88
6.3 Deciding . . . 92
6.4 Convective Reynold's Stress . . . 100
6.5 Summary of Results . . . 104

7 Higher Dimensional Models with Transport 110
7.1 Radiative Stars . . . 111
7.2 Convective Stars . . . 115
7.3 Crossover Behavior . . . 117

8 Time Dependence 125
8.1 Assumptions and Computational Methods . . . 125
8.2 Fully Radiative Stars . . . 129
8.3 Fully Convective Stars . . . 132
8.4 Mixed Stars . . . 138

II Applications in Astronomy 144

9 X-Ray Binaries 145
9.1 Accretion rate . . . 145
9.2 Pre-Roche Expansion . . . 147
9.3 Post-Roche Accretion . . . 152
9.4 Critical Accretion Dynamics . . . 158

9.5 Limit Cycles 163

10 Accretion Induced Collapse 173

11 Spotted Black Widows 179
11.1 Setup 180
11.2 Main Sequence Solutions 183
11.3 Brown Dwarfs 190

12 Banded Stars 198

Appendices 204

A Viscosity Code 204

B Acorn Stellar Integration Code 207
B.1 Opal and Ferguson Opacity Table Parser 207
B.2 Stellar Integration Code 211

C Gob Stellar Integration Code 239

D Anisotropy Code 266

E Reference Stellar Models 271

Bibliography 291

Definition of Symbols

Symbol	Name	Definition/Value/[Units]
log	Logarithm base 10	
ln	Logarithm base e	
G	Newton's Constant	$6.673 \times 10^{-8}\mathrm{erg}\frac{\mathrm{cm}}{\mathrm{g}^2}$
$M_\odot$	Solar Mass	$1.98855 \times 10^{33}\mathrm{g}$
$R_\odot$	Solar Radius	$6.955 \times 10^{10}\mathrm{m}$
$L_\odot$	Solar Luminosity	$3.83 \times 10^{33}\mathrm{erg/s}$
m_p	Proton Mass	$1.6605 \times 10^{-24}\mathrm{g}$
a	Radiation Constant	$7.57 \times 10^{-15}\frac{\mathrm{erg}}{\mathrm{cm}^3\mathrm{K}^4}$
c	Speed of Light	$2.99792458 \times 10^{10}\mathrm{cm/s}$
k_B	Boltzmann Constant	$1.38065 \times 10^{-16}\mathrm{erg/K}$
σ	Stefan-Boltzmann Constant	$5.6703 \times 10^{-5}\mathrm{erg/s/cm^2/K^4}$
R_y	Rydberg - Hydrogen Ionization Energy	$2.179872 \times 10^{-11}\mathrm{erg}$
q	Electron Charge Magnitude	$4.80321 \times 10^{-10}\sqrt{\mathrm{erg}\cdot\mathrm{cm}}$
M	Stellar Mass	$[M_\odot]$
M_p	Pulsar Mass	$[M_\odot]$
Σ	Column Density	$[\mathrm{g/cm^2}]$
Σ_h	Heating Column Density	$[\mathrm{g/cm^2}]$
κ	Mass Attenuation Coefficient	$[\mathrm{cm^2/g}]$
R	Stellar Radius	$[R_\odot]$
R_0	Orbital Radius	[cm]
R_b	Roche Lobe Radius	[cm]
$\mathcal{P}$	Orbital Period	[s]
$\mathcal{P}_p$	Pulsar Rotation Period	[s]
ω	Pulsar frequency	[rad/s]
z	Depth	$[cm]$
g	Acceleration due to Gravity	$\frac{GM}{R^2}$
P	Pressure	$[\mathrm{erg/cm^3}]$
ρ	Density	$[\mathrm{g/cm^3}]$
T	Temperature	[K]
u	Specific Internal Energy	$[\mathrm{erg/cm^3}]$
s	Specific Entropy	$[\mathrm{erg/K/cm^3}]$
F_b	Flux due to Nuclear Processes	$[\mathrm{erg/cm^2/s}]$
L_{in}	Luminosity due to Nuclear Processes	[erg/s]
F_r	Radiative Flux	$\frac{4acT^3}{3\kappa\rho}\partial_z T$
L_e	External Luminosity	[erg/s]
k	Thermal Conductivity	[erg/cm/s/K]
k_{rad}	Radiative Thermal Conductivity	$\frac{4acT^3}{3\rho\kappa}$
c_v	Specific Heat Capacity (Constant Volume)	$[k_B/\mu]$
c_p	Specific Heat Capacity (Constant Pressure)	γc_v
γ	Adiabatic Index	$\frac{c_p}{c_v}$
μ	Mean Free Particle Mass	$\frac{\rho k T}{p}$
v_s	Speed of Sound	$\sqrt{\frac{\gamma p}{\rho}}$
h_s	Pressure Scale Height	$\frac{dz}{d\ln p} = \frac{p}{\rho g}$

Symbol	Name	Definition/Value/[Units]
∇	Temperature Gradient	$\frac{d\ln T}{d\ln P}$
∇_{rad}	Radiative Temperature Gradient	$\frac{3\kappa p F_b r^2}{4acGMT^4}$
∇_{ad}	Adiabatic Temperature Gradient	$1-\frac{1}{\gamma}$
l	Convective Length-scale	[cm]
$\aleph$	Convective Scale Factor	l/h_s
Γ	Convective Efficiency	
∇_{conv}	Convective Gradient	
v_c	Convective Speed	[cm/s]
F_c	Convective Flux	$F_{net}-F_r$
v_0	Wind Speed	
v_ϕ	Circumferential Wind Speed	
∇_c	Circumferential Temperature Gradient	$\partial_\phi \ln T$
Δz	Region Thickness	[cm]
τ_t	Cooling Time	$\frac{\text{Heat Content}}{\text{Non-Transient Flux}}=\frac{c_pT(\Delta z)}{F_b}=\frac{\gamma p(\Delta z)}{F_b}$
τ_w	Wind Circulation Time	$\frac{2\pi r}{v_w}$
ν	Kinematic Viscosity	[cm^2/s]
N	Brunt-Vaisala Frequency	$\sqrt{g\partial_z \ln\rho}$ or $\sqrt{g\partial_z s/\gamma}$
Ri	Richardson Number	$\frac{N^2}{(dv/dz)^2}$
Ri$_c$	Critical Richardson Number	
Re	Reynolds Number	vd/ν with characteristic flow diameter d
Re$_c$	Critical Reynolds Number	
β	Thermal Expansion Coefficient	[K^{-1}]
α	Thermal Diffusivity	$\frac{k}{c_p}$
Ra	Rayleigh Number	$\frac{\beta g l^3 \Delta T}{\alpha\nu}$
Ra$_c$	Critical Rayleigh Number	$\sim 10^3$
P$_e$	Péclet Number	$\frac{vl}{\alpha}$
r	Spherical Radial Coordinate	
θ	Spherical Polar Angle	
ϕ	Spherical Azimuthal/Cylindrical Polar Angle	
s	Cylindrical Radial Angle	

List of Figures

1.1 Depiction of a pulsar and its companion. Note that none of the depictions are to scale. The companion orbits with angular velocity equal to its rotational angular velocities due to tidal locking effects. The pular and companion are separated by a distance R_o. Their masses are M_p and M respectively. The star has radius R. The heating zone is, for any kind of radiation, the region of unit optical depth given that the radiation is incident from one side and that the source is far enough away that it may be viewed as a planar wavefront. 8
1.2 $\log \kappa^{-1}$ is plotted versus $\log E$. The former is measured in g/cm^2 and the latter in eV. Data was extracted manually from plots in the Particle Data Group book[6], and so has some uncertainty associated with the conversion process. 10
1.3 $\log \Sigma$ is plotted versus $\log E$. The former is measured in g/cm^2 and the latter in eV. 11

2.1 The vertical axis is $\log \rho$ (with ρ measured in g/cm^3), the horizontal is $\log T$ (with T measured in K), and the color represents $\log \kappa$ (with κ measured in cm^2/g. White regions are those without data. 19

[6] ´J. et al Beringer. “Particle Data Group”. In: *Phys. Rev. D* 86 (2012), p. 010001.

2.2 Radial coordinate (in cm) versus log of Σ (in g/cm^2) for nine different scenarios. Σ here is computed as the mass above the point of interest divided by $4\pi R^2$. The columns are the three different stars under consideration. Moving left to right, they are $M = M_\odot$,$L_{in} = L_\odot$,$R = R_\odot$, $M = 0.3M_\odot$,$L_{in} = 10^{-2}L_\odot$,$R = 0.43R_\odot$, and $M = 0.02M_\odot$,$L_{in} = 10^{-4}L_\odot$,$R = 0.14R_\odot$. The rows represent different quantities of external luminosity. From top to bottom, these are $L_e = 0, L_e = L_\odot \frac{R^2}{R_\odot}^2, L_e = 10L_\odot \frac{R^2}{R_\odot}^2$. The vertical grey bar goes from the edge of the photosphere (where $\tau = 2/3$) to the heating depth ($\Sigma = 10^3$g/cm^2). Blue regions are dominated by convective heat transport, red by radiative transport. 21

2.3 Log of T (in K) versus log of Σ (in g/cm^2) for the same nine scenarios defined in figure 2.2. Σ here is computed as the mass above the point of interest divided by $4\pi R^2$. The columns are the three different stars under consideration. The rows represent different quantities of external luminosity. The vertical grey bar goes from the edge of the photosphere (where $\tau = 2/3$) to the heating depth ($\Sigma = 10^3$g/cm^2). Blue regions are dominated by convective heat transport, red by radiative transport. 23

2.4 Log of pressure scale height versus log of Σ (in g/cm^2) for the same nine scenarios defined in figure 2.2. The columns are the three different stars under consideration. The rows represent different quantities of external luminosity. The vertical grey bar goes from the edge of the photosphere (where $\tau = 2/3$) to the heating depth ($\Sigma = 10^3$g/cm^2). Blue regions are dominated by convective heat transport, red by radiative transport. 24

2.5 Log of convective efficiency (Γ, see text) versus log of Σ (in g/cm^2) for the same nine scenarios defined in figure 2.2. The columns are the three different stars under consideration. The rows represent different quantities of external luminosity. The vertical grey bar goes from the edge of the photosphere (where $\tau = 2/3$) to the heating depth ($\Sigma = 10^3$g/cm^2). Blue regions are dominated by convective heat transport, and all other regions have been omitted due to Γ only being defined in convective zones. 26

2.6 The vertical axis is $\log\rho$ (with ρ measured in g/cm^3), the horizontal is $\log T$ (with T measured in K), and the color represents $\log\kappa$ (with κ measured in cm^2/g. White regions are those without data. The nine stellar models defined in figure 2.2 are plotted as tracks on top of the opacity. The terminus marker indicates which track is which: the three sizes of markers correspond in increasing order to the three stellar masses under consideration, and the three kinds of markers correspond in order of increasing number of sides to increasing external illumination. Blue regions are dominated by convective heat transport, red by radiative transport. 27
2.7 The log of f is plotted versus $\log(L_e/L_{i,\mathrm{old}})$ with $\beta = 4+2/3$ in orange and $\beta = 0$ in blue. These solutions were determined numerically in Mathematica. 33

4.1 The vertical axis is $\log\rho$ (with ρ measured in g/cm^3), the horizontal is $\log T$ (with T measured in K), and the color represents $\log\nu$ (with ν measured in cm^2/s. White regions are those without data. 52
4.2 The vertical axis is $\log\rho$ (with ρ measured in g/cm^3), the horizontal is $\log T$ (with T measured in K), and the color represents the log of the anisotropy factor A. White regions are those without data. 55
4.3 The vertical axis is $\log\rho$ (with ρ measured in g/cm^3), the horizontal is $\log T$ (with T measured in K), and the color represents the log of the anisotropy factor A. White regions are those without data. 56

8.1 $\Delta T/T_0$ (top) and $L/L_\odot$ (bottom) versus $\log\Sigma$ (in g/cm^2) for a star of mass $M_\odot$, radius $R_\odot$, and luminosity $100L_\odot$. The external heat was put in at $\Sigma = 10^3$g/cm^2 and linearly increased from zero to $100L_\odot$ over the course of 10^8s, which is where the simulation ends. Color represents time, with the simulation beginning at violet and ending with red. 130
8.2 $\Delta T/T_0$ (top) and $L/L_\odot$ (bottom) versus $\log\Sigma$ (in g/cm^2) for a star of mass $M_\odot$, radius $R_\odot$, and luminosity $100L_\odot$. The external heat was put in at $\Sigma = 10^3$g/cm^2 and linearly increased from zero to $100L_\odot$ over the course of 10^8s, after which the simulation continued for another 10^8s to allow for equilibration. Color represents time, with the simulation beginning at violet and ending with red. 131

8.3 $\Delta T/T_0$ (top) and $L/L_\odot$ (bottom) versus $\log\Sigma$ (in g/cm^2) for a star of mass $M_\odot$, radius $R_\odot$, and luminosity $100L_\odot$. The external heat was put in at $\Sigma = 10^3$g/cm^2 and linearly decreased from $100L_\odot$ to zero over the course of 10^8s. Color represents time, with the simulation beginning at violet and ending with red. 133
8.4 $\Delta T/T_0$ (top) and $L/L_\odot$ (bottom) versus $\log\Sigma$ (in g/cm^2) for a star of mass $0.3M_\odot$, radius $2.65R_\odot$, and luminosity $0.1L_\odot$. The external heat was put in at $\Sigma = 10^3$g/cm^2 and linearly decreased from $0.1L_\odot$ to zero over the course of 10^8s. Color represents time, with the simulation beginning at violet and ending with red. 134
8.5 $\Delta T/T_0$ (top) and $L/L_\odot$ (bottom) versus $\log\Sigma$ (in g/cm^2) for a star of mass $0.3M_\odot$, radius $2.65R_\odot$, and luminosity $0.1L_\odot$. The external heat was put in at $\Sigma = 10^3$g/cm^2 and linearly decreased from $0.1L_\odot$ to zero over the course of 10^8s. The simulation was then run for an additional 10^8s with no external heating. Color represents time, with the simulation beginning at violet and ending with red. 135
8.6 $\Delta T/T_0$ (top) and $L/L_\odot$ (bottom) versus $\log\Sigma$ (in g/cm^2) for a star of mass $0.3M_\odot$, radius $2.65R_\odot$, and luminosity $0.1L_\odot$. The external heat was put in at $\Sigma = 10^3$g/cm^2 and linearly decreased from $L_\odot$ to zero over the course of 10^8s. The simulation was then run for an additional 10^8s with no external heating. Color represents time, with the simulation beginning at violet and ending with red. 136
8.7 $\Delta T/T_0$ (top) and $L/L_\odot$ (bottom) versus $\log\Sigma$ (in g/cm^2) for a star of mass $M_\odot$, radius $R_\odot$, and luminosity $L_\odot$. The external heat was put in at $\Sigma = 10^3$g/cm^2 and linearly decreased from $L_\odot$ to zero over the course of 10^8s. Color represents time, with the simulation beginning at violet and ending with red. 140
8.8 $\Delta T/T_0$ (top) and $L/L_\odot$ (bottom) versus $\log\Sigma$ (in g/cm^2) for a star of mass $0.3M_\odot$, radius $2.65R_\odot$, and luminosity $0.1L_\odot$. The external heat was put in at $\Sigma = 10^3$g/cm^2 and linearly decreased from $10L_\odot$ to zero over the course of 10^8s. The simulation was then run for an additional 10^8s with no external heating. Color represents time, with the simulation beginning at violet and ending with red. 141

8.9 $\Delta T/T_0$ (top) and $L/L_\odot$ (bottom) versus $\log \Sigma$ (in g/cm^2) for a star of mass $M_\odot$, radius $R_\odot$, and luminosity $L_\odot$. The external heat was put in at $\Sigma = 10^3$g/cm^2 and linearly decreased from $L_\odot$ to zero over the course of 10^8s. It was then run for another 10^8s at that value. Color represents time, with the simulation beginning at violet and ending with red. 142
8.10 $\Delta T/T_0$ (top) and $L/L_\odot$ (bottom) versus $\log \Sigma$ (in g/cm^2) for a star of mass $M_\odot$, radius $R_\odot$, and luminosity $L_\odot$. The external heat was put in at $\Sigma = 10^3$g/cm^2 and immediately decreased from $L_\odot$ to zero over the course of 10^8s before being run for another 10^9s. Color represents time, with the simulation beginning at violet and ending with red. . . 143

9.1 The vertical axis is $\log \mathcal{P}$ in seconds, the horizontal axis is the companion mass M in solar masses, and the color represents the log of the expansion timescale $h_s/\dot{R}$ in seconds. The four different plots correspond to four different pulsar luminosities. 153
9.2 The vertical axis is $\log \mathcal{P}$ in seconds, the horizontal axis is the companion mass M in solar masses, and the color represents the log of $\tau_{\text{disk}}/\tau_{\text{exp}}$. The four plots correspond to different pulsar luminosities. . 157
9.3 The vertical axis is $\log \mathcal{P}$ in seconds, the horizontal axis is the companion mass M in solar masses, and the color represents the log of the ratio of the quick contraction length to the scale height. The four plots correspond to different pulsar luminosities. 161
9.4 The vertical axis is $\log \mathcal{P}$ in seconds, the horizontal axis is the companion mass M in solar masses, and the color represents the log of the contraction timescale. The four plots correspond to different pulsar luminosities. 162
9.5 The vertical axis is $\log \mathcal{P}$ in seconds, the horizontal axis is the companion mass M in solar masses, and the color represents the log of the ratio of the critical disk viscous timescale to the contraction timescale. The four plots correspond to different pulsar luminosities. 164
9.6 The vertical axis is $\log \mathcal{P}$ in seconds, the horizontal axis is the companion mass M in solar masses, and the color represents the type of limit cycle. Blue is type 1, Green is type 2, Maroon is type 3. The four plots correspond to different pulsar luminosities. 169

10.1 The vertical axis is $M/M_\odot$, the horizontal axis is $M_c/M_\odot$, with both axes log-scaled. The color represents the ratio $R_{\max}/30R_\odot$, the denominator being the approximate Roche radius for the period and mass range of interest, and the numerator being the post-expansion radius of the red giant of interest. 177

11.1 The vertical axis is $\mathcal{P}$ in seconds, the horizontal axis is the companion mass in solar masses, with both axes log-scaled. The color represents the log of the day/night flux ratio $\log F_{\rm day}/F_{\rm night}$. The four different plots correspond to four different pulsar luminosities. The black line corresponds to the Roche cutoff. 186

11.2 The vertical axis is $\mathcal{P}$ in seconds, the horizontal axis is the companion mass in solar masses, with both axes log-scaled. The color represents the log of the day/night flux ratio $\log \Delta F/F$. The four different plots correspond to four different pulsar luminosities. The black line corresponds to the Roche cutoff. The white regions above the Roche cutoff have $\Delta F = 0$ due to heat bottling. 187

11.3 The vertical axis is $\mathcal{P}$ in seconds, the horizontal axis is the companion mass in solar masses, with both axes log-scaled. The color represents the log of the day/night flux ratio $\log F_{\rm day}/(F_i+F_e)$. The four different plots correspond to four different pulsar luminosities. The black line corresponds to the Roche cutoff. 188

11.4 The vertical axis is $\mathcal{P}$ in seconds, the horizontal axis is the companion mass in solar masses, with both axes log-scaled. The color represents the log of the day/night flux ratio $\log W/(F_i + F_e)$. The four different plots correspond to four different pulsar luminosities. The black line corresponds to the Roche cutoff. Note that the white region above the Roche cutoff corresponds to the case $W = 0$ 189

11.5 The vertical axis is $\mathcal{P}$ in seconds, the horizontal axis is the companion mass in solar masses, with both axes log-scaled. The color represents the log of the day/night flux ratio $\log F_{\rm night}/F_i$. The four different plots correspond to four different pulsar luminosities. The black line corresponds to the Roche cutoff. 191

11.6 Top: $\Delta F/F_e$ is shown as a function of $\log\chi$. Bottom: $\log F_{\rm day}/F_{\rm night}$ is shown as a function of $\log\chi$. 194

List of Tables

6.1 Computed parameterization of circumferential heat transport by winds. The first column specifies what case is under consideration. All possible cases are enumerated here. The remaining columns specify y, a prefactor on the transport as well as q, a, b, the exponents on $\Delta T/T$, $l/2\pi R$, and Ro respectively. Note that factors of γ and $\aleph$ have been neglected in assembling this table. 105

6.2 Critical thermal anisotropy values are listed for each case of interest. Note that factors of γ and $\aleph$ have been neglected in assembling this table. 107

Motivation

If you haven't found something strange during the day, it hasn't been much of a day.

– John Archibald Wheeler

Pulsars, highly magnetic compact stellar remnants, exhibit some of the most unusual behaviors in the universe by virtue of existing at length and energy scales where general relativity and quantum field theory are both relevant. Pulsar gravitational fields are typically so strong that in binary pairs they emit significant gravitational radiation. The magnetic field near a pulsar's surface is strong enough that the index of refraction of the vacuum deviates significantly from unity, and particle pair creation helps create an ionized wind which travels relativistically away from the pulsar[7].

Most of what is known of pulsars comes from radio timing data[8]. Pulsars may be thought of as spherical magnetic dipoles approximately 10km in radius with surface magnetic fields between 10^8Gauss and 10^{15}Gauss, spinning with periods between millisecond and second timescales[9]. As a result of the large electric fields created by the rotating magnetic dipole moment, particles are created and carry energy, both kinetic and in the form of a Poynting flux, away from the pulsar. As these particles move they also radiate gamma-rays. Observationally, this means that pulsars appear in a wide band of radio frequencies as a periodic short pulse, while also being active through very high energies. The timing of these pulses has informed much of what is currently known about pulsars.

---

[7] Padmanabhan, op. cit.

[8] Dipankar Bhattacharya. "The Evolution of the Magnetic Fields of Neutron Stars". In: *J. Astrophys. Astr.* 16 (Mar. 1994), pp. 217–232. URL: `http://www.ias.ac.in/jarch/jaa/16/217-232.pdf`.

[9] Idem, "The Evolution of the Magnetic Fields of Neutron Stars"; José A. Pons et al. "Evidence for Heating of Neutron Stars by Magnetic-Field Decay". In: *Phys. Rev. Lett.* 98 (7 Feb. 2007), p. 071101. DOI: `10.1103/PhysRevLett.98.071101`. eprint: `http://arxiv.org/pdf/astro-ph/0607583.pdf?origin=publication_detail`. URL: `http://link.aps.org/doi/10.1103/PhysRevLett.98.071101`.

More specifically, pulsars have masses and radii in a very small range constrained by models of the degenerate nuclear equation of state[10]. From dispersion delay data at different frequencies it is possible to determine the electron column density in the interstellar medium between Earth and the pulsar, which can give a distance estimate[11]. Measurement of the pulse period gives the angular frequency ω. Combined with the mass and radius this gives the rotational energy of the pulsar:

$$E = \frac{1}{2} I \omega^2 = \frac{1}{5} M R^2 \omega^2 \tag{1}$$

Measurement of the rate at which the pulse period changes gives $\dot{\omega}$, which then gives the rate at which the pulsar rotational energy changes:

$$\dot{E} = \frac{2}{5} M R^2 \omega \dot{\omega} \tag{2}$$

Equating this with the energy loss rate of a magnetic dipole then gives the surface dipole magnetic field. Measurement of $\dot{\omega}$ can also give insight into the mechanisms transferring angular momentum to or from the pulsar by giving an estimate of the braking index[12].

While these techniques give significant insight into the properties of the pulsar, they give very little information regarding the surrounding environment. In particular, the properties of the pulsar wind are currently not very well known. While it is known that some fraction of the outgoing electromagnetic flux must be converted into a particle flux at the light cylinder of radius

$$R_l = \frac{c}{\omega}, \tag{3}$$

little is known of the nature of this conversion and the effect it has on the radiation portion of the energy flux. Recently, a number of binary systems composed of a pulsar and star orbiting it have been discovered in which the pulsar wind causes observable changes in the companion star[13]. If the companion star has a mass less

[10] Padmanabhan, op. cit.; J. M. Lattimer and M. Prakash. "Neutron Star Structure and the Equation of State". In: *The Astrophysical Journal* 550.1 (2001), p. 426. eprint: `http://arxiv.org/abs/astro-ph/0002232`. URL: `http://stacks.iop.org/0004-637X/550/i=1/a=426`.

[11] Andrea N Lommen and Paul Demorest. "Pulsar timing techniques". In: *Classical and Quantum Gravity* 30.22 (2013), p. 224001. eprint: `http://arxiv.org/abs/1309.1767`. URL: `http://stacks.iop.org/0264-9381/30/i=22/a=224001`.

[12] Padmanabhan, op. cit.

[13] R. P. Breton et al. "Discovery of the Optical Counterparts to Four Energetic Fermi Millisecond Pulsars". In: *The Astrophysical Journal* 769 (2013), p. 108. URL: `http://arxiv.org/abs/1302.1790`.

than the $0.08 M_\odot$ minimum required to sustain fusion, the system is known as a Black Widow[14], and if the pulsar wind heats the companion and causes it to swell to fill its Roche lobe, the system is known as a Redback[15].

In the vast majority of Black Widows, even heating is seen on the pulsar-facing side[16]. There is one, however, known as PSR J1544-4937, in which the heating appears to be highly concentrated towards a small set of points on the companion. This indicates effects involving the interaction between the wind and the companion magnetosphere.

In the case of Redbacks, it is possible that Roche lobe-filling companions can begin an accretion process onto the pulsar as a result of heating from the wind. If this occurs, the system can become an X-ray binary. There are several known cases of X-ray binaries which turn on and off on timescales of ~ 10yrs[17]. This may be due to the accretion disk burying the magnetic field of the pulsar, allowing the companion to cool and thereby halting the accretion process[18]. Under this model, when the accretion rate drops sufficiently the process begins again.

Both kinds of systems offer an opportunity to learn more about the pulsar wind, in particular as the effects of the wind on the companion are strongly influenced by its composition. For typical low-frequency radiation (anything ranging up to X-rays in energy), the region which the wind heats is in the upper atmosphere of the star, near the photosphere. The result is that the radiation is just re-radiated without significantly altering the structure of the atmosphere. The net effect is a rise in

[14] Roberts, op. cit.; D. J. Stevenson. "The search for brown dwarfs". In: *Annual Review of Astronomy and Astrophysics* 29 (1991), pp. 163–193. DOI: `10.1146/annurev.aa.29.090191.001115`.

[15] Hai-Liang Chen et al. "Formation of Black Widows and Redbacks—Two Distinct Populations of Eclipsing Binary Millisecond Pulsars". In: *The Astrophysical Journal* 775.1 (2013), p. 27. eprint: `http://arxiv.org/abs/1308.4107`. URL: `http://stacks.iop.org/0004-637X/775/i=1/a=27`.

[16] Reynolds et al., op. cit.; Roger W. Romani et al. "PSR J1311–3430: A Heavyweight Neutron Star with a Flyweight Helium Companion". In: *The Astrophysical Journal Letters* 760.2 (2012), p. L36. eprint: `http://arxiv.org/abs/1210.6884`. URL: `http://stacks.iop.org/2041-8205/760/i=2/a=L36`; M. H. van Kerkwijk, R. P. Breton, and S. R. Kulkarni. "Evidence for a Massive Neutron Star from a Radial-velocity Study of the Companion to the Black-widow Pulsar PSR B1957+20". In: *The Astrophysical Journal* 728.2 (2011), p. 95. eprint: `http://arxiv.org/abs/1009.5427`. URL: `http://stacks.iop.org/0004-637X/728/i=2/a=95`.

[17] Icdem, B. and Baykal, A. "Viscous timescale in high mass X-ray binaries". In: *Astronomy and Astrophysics* 529 (2011), A7. DOI: `10.1051/0004-6361/201015810`. eprint: `http://arxiv.org/abs/1102.4203`. URL: `http://dx.doi.org/10.1051/0004-6361/201015810`.

[18] J. Hessels. "M28I and J1023+0038: The Missing Links Go Missing, but Provide a New Link". In: NS Workshop. Dec. 2013. URL: `http://www.astro.uni-bonn.de/NS2013-2/Hessel_M28i.pdf`.

temperature on the near-side according to the Stefan-Boltzmann law:

$$4\pi R^2 \sigma T_{new}^4 = 4\pi R^2 \sigma T_{old}^4 + L_e. \tag{4}$$

The far-side does not heat at all, as there is no time to move the absorbed heat around the star before reemission occurs.

When the radiation is higher in energy, or is made of massive particles, the situation is somewhat different. High energy radiation can penetrate quite deep into the star, as will be discussed later. Massive particles can likewise make it quite far, particularly if they are uncharged. Charged massive particles are, however, limited by the ionization zone in how far they may travel. Regardless of the specific form of the external heating, when it occurs at depth the picture is very different. In particular, the heat has some time to be redistributed within the star rather than immediately escaping to the near-side. The formal statement of this effect is that the time it takes for the heat to be nontrivially redistributed is now comparable to or shorter than the radiative relaxation time. Profound structural changes in the stellar atmosphere may occur, including the excitation of gravity waves, strong zonal winds, tropical hurricanes, and the inducement of swelling in the deeper regions of the atmosphere. This last symptom of external heating may be responsible for the observed Roche-lobe filling in certain Redback systems, with the eponymous thermal difference on the surface between the two sides of the star being due to the non-penetrative flux of the Pulsar wind.

As these phenomena couple heat transport, fluid mechanics, orbital mechanics, and various pieces of thermodynamic microphysics, we will discuss the physics first, and then the astronomy. Along the way, we will use examples from astronomy to illustrate relations, gain intuition, and build models, but only at the end will the astrophysical phenomena of interest be discussed in full.

Part I

Physics

1

Geometry and Optical Depth

, .

There is geometry in the humming of the strings, there is music in the spacing of the spheres.

– Pythagoras

The geometry of the situations of interest is outlined in Fig. 1.1. The companion star and pulsar orbit their center of mass with angular velocity Ω. The companion is tidally locked, and hence Ω is also its rotation rate. The pulsar, on the other hand, has rotation rate $\omega \gg \Omega$. The two objects are separated by distance R_o, and have masses M_p and M for the pulsar and companion respectively. The star has radius R. Note that the relative distances depicted are not shown to scale. The heating zone is, for any kind of radiation, the region surrounding the surface of unit optical depth. In the cases of interest the source is positioned on one side of the companion and is far enough away that it may be viewed as roughly a planar wavefront.

To determine where the heating zone lies, we must examine the optical depth associated with various kinds of radiation incident on the surface of the star. Below 10keV, the chief scattering processes are resonant absorption and Rayleigh scattering[1]. Above this scale, Compton scattering becomes the dominant process,until approximately 1MeV $\sim 2m_e$, at which point the dominant process is pair production. This state of affairs continues to arbitrarily high energies once the electron-positron pair production threshold is crossed. The use of the pair production decay channel, however, means that there will be more particles present after the initial scattering, and these may continue moving through the star for some distance before further scattering thermalizes them. If the resulting particles have energies above some critical level, the dominant process once all channels and possibilities are accounted for will continue to be pair production.

The net result of all of this is that for incident radiation below a critical energy, a single scattering event suffices and the cross-section directly gives the depth at which the radiation deposits heat. This gives

$$\Sigma = \frac{1}{\kappa}, \tag{1.1}$$

where κ is the mass attenuation coefficient corresponding to the material and particle kind. Above the critical energy, the resulting particles from the first scattering continue to produce further particles until their descendents drop below the critical energy and produce heat. At each stage in the shower, additional particles are produced with energies approximately two times lower than what they started with, so if E_γ

[1] J. et al Beringer. "Particle Data Group". In: *Phys. Rev. D* 86 (2012), p. 010001.

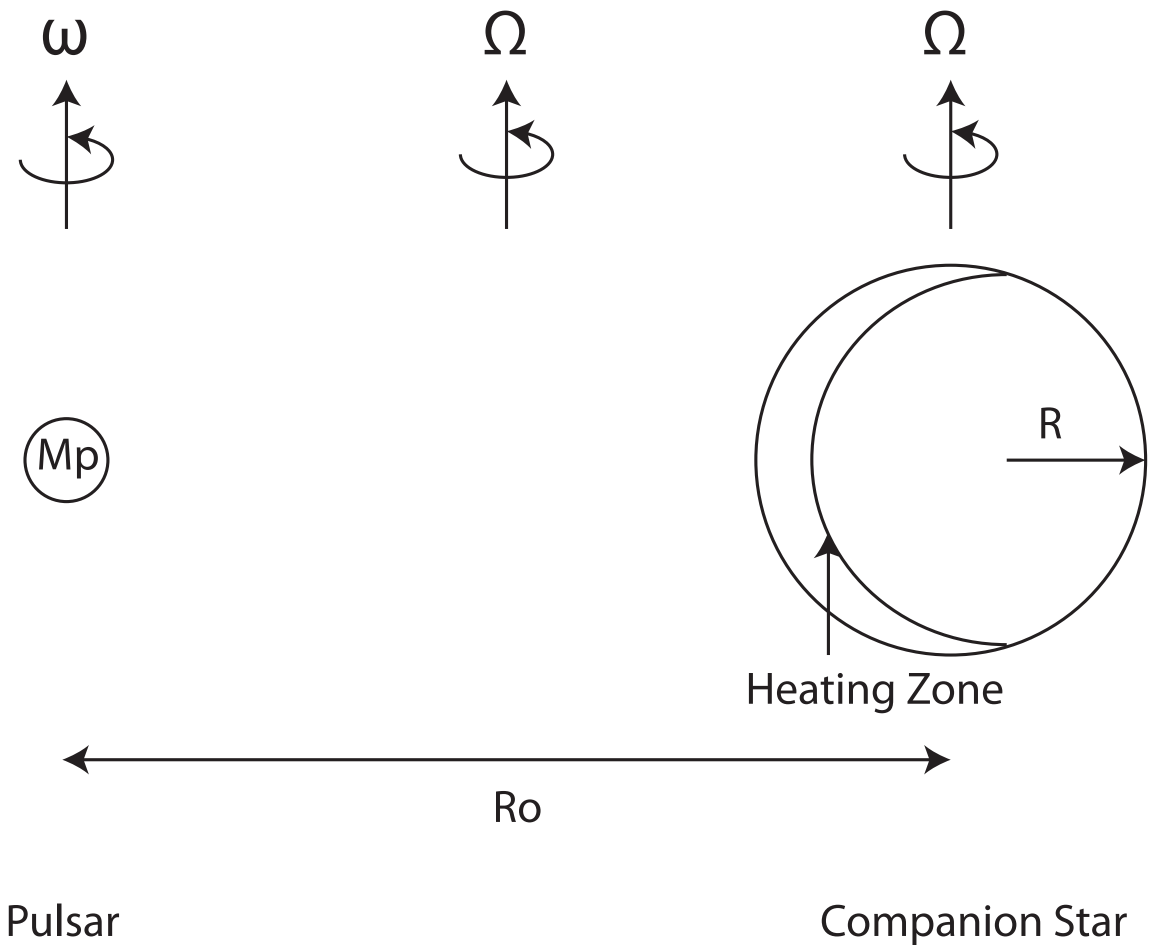

Figure 1.1: Depiction of a pulsar and its companion. Note that none of the depictions are to scale. The companion orbits with angular velocity equal to its rotational angular velocities due to tidal locking effects. The pular and companion are separated by a distance R_o. Their masses are M_p and M respectively. The star has radius R. The heating zone is, for any kind of radiation, the region of unit optical depth given that the radiation is incident from one side and that the source is far enough away that it may be viewed as a planar wavefront.

is the energy of the photon and E_{crit} is the critical energy, a total of approximately $\log_2(E_\gamma/E_{crit})$ are created. If the scattering cross-section at each stage is roughly constant, as is expected in the case of energies above GeV scales[2], then this means that the column density at which heat is produced should be

$$\Sigma = \frac{1}{\kappa}\left(1 + \log_2 \frac{E_\gamma}{E_{crit}}\right),$$

The critical energy is given approximately[3] in gases by

$$E_{crit} = \frac{710\text{MeV}}{Z + 0.92},$$

where Z is the number of protons in a nucleus. For hydrogen this simplifies to

$$E_{crit} = 370\text{MeV}.$$

Plots of κ^{-1} and the corresponding Σ are shown in Fig. 1.2 and Fig. 1.3 respectively.

For hydrogen, the value of κ^{-1} is approximately 100g/cm^2 for all energies beyond E_{crit} which have been measured[5], going up through 100GeV. Thus

$$\Sigma = 100\frac{\text{g}}{\text{cm}^2}\left(1 + \log_2 \frac{E_\gamma}{370\text{MeV}}\right).$$

Typical pulsar photon energies in the upper end of the spectrum are of order hundreds of GeV[6]. Substituting this in gives roughly

$$\Sigma_h = 10^3\frac{\text{g}}{\text{cm}^2}. \tag{1.2}$$

This is the column density at which a stellar companion transforms the pulsar's gamma rays into heat, and we will use this value in calculations involving the heating depth. To most appropriately model the physical process of particle showers and absorption, we will treat the incident luminosity as following

$$L_e(\Sigma) = L_e e^{-\Sigma/\Sigma_h}, \tag{1.3}$$

[2] Ibid.

[3] Ibid.

[5] Ibid.

[6] A. Smith David. "Gamma Ray Pulsars with the Fermi LAT". in: 3rd Fermi Symposium. May 2011. URL: `http://fermi.gsfc.nasa.gov/science/mtgs/symposia/2011/program/session14/Smith_FermiPSRs.pdf`; H. et al Anderhub. "Search for Very High Energy Gamma-ray Emission from Pulsar-Pulsar Wind Nebula Systems with the MAGIC Telescope". In: *The Astrophysical Journal* 710.1 (2010), p. 828. URL: `http://stacks.iop.org/0004-637X/710/i=1/a=828`.

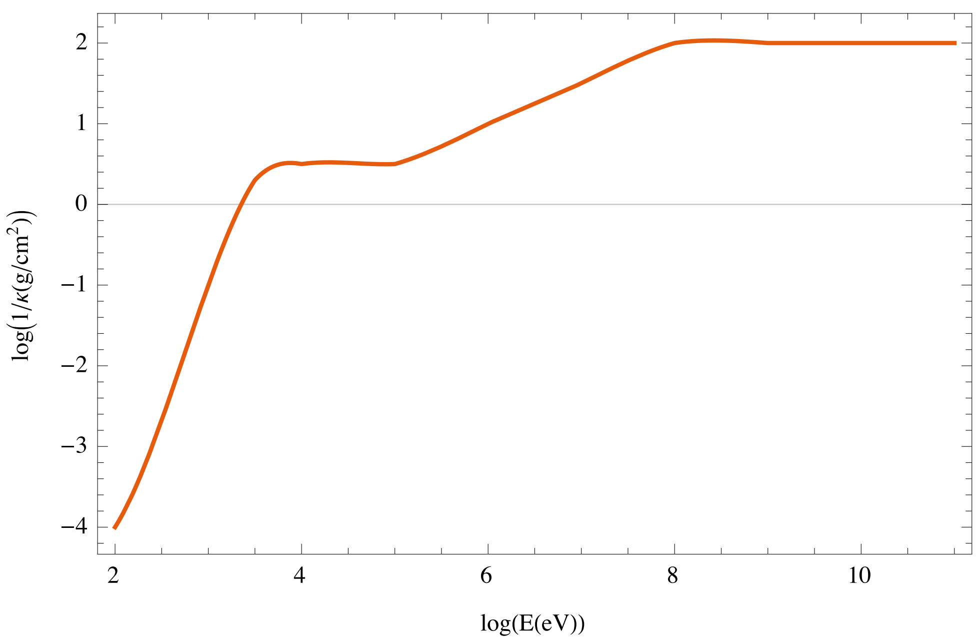

Figure 1.2: $\log \kappa^{-1}$ is plotted versus $\log E$. The former is measured in g/cm^2 and the latter in eV. Data was extracted manually from plots in the Particle Data Group book[4], and so has some uncertainty associated with the conversion process.

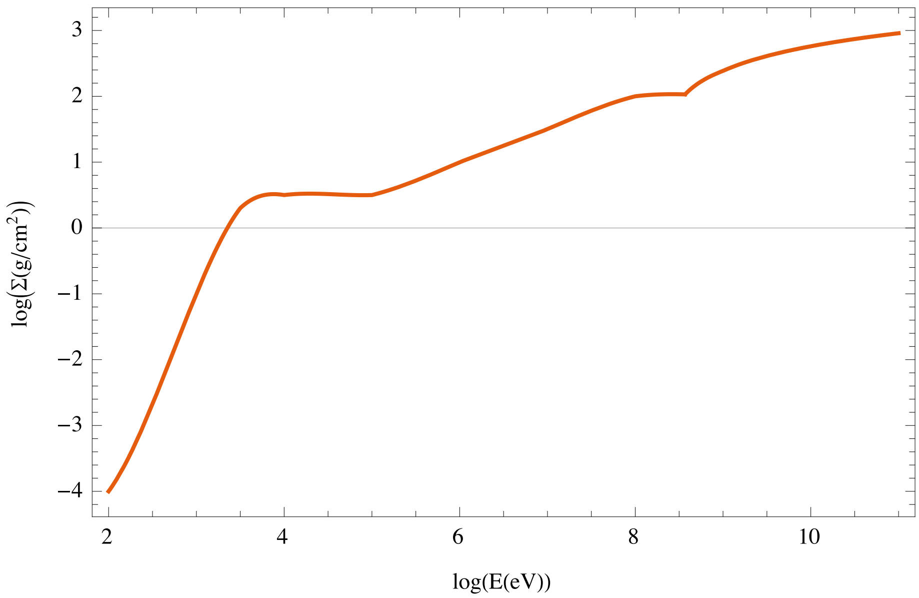

Figure 1.3: $\log \Sigma$ is plotted versus $\log E$. The former is measured in $\mathrm{g/cm^2}$ and the latter in eV.

where L_e measures only the high-energy photons. Low energy photons are ignored, as they are absorbed and reemitted soon thereafter in the photosphere.

Armed with this information regarding the structure of the heating zone, we can in principle take a three-dimensional model of a star and compute the spatial dependence of the heating. Again, in principle, this may be used to compute the resulting effects on the star. For the purposes of gaining physical intuition, however, this is not the most effective way to proceed, for there are many simplifications which may save substantially on computational effort and may make clearer the relevant physics.

The most basic model for the companion star which captures some of the physics of interest is to treat it as one-dimensional, and ignore the azimuthal symmetry breaking which results from the tidal locking. In this case, the star is parametrized by a series of functions of the radial coordinate, such as temperature, pressure, and so on. Though this model neglects a significant physical asymmetry, it is advantageous in its mathematical and computational simplicity, and so will be our starting point. Within the context of this model, we will treat all physical quantities as their averages over the angular coordinates, such that the externally incident flux will sum up to the same total luminosity. As a result, this model is often referred to as the plane-parallel or isotropic atmosphere, for in it there is only one coordinate (depth) which matters.

After this model, the next modification will be to examine higher-dimensional models. We will examine both two-dimensional models which add just the azimuthal coordinate ϕ and fully three dimensional models. In the former, we will treat all quantities as their average over the spherical polar angle θ, while the latter holds the full dimensionality of the system.

Beyond spatial dimensions, there is also the question of time. Initially we will consider all solutions in the steady-state. After this, we will shift to considering the time-dependence of these models, and exa mine both the stability of the steady-state solutions and the means by which they are reached.

References

Anderhub, H. et al. “Search for Very High Energy Gamma-ray Emission from Pulsar-Pulsar Wind Nebula Systems with the MAGIC Telescope”. In: *The Astrophysical Journal* 710.1 (2010), p. 828. URL: `http://stacks.iop.org/0004-637X/710/i=1/a=828` (cit. on p. 9).

Beringer, J. et al. “Particle Data Group”. In: *Phys. Rev. D* 86 (2012), p. 010001 (cit. on pp. 7, 9).

Smith David, A. “Gamma Ray Pulsars with the Fermi LAT”. In: 3rd Fermi Symposium. May 2011. URL: `http://fermi.gsfc.nasa.gov/science/mtgs/symposia/2011/program/session14/Smith_FermiPSRs.pdf` (cit. on p. 9).

2

One-Dimensional Model

There is a computer disease that anybody who works with computers knows about. It's a very serious disease and it interferes completely with the work. The trouble with computers is that you "play" with them!

– Richard P. Feynman[1]

2.1 Equations of Stellar Structure

In the isotropic steady-state model, we treat all quantities in the companion as functions of r, the distance from its center. No other independent variable enters in this model, as t is forbidden by the steady-state assumption and θ and ϕ are forbidden by the isotropy assumption. Thus we write temperature as $T(r)$, pressure as $P(r)$, and so on.

To a very good approximation, we may neglect the variation in the composition of the star with position. That is, we treat all compositional variables as global constants, such that $X(r) = X_0$, the hydrogen mass fraction in the star, and likewise for all other such quantities. In making this approximation we mainly lose accuracy in calculating the properties of convection zones, though there our accuracy is primarily limited by the uncertainty in the choice of mixing length, and so this loss is acceptable.

The remaining spatial variables are then only thermodynamic ones. Of these, one might pick as "fundamental" ones the pressure, temperature, density, and mean

[1] Richard P. Feynman. *Los Alamos From Below*. `https://www.youtube.com/watch?v=0ogSC6JKkrY`. Feb. 6, 1975. URL: `http://calteches.library.caltech.edu/34/3/FeynmanLosAlamos.htm`.

molecular weight[2]. All other quantities of interest may be derived from these. We may, however, eliminate μ, for it is a direct function of T. This follows from the fact that we have held compositional variables fixed, such that μ varies only through ionization.[3]. This variation occurs mainly when $k_B T$ is comparable to $13.6eV$, and is generally taken to happen between $10^{3.8}$K and $10^{4.1}$K. The value of $13.6eV$, of course, is the ionization energy of hydrogen.

Using the equation of state, we may eliminate yet another function, to reduce the total count of "fundamental" thermodynamic variables at each point to two. The equation of state is most generally written as

$$P = f(\rho, T), \tag{2.1}$$

though it is usually well approximated by the form

$$\mu P = \rho k_B T + \frac{1}{3} a T^4, \tag{2.2}$$

where the second term is included to accommodate radiation pressure. At low temperatures the second term may be dropped, yielding the familiar ideal gas law. Regardless of the specific form, we will use the equation of state to eliminate the density from consideration, and hence write

$$\rho = g(P, T). \tag{2.3}$$

Our ability to write it in this form comes from P being monotonic in ρ and T. We choose ρ rather than T or P because we generally wish to compute heat transport properties in terms of temperature, and in hydrostatic equilibrium the pressure is computable by a straightforward integral. As a result, we are left with two basic functions, $P(r)$ and $T(r)$, which fully characterize the star to within our various approximations.

It will often be more convenient to replace r with m, the mass above a particular radius, as the independent variable. As m is monotonically decreasing with r this is a perfectly well-defined transformation. We thus write $P = P(m), T = T(m)$. In this language, the condition of hydrostatic equilibrium may be cast into a convenient form, as

$$\frac{dP}{dr} = -\rho g \rightarrow \frac{dP}{dm} = \frac{g}{4\pi r^2}. \tag{2.4}$$

Now over the depth ranges of interest, as will be verified later, r varies only slightly relative to R. As a result, we may neglect its variation in computing quantities

[2]Other valid choices include specific energy, specific entropy, sound speed, etc.

[3]At high pressures it may also depend on pressure, and indeed we will account for this

in which r appears as a multiplicative factor. This is known as the thin-envelope assumption, and has several useful implications. For instance, we may approximate the gravity of the star as being fixed at

$$g \equiv \frac{GM}{R^2}. \tag{2.5}$$

As a result, we may write the condition of hydrostatic equilibrium as

$$\frac{dP}{dm} = \frac{GM}{4\pi R^4}. \tag{2.6}$$

Using the boundary condition $P(r = \infty) = 0, m(r = \infty) = 0$ we find

$$P(m) = \frac{GMm}{4\pi R^4}. \tag{2.7}$$

Note that we may also use the variable

$$\Sigma \equiv \frac{m}{4\pi R^2} \tag{2.8}$$

as the independent variable. Given that this is the form in which we know the heating depth, we will often switch to using this rather than m.

Given $T(m)$, in addition to what we have found so far, we will know the structure of the star to within the bounds of our approximations. As a result, we know that $T(m)$ must depend in some fashion on the luminosity of the star and on the external illumination we hope to investigate, for these quantities appear nowhere else and they seem quite important. To that end, consider the outer boundary condition on the star. There are a variety of models for this[4], but most treat the low-m regime by some gas-radiation dilution model and use this to find the optical depth along the radial direction. From there, it is typically asserted that

$$L = 4\pi R^2 \sigma T^4 \tag{2.9}$$

at the place where the optical depth $\tau = 2/3$. This is just an application of the Stephan-Boltzmann radiation law to a gray-body atmosphere, with an effective treatment for the differing rates at which different frequencies of radiation escape at low optical depth. We will not go into the specific details of the model we used, and merely state that they are those described in Ref.[5].

[4] B. Paczyński. "Envelopes of Red Supergiants". In: *Acta Astronomica* 19 (1969), p. 1.
[5] Ibid.

From this upper boundary condition on T, we may integrate towards higher m using the equation

$$\frac{dT}{dm} = \left(\frac{d\ln T}{d\ln P}\right)\frac{T}{P}\frac{dP}{dm} = \nabla\frac{T}{P}\frac{dP}{dm}, \tag{2.10}$$

where the second equality defines the symbol ∇ and where the derivative with respect to $\ln P$ is taken along the radial direction. This last point is not relevant in an isotropic star, where ∇T and ∇p are aligned, but will become important when we move to higher dimensional models.

Of course, there is no physical content in Eq. (2.10): it is simply a true statement regarding differentiable functions. The reason we bother to cast the problem in this form is that ∇ may often be expressed simply. In regions of the star where heat is transported radiatively,

$$\nabla = \nabla_{rad} = \frac{3\kappa PL}{16\pi acGMT^4}, \tag{2.11}$$

where κ is the Rosseland mean opacity of the stellar material, and is generally a function of P and T. On the other hand, when the region of interest is unstable against convection, the thermal gradient ∇ is somewhat more complicated. If convection is efficient, then the convective gradient matches the adiabatic gradient, such that

$$\nabla = \nabla_{ad} = \left.\frac{d\ln T}{d\ln P}\right|_s. \tag{2.12}$$

This gradient is typically 0.4 for monatomic gas and for fully ionized gas, and drops to $0.1 - 0.2$ in the ionization zone. If, on the other hand, convection is inefficient, then matters become somewhat more complex, as then both radiation and convection contribute nontrivially to thermal transport. The full solution for the convective gradient in this case is somewhat complicated, and involves the root of a cubic with a closed form which does not yield much intuition. Various methods of numerical solution have been developed[6], and will be employed in the next section. As will be shown later, however, convection is usually highly efficient in the cases of interest, and so setting $\nabla = \nabla_{ad}$ in convecting regions is generally accurate.

It is worth noting that the question of convective stability is much simpler in stars than in other contexts. The microscopic viscosity of stellar atmospheres is generally far too low to stop convection[7]. This is a statement about the typically large value of the Rayleigh number whenever the radiative gradient exceeds the adiabatic one. Thus

[6] Ibid.

[7] This will be discussed at length when we examine the properties of fluids in motion for higher dimensional heat transport

in the absence of shear turbulence the primary criterion determining if convection occurs is

$$\nabla_{rad} > \nabla_{ad}. \tag{2.13}$$

If this condition is satisfied then convection occurs. Loosely speaking this criterion may be thought of as indicating that the temperature gradient needed to carry the thermal flux through radiation is too high relative to the buoyancy experienced by an adiabatically expanding packet of gas. The result is a convective instability.

The only remaining piece of physics we need to compute stellar structures with the above equations is κ. This we take from tables such that those of OPAL[8] and Ferguson[9], as discussed in Appendix B.1. A plot of the opacities produced by these tables at $X = 0.7, Y = 0.27, Z = 0.03$ is shown in figure 2.1.

2.2 Simulations

Armed with the equations of stellar structure, we may simulate a variety of stars numerically to see how they respond to different amounts of external illumination. The purpose of these initial simulations is to gain intuition for the relevant phenomenology, and to determine reasonable ranges for the various parameters such as temperature, pressure, and so on.

Initially, all simulations were done using a modified version of the Gob software package, originally written for Red Giant envelope integration[10]. The original and modified codes may be found in Appendix C. A modern code known as Acorn was then written as part of this thesis to incorporate recent advances in low-temperature stellar opacity models. In addition, it uses a much finer adaptive mass grid, resulting in more accurate and smoother stellar profiles[11]. This code was then verified in the high-temperature limit against Gob, and the microphysical inputs were verified independently in the low-temperature limit. The details of this code may be found in Appendix B.2, with details on the opacity tables and associated interpolation routines in Appendix B.1. The code solves precisely the same equations as Gob[12], with the

[8] C. A. Iglesias and F. J. Rogers. "Updated Opal Opacities". In: *The Astrophysical Journal* 464 (June 1996), p. 943. DOI: 10.1086/177381.

[9] Jason W. Ferguson et al. "Low-Temperature Opacities". In: *The Astrophysical Journal* 623.1 (2005), p. 585. URL: http://stacks.iop.org/0004-637X/623/i=1/a=585.

[10] Paczyński, op. cit.

[11] The smoothness of the resulting profiles is particularly important, as we will use the output from the steady-state code as the input to the transient code, which requires evaluating numerical derivatives in mass.

[12] Paczyński, op. cit.

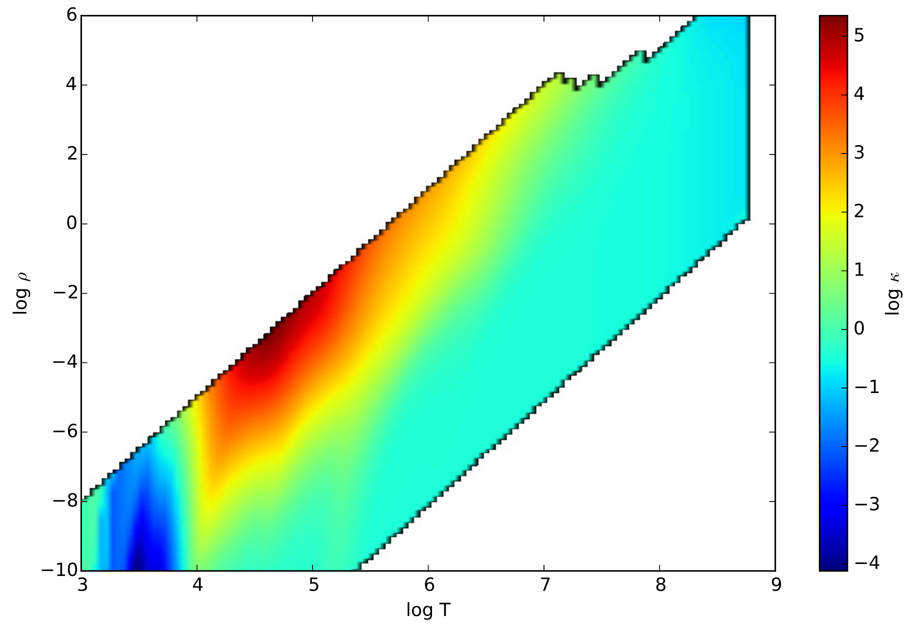

Figure 2.1: The vertical axis is $\log \rho$ (with ρ measured in g/cm^3), the horizontal is $\log T$ (with T measured in K), and the color represents $\log \kappa$ (with κ measured in cm^2/g. White regions are those without data.

addition of the thin envelope assumption, such that $M-m$ and r are taken not to change, except where they appear explicitly as parameters for differentiation.

Though Acorn only computes stellar envelopes, this is more than enough to examine the vicinity of Σ_h. The heat input was modeled by changing the luminosity of the star as a function of column density, according to

$$L(\Sigma) = L_{in} + L_e e^{-\Sigma/\Sigma_h}. \tag{2.14}$$

A value of $\Sigma_h = 10^3 \mathrm{g/cm^2}$ was used here, as per the discussion in Chapter 1.

To begin with, we consider models where the external illumination is imposed whilst holding the star's radius and intrinsic luminosity fixed. The following three representative models for companion stars were chosen for the simulations:

- The Sun: $M = M_\odot$,$L_{in} = L_\odot$,$R = R_\odot$
- Low-mass nuclear-burning: $M = 0.3M_\odot$,$L_{in} = 10^{-2}L_\odot$,$R = 0.43R_\odot$
- Brown dwarf: $M = 0.02M_\odot$,$L_{in} = 10^{-4}L_\odot$,$R = 0.14R_\odot$

The full output from Acorn for each of these cases for a variety of external luminosities may be found in Appendix E.

The first aspect of these models worth investigating is the region of validity of the thin-envelope approximation, which is the assumption that $r \approx R$ everywhere in the envelope. To see where this holds, we have plotted the radius as a function of Σ in figure 2.2. For the $1M_\odot$ star, the thin-envelope approximation is good down to $\Sigma = 10^6 \mathrm{g/cm^2}$ or so, where deviations reach roughly 10%. For the $0.3M_\odot$ star, the approximation is valid everywhere with no external heating, down to $\Sigma = 10^7 \mathrm{g/cm^2}$ for $L_e = L_i$, and to $\Sigma = 10^6 \mathrm{g/cm^2}$ for $L_e = 10L_i$. For both of these stars, deviations grow rapidly past the regime of validity. Finally, for the $0.02M_\odot$ star, the approximation is typically only valid within 10% down to Σ_h. Past this, however, deviations grow much more slowly than for the other two stars, and so the approximation may be safely used down to around $10^5 \mathrm{g/cm^2}$, where deviations reach 15%. Fortunately there are no phenomena which are both sensitive to the high-Σ failure of this approximation and are of significant quantitative interest, so this approximation is a safe one to make. Subsequent plots will be truncated in their range of Σ to that in which the approximation is valid to within 50%.

We now turn to the thermal structure of the star. Figure 2.3 shows the log of temperature versus the log of column density for nine scenarios. The three stars of interest are represented by the columns, while three different external luminosities are represented by the rows. The top row has no external illumination, the middle

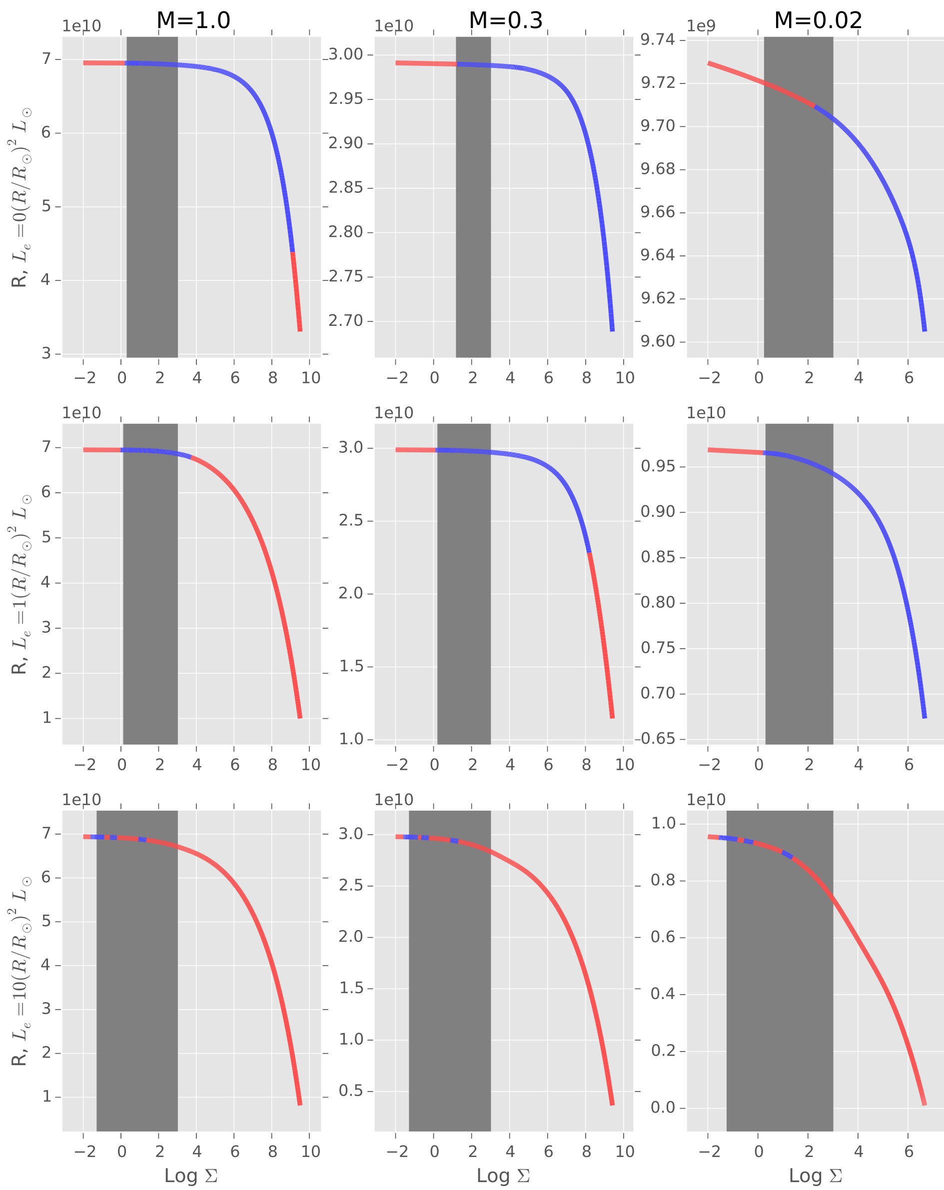

Figure 2.2: Radial coordinate (in cm) versus log of Σ (in g/cm^2) for nine different scenarios. Σ here is computed as the mass above the point of interest divided by $4\pi R^2$. The columns are the three different stars under consideration. Moving left to right, they are $M = M_\odot$,$L_{in} = L_\odot$,$R = R_\odot$, $M = 0.3M_\odot$,$L_{in} = 10^{-2}L_\odot$,$R = 0.43R_\odot$, and $M = 0.02M_\odot$,$L_{in} = 10^{-4}L_\odot$,$R = 0.14R_\odot$. The rows represent different quantities of external luminosity. From top to bottom, these are $L_e = 0, L_e = L_\odot \frac{R^2}{R_\odot}^2, L_e = 10L_\odot \frac{R^2}{R_\odot}^2$. The vertical grey bar goes from the edge of the photosphere (where $\tau = 2/3$) to the heating depth ($\Sigma = 10^3$g/cm^2). Blue regions are dominated by convective heat transport, red by radiative transport.

row has the illumination equal to $L_\odot R^2/R_\odot^2$, and the bottom row has it equal to ten times that. Note that for each mass, the radius was held constant. As a result, the top row represents a nearly unmodified system, while the bottom row represents a system dominated by the external heating.

Looking first at the sun, we see that adding external heating begins by shutting down convection at the base of the envelope, and eventually leads to almost completely radiative transport at high external luminosity. The only regions which remain convective are those in the vicinity of the ionization zone, where the adiabatic gradient is very low to begin with. This may be understood as a result of the external heat decreasing the temperature gradient between the core and the heating depth, while increasing it between this depth and the surface. In the former region this suffices to switch the transport from convective to radiative, while the latter is very stable against convection and so remains radiative. That the effect of the heating is so much deeper than the heating depth may be viewed as due to the imposition of a different boundary condition at this depth. In particular, the fact that we maintain a fixed radius as we vary the flux means that the surface temperature scales as $L_{net}^{1/4}$. In the $0.3M_\odot$ star we see the same thing, though with convection holding on in a larger region in the middle plot. In the $0.02M_\odot$ star, the same process is evidently occurring, though the transition to radiative transport is not apparent until the final plot. This is as we expect: at the lower temperatures which dominate in these stars, radiative transport is less efficient and so the need for convective heat transport is greater.

One interesting feature of note is the change in thermal gradient between $T = 10^4$K and $T = 10^{4.5}$K. This occurs when the ionization zone is convective, which it almost always is, and results from a decrease in the adiabatic gradient within the zone. The reason this feature is not visible in each of the nine scenarios plotted in figure 2.3 is that in not all scenarios does the ionization zone fall within the envelope.

The next aspect of these models worth examining is the pressure scale height, h_s. This sets the characteristic length scale for turbulence, wind shearing, and convective motion, and so will be of interest at every stage of our analysis. The log of this height is shown in figure 2.4. In each of the models, h_s increases monotonically into the star past the photosphere, starting around $10^{6.5}$cm near the surface and reaching values only a few orders of magnitude smaller than R at the base of the envelope. In general, we expect h_s to follow a power-law as a function of Σ, and indeed this is what we see. Deviations from this are typically due to changes in the mode of heat transport, or to the ionization of material at various points.

Now we may also compute the efficiency of convection, Γ, defined as the ratio of the heat carried by a convecting gas packet to the heat lost radiatively along the

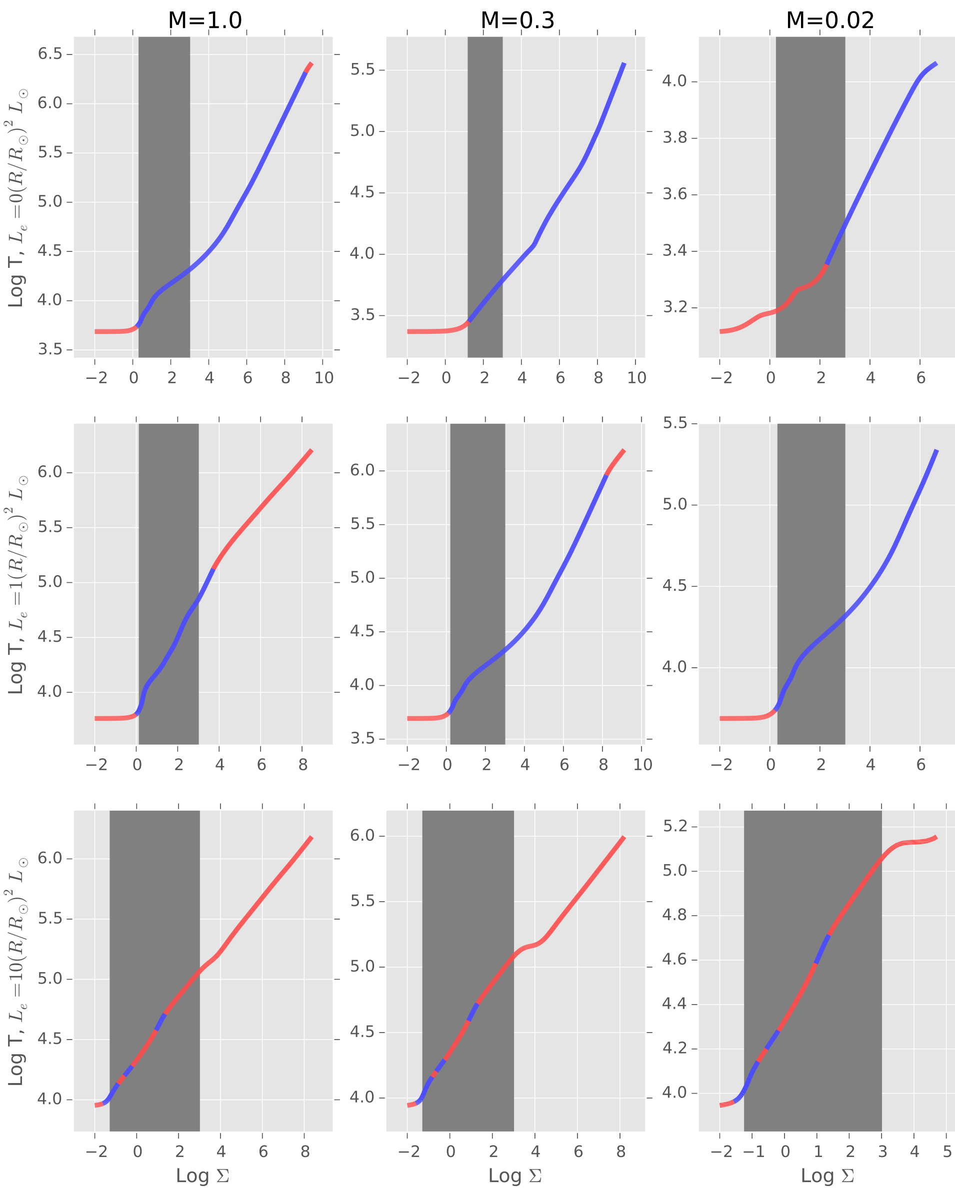

Figure 2.3: Log of T (in K) versus log of Σ (in g/cm^2) for the same nine scenarios defined in figure 2.2. Σ here is computed as the mass above the point of interest divided by $4\pi R^2$. The columns are the three different stars under consideration. The rows represent different quantities of external luminosity. The vertical grey bar goes from the edge of the photosphere (where $\tau = 2/3$) to the heating depth ($\Sigma = 10^3$g/cm^2). Blue regions are dominated by convective heat transport, red by radiative transport.

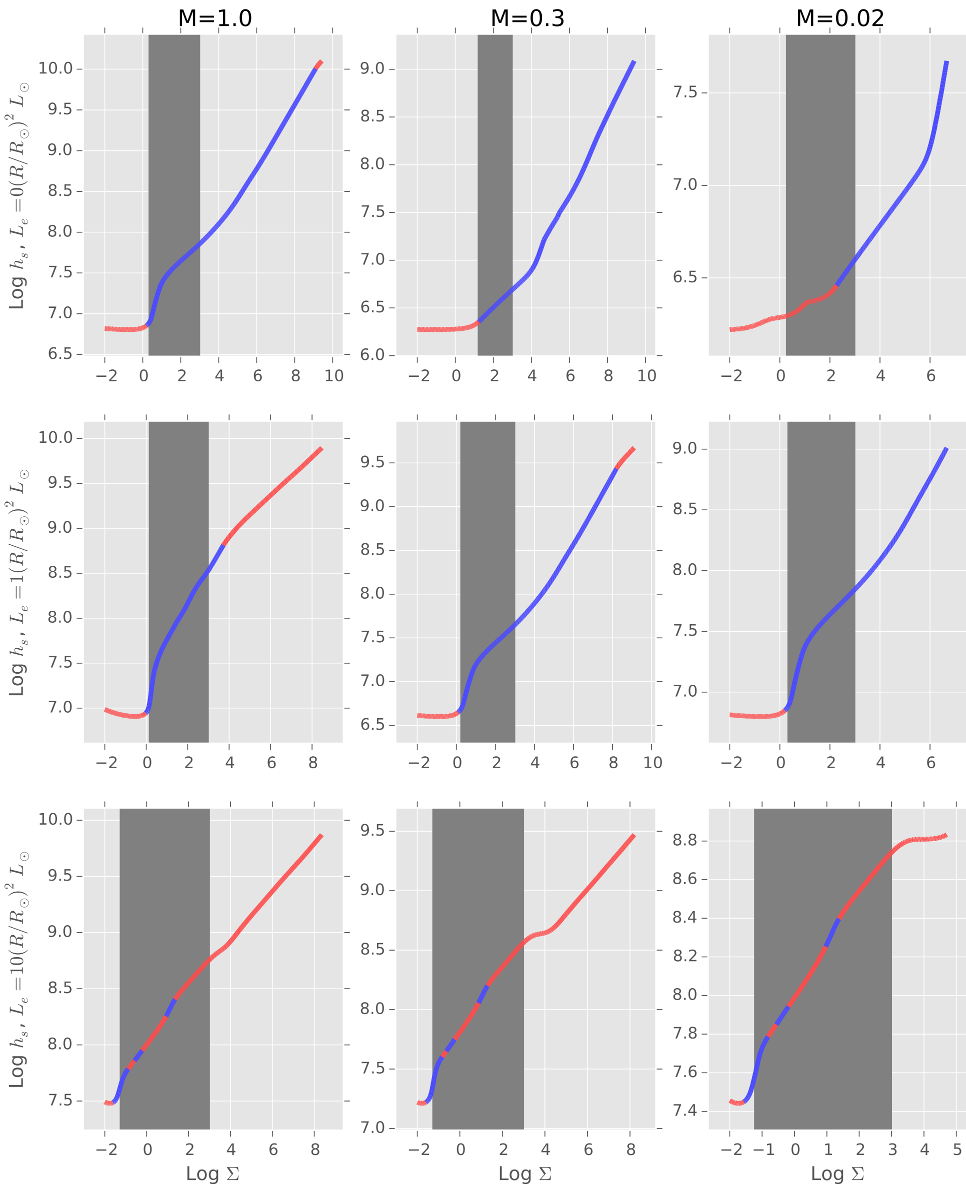

Figure 2.4: Log of pressure scale height versus log of Σ (in g/cm^2) for the same nine scenarios defined in figure 2.2. The columns are the three different stars under consideration. The rows represent different quantities of external luminosity. The vertical grey bar goes from the edge of the photosphere (where $\tau = 2/3$) to the heating depth ($\Sigma = 10^3$g/cm^2). Blue regions are dominated by convective heat transport, red by radiative transport.

way. While a variety of expressions exist for this, we will make use of the one used in the Gob stellar integration code[13]. The results of doing so are shown in figure 2.5. This quantity is of interest because it is a good indicator of the extent to which the balance between convection and radiation has been altered by the external heating, as well as because it indicates the extent to which the convective gradient deviates from the adiabatic one. In each of the unperturbed stars, convection is either highly efficient at the heating depth or becomes very efficient close to the heating depth. In shallower regions the efficiency decreases until convection ceases, with a sharp drop in efficiency at the boundary. Importantly, the region over which the efficiency is low is very small, as the slope of Γ with respect to Σ is large near the radiative-convective transition. In the perturbed stars, convection does not always occur in the same region, as the additional heat may turn it off in the vicinity of the surface, but where it does occur all of the same statements regarding its efficiency hold.

Finally, it is also useful to examine how κ varies through each of the stellar models of interest, and so this is shown in figure 2.6. Referencing figure 2.1, we see a few points worthy of discussion. First, many of the stellar tracks go outside of the known opacity data. In most of these cases the stars are convective, with highly efficient convection, and so the opacity is irrelevant. In every combination of the two low-mass stars with the two lowest-heating values, however, we get a radiative region outside of the known opacity data. In each case the issue arises because ρ is too large. The opacity tables are internally stored using ρ/T^3 and T as the independent variables[14]. Below 10^6K the tables form a rectangular grid in these variables. As a result, these tracks have exceeded the maximum value of ρ/T^3 for which we have data, while remaining in an acceptable temperature range. The simulation code in these cases simply returns the opacity at the correct temperature and maximum value of ρ/T^3 for which data exists. Fortunately, however, examination of the corresponding regions in figure 2.3 indicates that these regions are actually quite small in pressure-space, and only appear stretched in this plot out because ρ changes more rapidly here.

The second feature worth noting is that the convergence of the various tracks corresponding to the radiative atmospheres supports our conclusions regarding the decay of heating into radiative zones. Likewise, the lack of convergence between the analogous convective envelopes supports our conclusions regarding the continuation of heating into convection zones. Additionally, the vast majority of each track, whether measured by pressure-space or arc-length in $\log\rho, \log T$ space, is spent in regions

[13]Ibid.

[14]The first of these, ρ/T^3, is often called R, and usually defined with ρ measured in units of 1g/cm^3 and T measured in units of 10^6K.

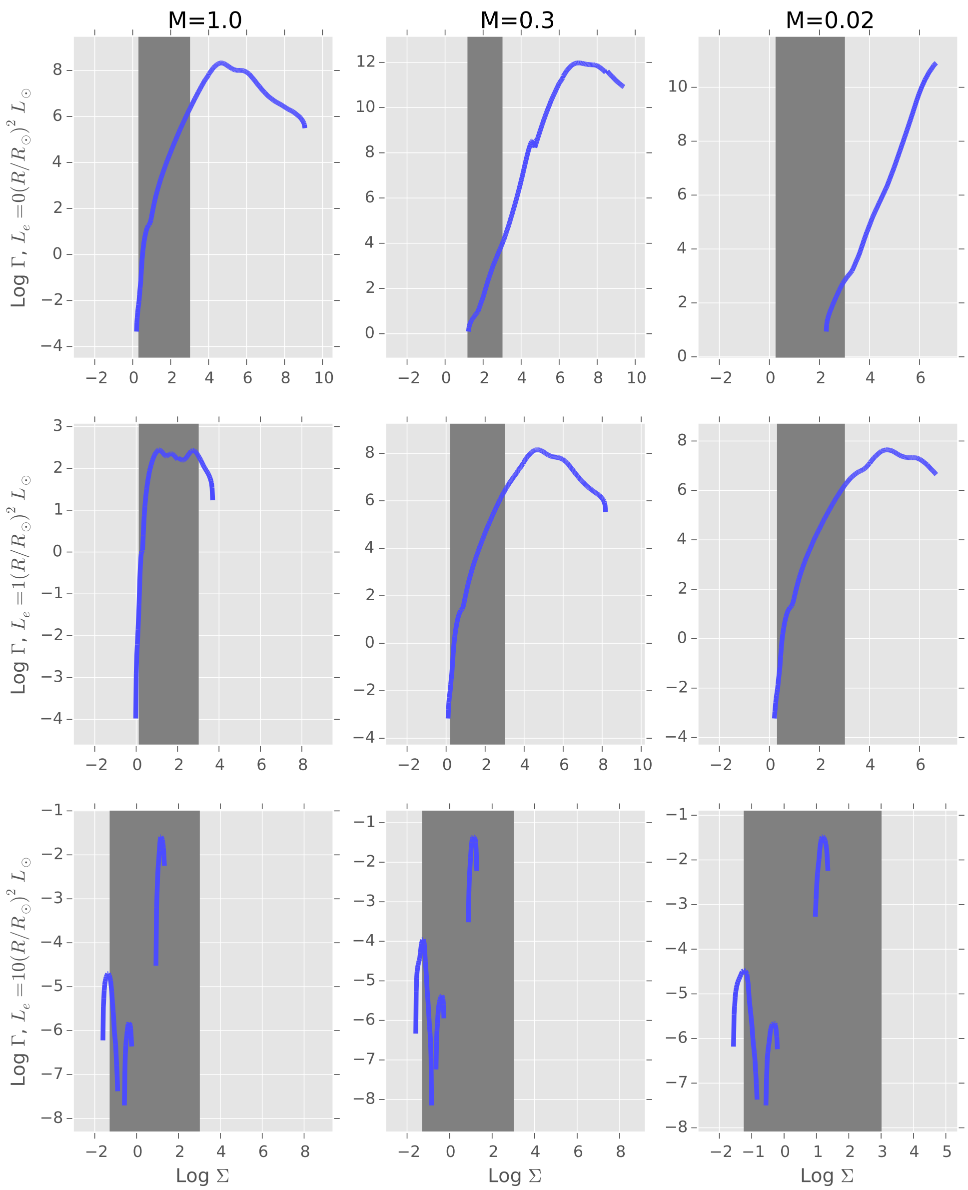

Figure 2.5: Log of convective efficiency (Γ, see text) versus log of Σ (in g/cm^2) for the same nine scenarios defined in figure 2.2. The columns are the three different stars under consideration. The rows represent different quantities of external luminosity. The vertical grey bar goes from the edge of the photosphere (where $\tau = 2/3$) to the heating depth ($\Sigma = 10^3$g/cm^2). Blue regions are dominated by convective heat transport, and all other regions have been omitted due to Γ only being defined in convective zones.

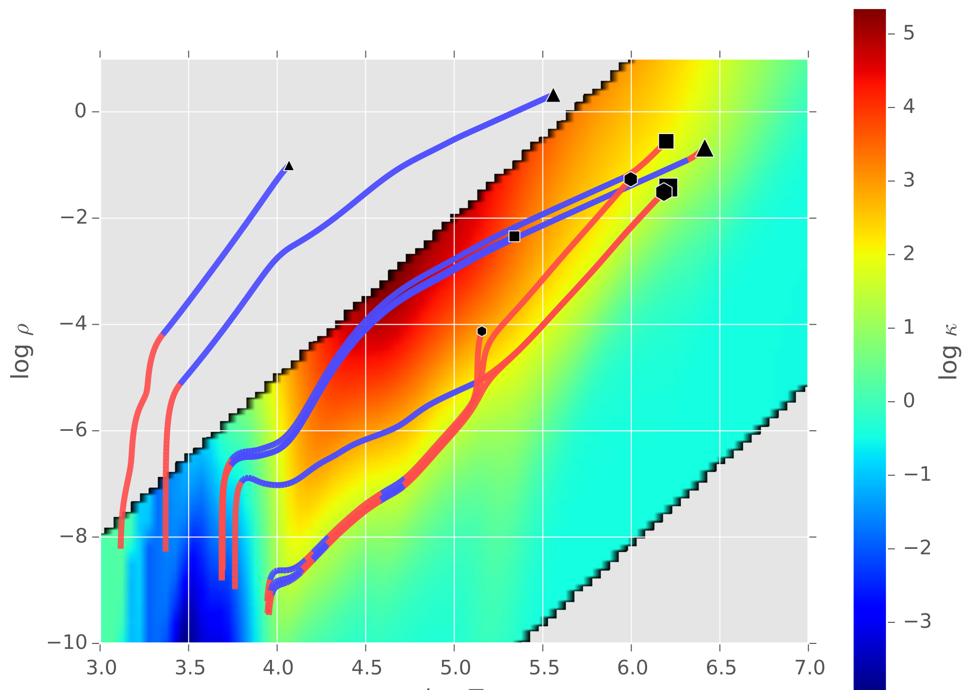

Figure 2.6: The vertical axis is $\log \rho$ (with ρ measured in g/cm^3), the horizontal is $\log T$ (with T measured in K), and the color represents $\log \kappa$ (with κ measured in cm^2/g. White regions are those without data. The nine stellar models defined in figure 2.2 are plotted as tracks on top of the opacity. The terminus marker indicates which track is which: the three sizes of markers correspond in increasing order to the three stellar masses under consideration, and the three kinds of markers correspond in order of increasing number of sides to increasing external illumination. Blue regions are dominated by convective heat transport, red by radiative transport.

where

$$\left.\frac{\partial \kappa}{\partial T}\right| < 0. \tag{2.15}$$

This fact will become relevant later in the next section. Finally, the fact that the minimum in κ lies at temperatures comparable to those in the ionization zone means that ∇_{rad} tends to peak where ∇_{ad} is at a minimum, which encourages the formation of a convection region around the ionization zone. This is seen even in the case of heavy external illumination, which generally pushes stars towards radiative transport even at depths much below where the additional heat is deposited.

2.3 Luminosity and Radial Variation

The simulations in the previous section were done with the radius and internal luminosity of the star fixed. To be completely accurate, we should really do a boundary condition matching between the photosphere and the nuclear burning region, as is done in codes like MESA[15]. Instead, we will perform a much simpler process, which consists of identifying roughly what the temperature change in the bulk of the star is, and using that, along with the dependence of nuclear burning on temperature, to estimate the balance between changing radius, changing surface temperature, and changing internal luminosity.

To begin, let P_b be the pressure at which the star changes from being convective to being radiative. We usually expect stars to be convective for $P < P_b$ and radiative for $P > P_b$[16]. This is obviously not always the case, as there can be small regions where convection turns on and off, but as a coarse view of things this is a good approximation. Note that for fully radiative stars $P_b = 0$ and for fully convective stars $P_b = P_{\text{core}} \approx \frac{2 g_{\text{surf}} M}{4\pi R^2}$. The mixed case, where $0 < P_b < P_{\text{core}}$, arises for stars of mass $M \in [0.43, 2] M_\odot$[17].

[15] Bill Paxton et al. "Modules for Experiments in Stellar Astrophysics (MESA): Planets, Oscillations, Rotation, and Massive Stars". In: *The Astrophysical Journal Supplement Series* 208.1 (2013), p. 4. URL: `http://stacks.iop.org/0067-0049/208/i=1/a=4`.

[16] The reason we expect convection on top is that ∇_{rad} decreases rapidly with temperature. In an efficient convection zone $T \propto P^{\nabla_{ad}}$, where ∇_{ad} is usually around 0.4 except in the ionization zone, where it drops to 0.1. ∇_{rad}, on the other hand, usually goes roughly as $PT^{-5} \propto P^{1-5\nabla_{ad}}$ in the star's interior. When we look past the ionization zone, the exponent is negative, and so ∇_{rad} eventually drops below ∇_{ad} at high pressure. There may of course be brief changes between convective and radiative heat transport in the ionization zone, but below that region our arguments should hold. Note that in computing ∇_{rad} we have factored in the approximate dependence of the opacity on temperature and pressure.

[17] Maurizio Salaris and Cassisi Santi. *Evolution of stars and stellar populations.* Vol. 1. ISBN:

If the star's surface heats up by an amount ΔT, we may ask how much of a change this causes in the matter below. In the radiation region, we know that

$$\frac{dT}{dP} = \frac{3\kappa L}{16\pi acGmT^3}, \tag{2.16}$$

where m is the mass below the pressure of interest. If we perturb this equation by letting $T \to T + \delta T$, and assume that $T(P)$ is a solution to the equation, then

$$\frac{d(\delta T)}{dP} = \frac{dT}{dP}\left(\left.\frac{\partial \ln \kappa}{\partial T}\right|_P - 3\frac{1}{T}\right)\delta T. \tag{2.17}$$

Now κ usually decreases with increasing temperature, at least once you look deeper than the upper envelope, so the perturbation decreases exponentially as one goes to higher pressures. This is consistent with the valve modelof radiative zones[18]. For fully radiative stars, then, we expect as a result that keeping R and L_{in} fixed is appropriate.

In the convecting region things are somewhat more complicated. We know that $T \propto P_c^{\nabla} \approx P^{\nabla_{ad}}$. If the temperature at some pressure P_0 is increased by T_0, then the temperature changes all the way from P_0 to P_b following the convective gradient. For stars which have some nontrivial convection zone, let ΔT_0 be the temperature change at P_0, where we now restrict $P_0 < P_b$ and pick P_0 at the lowest possible pressure below the photosphere. Recall that the radius of the star obeys

$$\frac{dr}{dm} = \frac{1}{4\pi r^2 \rho}. \tag{2.18}$$

This may also be written as

$$\frac{dr^3}{dm} = \frac{3}{4\pi\rho}. \tag{2.19}$$

Differentiating with respect to time gives

$$\frac{d}{dm}\left(\frac{dr^3}{dt}\right) = \frac{-3}{4\pi\rho}\left(\frac{d\ln\rho}{dt}\right) = -\frac{dr^3}{dm}\left(\frac{d\ln\rho}{dt}\right). \tag{2.20}$$

At fixed pressure, $d\ln\rho = -d\ln T$, neglecting the small space occupied by the ionization zone, so

$$\frac{d\ln\rho}{dt} = -\frac{d\ln T}{dt}. \tag{2.21}$$

0-470-09220-3. John Wiley Sons, 2005, pp. 138–140.

[18] H. Ritter, Z.-Y. Zhang, and U. Kolb. "Irradiation and mass transfer in low-mass compact binaries". In: *Astronomy and Astrophysics* 360 (Aug. 2000), p. 969. eprint: `astro-ph/0005480`.

As a result,

$$\frac{d}{dm}\left(\frac{dr^3}{dt}\right) = \frac{dr^3}{dm}\frac{d\ln T}{dt}. \tag{2.22}$$

Integrating assuming fixed radius at the base of the convection zone allows us to write

$$\frac{d\mathcal{V}_c}{dt} = \mathcal{V}_c\frac{d\ln T}{dt}, \tag{2.23}$$

or

$$\frac{d\ln\mathcal{V}_c}{dt} = \frac{d\ln T}{dt}, \tag{2.24}$$

where $\mathcal{V}_c$ is the volume of the convection zone. Integrating with respect to time yields

$$\Delta\ln\mathcal{V}_c = \Delta\ln T. \tag{2.25}$$

If the position of the base of the convection zone is fixed and near the core, then this reduces to

$$\Delta\ln R = \frac{1}{3}\Delta\ln T. \tag{2.26}$$

In the case of fully convective stars a fixed base is a fine assumption: ∇_{rad} is so much greater than ∇_{ad} that P_b is just the core pressure. In the case of fully radiative stars, we are likewise fine: increasing T just lowers ∇_{rad}, reinforcing the fact that $\nabla_{rad} < \nabla_{ad}$. Thus we do not expect that if $\mathcal{V}_c$ is zero for some T, it will become nonzero at a larger T. Between these two cases, we may compute the change that a temperature perturbation has on the convective-radiative boundary.

Suppose that $T(P)$ is the unperturbed state and $\delta T(P)$ is the perturbation. Then

$$\nabla_{ad} = \nabla_{rad}\left(P_b', T+\delta T\right) = \nabla_{rad}\left(P_b, T\right), \tag{2.27}$$

and so

$$\therefore \partial_P\nabla_{rad}dP_b + \partial_T\nabla_{rad}\partial_P T dP_b + \partial_T\nabla_{rad}\delta T = 0. \tag{2.28}$$

From this it follows that

$$\frac{dP_b}{dT} = -\frac{P}{T}\left(\frac{\partial_{\ln T}\nabla_{rad}}{\partial_{\ln p}\nabla_{rad} + \nabla\partial_{\ln T}\nabla_{rad}}\right) = -\frac{P}{T}\left(\frac{-3+\partial_{\ln T}\ln\kappa}{1+\nabla\left(-3+\partial_{\ln T}\ln\kappa\right)}\right). \tag{2.29}$$

As $\nabla = \nabla_{ad}$ at the transition point, this simplifies to

$$\frac{dP_b}{dT} = -\frac{P}{T}\left(\frac{-3+\partial_{\ln T}\ln\kappa}{1+\nabla_{ad}\left(-3+\partial_{\ln T}\ln\kappa\right)}\right). \tag{2.30}$$

Now $\partial_{\ln T} \ln \kappa$ (holding P fixed) at high temperature and pressure is generally around -3, and ∇_{ad} under the same conditions is usually around 0.4, so this expression is actually negative, with magnitude roughly given by $-4P/T$. Thus

$$\nabla_b \equiv -\frac{d \ln P_b}{d \ln T} \approx 4. \tag{2.31}$$

As $\ln T$ changes by the same amount everywhere in the convection zone, we may substitute T_0 for T and obtain the same result. This is consistent with what we see in the top-left and middle-left of Figure 2.3, where $\log T$ changes by one near the base of the sun's envelope and $\log P_b$ changes by five or so towards the surface.

We may now examine the behavior of the radius of the base of the convection zone. Let this radius be R_{base}, the initial temperature at P_0 be $T_{0,i}$, and the final temperature at P_0 be $T_{0,f}$. Using this, we write

$$\frac{dR_{\text{base}}}{d \ln T_0} = \frac{dR_{\text{base}}}{d \ln P_b}\frac{d \ln P_b}{d \ln T_0} = -\nabla_{ad} h_s \frac{d \ln P_f}{d \ln T_0} = \nabla_{ad} \nabla_b h_s. \tag{2.32}$$

Recalling that h_s is a function only of T, we may find h_s at the base using only knowledge of the way the temperature at the base of the convection zone changes. That is,

$$\frac{d \ln T_b}{d \ln T_0} = \left.\frac{\partial \ln T_b}{\partial \ln T_0}\right|_{P_b} + \left.\frac{\partial \ln T_b}{\partial \ln P_b}\right|_{T_0} \left.\frac{d \ln P_b}{d \ln T_0}\right|_{T_0} = 1 - \nabla_{ad}\nabla_b. \tag{2.33}$$

Thus

$$\frac{dh_s}{d \ln T_0} = h_s \left(1 - \nabla_{ad}\nabla_b\right), \tag{2.34}$$

and hence

$$h_{s,f} = h_{s,i} \left(\frac{T_{0,f}}{T_{0,i}}\right)^{1-\nabla_{ad}\nabla_b}. \tag{2.35}$$

Now the difference between $R_{i,0}$ and $Rf, 0$ is given by

$$R_{i,0} - R_{f,0} = \int_{P_0}^{P_f} \frac{dr}{dP} dP = \frac{h_{s,i}}{\nabla_{ad}} \left(1 - \left(\frac{P_{0,i}}{P_{b,i}}\right)^{\nabla}_{ad}\right), \tag{2.36}$$

so putting it all together we find

$$\frac{dR}{d\ln T_0} = \left.\frac{\partial R}{\partial \mathcal{V}_c}\right|_{R_{\rm base}} \frac{d\mathcal{V}_c}{d\ln T_0} + \frac{dR_{\rm base}}{d\ln T_0} \tag{2.37}$$

$$= \left.\frac{\partial R}{\partial \mathcal{V}_c}\right|_{R_{\rm base}} \left(\mathcal{V}_c - 4\pi R_{\rm base}^2 \frac{dR_{\rm base}}{d\ln T_0}\right) + \frac{dR_{\rm base}}{d\ln T_0} \tag{2.38}$$

$$= \frac{R}{3\mathcal{V}_c} \left(\mathcal{V}_c - 4\pi R_{\rm base}^2 \frac{dR_{\rm base}}{d\ln T_0}\right) + \frac{dR_{\rm base}}{d\ln T_0} \tag{2.39}$$

$$= \frac{R}{3} + \frac{dR_{\rm base}}{d\ln T_0}\left(1 - \frac{R_{\rm base}^2}{R^2}\right) \tag{2.40}$$

$$= \frac{R}{3} + \nabla_{ad}\left(R_{i,0} - R_{f,0}\right)\left(\frac{T_{0,f}}{T_{0,i}}\right)^{1-\nabla_{ad}\nabla_b}\left(1 - \frac{R_{\rm base}^2}{R^2}\right). \tag{2.41}$$

Past the initial small changes in temperature, the second term is negligible, so we find that we are actually justified in writing

$$\Delta \ln R = \frac{1}{3}\Delta \ln T \tag{2.42}$$

for convecting stars. To combine the cases of convection and radiation, we write

$$\Delta \ln R = \min\left(\frac{1}{12}\ln\frac{P_b}{P_0}, \frac{1}{3}\Delta \ln T\right). \tag{2.43}$$

The picture, then, is that fully radiative stars have fixed R, L_{in}, and fully convective stars have $\Delta \ln R = \frac{1}{3}\Delta \ln T$. To determine the change in L_{in} for a fully convective star, we note that nuclear burning typically scales as T^β for some $\beta > 0$. Thus we may write the energy balance in such a star as

$$4\pi R^2 \sigma T_{\rm surf,new}^4 = L_e + L_{in,old}\left(\frac{T_{\rm surf,new}}{T_{\rm surf,old}}\right)^\beta, \tag{2.44}$$

where we have made use of the fact that the surface temperature ratio between the perturbed and unperturbed cases is the same as the core temperature ratio between the two cases. Substituting in what we know for the dependence of R on T gives

$$4\pi R_{\rm old}^2 \sigma T_{\rm surf,new}^{4+2/3} T_{\rm surf,old}^{-2} = L_e + L_{i,\rm old}\left(\frac{T_{\rm surf,new}}{T_{\rm surf,old}}\right)^\beta. \tag{2.45}$$

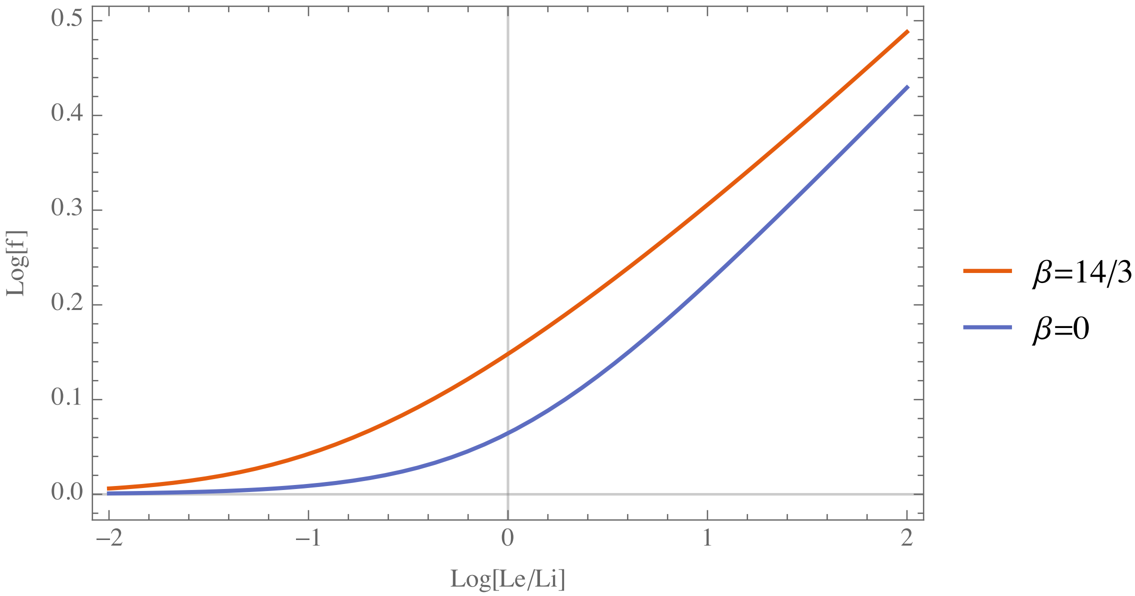

Figure 2.7: The log of f is plotted versus $\log(L_e/L_{i,\mathrm{old}})$ with $\beta = 4 + 2/3$ in orange and $\beta = 0$ in blue. These solutions were determined numerically in Mathematica.

Using $L_{i,\mathrm{old}} = 4\pi R_{\mathrm{old}}^2 \sigma T_{\mathrm{surf,old}}^4$ and letting $f \equiv T_{\mathrm{surf,new}}/T_{\mathrm{surf,old}}$, we find

$$\frac{L_e}{L_{i,old}} = f^{4+2/3} - f^{\beta}. \tag{2.46}$$

Fully convective stars tend to be cooler ones, for which $\beta \approx 4$, so we may numerically solve this for a variety of cases. The results of this are shown in orange in figure 2.7. Note that when the impact on nuclear burning is included in the solution, the result exceeds what we would otherwise find. This aligns with our intuition that heating the star causes it to burn faster, which causes it to heat more. The trend is close to linear, past $L_e = L_{i,\mathrm{old}}$, with a slope of roughly $1/6$, so loosely speaking $T \propto L_e^{1/6}$, $R \propto L_e^{1/6}$, and $L_{in} \propto L_e^{2/3}$. In the case that the convection zone goes deep into the star but does not reach near the nuclear burning region, we expect instead that L_{in} will be constant and that $R \propto T \propto (L_e + L_{in})^{3/14}$, as plotted in blue in figure 2.7.

Note that if $\beta > 14/3$ then Eq. (2.46) has no solutions. This reflects the fact that in such a system, heating the star causes the nuclear burning rate to go up faster than the surface flux can accommodate, further heating the star. The end of such a process occurs by weakening the coupling between the surface and the core of the star by turning off convection in the vicinity of the core. Further note that if the star is not heated by nuclear burning, the only thermodynamically allowed equilibrium has the external illumination only stemming the loss of heat, not raising the temperature.

It appears, in summary, that the only stars which will respond to the external illumination by swelling are those which are nuclear burning and mostly convective, and that the response is greatest in those which are convective all the way down to the nuclear burning regions. In these, the swelling is increased by the fact that the nuclear burning increases in extent to match the hotter core temperatures.

In the next several chapters we will move to higher-dimensional models and perform the same kind of analysis to determine what, if any, impact the anisotropy in the external heating has, and how this impact depends on the parameters of the system.

References

Ferguson, Jason W. et al. "Low-Temperature Opacities". In: *The Astrophysical Journal* 623.1 (2005), p. 585. URL: http://stacks.iop.org/0004-637X/623/i=1/a=585 (cit. on p. 18).

Feynman, Richard P. *Los Alamos From Below*. https://www.youtube.com/watch?v=OogSC6JKkrY. Feb. 6, 1975. URL: http://calteches.library.caltech.edu/34/3/FeynmanLosAlamos.htm (cit. on p. 14).

Iglesias, C. A. and F. J. Rogers. "Updated Opal Opacities". In: *The Astrophysical Journal* 464 (June 1996), p. 943. DOI: 10.1086/177381 (cit. on p. 18).

Paczyński, B. "Envelopes of Red Supergiants". In: *Acta Astronomica* 19 (1969), p. 1 (cit. on pp. 16–18, 25).

Paxton, Bill et al. "Modules for Experiments in Stellar Astrophysics (MESA): Planets, Oscillations, Rotation, and Massive Stars". In: *The Astrophysical Journal Supplement Series* 208.1 (2013), p. 4. URL: http://stacks.iop.org/0067-0049/208/i=1/a=4 (cit. on p. 28).

Ritter, H., Z.-Y. Zhang, and U. Kolb. "Irradiation and mass transfer in low-mass compact binaries". In: *Astronomy and Astrophysics* 360 (Aug. 2000), p. 969. eprint: astro-ph/0005480 (cit. on p. 29).

Salaris, Maurizio and Cassisi Santi. *Evolution of stars and stellar populations*. Vol. 1. ISBN: 0-470-09220-3. John Wiley Sons, 2005, pp. 138–140 (cit. on p. 28).

3

Higher Dimensional Models

All of the analysis thus far has been one dimensional. We now describe a framework for computing higher dimensional steady state effects in certain limits. Recall that in hydrostatic equilibrium,

$$\boldsymbol{\nabla} p = \rho \left(\boldsymbol{c} - \boldsymbol{g} \right), \tag{3.1}$$

where $\boldsymbol{c}$ captures all rotational acceleration effects. We also have that in steady state and without any input heating or winds, the thermal flux obeys

$$\boldsymbol{\nabla} \cdot \boldsymbol{F} = 0. \tag{3.2}$$

In the presence of an input heat power density ε, this changes to

$$\boldsymbol{\nabla} \cdot \boldsymbol{F} = \varepsilon. \tag{3.3}$$

The boundary condition on this equation at the star's edge is a free one, with the flux at $r = \infty$ dropping to zero. This results from the thermal flux proceeding out of the star at the photosphere with no reflection. The star's photospheric temperature is determined by

$$\sigma T^4 = \boldsymbol{F} \cdot \hat{n} \tag{3.4}$$

at the photosphere's base, usually defined as the point where $\tau = 2/3$. Finally, if winds are introduced, the flux divergence becomes[1]

$$\boldsymbol{\nabla} \cdot \boldsymbol{F} = \varepsilon - c_p T \boldsymbol{v} \cdot \left(\boldsymbol{\nabla} \ln T - \nabla_{ad} \boldsymbol{\nabla} \ln p \right). \tag{3.5}$$

[1]Rudolf Kippenhahn, Alfred Weigert, and Achim Weiss. *Stellar Structure and Evolution*. Springer, 2012. ISBN: 978-3-642-30304-3.

Note that $\boldsymbol{F}$ includes convective and radiative effects only. Further note that ε must include the effects of viscous dissipation on the winds in order for this formalism to be self-consistent.

In general, we expect that we may write the thermal flux in terms of the temperature distribution as

$$\boldsymbol{F} = -k\boldsymbol{\nabla}T, \tag{3.6}$$

where k may depend on the temperature, the pressure, and the gradients thereof. Note that this holds even for convective flux, though in the case of convection the thermal conductivity will be a rank two tensor, reflecting the potentially anisotropic nature of the thermal diffusion supported by convection. It is tempting to argue that this anisotropy may be handled by superposing an advective flow on top of the underlying convection cell, and this is mathematically a valid option, but it leads to multiple different advective terms of distinct physical origin, which is not an appealing solution. Thus we will not hide from the complexity of anisotropic thermal conduction by convection. Generally speaking the convective conductivity along $\boldsymbol{\nabla}p$ will be given by the usual expression, but with ∇ computed taking into account the angle α of misalignment between the temperature and pressure gradients. More formally, ∇ may be defined in this context as

$$\nabla \equiv \frac{\partial \ln T}{\partial \ln p}, \tag{3.7}$$

where the partial derivatives are taken following the pressure gradient. The transverse components of the convective conductivity are then given by the transverse size of the convection cell, as will be discussed in a later chapter. Qualitatively, everything else remains the same for the convective aspect of the flow[2].

In the case where k is a nontrivial tensor, it is not generally possible to avoid using T as an intermediate result. Having said this, there are several things we can determine which at least constrain the form of k. First, k must be invertible, as the null space of k must consist solely of the trivial vector, or else arbitrary temperature gradients along a given axis could result in no flux. Additionally, when $\boldsymbol{\nabla}T$ and $\boldsymbol{\nabla}p$ align, the flux is entirely along the preferred direction this picks out. Similarly, if $\boldsymbol{\nabla}T$ is perpendicular to $\boldsymbol{\nabla}p$, the flux is entirely along $\boldsymbol{\nabla}T$. Thus k must be diagonal in

[2]Pierre Lesaffre et al. "A two-dimensional mixing length theory of convective transport". In: *Monthly Notices of the Royal Astronomical Society* (2013). DOI: `10.1093/mnras/stt317`. eprint: `http://mnras.oxfordjournals.org/content/early/2013/03/20/mnras.stt317.full.pdf+html`. URL: `http://mnras.oxfordjournals.org/content/early/2013/03/20/mnras.stt317.abstract`.

any orthonormal basis which has one basis element parallel to the pressure gradient. In this basis, k^{-1} is just the element-wise reciprocal of k along the diagonal.

In the case where k may vary spatially and is a scalar, $\boldsymbol{\nabla} \times \boldsymbol{F}$ may be nonzero. In particular,

$$\boldsymbol{\nabla} \times \boldsymbol{F} = -k\boldsymbol{\nabla} \times \boldsymbol{\nabla} T - \boldsymbol{\nabla} k \times \boldsymbol{\nabla} T = -\boldsymbol{\nabla} k \times \boldsymbol{\nabla} T = \boldsymbol{\nabla} \ln k \times \boldsymbol{F}, \tag{3.8}$$

which allows $\boldsymbol{F}$ to be computed without computing T as an intermediate result, so long as the functional form of k is known.

In general, a vector field may be written as the sum of a field with zero curl and a field with zero divergence. Suppose that

$$\boldsymbol{\nabla} \cdot \boldsymbol{G} = 0 \tag{3.9}$$

and

$$\boldsymbol{\nabla} \times \boldsymbol{H} = 0. \tag{3.10}$$

Then we write

$$\boldsymbol{F} = \boldsymbol{G} + \boldsymbol{H}. \tag{3.11}$$

Thus all said we have, in the special case where k is a scalar,

$$\boldsymbol{\nabla} \cdot \boldsymbol{H} = \varepsilon \tag{3.12}$$

$$\boldsymbol{\nabla} \times \boldsymbol{H} = 0 \tag{3.13}$$

$$\boldsymbol{\nabla} \cdot \boldsymbol{G} = 0 \tag{3.14}$$

$$(\boldsymbol{\nabla} - \boldsymbol{\nabla} \ln k) \times \boldsymbol{G} = \boldsymbol{\nabla} \ln k \times \boldsymbol{H}. \tag{3.15}$$

The solution for $\boldsymbol{H}$ is given by the familiar electrostatics Green's function as

$$\boldsymbol{H}(\boldsymbol{r}) = \int d^3\boldsymbol{r'} \frac{\varepsilon(\boldsymbol{r'})(\boldsymbol{r} - \boldsymbol{r'})}{4\pi \left|\boldsymbol{r} - \boldsymbol{r'}\right|^3}. \tag{3.16}$$

In the case where winds are important, the appropriate substitution of must be made to incorporate them into Eq. (3.16). Given k, then, this serves as the source term which determines $\boldsymbol{G}$.

There are several options to complete the solution given k. One is to directly invert the differential operator acting on $\boldsymbol{G}$. This may be done, for instance, via eigenfunction expansion into either a plane wave basis or a vector spherical harmonic basis. Another solution involves numerical inversion of the differential operator over a spatial grid. Direct exact solutions, however, are of limited utility due to the fact that k is ultimately a nonlinear and non-local function of $\boldsymbol{F}$. Even if this were not the case for k, it would still be the case for the wind distribution. As a result, once a 'good-enough' approximation of the flux is obtained, k and the wind distribution should be recomputed to allow for further refinement of $\boldsymbol{F}$. It follows that an iterative (perturbative) or quickly-converging eigenfunction expansion solution is preferred.

Suppose that k (scalar or tensor) is known as a function of T, ∇T, p, and ∇p. If, additionally, the boundary of the star is a known surface $\partial\Omega$ with normal vector $\hat{n}$, then we may determine the temperature and pressure analogously to how Gob or other atmospheric integration codes handle it. That is, we may first set ρ and p in accordance with standard photospheric prescriptions on $\partial\Omega$. The temperature is set by Eq. (3.4). Given an estimate of $\boldsymbol{F}$, Eq. (3.6) may be combined with the hydrostatic equilibrium condition Eq. (3.1) to integrate the pressure and temperature inward, recomputing the density at each stage. Using the new state of the star, k may be recomputed and used to form a new estimate of $\boldsymbol{F}$.

As an example of an iterative method for determining the flux, let $\boldsymbol{G}_0$ be the solution to

$$\nabla \times \boldsymbol{G}_0 = \nabla \ln k \times \boldsymbol{H}$$

and letting $\boldsymbol{G}_n$ be the solution to

$$\nabla \times \boldsymbol{G}_n = \nabla \ln k \times \boldsymbol{G}_{n-1},$$

given by treating the right side as the source current for a Biot-Savart-like law. The full solution may then be written as

$$\boldsymbol{G} = \sum_{n=0}^{\infty} G_n. \tag{3.17}$$

Of course the convergence of this series is not guaranteed. In fact, as we will show later, this series will generally not converge, so eigenfunction expansion is a more promising route. The case may be improved by alternating iterations of this series method with iterations of recomputing k, as this minimizes the distance that the solution moves from self-consistency in any step, but ultimately other methods will prove preferable.

3.1 Zero-Wind Analytic Model

Before doing anything as involved as the above process, it is worth extracting as much information as possible analytically. As a toy model, suppose that k is a scalar function of just T and p, and is a power-law thereof, such that

$$k = wT^a P^b. \tag{3.18}$$

The former assumption amounts to specifying that we are in the radiative zone, while the latter amounts to specifying that we don't cross between regions with substantively different power laws. This is actually not very constraining, as may be seen in figure 2.1. Furthermore, suppose that we neglect all wind effects. In later sections we will remove this assumption.

Take the external heating to be put in at a point, which by choice of axis we set to be at $\boldsymbol{r}_h = r_h \hat{z}$. Eq. (3.16) then gives

$$\boldsymbol{H}(\boldsymbol{r}) = \frac{1}{4\pi}\left(\frac{L_i \hat{r}}{r^2} + \frac{L_e(\boldsymbol{r}-\boldsymbol{r}_h)}{|\boldsymbol{r}-\boldsymbol{r}_h|^3}\right). \tag{3.19}$$

The source term leading to $\boldsymbol{G}_0$ is then

$$\boldsymbol{\nabla} \ln k \times \boldsymbol{H} = (a\boldsymbol{\nabla} \ln T + b\boldsymbol{\nabla} \ln p) \times \boldsymbol{H}. \tag{3.20}$$

To leading order, $\boldsymbol{\nabla} T$ is parallel to $\boldsymbol{H}$ (treating $\boldsymbol{G}_0$ as a perturbation), so

$$\boldsymbol{\nabla} \ln k \times \boldsymbol{H} = b\boldsymbol{\nabla} \ln p \times \boldsymbol{H} = \frac{b}{h_s}\hat{g} \times \boldsymbol{H}. \tag{3.21}$$

Rotational effects are a perturbation on $\hat{g}$ so we take $\hat{g}$ to be $-\hat{r}$. As a result,

$$\boldsymbol{\nabla} \ln k \times \boldsymbol{H} = -\frac{b}{h_s}\hat{r} \times \frac{1}{4\pi}\left(\frac{L_i \hat{r}}{r^2} + \frac{L_e(\boldsymbol{r}-\boldsymbol{r}_h)}{|\boldsymbol{r}-\boldsymbol{r}_h|^3}\right) = \frac{bL_e \hat{r} \times \boldsymbol{r}_h}{4\pi h_s |\boldsymbol{r}-\boldsymbol{r}_h|^3} = \frac{-br_h L_e \hat{\phi}}{4\pi h_s |\boldsymbol{r}-\boldsymbol{r}_h|^3}. \tag{3.22}$$

3.1.1 Iterative Method

Now suppose we adopt the iterative scheme described earlier. Then

$$\boldsymbol{\nabla} \times \boldsymbol{G}_0 = -\frac{br_h L_e \hat{\phi}}{4\pi h_s |\boldsymbol{r}-\boldsymbol{r}_h|^3}, \tag{3.23}$$

where the scale height is to be evaluated at the sample place as the curl, given by $\boldsymbol{r}$. Outside of the star this quantity diverges, and so the curl of $\boldsymbol{G}_0$ becomes zero. Note that the nonzero circulating flux outside of the star is not unphysical, though the representation of the flux in this manner is somewhat nonstandard. For a simple example, consider a planar light emitter which emits collimated light normal to its surface, with flux which varies along the plane. The curl of the flux field above this surface is evidently nonzero.

From symmetry considerations it is evident that $\boldsymbol{G}_0$ describes a circulating flux between the heating point and the opposing point on the star. The net flux transported due to all $\boldsymbol{G}$ terms is zero due to their uniformly vanishing divergences. The primary effect of these flux loops then is to change the distribution of heat in the interior. In particular, suppose that $b \geq 0$[3]. The circulating flux lines then proceed toward the point $\boldsymbol{r}_h$ outside the star and away from it within the star.

We may compute the net flux which is transported from one side to the other within the star. To do so, first note that $\boldsymbol{G}_0$ may be written as a curl of another vector field due to its vanishing divergence. This vector field may be written as

$$\boldsymbol{A}_0(\boldsymbol{r}) = \int d^3\boldsymbol{r}' \frac{\boldsymbol{\nabla} \times \boldsymbol{G}_0}{4\pi \left|\boldsymbol{r} - \boldsymbol{r}'\right|} = \int d^3\boldsymbol{r}' \frac{-b r_h L_e \hat{\phi}}{(4\pi)^2 h_s \left|\boldsymbol{r} - \boldsymbol{r}_h\right|^3 \left|\boldsymbol{r} - \boldsymbol{r}'\right|}. \tag{3.24}$$

From symmetry considerations we know that this will go along $-\hat{\phi}$ at $\boldsymbol{r}$. The magnitude will be dominated by contributions near $\boldsymbol{r}_h$, and so may be estimated as

$$A_0 \approx \frac{b r_h L_e}{(4\pi)^2 h_s \left|\boldsymbol{r} - \boldsymbol{r}_h\right|} \tag{3.25}$$

up to corrections of order unity given roughly by the log of the ratio of $r - r_h$ to the size of the heating region, which in practice will be finite. Note that the scale height here is that at $\boldsymbol{r}_h$. The integrated flux through the star is therefore

$$L_{int} = -\int d^2\boldsymbol{r} \hat{z} \cdot \boldsymbol{G}_0 = -\int_0^{2\pi} d\phi r \boldsymbol{A}_0 \cdot \hat{\phi} = \frac{2\pi r b r_h L_e}{(4\pi)^2 h_s \sqrt{r^2 + r_h^2}}. \tag{3.26}$$

In general we expect $r_h \approx r$ so

$$L_{int} \approx \frac{rb}{8\sqrt{2}\pi h_s} L_e. \tag{3.27}$$

In general, $h_s \ll r$ and b is of order unity, so this significantly exceeds the input luminosity, and indeed indicates that the circulating flux significantly exceeds the conservative flux $\boldsymbol{H}$. This indicates that the curl operator has eigenvalues which are typically much less than those of the $\boldsymbol{\nabla} \ln k \times$ operator, invalidating an iterative method of this form. This result is more general than the specific form of k used. To see this, suppose we let b depend on P and T. None of the above results change so long as $|br/h_s| \gg 1$, for we only relied on local properties of b until performing

[3]This will generally be true, as can be seen by noting that at fixed T, $\rho \propto P$, and by examining figure 2.1. Note that $k \propto \kappa P$.

integration, and in the integration procedure all symmetry constraints remain because b reflects the underlying symmetry in T and P. As a result, all that changes is that the integration replaces b with some weighted average of its value over the star at r_h, which cannot produce values orders of magnitude smaller than unity, given that b undergoes no sign changes and is typically of order unity at the densities of interest. Intuitively this result concerning the eigenvalues of $\boldsymbol{\nabla} \ln k \times$ arises because all material properties of the star change on scales on the order of a pressure scale height, while flux variations have a characteristic scale which goes as the stellar radius.

3.1.2 Eigenfunction Expansion

Having demonstrated that a straightforward iterative series expansion is invalid for this kind of problem, we now turn to eigenfunction expansion. The most convenient basis for doing this is that of vector spherical harmonics. These are defined as

$$\boldsymbol{Y}_{lm} = \hat{r} Y_{lm} \tag{3.28}$$

$$\boldsymbol{\Psi}_{lm} = r \boldsymbol{\nabla} Y_{lm} \tag{3.29}$$

$$\boldsymbol{\Phi}_{lm} = \boldsymbol{r} \times \boldsymbol{\nabla} Y_{lm}, \tag{3.30}$$

where the gradient operators are constrained to the surface of the unit sphere, Y_{lm} are the usual scalar spherical harmonics, and $-l \leq m \leq l$ as usual. These operators are mutually orthogonal, and their norms are 1, $l(l+1)$, and $l(l+1)$ respectively. Given a field $\boldsymbol{A}$, we may write

$$\begin{aligned}
\boldsymbol{A} &= \sum_{l=0}^{\infty} \sum_{m=-l}^{l} A_{lm,1} \boldsymbol{Y}_{lm} + A_{lm,2} \boldsymbol{\Psi}_{lm} + A_{lm,3} \boldsymbol{\Phi}_{lm}, \\
\boldsymbol{\nabla} \times \boldsymbol{A} &= \sum_{l=0}^{\infty} \sum_{m=-l}^{l} -\frac{l(l+1)}{r} A_{lm,3} \boldsymbol{Y}_{lm} - \left(\partial_r + \frac{1}{r} \right) A_{lm,3} \boldsymbol{\Psi}_{lm} \\
&\quad + \left(-\frac{A_{lm,1}}{r} + \left(\partial_r + \frac{1}{r} \right) A_{lm,2} \right) \boldsymbol{\Phi}_{lm}, \\
\hat{r} \times \boldsymbol{A} &= \sum_{l=0}^{\infty} \sum_{m=-l}^{l} -A_{lm,3} \boldsymbol{\Psi}_{lm} + A_{lm,2} \boldsymbol{\Phi}_{lm}, \\
\boldsymbol{\nabla} \cdot \boldsymbol{A} &= \sum_{l=0}^{\infty} \sum_{m=-l}^{l} \left(\partial_r A_{lm,1} + \frac{2}{r} A_{lm,1} - \frac{l(l+1)}{r} A_{lm,2} \right) Y_{lm}.
\end{aligned} \tag{3.31}$$

Note that the coefficients in these expansions are all functions just of r. Expanding both $\boldsymbol{H}$ and $\boldsymbol{G}$ in this manner yields

$$\begin{aligned}\left(\boldsymbol{\nabla}+\frac{\hat{r}b}{h_s}\right)\times\boldsymbol{G} &= \sum_{l=0}^{\infty}\sum_{m=-l}^{l} -\frac{l(l+1)}{r}G_{lm,3}\boldsymbol{Y}_{lm} - \left(\partial_r+\frac{1}{r}+\frac{b}{h_s}\right)G_{lm,3}\boldsymbol{\Psi}_{lm} \\ &\quad + \left(-\frac{G_{lm,1}}{r}+\left(\partial_r+\frac{1}{r}+\frac{b}{h_s}\right)G_{lm,2}\right)\boldsymbol{\Phi}_{lm} \\ &= -\frac{b}{h_s}\sum_{l=0}^{\infty}\sum_{m=-l}^{l} -H_{lm,3}\boldsymbol{\Psi}_{lm}+H_{lm,2}\boldsymbol{\Phi}_{lm}.\end{aligned} \tag{3.32}$$

Note that $\boldsymbol{\nabla}\times\boldsymbol{H}=0$ implies that $H_{lm,3}=0$. The orthogonality of the vector spherical harmonics, combined with the divergence-free nature of $\boldsymbol{G}$, then allows us to write

$$-\frac{l(l+1)}{r}G_{lm,3}=0 \tag{3.33}$$

$$-\left(\partial_r+\frac{1}{r}-\frac{b}{h_s}\right)G_{lm,3}=0 \tag{3.34}$$

$$\left(\partial_r+\frac{1}{r}-\frac{b}{h_s}\right)G_{lm,2}-\frac{G_{lm,1}}{r}=-\frac{b}{h_s}H_{lm,2} \tag{3.35}$$

$$\partial_r G_{lm,1}+\frac{2}{r}G_{lm,1}-\frac{l(l+1)}{r}G_{lm,2}=0. \tag{3.36}$$

The first condition gives us $G_{lm,3}=0$. The second condition is then trivially satisfied. The third and fourth conditions must be combined to obtain a solution. Using the fourth to obtain the second coefficient, we write

$$\left(\partial_r+\frac{1}{r}-\frac{b}{h_s}\right)\left[\frac{r}{l(l+1)}\left(\partial_r G_{lm,1}+\frac{2}{r}G_{lm,1}\right)\right]-\frac{G_{lm,1}}{r}=-\frac{b}{h_s}H_{lm,2}. \tag{3.37}$$

Once a solution to this is known, the value of $G_{lm,2}$ may be computed directly.

The differential equation of interest may be solved numerically without much difficulty, given H_{lm}, but for the purposes of our rough calculations suppose we insist that $G_{lm,1}$ changes with characteristic scale of order the stellar radius. This amounts to insisting that ∂_r has eigenvalues of order $1/r$. Given that $h_s \ll r$ we may write

$$-\frac{b}{h_s}\left(\frac{r}{l(l+1)}\partial_r G_{lm,1}+\frac{2}{l(l+1)}G_{lm,1}\right)=-\frac{b}{h_s}H_{lm,2}, \tag{3.38}$$

or

$$\frac{r}{l(l+1)}\partial_r G_{lm,1} + \frac{2}{l(l+1)} G_{lm,1} = H_{lm,2}. \tag{3.39}$$

To simplify matters somewhat, we consider a modified version of the input heating considered earlier. In this case, the input heat takes on the form

$$\varepsilon = \frac{\delta(r-r_h)}{4\pi r_h^2}\left[L_{e,0}Y_{00} + L_{e,1}\left(Y_{1,-1} - Y_{1,1}\right)\right]. \tag{3.40}$$

This qualitatively reproduces the expected heating behavior, with preferential heating on one side but without any net cooling, so long as $L_{e,0} > \sqrt{6}L_{e,1}$. The heating all occurs at a radius r_h, with maximum heating on the positive $\hat{x}$ side. The source term $\boldsymbol{\nabla} \ln k \times \boldsymbol{H}$ is not impacted in any way by the $Y_{0,0}$ term, as this term produces a radial flux field. The remaining terms give rise to a flux field which contributes to the source term. The equations governing this field are given by

$$\partial_r H_{1,\pm1,1} + \frac{2}{r} H_{1,\pm1,1} - \frac{2}{r} H_{1,\pm1,2} = \frac{\delta(r-r_h)}{4\pi r_h^2}\left(\mp L_{e,1}\right), \tag{3.41}$$

$$H_{1,\pm1,3} = 0 \tag{3.42}$$

$$-\frac{H_{1,\pm1,1}}{r} + \left(\partial_r + \frac{1}{r}\right) H_{1,\pm1,2} = 0. \tag{3.43}$$

The first of these relations arises from the divergence condition $\boldsymbol{H}$, while the second two arise from the requirement that the curl of $\boldsymbol{H}$ vanish. The general solution to this set of equations is

$$H_{1,\pm1,1} = \frac{A}{r^3} + B + \frac{\mp L_{e,1}(r^3 + 2r_h^3)\Theta(r-r_h)}{12\pi r^3 r_h^2} \tag{3.44}$$

$$H_{1,\pm1,2} = -\frac{A}{2r^3} + B + \frac{\mp L_{e,1}(r^3 - r_h^3)\Theta(r-r_h)}{12\pi r^3 r_h^2} \tag{3.45}$$

$$H_{1,\pm1,3} = 0, \tag{3.46}$$

where $\Theta(x)$ is the Heaviside step function and the constants A and B are to be fixed by boundary condition considerations. In this case, we want the flux to drop to zero at infinity, and we want it to be finite at finite radius. As a result, both constants are zero and we have

$$H_{1,\pm1,1} = \frac{\mp L_{e,1}(r^3 + 2r_h^3)\Theta(r-r_h)}{12\pi r^3 r_h^2} \tag{3.47}$$

$$H_{1,\pm1,2} = \frac{\mp L_{e,1}(r^3 - r_h^3)\Theta(r-r_h)}{12\pi r^3 r_h^2} \tag{3.48}$$

$$H_{1,\pm1,3} = 0. \tag{3.49}$$

Using this to solve for $G_{1,\pm1,1}$ in the simplified differential equation gives

$$G_{1,\pm1,1} = \frac{\mp L_{e,1}(r-r_h)^2(r+2r_h)\Theta(r-r_h)}{12\pi r^3 r_h^2}, \tag{3.50}$$

where we have already imposed the condition that this converge at the origin. To obtain the flux from one side of the star to the other from this, we note that $G_{lm,1}$ doesn't contribute to the flux through a slice of the star which cuts it in half. The only such contribution arises from the angular terms. We already know that $G_{lm,3} = 0$, so we just need to compute $G_{lm,2}$. This may be done as described previously, yielding

$$G_{1,\pm1,2} = \frac{\mp L_{e,1}}{12\pi r^2 r_h^2}\left(\frac{(r-r_h)^2(r+2r_h)\delta(r-r_h)}{2} + \frac{(r^3-r_h^3)\Theta(r-r_h)}{r}\right). \tag{3.51}$$

Only the portion of the vector field directed along $\hat{\phi}$ contributes to the flux through the plane separating the two halves of the star, and this is given by

$$G_{\pm\phi} = \pm\sqrt{\frac{3}{2\pi}}\frac{L_{e,1}}{12\pi r^2 r_h^2}\left(\frac{(r-r_h)^2(r+2r_h)\delta(r-r_h)}{2} + \frac{(r^3-r_h^3)\Theta(r-r_h)}{r}\right), \tag{3.52}$$

where we have set $\phi = \pi/2$. Integrating this over the plane of interest then yields

$$L = \int_0^R dr \int_0^{\pi/2} d(\cos\theta) r(G_\phi - G_{-\phi}) = 4\int_0^R rG_\phi = \frac{(R-r_h)^2(R+2r_h)}{2\sqrt{6}\pi^{3/2}Rr_h^2}L_{e,1}, \tag{3.53}$$

where R is the stellar radius and L is the total power flowing from one side of the star to the other as a result of the circulation field. In typical situations, $R - r_h \ll R$, so

$$L \approx L_{e,1}\frac{1}{20}\left(1 - \frac{r_h}{R}\right)^2. \tag{3.54}$$

By comparison, the flux due to the curl-free term is given by the incident flux times the ratio of the solid angle that the plane of interest sweeps as seen from the heating point, which is roughly $2\pi/3$, to the total solid angle of 4π, so in most cases this term dominates over the circulation term. One important consequence of Eq. (3.54) is that as the heat is deposited deeper, the flux which manages to find its way to the opposing side increases as expected.

Interestingly, this result is independent of a, b. So long as they do not vary substantially on a spherical shell, this independence should hold. Additionally, note that the situation in any case is very different from that of an isotropic star, wherein half of the heating flux is present on each side. This is a result of the fact that a spherically symmetric shell of heating cannot alter the flux inside it, while an anisotropic heating shell can.

It is worth noting two effects which we have not considered here. The first is the potential for a more complex thermal conductivity structure due to convection, and the second is that of wind transport/dissipation. In the case of the former, the key effect will be the potential for significantly greater conductivity gradients misaligned with the thermal gradient. In the case of the latter, the key effect will be additional heating terms, manifesting as regions of nonzero ε, even when no heating is present at those locations. Finally, rotation plays a role in determining how these complications alter the situation. Estimating the significance of these effects is the subject of subsequent sections.

3.2 Zero-Divergence Wind Model

Suppose that we insist that the flux divergence be made zero by wind transport. This represents the opposite limit of the previous section solution. This condition means that we require

$$\varepsilon = c_p T \boldsymbol{v} \cdot \left(\boldsymbol{\nabla} \ln T - \nabla_{ad} \boldsymbol{\nabla} \ln p \right). \tag{3.55}$$

Recall that $c_p = \gamma c_v$ and that up to factors of order unity $c_v = k_B T/\mu$, so

$$\varepsilon = \gamma p \boldsymbol{v} \cdot \left(\boldsymbol{\nabla} \ln T - \nabla_{ad} \boldsymbol{\nabla} \ln p \right). \tag{3.56}$$

This relation would be precisely correct if we neglected convection in computing $\boldsymbol{F}$. This is not how we are treating the heat flux, however, so we need to correct this relation by subtracting out the convective term. The convective term arises from gas traveling in a circulatory fashion up and down a pressure gradient. As a result, this subtraction may be done by requiring $\boldsymbol{v} \perp \boldsymbol{\nabla} p$. This is essentially the geostrophic flow condition. One might object to this requirement by citing Kelvin-Helmholtz instability, but such processes separate in our treatment to convection and advection, as in a convective roll. Likewise one might object to this requirement by arguing that winds can move along pressure gradients in radiative regions. While this is true, such winds cannot be driven by thermal processes, as the region must, by definition, be stable against convection. Objections case aside, we impose this requirement, and the criterion reduces to

$$\varepsilon = \gamma p \boldsymbol{v} \cdot \boldsymbol{\nabla} \ln T \sim \frac{\Sigma g}{h_s} \boldsymbol{v} \cdot \hat{e}_T, \tag{3.57}$$

where $\hat{e}_T$ is the unit vector along the thermal gradient. The approximate form comes from noting that if the flux has zero divergence except in the core, then the thermal gradient must be purely radial. Now we know that neglecting viscous losses,

$$\varepsilon \approx \frac{L_e}{2\pi R^2}\left[1-\exp\left(-\Sigma/\Sigma_h\right)\right], \tag{3.58}$$

where we are taking the illumination to occur on one side only. As a result,

$$\boldsymbol{v}\cdot\hat{e}_T \approx \frac{L_e h_s}{2\pi g \Sigma R^2}\left[1-\exp\left(-\Sigma/\Sigma_h\right)\right]. \tag{3.59}$$

Usually $R \sim 10^{10}$cm, $h_s \sim 10^7$cm, $g \sim 10^4$cm/s^2, $L_e \sim 10^{33}$erg/s, and $\Sigma_h = 10^3$g/cm^2, so this has a maximum value of

$$\boldsymbol{v}\cdot\hat{e}_T \sim 10^{12}\text{cm/s}. \tag{3.60}$$

This is an absurd value, greater than the speed of light, and indicates a breakdown in the assumption that the divergence of the flux remains zero. In particular, it arises from the characteristic scale over which T changes in the absence of a flux divergence being much greater than the characteristic scale over which ε changes. As the wind clearly cannot move enough heat to keep the divergence at zero, the temperature profile will shift to accommodate the shorter length scale.

Evidently the true steady state, if one exists, lies somewhere in between the two models considered thus far. The star likely adjusts its radial transport to handle much of the flux divergence, and then sets up some non-radial flux transport, which then allows the wind to move non-radially to dissipate some of the flux divergence. As a result, the star must exhibit some anisotropy, but it is possible that below a certain depth winds succeed in isotropizing the thermal structure. This model will serve as a template for subsequent analyses.

References

Kippenhahn, Rudolf, Alfred Weigert, and Achim Weiss. *Stellar Structure and Evolution*. Springer, 2012. ISBN: 978-3-642-30304-3 (cit. on p. 36).

Lesaffre, Pierre et al. "A two-dimensional mixing length theory of convective transport". In: *Monthly Notices of the Royal Astronomical Society* (2013). DOI: 10.1093/mnras/stt317. eprint: http://mnras.oxfordjournals.org/content/early/2013/03/20/mnras.stt317.full.pdf+html. URL: http://mnras.oxfordjournals.org/content/early/2013/03/20/mnras.stt317.abstract (cit. on p. 37).

4

Review of Fluid Mechanics

Big whirls have little whirls that feed on their velocity,
and little whirls have lesser whirls and so on to viscosity.
– Lewis Fry Richardson

To understand how wind flow works in stars, it is worth reviewing the basic fluid mechanics involved. In general, fluid mechanics problems are exceedingly difficult to solve, either analytically or numerically. As a result, we will exploit the fact that such problems may often be broadly characterized by only a few dimensionless numbers. This reduces the complexity of the problems, and allows us to reduce many scenarios to the same mathematics. Before discussing these numbers, however, we must address a dimensionful property of fluids: viscosity.

4.1 Microscopic Viscosity

Intuitively viscosity is a measure of the resistance of a fluid to shearing. The term usually refers to a material property, rather than a property of fluid flow. As both notions are important, viscosity as a material property and viscosity as a property of fluid flow, we will use "microscopic viscosity" to denote the material property and "turbulent viscosity" or "effective viscosity" to denote the flow property. The latter will be discussed at length later in this chapter, while here we will focus on the former.

In this analysis, we take the companion stars of interest to be primarily hydrogen, with some helium present in small quantities. At temperatures higher than those in the ionization zone, in the regime where $\mu = \frac{1}{2}m_p$, the Spitzer estimate gives the microscopic viscosity as[1]

$$\nu = 5.2 \times 10^{-15} \frac{T^{5/2}}{\rho \ln \Lambda} \frac{\mathrm{cm}^2}{\mathrm{s}}, \tag{4.1}$$

where T is made dimensionless by dividing out by K, and likewise for ρ by dividing out by g/cm^3. The quantity $\ln \Lambda$ is given by[2]

$$\ln \Lambda = \begin{cases} -17.4 + 1.5 \ln T - 0.5 \ln \rho & T < 1.1 \times 10^5 \mathrm{K} \\ -12.7 + \ln T - 0.5 \ln \rho & T > 1.1 \times 10^5 \mathrm{K} \end{cases}, \tag{4.2}$$

where everything is in the same units as before.

To obtain a broader range of microscopic viscosities, we turn to tables of this value at various temperatures and pressures[3]. The results, computed for a mixture of 85% hydrogen and 15% helium, indicate that $\rho\nu$ is roughly constant, ranging from 3×10^6g/cm/s to 3×10^7g/cm/s. The tabulated data allows us to compute ν for temperatures ranging from 3600K up to 10^5K, and pressures ranging from 10^3erg/cm^3 up to 10^{11}erg/cm^3. Between this and the Spitzer estimate, then, we have covered the entire range of interest for stellar atmospheres except for very low temperatures in the outer regions of brown dwarfs. These regions, however, are not of much interest, as the transport phenomena of interest occur much deeper in the star. Furthermore, unlike the case for opacity, the underlying physics behind microscopic viscosities is not expected to change significantly at these lower temperatures. Thus reasonable extensions of the low-temperature viscosity model may be used, with the understanding that they are only accurate as order-of-magnitude estimates.

Next we consider the viscosity of radiation, which was not included in either the data table nor the Spitzer estimate. The radiative viscosity is given by[4]

$$\nu_{rad} = \frac{aT^4}{c\kappa\rho}. \tag{4.3}$$

This is usually much smaller even than the microscopic viscosity of hydrogen. To see this, we may non-dimensionalize T, κ, and ρ and evaluate the constant factors to find

$$\nu_{rad} \approx 3 \times 10^{-5} T_5^4 \rho_0^{-1} \kappa_0^{-1} \frac{\mathrm{cm}^2}{\mathrm{s}}, \tag{4.4}$$

[1] Daniel Kagan and J. Craig Wheeler. "The Role of the Magnetorotational Instability in the Sun". In: *The Astrophysical Journal* 787.1 (2014), p. 21. URL: `http://stacks.iop.org/0004-637X/787/i=1/a=21`.

[2] Ibid.

[3] F. N. Edmonds Jr. "The Coefficients of Viscosity and Thermal Conductivity in the Hydrogen Convection Zone." In: *The Astrophysical Journal* 125 (Mar. 1957), p. 535. DOI: `10.1086/146327`.

[4] Rudolf Kippenhahn, Alfred Weigert, and Achim Weiss. *Stellar Structure and Evolution*. Springer, 2012. ISBN: 978-3-642-30304-3.

where factors with subscripts are given numerically by the quantity divided by ten to the power of the subscript in the C.G.S.K unit system as usual. While this is much less than the microscopic viscosity over the entire range of tabulated data, at high temperatures it will overtake the Spitzer data due to a higher power of T appearing in the numerator.

To compute ν over the entire range of available data, an interpolation code was written which makes use of both the Spitzer form and the data tables. It returns an error whenever the data is outside of the range of validity of both, taking the Spitzer formula to be only valid above the ionization temperature $10^{4.1}$K. In places where both sources contained valid data, the tabulated version was used. In addition, it computes the radiative viscosity and adds it to the viscosity obtained from the other sources. The radiation merely provides an additional avenue for momentum transport, and so linear combination is appropriate. The full code may be found in Appendix A. The output from this code is shown in figure 4.1. Following the trajectories shown in the one-dimensional modeling chapter, we see that the viscosity is typically between $1\mathrm{cm}^2/\mathrm{s}$ and $10^4\mathrm{cm}^2/\mathrm{s}$, with higher temperature stars reaching at most $10^5\mathrm{cm}^2/\mathrm{s}$.

The one remaining question needed to determine the viscous microphysics of interest is that of the impact of magnetic fields. At temperatures where the ionization fraction is low, the magnetic field by and large does not interact with the gas, and so at low temperatures the above results are accurate independent of the magnetic field. The remaining effect of interest then is that of the solar magnetic field on momentum transport in plasma. Once ionization occurs, the magnetic field can introduce preferred directions of momentum transport, significantly altering the shear properties of the medium. This occurs when the thermal gyroradius is less than the mean free path of the ions. The intuition behind this is that it occurs when the magnetic field has a chance to order the system in between randomizing collisions.

Detailed calculations of this effect have been done[5], with the result that the anisotropy in the viscosity is of order

$$t_{ci}^{-2}\omega_{ci}^{-2}, \tag{4.5}$$

where t_{ci} is the self-collision time for positive ions and ω_{ci} is the gyrofrequency of these same ions in the magnetic field. Both quantities are to be computed assuming thermal equilibrium. More specifically, the quantity in Eq. (4.5) gives the approximate ratio of the visocosity of a velocity gradient perpendicular to the velocity, holding the velocity perpendicular to the magnetic field, to the viscosity in the absence of a magnetic

[5] Jr. Lyman Spitzer. *Physics of Fully Ionized Gases.* Vol. 1. ISBN 978-0-486-44982-1. Dover, 2006.

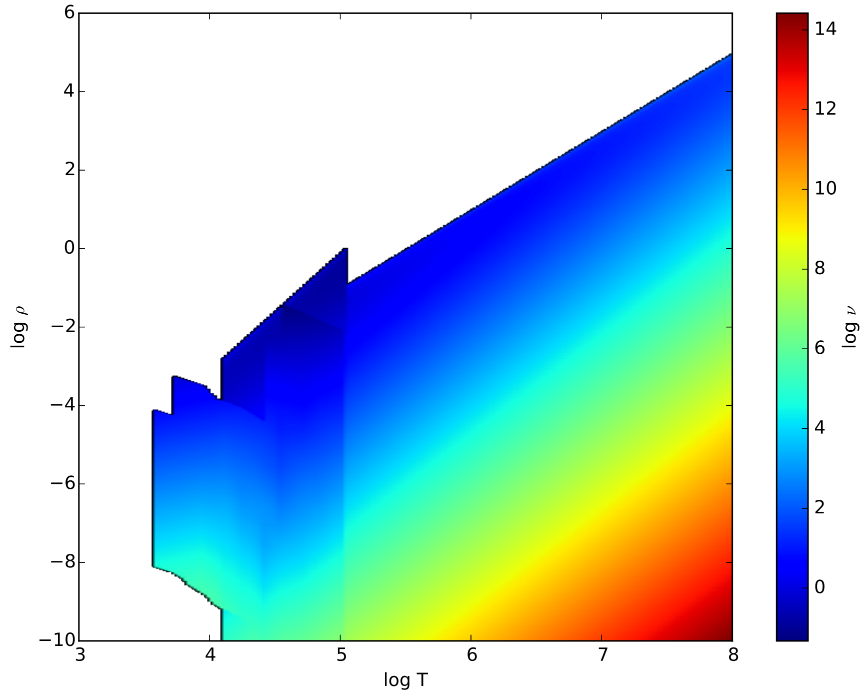

Figure 4.1: The vertical axis is $\log \rho$ (with ρ measured in g/cm^3), the horizontal is $\log T$ (with T measured in K), and the color represents $\log \nu$ (with ν measured in cm^2/s. White regions are those without data.

field. If this quantity exceeds unity then the magnetic field may be ignored, and the anisotropy disappears.

To compute the anisotropy, then, we note that t_{ci} is given by the mean free path of the ions divided by their typical thermal velocities. Thus

$$t_{ci} = \frac{\lambda}{\sqrt{\langle v^2 \rangle}} = \frac{\nu}{\langle v^2 \rangle}. \tag{4.6}$$

Note that in the final equality here, ν is the non-magnetic microscopic viscosity. The thermal gyroradius is given by

$$r_g = \frac{m_u c \sqrt{\langle v^2 \rangle}}{qB}, \tag{4.7}$$

Thus

$$\omega_{ci} = \frac{\sqrt{\langle v^2 \rangle}}{r_g} = \frac{qB}{m_u c}. \tag{4.8}$$

As a result, the anisotropy factor is

$$\frac{1}{t_{ci}^2 \omega_{ci}^2} = \frac{m_u^2 c^2 \langle v^2 \rangle^2}{q^2 B^2 \nu^2} = \frac{9 k_B^2 T^2 c^2}{q^2 B^2 \nu^2} = \frac{9 p^2 \mu^2 c^2}{\rho^2 q^2 B^2 \nu^2}. \tag{4.9}$$

To produce a factor which has the appropriate temperature dependence at low temperatures, we note that the anisotropy only impacts the ionized portion of the gas. As a result, we may separate the gas into its ionized and neutral portions, compute their viscosities, and then add them. The corrected anisotropy factor is then

$$m_p^{-1} \left(2\mu - m_p + 2 \frac{m_p - \mu}{t_{ci}^2 \omega_{ci}^2} \right). \tag{4.10}$$

As an estimate of the magnitude of the anisotropy factor when $\mu = m_p/2$, we may take typical values of ν to be $\sim \rho^{-1} 10^7$g/cm/s, and hence

$$\frac{1}{t_{ci}^2 \omega_{ci}^2} \sim \frac{9 p^2 \mu^2 c^2}{q^2 B^2 10^{14}} \sim \frac{p^2 \mu^2 c^2}{q^2 B^2 10^{13}} \sim \frac{4 \times 10^{-21} p^2}{B^2}. \tag{4.11}$$

where all units have been omitted for clarity. As usual all quantities are in measured C.G.S.K units. In most stars of interest, $g \sim 10^4$cm/s^2, so near the surface this may be written as

$$\frac{1}{t_{ci}^2 \omega_{ci}^2} \sim \frac{4 \times 10^{-13} \Sigma^2}{B^2}. \tag{4.12}$$

As a quick estimate, suppose we plug in the sun's magnetic field of $\sim 10^{-2}G$. This yields an anisotropy factor of $4\times10^{-9}\Sigma^2$. Thus the viscosity is significantly anisotropic for $\Sigma < 6\times10^3\mathrm{g/cm}^2$. The viscosity code in Appendix A is capable of computing the minimum B field requires to induce significant anisotropy. In convection zones this is often irrelevant: the convective viscosity far exceeds the molecular viscosity. In radiative zones, the microscopic viscosity will play a role in determining the characteristic scale of turbulence[6]. In cases where the microscopic viscosity does matter in a regime in which there is magnetically-induced anisotropy, we will hold the field to be that inside a dipole, aligned with the star's rotation axis, and so the microscopic viscosity is just multiplied by the anisotropy factor. The code in Appendix A accepts an optional argument specifying this factor. In its absence, isotropy is assumed.

The anisotropy factor is shown for $B = 10^{-2}\mathrm{G}$ in figure 4.2 and $B = 10^3\mathrm{G}$ in figure 4.3. In the first case the anisotropy is minimal for most density-temperature combinations of interest, while the latter shows significant anisotropy in a wide enough range of densities and temperatures that most scenarios of interest are covered. The regions of greatest anisotropy are subject to some numerical noise, resulting from a breakdown in the assumption that all ionization is hydrogen ionization.

4.2 Reynolds Number

The first of our dimensionless numbers is the Reynolds number, defined as

$$\mathrm{Re} \equiv \frac{vl}{\nu}, \tag{4.13}$$

where v is a characteristic velocity scale for a shear flow, l is a characteristic length scale, and ν is the viscosity of the fluid. The precise meaning of ν in this context is somewhat complex, so we will discuss it further later on. The Reynolds number in non-stratified flow is the quantity which determines whether or not a flow is shear turbulent. Barring stabilizing factors which will be discussed below, the flow is turbulent when

$$\mathrm{Re} > \mathrm{Re}_c$$

for some critical Reynolds number Re_c. Typical values of this number are of order 10^3.

[6] This is a result of our use of the more modern Richardson criterion modified to incorporate the effect turbulence plays in aiding thermal diffusion.

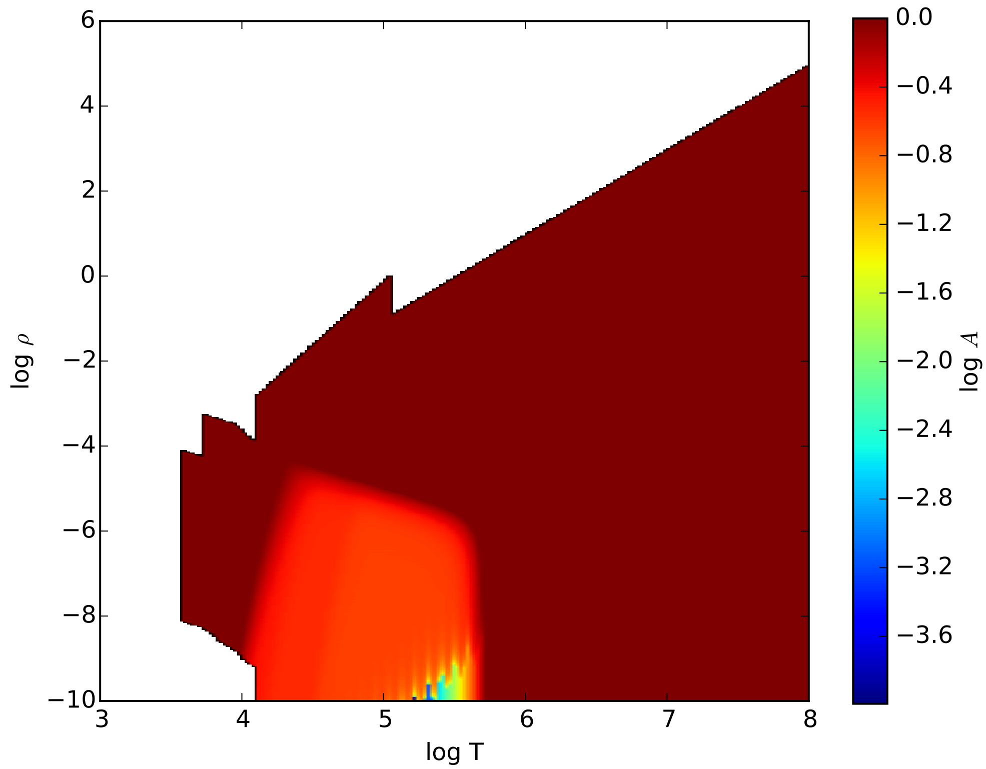

Figure 4.2: The vertical axis is $\log \rho$ (with ρ measured in g/cm^3), the horizontal is $\log T$ (with T measured in K), and the color represents the log of the anisotropy factor A. White regions are those without data.

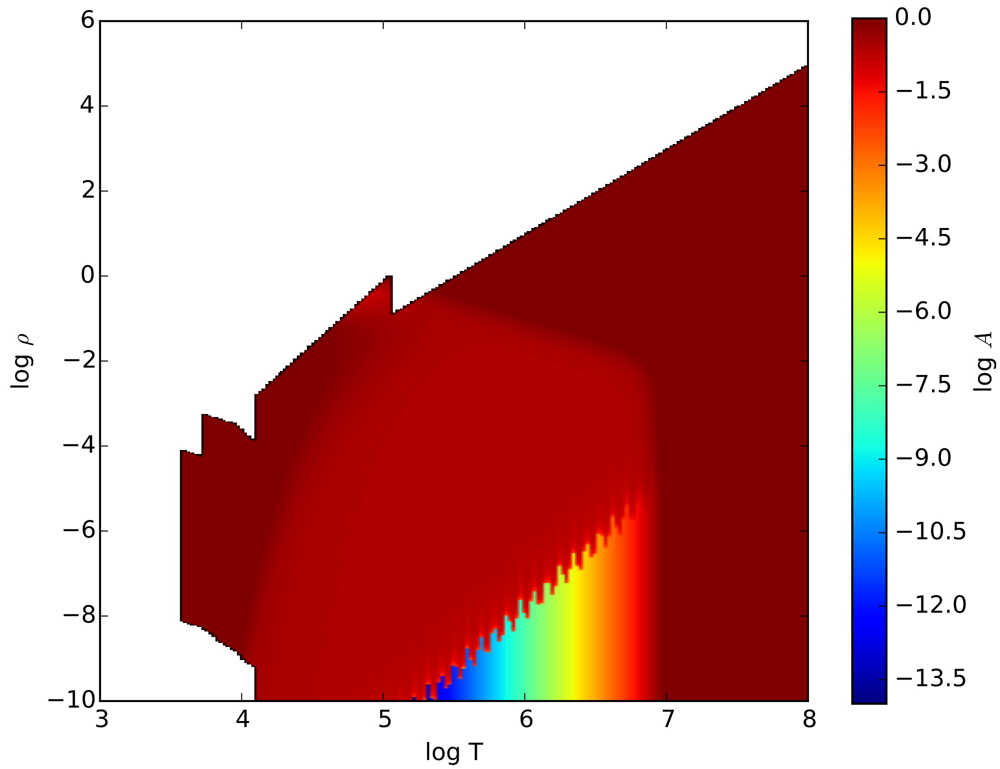

Figure 4.3: The vertical axis is $\log \rho$ (with ρ measured in g/cm^3), the horizontal is $\log T$ (with T measured in K), and the color represents the log of the anisotropy factor A. White regions are those without data.

4.3 Rayleigh Number

In addition to shear instability, it is possible for a fluid to be convectively unstable. This instability is quantified by the Rayleigh number, defined as

$$\mathrm{Ra} \equiv \frac{\beta g l^3 \Delta T}{\alpha \nu}, \tag{4.14}$$

where β is the thermal expansion coefficient and α is as defined previously. Convective instability occurs when $\nabla_{rad} > \nabla_{ad}$ and the Rayleigh number exceeds the critical Rayleigh number Ra_c, typically of order 10^3. The former condition is necessary for adiabatic expansion to lead to growing buoyant perturbations, while the latter is necessary for this expansion to not be overcome by viscous dissipation.

We claim that the Rayleigh number is typically so large that whenever the former condition is satisfied in a star the latter is as well. To begin, we write the Rayleigh number as

$$\mathrm{Ra} \approx \frac{\beta g \aleph^3 h_s^3 T \Delta \ln T}{\alpha \nu}. \tag{4.15}$$

Over a scale height, which is roughly what we expect the convection cell size to be, P changes by a factor of e and, we expect T to change by a multiplicative factor of similar magnitude. Thus $\Delta \ln T$ is of order unity, so

$$\mathrm{Ra} \approx \frac{\beta g \aleph^3 h_s^3 T}{\alpha \nu}. \tag{4.16}$$

Now β is typically of order T^{-1}, equaling

$$\beta = \frac{1}{V}\left(\frac{\partial V}{\partial T}\right)_p \sim \frac{1}{T}$$

so long as the ideal gas law holds. This only fails in the ionization zone, where β will be somewhat lower. Keeping this in mind, we find

$$\mathrm{Ra} \approx \frac{\xi g \aleph^3 h_s^3}{\alpha \nu}, \tag{4.17}$$

where ξ is the dimensionless constant giving the ratio of β to T^{-1}. Typical scale heights are around 300km, and typical values of g are around $10^4\mathrm{cm/s^2}$, so

$$\mathrm{Ra} \approx 3 \times 10^{26} \frac{\xi \aleph^3}{\alpha \nu}, \tag{4.18}$$

with all remaining quantities given in the usual c.g.s.k unit system. Now

$$\alpha = \frac{k_{rad}}{\rho c_p}, \tag{4.19}$$

so

$$\mathrm{Ra} \approx 3 \times 10^{26} \frac{\xi \aleph^3 \rho c_p}{k_{rad} \nu}. \tag{4.20}$$

We expect c_p to be of order $k_B/\mu \approx \rho 10^8 \mathrm{erg/K/cm}^3$, so

$$\mathrm{Ra} \approx 2 \times 10^{34} \frac{\xi \aleph^3}{k_{rad} \nu}. \tag{4.21}$$

Typical values of $\aleph$ are between unity and two. Taking the lower end gives

$$\mathrm{Ra} \approx 2 \times 10^{34} \frac{\xi}{k_{rad} \nu}. \tag{4.22}$$

As was argued earlier, the maximum value of ν for the stellar models of interest is around 10^5cms, so in a worst case scenario

$$\mathrm{Ra} \approx 2 \times 10^{29} \frac{\xi}{k_{rad}}. \tag{4.23}$$

Now k_{rad} may be computed directly as

$$k_{rad} = \frac{4acT^3}{3\rho\kappa}, \tag{4.24}$$

where κ is within a few orders of magnitude of $1\mathrm{cm}^2/\mathrm{g}$. Thus

$$k_{rad} = 10^8 \frac{T_4^3}{\rho_1}, \tag{4.25}$$

where T_4 is $T/10^4$K and ρ_1 is $\rho \mathrm{cm}^3/\mathrm{g}$. It follows that, again in a worst case,

$$\mathrm{Ra} \approx 2 \times 10^{21} \frac{\xi \rho_1}{T_4^3}. \tag{4.26}$$

Even supposing that ξ and ρ_1 are both quite a few orders of magnitude below unity, and taking T to be 10^6K, the Rayleigh number still exceeds its critical value. Thus we are safe assuming that whenever convection is indicated by the thermal gradient criterion it occurs.

4.4 Richardson Number

The next dimensionless number of interest is the Richardson number, defined as

$$\mathrm{Ri} \equiv \frac{N^2}{(dv/dz)^2}, \tag{4.27}$$

where

$$N^2 = g\frac{d\ln\rho}{dz} \tag{4.28}$$

defines the Brunt-Vaisala frequency N and dv/dz is the vertical velocity shear. The Richardson number quantifies the competition between buoyant stabilizing forces and shear instability. In particular, an oft-cited[7] necessary but not sufficient criterion for instability is that

$$\mathrm{Ri} < \mathrm{Ri}_c \approx 0.25. \tag{4.29}$$

There is, however, significant evidence, both experimental and theoretical, against this criterion[8]. There are two problems. The first is that turbulence mixes the fluid, which counteracts the entropic stratification that would otherwise stabilize it. As a result, the fluid is actually unstable over a wider range of parameter space than this criterion indicates. The second is that more modern experimental evidence suggests that even when this mixing is minimal, the critical value should be closer to

[7] Richard Lyons, A. H. Panopsky, and Sarah Wollaston. "The Critical Richardson Number and Its Implications for Forecast Problems". In: *Journal of Applied Meteorology* 3 (Jan. 1964), pp. 136–142. URL: http://journals.ametsoc.org/doi/pdf/10.1175/1520-0450(1964)003%3C0136:TCRNAI%3E2.0.CO;2.

[8] E. Schatzman, J.P. Zahn, and P. Morel. "Shear turbulence beneath the solar tachocline". In: *Astronomy and Astrophysics* (Oct. 2000). eprint: http://arxiv.org/pdf/astro-ph/0010543v1.pdf; E. C. Itsweire, K. N. Helland, and C. W. Van Atta. "The evolution of grid-generated turbulence in a stably stratified fluid". In: *Journal of Fluid Mechanics* 162 (Jan. 1986), pp. 299–338. ISSN: 1469-7645. DOI: 10.1017/S0022112086002069. URL: http://journals.cambridge.org/article_S0022112086002069; A. Maeder. "Stellar rotation: Evidence for a large horizontal turbulence and its effects on evolution". In: *Astronomy and Astrophysics* 399.1 (2003), pp. 263–269. DOI: 10.1051/0004-6361:20021731. eprint: http://arxiv.org/abs/astro-ph/0301258. URL: http://dx.doi.org/10.1051/0004-6361:20021731; Prat, V. and Lignières, F. "Turbulent transport in radiative zones of stars". In: *Astronomy and Astrophysics* 551 (2013), p. L3. DOI: 10.1051/0004-6361/201220577. eprint: http://arxiv.org/abs/1301.4151. URL: http://dx.doi.org/10.1051/0004-6361/201220577; S. Mathis, A. Palacios, and J.-P. Zahn. "On shear-induced turbulence in rotating stars". In: *Astronomy and Astrophysics* 425.1 (2004), pp. 243–247. DOI: 10.1051/0004-6361:20040279. eprint: http://arxiv.org/abs/astro-ph/0403580. URL: http://dx.doi.org/10.1051/0004-6361:20040279.

unity than to 0.25[9]. In convection zones this may be remedied by setting the critical Richardson number to

$$\mathrm{Ri}_c = \max\left(1, \frac{1}{\mathrm{P}_e}\right), \tag{4.30}$$

where Pe is the Péclet number, defined in this context as

$$\mathrm{P}_e = \frac{v_c l}{\alpha} \tag{4.31}$$

and α is the thermal diffusivity. Outside of convective layers, the criterion may be modified by replacing the Péclet as written above with one computed using the characteristic velocity and length scale of turbulent eddies.[10] In both cases, this criterion takes into account the action of heat transport to lower buoyant effects. Notice that this criterion in the non-convecting case presumes the existence of turbulence from the start, and is primarily making a statement regarding the characteristic scale of the turbulence. This, in effect, neglects the microscopic viscosity of the fluid, which is akin to arguing that

$$\nu \ll v\Delta z, \tag{4.32}$$

where v and Δz are the maximum turbulence speed and size allowed by the modified Richardson criterion. This condition is satisfied by taking

$$\frac{\nu}{v\Delta z} \leq \frac{1}{\mathrm{Re}_c} \ll 1. \tag{4.33}$$

Should this condition fail, the flow cannot be turbulent anyway via the Reynolds criterion, as the turbulence velocity and length scale cannot be smaller than those of the shear which produces it, and so it suffices to require both the Reynolds criterion and the Richardson criterion, without having an additional condition regarding the microscopic viscosity.

At this stage it is worth introducing the idea of an effective viscosity. This is the viscosity that one would measure in a turbulent flow by using the definition of viscosity as the force per unit area per unit shear across a fluid. A key property of an effective viscosity, as will be discussed at length in the following sections, is that it is dependent on the length scale over which the shear occurs. In the context of the Reynolds criterion, the question of stability becomes one of the effective viscosity of

[9] V. M. Canuto. “Turbulence in Stars. II. Shear, Stable Stratification, and Radiative Losses”. In: *The Astrophysical Journal* 508.2 (1998), p. 767. URL: `http://stacks.iop.org/0004-637X/508/i=2/a=767`.

[10] Ibid.

any non-shear turbulent processes. In the context of the Richardson criterion, what occurs is the production in any Reynolds-unstable flow of turbulence up to a critical effective viscosity scale, defined by the criterion, and it is this effective viscosity which is seen by the large-scale flow. Thus the Richardson criterion is perhaps better viewed as setting a viscosity scale than making definitive statements about flow stability.

This is not the end of the story of the Richardson criterion, however. The actual Richardson criterion must account for the fact that in a stratified flow, there is a difference between the horizontal turbulent viscosity and the vertical turbulent viscosity. In order to accommodate this, we use as our criterion[11]:

$$\frac{v\Delta z}{(k_{rad}+\nu_h)}N_T^2 + \frac{v\Delta z}{\nu_h}N_\mu^2 < \left(\frac{dv}{dz}\right)^2, \tag{4.34}$$

where v and Δz are the speed and size of the largest eddies which are isotropic, ν_h is the turbulent viscosity for horizontal motions, k_{rad} is the thermal diffusivity due to radiation transport, and N_T and N_μ partition the Brunt-Vaisala frequency into pieces corresponding to the thermal and chemical gradients respectively. This takes into account all of the effects discussed thus far. We will examine in detail the computation of this criterion in the section on vertical shear.

4.5 Rossby Number

The next dimensionless number of interest is the Rossby number, which determines the circumstances under which the Coriolis force has a significant impact on the motion of a fluid. Given a characteristic speed v and a characteristic length scale x, the Rossby number is defined as

$$\mathrm{Ro} \equiv \frac{v}{2x\Omega\sin\theta}, \tag{4.35}$$

where Ω and θ are defined as usual. Note that v is defined in a reference frame rotating at Ω, as fluid at rest in the rotating frame does not experience a Coriolis force. When this number is large relative to unity, the Coriolis force is negligible and so may be neglected. In the opposing limit, the Coriolis force dominates the flow, and geostrophic balance is likely. When the Rossby number is of order unity, the Coriolis force must typically be taken into account, but need not be the dominant effect. We will usually use $x = R$, such that the Rossby number refers to motion around the star.

[11] S. Mathis, A. Palacios, and J.-P. Zahn, op. cit.

4.6 Mach Number

The final dimensionless number of interest is the Mach number, defined as the ratio of the flow speed to the fluid's sound speed. That is,

$$\mathrm{Ma} \equiv \frac{v}{v_s}. \tag{4.36}$$

The sound speed is generally given as

$$v_s = \sqrt{\frac{P}{\rho}}, \tag{4.37}$$

where

$$\gamma = \frac{c_p}{c_v} \tag{4.38}$$

is the adiabatic index of the fluid. For a monatomic gas outside of the ionization zone, this is 5/3. Inside the ionization zone, it falls to roughly unity[12]. From our perspective, the Mach number is important primarily because for Ma > 1, turbulent losses become extreme, so we may safely assume that $v < v_s$.

[12] Donald D. Clayton. *Principles of Stellar Evolution and Nucleosynthesis.* Vol. 1. ISBN: 978-0521566315. University of Chicago Press, 1968.

References

A. Maeder. "Stellar rotation: Evidence for a large horizontal turbulence and its effects on evolution". In: *Astronomy and Astrophysics* 399.1 (2003), pp. 263–269. DOI: 10.1051/0004-6361:20021731. eprint: http://arxiv.org/abs/astro-ph/0301258. URL: http://dx.doi.org/10.1051/0004-6361:20021731 (cit. on p. 59).

Canuto, V. M. "Turbulence in Stars. II. Shear, Stable Stratification, and Radiative Losses". In: *The Astrophysical Journal* 508.2 (1998), p. 767. URL: http://stacks.iop.org/0004-637X/508/i=2/a=767 (cit. on p. 60).

Clayton, Donald D. *Principles of Stellar Evolution and Nucleosynthesis.* Vol. 1. ISBN: 978-0521566315. University of Chicago Press, 1968 (cit. on p. 62).

Edmonds Jr., F. N. "The Coefficients of Viscosity and Thermal Conductivity in the Hydrogen Convection Zone." In: *The Astrophysical Journal* 125 (Mar. 1957), p. 535. DOI: 10.1086/146327 (cit. on p. 50).

Itsweire, E. C., K. N. Helland, and C. W. Van Atta. "The evolution of grid-generated turbulence in a stably stratified fluid". In: *Journal of Fluid Mechanics* 162 (Jan. 1986), pp. 299–338. ISSN: 1469-7645. DOI: 10.1017/S0022112086002069. URL: http://journals.cambridge.org/article_S0022112086002069 (cit. on p. 59).

Kagan, Daniel and J. Craig Wheeler. "The Role of the Magnetorotational Instability in the Sun". In: *The Astrophysical Journal* 787.1 (2014), p. 21. URL: http://stacks.iop.org/0004-637X/787/i=1/a=21 (cit. on p. 50).

Kippenhahn, Rudolf, Alfred Weigert, and Achim Weiss. *Stellar Structure and Evolution.* Springer, 2012. ISBN: 978-3-642-30304-3 (cit. on p. 50).

Lyman Spitzer, Jr. *Physics of Fully Ionized Gases.* Vol. 1. ISBN 978-0-486-44982-1. Dover, 2006 (cit. on p. 51).

Lyons, Richard, A. H. Panopsky, and Sarah Wollaston. "The Critical Richardson Number and Its Implications for Forecast Problems". In: *Journal of Applied Meteorology* 3 (Jan. 1964), pp. 136–142. URL: http://journals.ametsoc.org/doi/pdf/10.1175/1520-0450(1964)003%3C0136:TCRNAI%3E2.0.CO;2 (cit. on p. 59).

Prat, V. and Lignières, F. "Turbulent transport in radiative zones of stars". In: *Astronomy and Astrophysics* 551 (2013), p. L3. DOI: 10.1051/0004-6361/201220577. eprint: http://arxiv.org/abs/1301.4151. URL: http://dx.doi.org/10.1051/0004-6361/201220577 (cit. on p. 59).

S. Mathis, A. Palacios, and J.-P. Zahn. "On shear-induced turbulence in rotating stars". In: *Astronomy and Astrophysics* 425.1 (2004), pp. 243–247. DOI: 10.1051/0004-

6361:20040279. eprint: http://arxiv.org/abs/astro-ph/0403580. URL: http://dx.doi.org/10.1051/0004-6361:20040279 (cit. on pp. 59, 61).

Schatzman, E., J.P. Zahn, and P. Morel. "Shear turbulence beneath the solar tachocline". In: *Astronomy and Astrophysics* (Oct. 2000). eprint: http://arxiv.org/pdf/astro-ph/0010543v1.pdf (cit. on p. 59).

5

Stability and Turbulence

When I meet God, I am going to ask him two questions: Why relativity? And why turbulence? I really believe he will have an answer for the first.
– Werner Heisenberg

The key problem of interest in this chapter is that of determining the local flow patterns that stars may exhibit, with a particular eye to questions of viscous and turbulent losses as well as flow stability. In the fluid mechanics discussed thus far, only one kind of instability was considered at a time. This turns out to be insufficiently general. In the various stellar models under consideration, Σ_h is sometimes within the unperturbed convection zone and sometimes not. The latter case may be analyzed by only considering shear instability, but the former requires understanding how shear and convective instabilities interact. To understand this, we will consider a model of shear flow with convection and analyze it in general. We will then proceed to look at the case of shear flow alone, as the difference in stability criteria between vertical and horizontal shear is significant there. The next chapter will then take a broader view of wind in stars, and will piece together a global picture from these local parts.

In analyzing the stability of different kinds of flows in this chapter we will keep the thin-envelope approximation made in our earlier one-dimensional model. This is justified by the same reasoning used there, and allows us to assume that the regions of interest are always thin relative to R. This means that g is a constant in the regions of interest, and that the curvature of these regions may be neglected. It further tells us that the pressure in each region is just what is required to hold up the material above it.

In addition to the above conditions, we take the shear in all cases to be an amount v_0 over a convective mixing length $l = \aleph h_s$, where $\aleph > 1$ is of order unity. When convection occurs, we will take its eddy velocity to be v_c.

5.1 Sheared Convection

In the analysis to follow, we work within a single convection cell of linear dimension l. Additionally, we take the forces resulting from microscopic viscosity to be small relative to those resulting from the buoyancy which drives convection. This is justified by our argument in the previous chapter that in stars the Rayleigh number is large relative to its critical value.

Note that since, by assumption, the flow is convectively unstable, the Richardson criterion is automatically satisfied: $N^2 < 0$. There are several limits which are easily analyzed. First, suppose that $v_0 \gg v_c$, and that $\mathrm{Re} > \mathrm{Re}_c$. In this case, the convection acts as a perturbation to the shear turbulence: existing eddies due to the shear suffice to carry the convective heat flux with only minor additional anisotropy. This scenario will be stable then against convective turbulence, as the shear will carry the needed flux, but will be unstable against shear turbulence. On the other hand, if $v_c \gg v_0$ and $\mathrm{Re} < \mathrm{Re}_c$, the shear acts as a perturbation to the convective turbulence: the convective eddies suffice to carry the necessary momentum flux, again with only minor additional anisotropy. This scenario is thus stable against shear turbulence yet unstable against convective turbulence.

Another straightforward limit is that in which $\mathrm{Re} < \mathrm{Re}_c$ and $v_0 \gg v_c$. In this case, shear due to v_0 is insufficient on its own to cause an instability: the viscosity is high enough that the turbulence is dissipated as heat faster than it is created. If the flow is stable against shear turbulence, however, the thermal flux must be carried by convection. As $v_c \ll v_0$, the convection appears as a perturbation against the background shear and so the flow will remain shear-stable with a background convective instability. The convection will increase the effective viscosity of the flow, but this only serves to further reduce Re and hence further stabilize the shear flow. Thus in this case the flow is shear stable and convectively turbulent. This flow pattern is like that known in meteorological work as a longitudinal roll[1].

Likewise, in the case where $\mathrm{Re} \gg \mathrm{Re}_c$ and $v_c \gg v_0$, there will be shear turbulence which provides a perturbative background for convective turbulence. That is, the convection is necessary and proceeds effectively unimpeded, yet the shear flow experiences turbulence nonetheless. Each kind of turbulence will cause an increased

[1]S. Mergui, X. Nicolas, and S. Hirata. "Sidewall and thermal boundary condition effects on the evolution of longitudinal rolls in Rayleigh-Bénard-Poiseuille convection". In: *Physics of Fluids (1994-present)* 23.8, 084101 (2011), pages. DOI: http://dx.doi.org/10.1063/1.3605698. URL: http://scitation.aip.org/content/aip/journal/pof2/23/8/10.1063/1.3605698; R. A. Brown. "Longitudinal instabilities and secondary flows in the planetary boundary layer: A review". In: *Reviews of Geophysics* 18.3 (1980), pp. 683–697. ISSN: 1944-9208. DOI: 10.1029/RG018i003p00683. URL: http://dx.doi.org/10.1029/RG018i003p00683.

effective viscosity seen by the other, and so here, by requiring Re to be large, we really mean the effective Re taking into account the convective viscosity.

The four cases considered so far characterize the extreme possibilities. The remaining scenarios lie in the interior of the $(\mathrm{Re}, v_c/v_0)$ space. Starting with $v_c \ll v_0$ and $\mathrm{Re} \ll \mathrm{Re}_c$ and moving towards increasing Re, we see that the flow must transition from shear stable and convectively unstable to shear unstable and convectively stable. If we move instead in the direction of increasing v_c, there is no such transition, as the kind of instabilities remain the same in the low Re limit. On the other hand, in the high Re limit, moving from low v_c to high v_c causes a convectively stable flow to become convectively unstable. We expect then a rich set of transitions in the intermediate values of Re and v_0/v_c.

To fill in our understanding of this space, the scaling forms of different instabilities will be useful. These have historically been understood as energy transport relations in momentum-space, though they may also be viewed as a result of the application of the Momentum-Shell Renormalization Group methodology to fluid mechanics[2]. In this context, the RG flow amounts to an increase in viscosity with length scale, conditioned upon the existence of turbulence. The Kolmorogov relation plays the role of a trivial fixed point[3], as expected given its assumption of isotropy and scale-invariance.

Regardless of the interpretation, the key differences between convective and shear instabilities lie in how energy is transferred to different length scales. In a shear instability, energy begins on long scales and is transferred to short scales, where it is eventually dissipated. In a convective stability, on the other hand, the energy begins on all scales and is merely redistributed. This difference results in a difference in the scaling form of the resultant eddy velocity. Furthermore within a convective instability the scaling form varies as a function of length scale. Specifically, if ϵ_μ is the rate of viscous energy dissipation per unit mass, ϵ_T is the rate of thermal dissipation

[2] Victor Yakhot and StevenA. Orszag. “Renormalization group analysis of turbulence. I. Basic theory”. English. In: *Journal of Scientific Computing* 1.1 (1986), pp. 3–51. ISSN: 0885-7474. DOI: 10.1007/BF01061452. URL: http://dx.doi.org/10.1007/BF01061452; Ye Zhou, David W. McComb, and George Vahala. “Renormalization Group (RG) in Turbulence: Historical and Comparative Perspective”. In: (Aug. 1997). URL: http://ntrs.nasa.gov/archive/nasa/casi.ntrs.nasa.gov/19970028852.pdf; Dirk Barbi and Gernot Munster. *Renormalization Group Analysis of Turbulent Hydrodynamics*. May 2013. URL: http://arxiv.org/abs/1012.0461; L. Ts. Adzhemyan et al. “Renormalization-group approach to the stochastic Navier Stokes equation: Two-loop approximation”. In: *International Journal of Modern Physics B* 17.10 (2003), pp. 2137–2170. DOI: 10.1142/S0217979203018193. eprint: http://www.worldscientific.com/doi/pdf/10.1142/S0217979203018193. URL: http://www.worldscientific.com/doi/abs/10.1142/S0217979203018193.

[3] Yakhot and Orszag, op. cit.; Barbi and Munster, op. cit.

per unit mass, and r is the length scale of interest, then[4]

$$\begin{aligned} v_{small}^{convective} &\sim (\epsilon_\mu r)^{1/3}, \\ v_{long}^{convective} &\sim (\epsilon_T^2 \beta^4 g^4 r^3)^{1/5}, \\ v^{shear} &\sim (\epsilon_\mu r)^{1/3}, \end{aligned}$$

where β is the thermal expansion coefficient. For an ideal gas, $\beta = T^{-1}$. The crossover between the two behaviors for convection typically occurs at the Bolgiano length, given by[5]

$$L_B = \epsilon_\mu^{5/4} \epsilon_T^{-3/4} (\beta g)^{-3/2}. \tag{5.1}$$

That is, the small-scaling is expected for $r < L_B$ and the long scaling for $r > L_B$. Now the scaling relations may also be written in terms of macroscopic quantities as

$$\begin{aligned} v_{small}^{convective} &\sim v_c \left(\frac{L_B}{l}\right)^{3/5} \left(\frac{r}{L_B}\right)^{1/3}, \\ v_{long}^{convective} &\sim v_c \left(\frac{r}{l}\right)^{3/5}, \\ v^{shear} &\sim v_0 \left(\frac{r}{l}\right)^{1/3}. \end{aligned}$$

Note that the scaling forms are only precise when the length scale is much smaller than any large-scale features of the flow. The primary large-scale flow length scale in

[4] Emily S. C. Ching et al. "Scaling behavior in turbulent Rayleigh-Bénard convection revealed by conditional structure functions". In: *Phys. Rev. E* 87 (1 Jan. 2013), p. 013005. DOI: `10.1103/PhysRevE.87.013005`. URL: `http://link.aps.org/doi/10.1103/PhysRevE.87.013005`; F Rincon. *Theories of convection and the spectrum of turbulence in the solar photosphere.* Tech. rep. astro-ph/0611842. Contribution to the proceedings : 239 Convection in Astrophysics, International Astronomical Union., held 21-25 August, 2006 in Prague, Czech Republic. Nov. 2006. eprint: `http://arxiv.org/pdf/astro-ph/0611842.pdf`. URL: `http://cds.cern.ch/record/1001690/files/0611842.pdf`; Dan Škandera, Angela Busse, and Wolf-Christian Müller. *Scaling Properties of Convective Turbulence.* English. Ed. by Siegfried Wagner et al. Springer Berlin Heidelberg, 2009, pp. 387–396. ISBN: 978-3-540-69181-5. DOI: `10.1007/978-3-540-69182-2_31`. URL: `http://dx.doi.org/10.1007/978-3-540-69182-2_31`; Detlef Lohse and Ke-Qing Xia. "Small-Scale Properties of Turbulent Rayleigh-Benard Convection". English. In: *Annual Review Of Fluid Mechanics.* Annual Review of Fluid Mechanics 42 (2010), pp. 335–364. ISSN: 0066-4189. DOI: `10.1146/annurev.fluid.010908.165152`; G Boffetta et al. *Kolmogorov and Bolgiano scaling in thermal convection: the case of Rayleigh-Taylor turbulence.* Tech. rep. arXiv:1101.5917. Comments: 4 pages, 5 figures. Feb. 2011. URL: `http://arxiv.org/pdf/1101.5917.pdf`.

[5] Ching et al., op. cit.; Lohse and Xia, op. cit.; Boffetta et al., op. cit.

this problem is the pressure scale height, or equivalently the size of the convection cell, so use of these relations in the vicinity of the convection scale should be treated with some caution. Having said that, this warning is most applicable in cases with fixed boundary conditions constraining the flow. In stars, where the boundaries are typically free and the fluid properties are continuous, the scale at which boundary effects on the scaling must be considered is somewhat larger relative to l. As a result the line between large-scale flow and turbulent scaling is somewhat more blurred than usual, so the use of these equations in the vicinity of a scale or convective height is safer than might otherwise be expected.

As a rough model, then, we take the kind of turbulence present at any length scale to be the kind with the greatest eddy velocity at that scale. In computing stability criteria, we use the effective viscosity due to the effect we are not considering. This model is convenient in that it provides a way to deal continuously with the empty sections in the table classifying flow phases: effectively as one or the other parameter changes the length scales are shuffled around to determine the flow properties.

Within the context of this model, and in the case where both types of turbulence are present, there are three possibilities. Either the shear velocity curve intersects the long convective velocity curve above $r = l$, or the shear curve falls below both convective curves, or it intersects the convection curves below $r = l$. In the first case, shear turbulence dominates and the convective turbulence manifests as a slight anisotropy in the shear turbulent flow. In the second case, convection dominates and the shear turbulence manifests as a slight anisotropy in the convection. In the final case, convective turbulence dominates on long scales, shear turbulence on intermediate scales, and convective turbulence on shorter scales. Each of these cases may be analyzed separately for stability.

5.1.1 Shear-dominated flow

In the first case, the Reynold's number is given by

$$\mathrm{Re} = \frac{v_0 l}{\nu_{eff}}. \tag{5.2}$$

Now the tricky part here is determining a choice of ν_{eff}. It is tempting to declare the convective eddies irrelevant, as they are subdominant on all length scales. The problem with this is that stability is determined in the absence of the instability of interest. Thus we take the effective viscosity here to be that due to the convective eddies, and hence

$$\mathrm{Re} = \frac{v_0 l}{v_c l} = \frac{v_0}{v_c}. \tag{5.3}$$

Furthermore, by virtue of us considering this case we must have

$$v_0\left(\frac{r}{l}\right)^{\frac{1}{3}} > v_c\left(\frac{r}{l}\right)^{3/5} \forall r < l \rightarrow \frac{v_0}{v_c} > \left(\frac{r}{l}\right)^{\frac{4}{15}} \forall r < l \rightarrow \frac{v_0}{v_c} > 1. \tag{5.4}$$

As a result, for turbulent flow to arise from shearing we must have $v_0 > \mathrm{Re}_c v_c$, which trivially satisfies the condition that $v_0 > v_c$ because $\mathrm{Re}_c \approx 10^3$. The full criterion for this case to arise, then, is

$$\frac{v_0}{v_c} > \mathrm{Re}_c. \tag{5.5}$$

The dissipation in this case is

$$\frac{\text{Power}}{\text{Area}} = \frac{Fv_0}{\text{Area}} = v_0 \nu_{eff} \rho \frac{dv}{dz} = v_0^2 \nu_{eff} \frac{\rho}{l}. \tag{5.6}$$

Once more we must pick an effective viscosity. Here, however, the effective viscosity is that due to the turbulence itself. Using the simple Prandtl model, this is given by

$$\nu_{eff} = l v_0. \tag{5.7}$$

As a result,

$$\frac{\text{Power}}{\text{Area}} = v_0 \nu_{eff} \rho \frac{dv}{dz} = \rho v_0^3. \tag{5.8}$$

As the energy density of the wind is ρv_0^2, the time over which it dissipates in the absence of a driving force is l/v_0 and the distance it travels is l.

Note that in this case the heat flux is entirely carried by the turbulent motion the shear generates. This is much faster than the convective flux, and so the associated temperature gradient will be lower. This will cause the layer to become convectively stable, leaving shear instability as the only remaining form of turbulence. Of course, should the turbulence stop the layer will become convectively unstable on the cooling timescale of the layer, though for this to happen the shear velocity must slow down tremendously to accommodate the much lower molecular-scale viscosity.

Finally, note that stability of shear flow on one length scale does not guarantee stability on another, and likewise with instability. In particular, the numerator of the Reynold's number scales as r^2, while the denominator scales as $r^{1+\epsilon}, \epsilon \in \left\{\frac{1}{3}, \frac{3}{5}\right\}$. As a result, $\mathrm{Re} \sim r^{\epsilon'}, \epsilon' \in \left\{\frac{2}{3}, \frac{2}{5}\right\}$.

As $\epsilon' > 0$, it is possible for a shear flow which is unstable on long length scales to stabilize on short ones. This could occur if the larger scale shear flow breaks up into bands smaller than a pressure height, each of which is internally laminar with a turbulent region in between. The bulk convective motion is then restricted to work on this new scale. One might expect v_c to drop as a result, as the gas packets have less time to accelerate before turning around. More specifically, one would expect $v_c \propto \sqrt{l}$. This decrease, however, will lower the flux that the convection can carry, leading to an increase in the thermal gradient across the region. The flux carried goes as

$$F_c \propto c_p v_c \frac{dT}{dz} \propto \rho v_c \frac{dT}{dz} \propto \rho l \frac{dT}{dz}\sqrt{\left(\frac{dT}{dz}\right) - \left(\frac{dT}{dz}\right)_{ad}}. \tag{5.9}$$

As a result, decreasing l results in a necessary increase of the temperature gradient to carry the same flux. Now recall that

$$\frac{dT}{dz} = \frac{T d\ln T}{P d\ln P}\frac{dP}{dz} = -g\rho\frac{T}{P}\nabla = -\frac{g\mu}{k_B}\nabla, \tag{5.10}$$

so

$$F_c \propto l\nabla\sqrt{\nabla - \nabla_{ad}}. \tag{5.11}$$

The corresponding differential form is

$$dF_c \propto \nabla\sqrt{\nabla - \nabla_{ad}}dl + l\frac{3\nabla - 2\nabla_{ad}}{2\sqrt{\nabla - \nabla_{ad}}}d\nabla. \tag{5.12}$$

Setting this to zero yields

$$\frac{d\nabla}{dl} = \frac{2\nabla(\nabla - \nabla_{ad})}{l(2\nabla_{ad} - 3\nabla)}. \tag{5.13}$$

This is a negative quantity, as $\nabla \approx \nabla_{ad}$, so decreasing l increases ∇ as expected. Recalling that

$$v_c \propto l\sqrt{\nabla - \nabla_{ad}}, \tag{5.14}$$

we find

$$\frac{dv_c}{dl} \propto \sqrt{\nabla - \nabla_{ad}}\left(1 + \frac{\nabla}{2\nabla_{ad} - 3\nabla}\right) = \sqrt{\nabla - \nabla_{ad}}\left(1 + \frac{1}{2\frac{\nabla_{ad}}{\nabla} - 3}\right). \tag{5.15}$$

In general we expect $\nabla > \nabla_{ad}$ and $\nabla \approx \nabla_{ad}$ in a convection zone, so we expect $\nabla_{ad}/\nabla = 1 - \delta$ for small positive δ. Thus

$$\frac{dv_c}{dl} \propto \sqrt{\nabla - \nabla_{ad}}\left(1 + \frac{1}{-1 - 2\delta}\right) \approx 2\delta\sqrt{\nabla - \nabla_{ad}} \approx 2\delta^{3/2}. \tag{5.16}$$

This quantity is positive, so v_c decreases as the length scale drops. This raises the Reynold's number for the flow and destabilizes it, so we expect the flow to actually be unstable on all length scales despite the fact that $\epsilon' = \frac{2}{3}$. The effective viscosity will be similar to the general case of shear turbulent flow.

5.1.2 Convection-dominated flow

In the second case, convection dominates on all length scales. The instability criterion for convective flow is that

$$\mathrm{Ra} \equiv \frac{\beta g l^3 \Delta T}{\alpha \nu} > \mathrm{Ra}_c. \tag{5.17}$$

Now recall that

$$\beta \equiv \frac{\partial \ln V}{\partial T}|_P. \tag{5.18}$$

We expect that at fixed pressure, increasing the temperature of a gas always increases its volume, even when ionization effects are present[6]. In the ionization zone this may be a relatively small increase due to the fact that increasing T there leads primarily to an increase in ionization, and hence to a decrease in μ which partially offsets the decrease in P. Without going into detail in analyzing the equation of state there is not much more that can be said, so we simply remark that β will typically be a number of order T^{-1}. As ΔT is of order T on a scale height, these two will roughly cancel, leaving

$$\frac{g l^3}{\alpha \nu} > \mathrm{Ra}_c. \tag{5.19}$$

The viscosity here once more should not be the molecular viscosity, but rather the turbulent viscosity due to the shear flow in the absence of convection. This viscosity is given on the scale of interest by

$$\nu = l v_0, \tag{5.20}$$

so

$$\frac{g l^2}{\alpha v_0} > \mathrm{Ra}_c. \tag{5.21}$$

Now the thermal diffusivity α will be dominated by the shear turbulence, and so is roughly equal to $l v_0$. As a result,

$$\frac{g l}{v_0^2} > \mathrm{Ra}_c. \tag{5.22}$$

This is the necessary criterion for convection to dominate over an otherwise shear-turbulent flow.

[6] The fact that this does not hold for solids is a result of the global symmetry changes which can occur in phase transitions.

Given that this is the case, we also know that

$$v^{shear} \sim v_0 \left(\frac{r}{l}\right)^{1/3} < v^{convective}_{small} \sim v_c \left(\frac{L_B}{l}\right)^{3/5} \left(\frac{r}{L_B}\right)^{1/3}, \tag{5.23}$$

and hence

$$\frac{v_0}{v_c} < \left(\frac{L_B}{l}\right)^{3/5} \left(\frac{l}{L_B}\right)^{1/3} = \left(\frac{L_B}{l}\right)^{4/15}. \tag{5.24}$$

Now L_B is generally a small length scale, much smaller than l, such that the regime 'visible' to the turbulence has no externally imposed length-scale. As a result, we require

$$v_c \gg v_0. \tag{5.25}$$

In this case the dissipation of the shear is given by the convective viscosity, which serves to transport momentum efficiently around the region. Thus

$$\frac{\text{Power}}{\text{Area}} = \frac{Fv}{\text{Area}} = v_0 \nu_{eff} \rho \frac{dv}{dz} = v_0^2 \nu_{eff} \frac{\rho}{l} = v_0^2 v_c l \frac{\rho}{z_0} = v_c \left(\rho v_0^2\right). \tag{5.26}$$

We recognize the final quantity in parentheses as the energy density of the wind. The time the wind may travel before running out of energy is then this divided by the volumetric power loss, and so is l/v_c. As $v_c \gg v_0$ we expect then that the wind loses energy comparable to what it carries over a distance much shorter than l.

5.1.3 Mixed shear-convective flow

In this case, the convective and shear velocities are such that

$$v_c > v_0, \tag{5.27}$$

$$v_0 \left(\frac{r}{l}\right)^{1/3} = v_c \left(\frac{r}{l}\right)^{3/5}, r > L_B. \tag{5.28}$$

This implies that

$$1 > \frac{v_0}{v_c} > \left(\frac{L_B}{l}\right)^{\frac{4}{15}}. \tag{5.29}$$

A result of this is that the system is convective on long scales and experiences shear turbulence on short scales. The length scale of the transition is given by

$$r_{crit} = l \left(\frac{v_0}{v_c}\right)^{\frac{15}{4}} \tag{5.30}$$

In order for the shear to be unstable below this length scale, we require as before

$$\mathrm{Re} = \frac{\left(\frac{v_0}{l}\right) r_{crit}}{v_c\left(\frac{r_{crit}}{l}\right)^{\frac{3}{5}}} = \frac{v_0}{v_c}\left(\frac{r_{crit}}{l}\right)^{\frac{2}{5}} > \mathrm{Re}_c \to \left(\frac{v_0}{v_c}\right)^{\frac{5}{2}} > \mathrm{Re}_c \tag{5.31}$$

We therefore have

$$1 > \frac{v_0}{v_c} > \mathrm{Re}_c^{\frac{2}{5}}. \tag{5.32}$$

As $\mathrm{Re}_c \sim 10^3$, this is a contradiction, so it appears that this crossover behavior cannot happen. This could just be a result of one of our assumptions being too strong, however: we have taken the onset of shear turbulence to occur precisely at the point where, were it to happen, it would be dominant over convective turbulence. The necessary assumption, however, is only that it occurs below the scale at which it takes over and above the scale of L_B. Thus the criterion should be

$$r_{crit} < l\left(\frac{v_0}{v_c}\right)^{\frac{15}{4}} \to r_{crit} = \xi l\left(\frac{v_0}{v_c}\right)^{\frac{15}{4}}, \xi \leq 1 \tag{5.33}$$

$$\mathrm{Re} = \frac{\left(\frac{v_0}{l}\right) r_{crit}}{v_c\left(\frac{r_{crit}}{l}\right)^{\frac{3}{5}}} = \frac{v_0}{v_c}\left(\frac{r_{crit}}{l}\right)^{\frac{2}{5}} > \mathrm{Re}_c \to \xi^{\frac{2}{5}}\left(\frac{v_0}{v_c}\right)^{\frac{5}{2}} > \mathrm{Re}_c \tag{5.34}$$

$$\therefore \xi > \mathrm{Re}_c^{5/2}\left(\frac{v_0}{v_c}\right)^{-25/4} \to r_{crit} = l\left(\mathrm{Re}_c\frac{v_c}{v_0}\right)^{5/2}, \tag{5.35}$$

with the condition that the crossover behavior occurs only when

$$r_{crit} \geq L_B, 1 \geq \xi > \mathrm{Re}_c^{5/2}\left(\frac{v_c}{v_0}\right)^{25/4}. \tag{5.36}$$

Using $\mathrm{Re}_c \sim 10^3$ we find roughly

$$1 \geq \xi > 10\left(\frac{v_c}{v_0}\right)^{25/4}. \tag{5.37}$$

Given that $v_c > v_0$ we find that the above is a contradiction, and hence that the crossover behavior cannot happen. This confirms the conclusion from our earlier, somewhat simpler analysis.

5.2 Non-Convective Shear

Consider now the regime of shear flow in the absence of convection. Let the vertical shear be v_0 across a scale height, and let the horizontal shear be v_x across a distance x.

Suppose first that the flow is shear-unstable. This is a common state of affairs in the radiative zone[7], mainly due to the absence of a large turbulent viscosity. Recall that the Richardson criterion is

$$\frac{v\Delta z}{(\alpha+\nu_h)}N_T^2 + \frac{v\Delta z}{\nu_h}N_\mu^2 < \left(\frac{dv}{dz}\right)^2, \tag{5.38}$$

where v and Δz are the speed and size of the largest eddies which are isotropic, ν_h is the turbulent viscosity for horizontal motions, α is the thermal diffusivity, and N_T and N_μ partition the Brunt-Vaisala frequency into pieces corresponding to the thermal and chemical gradients respectively. Using the usual approximation of derivatives as quotients and rearranging terms gives

$$\frac{1}{(\alpha+\nu_h)}N_T^2 + \frac{1}{\nu_h}N_\mu^2 < \frac{1}{v\Delta z}\left(\frac{v_0}{h_s}\right)^2. \tag{5.39}$$

The frequency components may be computed as[8]

$$N_T^2 = \frac{g}{h_s}\left(\nabla_{ad}-\nabla\right)\left(\frac{\partial\ln\rho}{\partial\ln T}\right)_{p,\mu} = \frac{g}{h_s}\left(\nabla_{ad}-\nabla\right) \tag{5.40}$$

and

$$N_\mu^2 = \frac{g}{h_s}\left(\frac{\partial\ln\rho}{\partial\ln\mu}\right)_{p,T}\left(\frac{d\ln\mu}{d\ln p}\right) = \frac{g}{h_s}\left(\frac{d\ln\mu}{d\ln p}\right). \tag{5.41}$$

Note that the derivatives involving μ here are compositional derivatives, taken ignoring ionization effects. As we are generally neglecting compositional effects, we may just set $N_\mu^2 = 0$.

[7] S. Mathis, A. Palacios, and J.-P. Zahn. "On shear-induced turbulence in rotating stars". In: *Astronomy and Astrophysics* 425.1 (2004), pp. 243–247. DOI: 10.1051/0004-6361:20040279. eprint: http://arxiv.org/abs/astro-ph/0403580. URL: http://dx.doi.org/10.1051/0004-6361:20040279; A. Maeder. "Stellar rotation: Evidence for a large horizontal turbulence and its effects on evolution". In: *Astronomy and Astrophysics* 399.1 (2003), pp. 263–269. DOI: 10.1051/0004-6361:20021731. eprint: http://arxiv.org/abs/astro-ph/0301258. URL: http://dx.doi.org/10.1051/0004-6361:20021731.

[8] V. M. Canuto. "Turbulence in Stars. II. Shear, Stable Stratification, and Radiative Losses". In: *The Astrophysical Journal* 508.2 (1998), p. 767. URL: http://stacks.iop.org/0004-637X/508/i=2/a=767.

Putting all of this in the Richardson criterion yields

$$\frac{(\nabla_{ad} - \nabla)}{(\alpha + \nu_h)} < \frac{h_s}{gv\Delta z}\left(\frac{v_0}{l}\right)^2. \tag{5.42}$$

The vertical viscosity, ν_v may be viewed as set by saturating this criterion with $v\Delta z$, as this sets the size of the largest isotropic eddies. In the context of our previous scaling arguments this may be viewed as one of the fixed points of the renormalization process. Thus,

$$\nu_v = \frac{h_s v_0^2}{gl^2}\frac{\alpha + \nu_h}{\nabla_{ad} - \nabla}. \tag{5.43}$$

The interpretation of this result is somewhat subtle, and hence worth examining in detail. Suppose first that a flow has a velocity shear which makes it Reynolds unstable in both the vertical and horizontal directions. The Richardson criterion as stated indicates that there will be turbulence, but that the vertical action of the turbulence will be limited in its viscosity by the requirement that the criterion hold.

Now suppose that the shear is insufficient make the system unstable vertically in the Reynolds sense, but sufficient to make it unstable horizontally in the same sense. The vertical viscosity will then be the maximum of the turbulent viscosity again from the Richardson criterion and the microscopic viscosity. Here the Richardson criterion plays the role of suppressing the vertical extent of the turbulent eddies created by the horizontal shear.

Now if the horizontal shear is insufficient to make the system Reynolds unstable but the vertical shear is, the eddies will be dominated by the vertical shear. The anisotropy which forced us to consider the horizontal viscosity separately from the vertical value is not relevant in this case, as horizontally-generated turbulence must fight the buoyant effects in one direction and not in the other, while vertically generated turbulence is from the start fighting these effects. Setting $\nu_h = \nu_v$ yields then

$$\nu_h = \frac{\alpha v_0^2}{N_T^2 l^2}. \tag{5.44}$$

If neither shear suffices to make the system Reynolds unstable, then the viscosity in both directions is just the microscopic viscosity.

As a final note, whenever the horizontal viscosity is not simply the microscopic value, we need to specify it to close the equation specifying the vertical viscosity. This is done by letting

$$\nu_h = v_h x, \tag{5.45}$$

though it is left to the specific physical circumstances to determine x and v_h. We will address this question as it arises.

References

A. Maeder. “Stellar rotation: Evidence for a large horizontal turbulence and its effects on evolution”. In: *Astronomy and Astrophysics* 399.1 (2003), pp. 263–269. DOI: 10.1051/0004-6361:20021731. eprint: http://arxiv.org/abs/astro-ph/0301258. URL: http://dx.doi.org/10.1051/0004-6361:20021731 (cit. on p. 75).

Adzhemyan, L. Ts. et al. “Renormalization-group approach to the stochastic Navier Stokes equation: Two-loop approximation”. In: *International Journal of Modern Physics B* 17.10 (2003), pp. 2137–2170. DOI: 10.1142/S0217979203018193. eprint: http://www.worldscientific.com/doi/pdf/10.1142/S0217979203018193. URL: http://www.worldscientific.com/doi/abs/10.1142/S0217979203018193 (cit. on p. 67).

Barbi, Dirk and Gernot Munster. *Renormalization Group Analysis of Turbulent Hydrodynamics*. May 2013. URL: http://arxiv.org/abs/1012.0461 (cit. on p. 67).

Boffetta, G et al. *Kolmogorov and Bolgiano scaling in thermal convection: the case of Rayleigh-Taylor turbulence*. Tech. rep. arXiv:1101.5917. Comments: 4 pages, 5 figures. Feb. 2011. URL: http://arxiv.org/pdf/1101.5917.pdf (cit. on p. 68).

Brown, R. A. “Longitudinal instabilities and secondary flows in the planetary boundary layer: A review”. In: *Reviews of Geophysics* 18.3 (1980), pp. 683–697. ISSN: 1944-9208. DOI: 10.1029/RG018i003p00683. URL: http://dx.doi.org/10.1029/RG018i003p00683 (cit. on p. 66).

Canuto, V. M. “Turbulence in Stars. II. Shear, Stable Stratification, and Radiative Losses”. In: *The Astrophysical Journal* 508.2 (1998), p. 767. URL: http://stacks.iop.org/0004-637X/508/i=2/a=767 (cit. on p. 75).

Ching, Emily S. C. et al. “Scaling behavior in turbulent Rayleigh-Bénard convection revealed by conditional structure functions”. In: *Phys. Rev. E* 87 (1 Jan. 2013), p. 013005. DOI: 10.1103/PhysRevE.87.013005. URL: http://link.aps.org/doi/10.1103/PhysRevE.87.013005 (cit. on p. 68).

Lohse, Detlef and Ke-Qing Xia. “Small-Scale Properties of Turbulent Rayleigh-Benard Convection”. English. In: *Annual Review Of Fluid Mechanics*. Annual Review of Fluid Mechanics 42 (2010), pp. 335–364. ISSN: 0066-4189. DOI: 10.1146/annurev.fluid.010908.165152 (cit. on p. 68).

Mergui, S., X. Nicolas, and S. Hirata. “Sidewall and thermal boundary condition effects on the evolution of longitudinal rolls in Rayleigh-Bénard-Poiseuille convection”. In: *Physics of Fluids (1994-present)* 23.8, 084101 (2011), pages. DOI: http://

dx.doi.org/10.1063/1.3605698. URL: http://scitation.aip.org/content/aip/journal/pof2/23/8/10.1063/1.3605698 (cit. on p. 66).

Rincon, F. *Theories of convection and the spectrum of turbulence in the solar photosphere*. Tech. rep. astro-ph/0611842. Contribution to the proceedings : 239 Convection in Astrophysics, International Astronomical Union., held 21-25 August, 2006 in Prague, Czech Republic. Nov. 2006. eprint: http://arxiv.org/pdf/astro-ph/0611842.pdf. URL: http://cds.cern.ch/record/1001690/files/0611842.pdf (cit. on p. 68).

S. Mathis, A. Palacios, and J.-P. Zahn. "On shear-induced turbulence in rotating stars". In: *Astronomy and Astrophysics* 425.1 (2004), pp. 243–247. DOI: 10.1051/0004-6361:20040279. eprint: http://arxiv.org/abs/astro-ph/0403580. URL: http://dx.doi.org/10.1051/0004-6361:20040279 (cit. on p. 75).

Škandera, Dan, Angela Busse, and Wolf-Christian Müller. *Scaling Properties of Convective Turbulence*. English. Ed. by Siegfried Wagner et al. Springer Berlin Heidelberg, 2009, pp. 387–396. ISBN: 978-3-540-69181-5. DOI: 10.1007/978-3-540-69182-2_31. URL: http://dx.doi.org/10.1007/978-3-540-69182-2_31 (cit. on p. 68).

Yakhot, Victor and StevenA. Orszag. "Renormalization group analysis of turbulence. I. Basic theory". English. In: *Journal of Scientific Computing* 1.1 (1986), pp. 3–51. ISSN: 0885-7474. DOI: 10.1007/BF01061452. URL: http://dx.doi.org/10.1007/BF01061452 (cit. on p. 67).

Zhou, Ye, David W. McComb, and George Vahala. "Renormalization Group (RG) in Turbulence: Historical and Comparative Perspective". In: (Aug. 1997). URL: http://ntrs.nasa.gov/archive/nasa/casi.ntrs.nasa.gov/19970028852.pdf (cit. on p. 67).

6

Global Wind Patterns

More is different.

– P.W. Anderson

In the previous chapter we discussed notions of local stability in an attempt to determine the properties of winds on length scales of order l and below. We now turn to length scales of order R to determine the global flow pattern. We will use as our building blocks the flow patterns at scales of order l.

6.1 Turbulent Zonal Flow

It has long been known that the gas giant planets in our own solar system organize their winds, at least on the surface, into zonal jets. These jetstreams are both stable against perturbations with spherical harmonic number $m \neq 0$ and exhibit a characteristic energy scaling in the total spherical harmonic number n, namely as n^{-5}[1]. Note that m and n are defined as in the spherical harmonic Y_n^m, such that $-n \leq m \leq n$. This phenomenon was first explained by Peter Rhines[2] in the

[1]Boris Galperin, Semion Sukoriansky, and Huei-Ping Huang. "Universal n-5 spectrum of zonal flows on giant planets". In: *Physics of Fluids (1994-present)* 13.6 (2001), pp. 1545–1548. DOI: http://dx.doi.org/10.1063/1.1373684. URL: http://scitation.aip.org/content/aip/journal/pof2/13/6/10.1063/1.1373684; Semion Sukoriansky, Boris Galperin, and Nadejda Dikovskaya. "Universal Spectrum of Two-Dimensional Turbulence on a Rotating Sphere and Some Basic Features of Atmospheric Circulation on Giant Planets". In: *Phys. Rev. Lett.* 89 (12 Aug. 2002), p. 124501. DOI: 10.1103/PhysRevLett.89.124501. URL: http://link.aps.org/doi/10.1103/PhysRevLett.89.124501.

[2]Peter B. Rhines. "Waves and turbulence on a beta-plane". In: *Journal of Fluid Mechanics* 69 (03 June 1975), pp. 417–443. ISSN: 1469-7645. DOI: 10.1017/S0022112075001504. URL:

paper which established the Rhines arrest of the inverse energy cascade characterizing Kolmogorov turbulence. This has been investigated in a variety of contexts, ranging from experimental[3] to simulational[4], and has been found to be a universal property of quasi two-dimensional turbulence on a rotating sphere. The arrest is, contrary to the original claims by Rhines, not quite a halting of the cascade. Rather, in the absence of friction, the β effect merely slows the cascade of energy to longer length scales. Frictional effects have been found[5] to be responsible for the actual halting of the energy flow. The properties of the Rhines spectrum, as well as the conditions under which it arises, are the subject of this section.

The Rhines wavenumber is defined as[6]

$$k_R \equiv \sqrt{\frac{\Omega}{R v_0}}, \tag{6.1}$$

and the β-effect wavenumber is given by

$$k_\beta \equiv \left(\frac{\Omega^3}{R^3 \varepsilon} \right)^{1/5}, \tag{6.2}$$

where ε is the energy input per unit mass into the system. The driving force is typically assumed to be present either at all length scales, or just at the smallest length scales. Historically there has been some uncertainty as to which of k_R and k_β

http://journals.cambridge.org/article_S0022112075001504.

[3]J.M. Nguyen Duc, Ph. Caperan, and J. Sommeria. "An Experimental Study of the Inverse Cascade of Energy in Two-Dimensional Turbulence". English. In: *Advances in Turbulence*. Ed. by Geneviève Comte-Bellot and Jean Mathieu. Springer Berlin Heidelberg, 1987, pp. 265–268. ISBN: 978-3-642-83047-1. DOI: 10.1007/978-3-642-83045-7_30. URL: http://dx.doi.org/10.1007/978-3-642-83045-7_30; D. H. Atkinson, J. B. Pollack, and A. Seiff. "The Galileo probe Doppler wind experiment: Measurement of the deep zonal winds on Jupiter". In: *Journal of Geophysical Research* 103 (Sept. 1998), pp. 22911–22928. DOI: 10.1029/98JE00060.

[4]Sergey Danilov and David Gurarie. "Rhines scale and spectra of the β-plane turbulence with bottom drag". In: *Phys. Rev. E* 65 (6 June 2002), p. 067301. DOI: 10.1103/PhysRevE.65.067301. URL: http://link.aps.org/doi/10.1103/PhysRevE.65.067301; Seimion Sukoriansky, Nadejda Dikovskaya, and Boris Galperin. "On the Arrest of Inverse Energy Cascade and the Rhines Scale". In: *Journal of the Atmospheric Sciences* 64 (2006). URL: http://journals.ametsoc.org/doi/abs/10.1175/JAS4013.1; S. Danilov and D. Gurarie. "Scaling, spectra and zonal jets in beta-plane turbulence". In: *Physics of Fluids* 16 (July 2004), pp. 2592–2603. DOI: 10.1063/1.1752928; J. Verhoeven and S. Stellmach. "The compressional beta effect: A source of zonal winds in planets?" In: *Icarus* 237 (July 2014), pp. 143–158. DOI: 10.1016/j.icarus.2014.04.019. arXiv: 1404.6940 [astro-ph.EP].

[5]Danilov and Gurarie, op. cit.; Sukoriansky, Dikovskaya, and Galperin, op. cit.

[6]Sukoriansky, Galperin, and Dikovskaya, op. cit.

actually controls zonal flows, but this is actually a misguided question, for there is another quantity which plays a significant role. This is the frictional wavenumber, given by

$$k_{fr} \equiv (3C_k)^{3/2} \left(\frac{\lambda^3}{\varepsilon}\right)^{1/2}, \tag{6.3}$$

where C_k is a constant, roughly equal to 6[7], and

$$\lambda \equiv \frac{d \ln E}{dt}, \tag{6.4}$$

with E being the specific kinetic energy of the wind and the time derivative being taken assuming no power input into E. It is actually the combination of the frictional, Rhines, and β effect wavenumbers which controls the properties of zonal flows[8].

The Rhines cascade is then understood in the following way. Energy is injected at very short length scales (large k). Energy present at the length scale set by k_β or above ($k < k_\beta$) proceeds to march to longer length scales in the inverse cascade. This process halts when the energy reaches k_{fr}, for there the energy is transported to $k > k_\beta$ and hence transformed into heat. As a result, if $k_\beta > k_{fr}$, we expect energy to pile-up near k_{fr}. It can be shown that the pile-up actually occurs at k_R, which is proportional in the steady-state to k_{fr} with proportionality constant quite close to unity[9]. Due to anisotropy in the cascade, this energy preferentially piles up in the $m = 0$, $n = Rk_{fr}$ mode, leading to jetstreams following lines of constant latitude circling the star. On the other hand, if $k_\beta < k_{fr}$, the inverse cascade cannot proceed, for all of the modes which would undergo it have lost their energy to friction. In this case, Kolmogorov-style turbulence dominates at all scales.

There are two reasons that we are careful to make a distinction between k_R and k_{fr} despite their general steady-state interchangeability. The first is that physically, the distinction reveals that the underlying cause of the arrest of the inverse cascade lies with friction, rather than Rossby wave instability[10]. The second is that while they are close in the steady-state, the transient case with ε making a sudden change and then remaining constant reveals that they are not always the same. In particular, upon making a change to the driving force, it takes some time for the velocity profile to adapt. During this time, k_R and k_{fr} will disagree quite strongly, for the former

[7] Ibid.

[8] Idem, "Universal Spectrum of Two-Dimensional Turbulence on a Rotating Sphere and Some Basic Features of Atmospheric Circulation on Giant Planets"; Sukoriansky, Dikovskaya, and Galperin, op. cit.

[9] Idem, "On the Arrest of Inverse Energy Cascade and the Rhines Scale".

[10] Ibid.

tracks the velocity profile while the latter tracks the driving force. The two come to terms on timescales of order λ^{-1}, and so on timescales shorter than these the number of bands, determined by k_R, may deviate significantly from the steady-state value suggested by k_{fr}[11]. Generally, this manifests as k_R beginning very large and then shrinking to assume the proper proportionality with k_{fr}, at which point the final number of bands is achieved. In all problems of interest, we will verify that the relevant transient timescales are greater than λ^{-1}, and hence that we may neglect this effect.

In addition to being careful about timescales, we must also be cautious regarding dimensionality. A key assumption underlying the Rhines cascade is that the flow is quasi-two-dimensional. This assumption is valid in any system with significant pressure stratification, such that we do not expect winds which go significantly against the pressure gradient. To state this formally, suppose that we follow the path of some fluid as it performs a closed loop around the star. Let the mean pressure of the fluid along the loop be P_0. Let Δs be the maximum distance between the path of the fluid and the isobaric surface at P_0. We require then that

$$\Delta s \ll R, \tag{6.5}$$

such that the deviations are not relevant on the global scale. Note that we have implicitly treated the flow as occurring on top of an averaged flow background in speaking of isobaric surfaces. This is the usual way to examine fluctuations in a renormalized theory, but it can lead to incorrect conclusions when not kept in mind.

Now we may estimate Δs as

$$\Delta s \approx \frac{\rho v_0^2}{|\nabla P|} = l\frac{\rho v_0^2}{P} = l\gamma\frac{v_0^2}{v_s^2}. \tag{6.6}$$

As $l \ll R$, γ is of order unity, and $v_0 < v_s$, the last of these coming from the immense shock losses associated with supersonic flow, we find that the criterion in Eq. (6.5) will always be satisfied. Thus it is only the transient criterion we ever need check.

6.2 Alternative Patterns

In the case where $k_\beta < k_{fr}$, and in the presence of turbulence, there is no energy available at the modes which may contribute to the Rhines cascade. As a result, no pile-up of energy occurs at k_R. Additionally, the lack of an anisotropic cascade

[11] Ibid.

in momentum-space means that the turbulence ought to be isotropic except on the largest scales, where the pattern of flow is determined by the driving force. Likewise, if there is no turbulence, the flow is just determined by the driving and boundary conditions at length scales of order R.

Given that we are interested in cases where a star is being heated on one side but not the other, we expect that the tendency will be to have wind flow in the $\hat{\phi}$ direction, driven by a temperature differential. Precisely what happens is determined by the Rossby number, which supports two distinct limits. For $\mathrm{Ro} \gg 1$, taking the length scale to be R, the Coriolis force is negligible on the scale of the star, and so the wind can simply flow around along $\hat{\phi}$. On the other hand, if $\mathrm{Ro} \ll 1$, once more taking the length scale to be R, the Coriolis force is important, and will tend to wrap the wind into hurricanes. If the flow is turbulent, we will refer to these as Kolmogorov hurricanes, for then they support the familiar structure of nested vortices on many length scales.

6.2.1 Large Rossby Number

When the Rossby number is large, the wind moves in an essentially ballistic manner. As we have argued in discussing the Rhines scale, the flow may be considered to be quasi-two-dimensional, as we take the wind to move along isobars. Note that in this limit the rotation of the star is largely irrelevant. As a result, the system is axisymmetric about the line connecting the pulsar and the companion. In analyzing this case, then, we eschew our standard conventions for $\hat{z}$ and instead take $\hat{z}$ to lie along this line. The angular coordinates θ and ϕ are then redefined accordingly, so v_θ is now the wind speed from one side of the star to the other, while v_ϕ measures the wind speed along the symmetric direction.

Suppose that the star has some temperature differential ΔT between the day and night sides[12]. Then in moving around the star, the wind acts as a heat engine. The specific power it moves is given by

$$\varepsilon' = c_p \boldsymbol{v} \cdot \boldsymbol{\nabla} T. \tag{6.7}$$

Now the rate at which the wind may extract work from this process is just the heat engine efficiency multiplied by the specific power. Using the endoreversible heat engine efficiency, a common approximation used in place of the maximal Carnot

[12]This is equivalent to speaking about the amplitude of the first nontrivial spherical harmonic.

efficiency for real-world systems, we find that

$$\dot{W} = \left(1 - \sqrt{1 - \frac{\Delta T}{T}}\right)(c_p \boldsymbol{v} \cdot \boldsymbol{\nabla} T) \approx \frac{\Delta T}{2T}(c_p \boldsymbol{v} \cdot \boldsymbol{\nabla} T), \tag{6.8}$$

and so approximating the gradient yields

$$\dot{W} = \frac{c_p v_\theta \Delta T^2}{2\pi R T} = \frac{v_s^2 v_\theta}{2\pi R}\left(\frac{\Delta T}{T}\right)^2 \left(\frac{k_B}{c_v \mu}\right), \tag{6.9}$$

where the final term on the right is $3/2$ for an ideal gas and of order unity generally. The intuitive picture here is that the wind moves to the hot side of the star, picks up heat, and then moves to the cold side to release it. It then moves back to the hot side to warm up again, and the process repeats.

There are a variety of structures that the global flow could take on. One would simply be to set v_θ to some uniform nonzero value. Given that there is nothing driving the flow in the $\hat{\phi}$ direction, and no spontaneous symmetry breaking, we may then set $v_\phi = 0$ up to turbulent corrections. This has the disadvantage of causing a net mass flux across the star. This could be remedied by setting v_θ to some value which varies as a periodic function of ϕ, spontaneously breaking the axisymmetry. There is, however, no physical process giving the ϕ scale for this symmetry breaking. Additionally, this solution leads to a singularity in the continuity equation near the poles, which is somewhat harder to remove.

There are two natural ways to correct the problems uncovered in the previous examples. The first would be to make use of Hadley cells. These preserve axisymmetry and require no additional length scale. They respect the isobaric nature of the flow up to corrections of order h_s[13], but have the advantage that there is no longer a singularity in the continuity equation. The other possibility is to assume once more circumferential transport. The axis along which the the transport aligns would be set by some combination of the weak residual effects of rotation and the magnetic anisotropy in the underlying microscopic viscosity, both of which will tend to weakly align it with the star's rotation axis. The question is then of whether or not all of the gas moves with the same handedness around the star. There is no physical process which breaks the symmetry here, so if there are zones with alternating handedness we expect the scale of alternation to be R. In either case, we refer to the relevant speed as v_θ.

[13]That is, they have deviations of order h_s.

Using the above results, we may equate $\dot{W}$ totaled over a spherical shell of thickness l with the specific power lost to viscous drag, giving

$$4\pi R^2 l \frac{v_\theta v_s^2 \Delta T^2}{2\pi R T^2} = v_\theta^2 \left(4\pi R^2 \nu_v l^{-1} + 2\pi R l v^2 \nu_h R^{-1}\right)\left(\frac{k_B}{c_v \mu}\right) \tag{6.10}$$

$$= 2\pi l \nu_h v_\theta^2 \left(1 + 2\left(\frac{R}{l}\right)^2 \frac{\nu_v}{\nu_h}\right)\left(\frac{k_B}{c_v \mu}\right) \tag{6.11}$$

$$\therefore R v_s^2 \frac{\Delta T^2}{\pi T^2} = \nu_h v_\theta \left(1 + 2\left(\frac{R}{l}\right)^2 \frac{\nu_v}{\nu_h}\right)\left(\frac{k_B}{c_v \mu}\right). \tag{6.12}$$

Note that because $\dot{W}$ is always a small fraction of ε, we do not need to worry about including heat produced by viscous effects in the calculation of heat transport.

We must now consider the radiative and convective cases separately. In the radiative case,

$$\nu_h = v_\theta R \tag{6.13}$$

and

$$\nu_v = v_\theta^2 \frac{\alpha + \nu_h}{g l \aleph \left(\nabla_{ad} - \nabla\right)}. \tag{6.14}$$

As a result, we may write

$$v_s^2 \frac{\Delta T^2}{\pi T^2} = v_\theta^2 \left(1 + 2\left(\frac{R}{l}\right)^2 \left(1 + \frac{\alpha}{v_h}\right)\left(\frac{v_\theta^2}{g\aleph l}\right)\right)\left(\frac{k_B}{c_v \mu}\right) \tag{6.15}$$

$$= v_\theta^2 \left(1 + 2\left(\frac{R}{l}\right)^2 \left(1 + \frac{\alpha}{\nu_h}\right)\left(\frac{v_\theta^2}{v_s^2}\right)\left(\frac{\gamma}{\aleph^2}\right)\right)\left(\frac{k_B}{c_v \mu}\right) \tag{6.16}$$

$$= v_\theta^2 \left(1 + 2\left(\frac{R}{l}\right)^2 \left(1 + \frac{k}{\rho c_p v_\theta R}\right)\left(\frac{v_\theta^2}{v_s^2}\right)\left(\frac{\gamma}{\aleph^2}\right)\right)\left(\frac{k_B}{c_v \mu}\right). \tag{6.17}$$

Now note that

$$\frac{k}{\rho c_p v_\theta R} = \frac{F}{\rho c_p v_\theta R |\partial_r T|} = \frac{F P}{\rho c_p v_\theta R \nabla T |\partial_r P|} = \frac{F h_s}{\rho c_p T v_\theta R \nabla} = \frac{F}{v_\theta g R \rho \nabla}\left(\frac{k_B}{\mu c_p}\right). \tag{6.18}$$

The last term and ∇ are both of order unity. The flux is generally within two orders of magnitude of $10^{12}\mathrm{erg/cm^2}$, R is within an order of magnitude of 10^{10}cm, g is close to $10^4\mathrm{cm/s^2}$, so this term may be written roughly as $v_\theta^{-1}\rho^{-1}10^{-2}\mathrm{g/cm^2/s}$. In the limit of fast winds, we expect this to be small, and hence may neglect the vertical shear, while for slower winds or lower densities we may neglect the horizontal shear.

Regardless, solving for v_θ yields

$$v_\theta = \sqrt{\frac{\sqrt{1 + 8v_s^2 \frac{\Delta T^2}{\pi T^2} \left(\frac{c_v \mu}{k_B}\right) \left(\frac{R}{l}\right)^2 \left(1 + \frac{k}{\rho c_p v_\theta R}\right) \left(\frac{v_\theta^2}{v_s^2}\right) \left(\frac{\gamma}{\aleph^2}\right)} - 1}{4 \left(\frac{R}{l}\right)^2 \left(1 + \frac{k}{\rho c_p v_\theta R}\right) \left(\frac{v_\theta^2}{v_s^2}\right) \left(\frac{\gamma}{\aleph^2}\right)}}. \tag{6.19}$$

This may be simplified by dropping factors of $\aleph, \gamma, c_v\mu/k_B$, all of which are quite close to unity, and by assuming $\Delta T/T$ to be small. Doing so yields

$$v_\theta = v_s \frac{\Delta T}{\pi T}. \tag{6.20}$$

The heat transported is therefore

$$\varepsilon' = v_\theta c_p \frac{\Delta T}{\pi R} = \frac{1}{\pi R} v_s c_p T \left(\frac{\Delta T}{T}\right)^2 \approx \frac{v_s^3}{\pi R} \left(\frac{\Delta T}{T}\right)^2. \tag{6.21}$$

On the other hand, in the convective case

$$\nu_v = l \max\left(v_c, v_\theta\right), \tag{6.22}$$

while

$$\nu_h = \max\left(l v_c, R v_\theta\right). \tag{6.23}$$

As $R > l$, their ratio is 1 for $l v_c < R v_\theta$, R/l for $v_\theta > v_c$, and $R v_\theta / l v_c$ in between. As $R \gg l$, then, the term $(R/l)^2 \nu_h/\nu_v$ is always dominant over unity, so we may write

$$R v_s^2 \frac{\Delta T^2}{2\pi T^2} = \nu_v v_\theta \left(\frac{R}{l}\right)^2 \left(\frac{k_B}{c_v \mu}\right). \tag{6.24}$$

Once more we will drop the rightmost term, for it should be very close to unity. This done, we may substitute in the expression for ν_v and find

$$v_s^2 \left(\frac{\Delta T}{T}\right)^2 \left(\frac{l}{R}\right) = 2\pi v_\theta \max\left(v_c, v_\theta\right). \tag{6.25}$$

To solve this, we first assume $v_c > v_\theta$. This yields

$$v_\theta = \frac{v_s^2}{2\pi v_c} \left(\frac{\Delta T}{T}\right)^2 \left(\frac{l}{R}\right). \tag{6.26}$$

If this exceeds v_c then we next take $v_c < v_\theta$ and find

$$v_\theta = v_s \frac{\Delta T}{T} \sqrt{\frac{l}{2\pi R}}. \tag{6.27}$$

If $v_c > v_\theta$ then

$$\varepsilon' = v_\theta c_p \frac{\Delta T}{\pi R} = \frac{v_s^2 c_p T}{2\pi R v_c} \left(\frac{l}{R}\right) \left(\frac{\Delta T}{T}\right)^3 \approx \frac{v_s^4}{2\pi R v_c} \left(\frac{l}{R}\right) \left(\frac{\Delta T}{T}\right)^3, \tag{6.28}$$

while in the other case

$$\varepsilon' = v_\theta c_p \frac{\Delta T}{\pi R} = \frac{v_s c_p T}{\pi R} \left(\frac{\Delta T}{T}\right)^2 \sqrt{\frac{l}{2\pi R}} \approx 2 l^{-1} v_s^3 \left(\frac{l}{2\pi R}\right)^{3/2} \left(\frac{\Delta T}{T}\right)^2. \tag{6.29}$$

The similar structure of all of the heat transport equations indicates that we may simplify, and write them each as

$$\varepsilon' = \xi l^{-1} v_s^3, \tag{6.30}$$

where ξ is a dimensionless quantity given in the radiative case as

$$\xi = 2 \left(\frac{l}{2\pi R}\right) \left(\frac{\Delta T}{T}\right)^2, \tag{6.31}$$

in the convective $v_c > v_\theta$ case as

$$\xi = 2\pi \frac{v_s}{v_c} \left(\frac{l}{2\pi R}\right)^2 \left(\frac{\Delta T}{T}\right)^3, \tag{6.32}$$

and in the convective $v_c < v_\theta$ case as

$$\xi = 2 \left(\frac{l}{2\pi R}\right)^{3/2} \left(\frac{\Delta T}{T}\right)^2. \tag{6.33}$$

From the form of ξ we may gain some intuition about the system. To begin, note that ξ/l depends on l only in the convective case. This is because in the convective case the nature of the turbulence which resists moving heat circumferentially depends on l, whereas in the radiative case this dependence is not there, for the turbulence there depends only on the Richardson viscosity scale. Additionally, $l/2\pi R$ is typically of order 10^{-3}, while v_s/v_c is typically of order 10^3. If $\Delta T/T$ is smaller than unity, we see that the most efficient transport comes when the turbulence is suppressed by entropic stratification, as in the radiative case.

Note that the above expressions were derived assuming $\Delta T/T$ is somewhat smaller than unity. The functional forms become somewhat more complicated as the temperature difference increases, so we will keep in mind that there could be deviations from the above behavior and use them primarily as guidelines for intuition and estimation. Having said that, note that l/R is generally on the order of 10^{-3}, and v_s/v_c is generally not more than 10^3, so all of the cases considered thus far indicate that v_θ approaches v_s as ΔT approaches T. This behavior is expected regardless of the underlying turbulent model, so the fact that it occurs in all of the cases indicates that we are not missing substantial qualitative physics. Furthermore, when $v_\theta > v_s$, we simply substitute $v_\theta = v_s$ to get the correct physics, for winds generally cannot travel much above the sound speed without incurring tremendous losses. In this case,

$$\varepsilon' = v_\theta c_p \frac{\Delta T}{\pi R} \approx \frac{v_s^3 \Delta T}{\pi R T}. \tag{6.34}$$

6.2.2 Small Rossby Number

When the Rossby number for motion on scales of order R is small, the Coriolis force is extremely important, and will generally deflect winds into hurricanes. To see this, suppose that a wind is flowing with velocity $\boldsymbol{v}$. The Coriolis acceleration it experiences is

$$\boldsymbol{a} = 2\boldsymbol{v} \times \boldsymbol{\Omega}, \tag{6.35}$$

where $\boldsymbol{\Omega}$ is the angular velocity of the region of the star of interest about the stellar rotation axis, neglecting the contribution of the wind. As the wind follows isobaric surfaces, this acceleration must be projected onto these surfaces. This yields circular motion, for the acceleration is always perpendicular to the motion as a result of the cross product, and the radius is given by

$$r_{rot} = \frac{v}{2\Omega \cos\theta}. \tag{6.36}$$

The resulting motion is a hurricane with a Rossby number of one. As the star will be dominated by these storms in this limit, we are looking at a diffusive process with thermal diffusion constant

$$k = \rho c_p v r_{rot} = \frac{\rho c_p v^2}{2\Omega \cos\theta}. \tag{6.37}$$

The flux is $k\nabla T$. The circumferential part of this is

$$F \approx k\frac{\Delta T}{\pi R}. \tag{6.38}$$

A spherical shell of thickness dz then transmits power $2\pi R dz F$. Averaging this over the mass of the shell gives

$$\varepsilon = \frac{2\pi R dz F}{2\pi R^2 \rho dz} = \frac{k\Delta T}{\rho \pi R^2} = \frac{c_p v r_{rot} \Delta T}{\pi R^2} \approx \frac{r_{rot} v v_s^2 \Delta T}{\pi R^2 T}. \tag{6.39}$$

Note that the factor of two in the denominator rather than four arises because ε is the specific power removed from one side of the star and added to the other, so we use half of the area of the star.

Before addressing the problem of determining v, it is worth discussing the divergence of all of our expressions at $\theta = \pi/2$. At the equator of the star, geostrophic winds experience no Coriolis force. As a result, this region is automatically excluded from the low Rossby number regime, and so our results from the previous section should be used for low latitudes. To be formal, let $\theta_\pm$ be the angles at which $v/2\Omega R\cos\theta$ equals unity. Between these angles, we should use the ballistic high-Rossby number results. Outside of this range, the hurricane diffusion result should be used.

Returning, then, to the question of v, we must once more compute a balance between the work the wind may extract as it shuffles heat around and the power lost to viscous effects. By the same reasoning in the previous section, we find that

$$\dot{W} = \frac{v_s^2 v^2 \Delta T^2}{4\pi R T^2 \Omega \cos\theta}. \tag{6.40}$$

As $r_{rot} \ll R$, we compute the viscous losses over a single hurricane, giving

$$2r_{rot} l \frac{v_s^2 v^2 \Delta T^2}{4\pi R T^2 \Omega \cos\theta} = v^2 \left(\pi r_{rot}^2 \nu_v l^{-1} + 2\pi r_{rot} l \nu_h r_{rot}^{-1}\right) \tag{6.41}$$

$$\therefore \frac{v_s^2 \Delta T^2}{2\pi^2 R r_{rot} T^2 \Omega \cos\theta} = \left(\nu_v l^{-2} + 2\nu_h r_{rot}^{-2}\right). \tag{6.42}$$

Here $2r_{rot}l$ is the area of the surface that the flux passes through, πr_{rot}^2 is the area associated with bottom drag, and $2\pi r_{rot} l$ is the area associated with shearing along the isobar. Now we recognize that $2r_{rot}\Omega\cos\theta = v$, so

$$\frac{v_s^2 \Delta T^2}{\pi^2 R T^2} = v\left(\nu_v l^{-2} + 2\nu_h r_{rot}^{-2}\right). \tag{6.43}$$

We must now once more consider the radiative and convective cases separately. In the radiative case, the horizontal viscosity is

$$\nu_h = v r_{rot} = \frac{v^2}{2\Omega\cos\theta}. \tag{6.44}$$

The vertical viscosity is then

$$\nu_v = v^2 \frac{\alpha + \nu_h}{gl\aleph\left(\nabla_{ad} - \nabla\right)} = v^2 \frac{\alpha + \frac{v^2}{2\Omega\cos\theta}}{gl\aleph\left(\nabla_{ad} - \nabla\right)}, \tag{6.45}$$

so the power balance is

$$\begin{aligned}
\frac{v_s^2 \Delta T^2}{\pi^2 R T^2} &= v\left(\nu_v l^{-2} + 2\nu_h r_{rot}^{-2}\right) && (6.46)\\
&= v\left(\nu_v l^{-2} + 2v r_{rot}^{-1}\right) && (6.47)\\
&= v\left(\nu_v l^{-2} + 4\Omega\cos\theta\right) && (6.48)\\
&= v\left(v^2 \frac{\alpha + \frac{v^2}{2\Omega\cos\theta}}{gl^3\aleph\left(\nabla_{ad} - \nabla\right)} + 4\Omega\cos\theta\right). && (6.49)
\end{aligned}$$

This equation is quintic and unfortunately has no analytic roots. For small $\Delta T/T$, a linear expansion suffices, yielding

$$v = \frac{v_s^2 \Delta T^2}{4\pi^2 R T^2 \Omega\cos\theta} \tag{6.50}$$

and

$$\varepsilon' = \frac{r_{rot} v v_s^2 \Delta T}{\pi R^2 T} = \frac{v^2 v_s^2 \Delta T}{2\Omega\pi R^2 T\cos\theta} = \frac{v_s^6 \Delta T^5}{32\Omega^3\pi^5 R^4 T^5 \cos^3\theta}. \tag{6.51}$$

Note that the angles $\theta_\pm$ may be computed roughly as $\pi/2 \pm \sin^{-1}(v/\Omega R)$. In computing ε', we should be averaging over θ outside of this range. Equivalently, we should be requiring that $v/2\Omega R \leq \cos\theta$, so we should average $cos^{-3}\theta$ over the range from $\cos\theta = 1$ to $\cos\theta = v/2\Omega R$. As the integration measure on a sphere is $-d(\cos\theta)$, we need only multiply ε' by

$$-\int_{v/2\Omega R}^{1} u^{-3} du = \frac{1}{2}\left(1 - \frac{v^2}{4\Omega^2 R^2}\right). \tag{6.52}$$

For small v this is generally 1/2, but for large v it approaches zero and then becomes negative, an indicator that the high Rossby number calculations are more appropriate.

We now turn to the convective case. If $v > v_c$, both the horizontal and vertical viscosities are dominated by the shearing[14]. The length scale in the vertical direction remains l, but in the horizontal direction is now r_{rot}. As a result,

$$\frac{v_s^2 \Delta T^2}{\pi^2 R T^2} = v\left(\nu_v l^{-2} + 2\nu_h r_{rot}^{-2}\right) \tag{6.53}$$

$$= v\left(v l^{-1} + 2v r_{rot}^{-1}\right) \tag{6.54}$$

$$= v^2\left(l^{-1} + 2r_{rot}^{-1}\right) \tag{6.55}$$

$$= v^2 l^{-1} + 4\Omega v \cos\theta \tag{6.56}$$

$$\therefore v = 2\Omega l \cos\theta\left(\sqrt{1 + \frac{v_s^2 \Delta T^2}{4\Omega^2 \pi^2 R l T^2 \cos^2\theta}} - 1\right) \approx \frac{v_s^2 \Delta T^2}{4\pi^2 R T^2 \Omega \cos\theta}. \tag{6.57}$$

This is precisely the result from the radiative case, and the power transmitted is the same. This is a result of the shear turbulence dominating over convection, and of the Richardson viscosity being a higher order correction in $\Delta T/T$ to v.

Now suppose that $v < v_c$. The diffusion of heat is then convection dominated even in non-radial directions. As a result, the diffusion constant is just v_c times the horizontal length scale. In the model of isotropic turbulence, we expect the characteristic length scale to be l. On the other hand, if the star is rotating very rapidly, the Coriolis effect may make this impossible. Rapid rotation can introduce an anisotropy in the convection cells[15], and so we will take the scale of this turbulence to be the minimum of r_{rot} and l, where the former is computed for v_c. First suppose

[14] We call this a Kolmogorov hurricane, for it is a hurricane which exhibits Kolmogorov turbulence at all but the largest scales. This is in contrast to in the radiative case where significant anisotropies are present across many scales, and to the convective case with $v_c > v$, which is just convective diffusivity.

[15] H. Köhler. "Differential Rotation Caused by Anisotropic Turbulent Viscosity". In: *Solar Physics* 13 (July 1970), pp. 3–18. DOI: 10.1007/BF00963937; Pierre Lesaffre et al. "A two-dimensional mixing length theory of convective transport". In: *Monthly Notices of the Royal Astronomical Society* (2013). DOI: 10.1093/mnras/stt317. eprint: http://mnras.oxfordjournals.org/content/early/2013/03/20/mnras.stt317.full.pdf+html. URL: http://mnras.oxfordjournals.org/content/early/2013/03/20/mnras.stt317.abstract; P. Garaud et al. "A model of the entropy flux and Reynolds stress in turbulent convection". In: *Monthly Notices of the Royal Astronomical Society* 407 (Oct. 2010), pp. 2451–2467. DOI: 10.1111/j.1365-2966.2010.17066.x. arXiv: 1004.3239 [astro-ph.SR]; Richard J.A.M. Stevens, Herman J.H. Clercx, and Detlef Lohse. "Heat transport and flow structure in rotating RayleighâBÃ©nard convection". In: *European Journal of Mechanics - B/Fluids* 40 (2013). Fascinating Fluid Mechanics: 100-Year Anniversary of the Institute of Aerodynamics, {RWTH} Aachen University, pp. 41–49. ISSN: 0997-7546. DOI: http://dx.doi.org/10.1016/j.euromechflu.2013.01.004. URL: http://www.sciencedirect.com/science/article/pii/S0997754613000058.

that r_{rot} is larger than l. This is the case, for instance, on the sun, which is known to exhibit giant convection cells[16]. Then the diffusivity is just $v_c l$, so the heat transported is

$$\varepsilon' = \frac{v_c l v_s^2 \Delta T}{\pi R^2 T}. \tag{6.58}$$

Now suppose that l is the larger. Then

$$\varepsilon' = \frac{v_c r_{rot} v_s^2 \Delta T}{\pi R^2 T} = \frac{v_c^2 v_s^2 \Delta T}{2\Omega\pi R^2 T \cos\theta}. \tag{6.59}$$

Now when $\Delta T \sim T$, it would appear that none of the above expansions are sufficient even qualitatively, for certain effects (such Richardson stabilization) do not appear to leading order. However, all of the models under consideration give in this case

$$v \sim \frac{v_s^2}{R\Omega}. \tag{6.60}$$

In other words, the Mach number[17] reduces to the sound speed Rossby number[18]. To get a feel for these Mach numbers, let us write R in units of $R_\odot$, Ω in units of $2\pi/1$hour, and v_s as $10^6 T_4^{1/2}$cm/s, where T_4 is the surface temperature measured in units of 10^4K. Note that we use a sound speed which is a factor of a few higher than that corresponding to 10^4K, as the temperature in the regions which transport significant heat by sonic winds is typically somewhere between a factor of one and ten higher than that at the surface. Using these values, we find that

$$\frac{v}{v_s} \sim \frac{T_4^{1/2} P_{\mathrm{hour}}}{50(R/R_\odot)}, \tag{6.61}$$

where P_{hour} is the orbital period measured in hours. As a result, we see that only for very short orbital periods can $\Delta T/T$ be of order unity with v/v_s not of the same order. If such cases arise and are of interest, they may be handled by extrapolating the scaling with $\Delta T/T$ to the point where v/v_s is of order unity. We expect to incur minimal error by doing this, as the dynamic range of this scaling is at most 50.

6.3 Deciding

We are now interested in determining when to expect Rhines scaling and when an alternate wind pattern is applicable. The condition for Rhines jetstreams is $k_\beta > k_{fr}$.

[16] D. H. Hathaway, L. Upton, and O. Colegrove. "Giant Convection Cells Found on the Sun". In: *ArXiv e-prints* (Jan. 2014). arXiv: `1401.0551 [astro-ph.SR]`.

[17] This is the ratio v/v_s.

[18] This is the ratio $v_s/R\Omega$

Using the definition of each wavenumber we find

$$\left(\frac{\Omega^3}{R^3\varepsilon}\right)^{1/5} > (3C_k)^{3/2}\sqrt{\frac{\lambda^3}{\varepsilon}}. \tag{6.62}$$

Now making use of

$$\dot{E} = \varepsilon - \lambda E \tag{6.63}$$

and

$$E = \frac{1}{2}v_\phi^2, \tag{6.64}$$

we find that in steady-state

$$\varepsilon = \frac{1}{2}\lambda v_\phi^2, \tag{6.65}$$

and hence our condition is

$$\left(\frac{2\Omega^3 v_\phi^3}{R^3\lambda}\right)^{1/5} > (3C_k)^{3/2}\sqrt{2}\lambda. \tag{6.66}$$

The Rossby number for flow around the star is roughly

$$\mathrm{Ro} = \frac{v_\phi}{2\pi R\Omega}. \tag{6.67}$$

Using this we may write $v_\phi = 2\pi R\Omega\mathrm{Ro}$, such that

$$\left(\frac{16\pi^3\Omega^6}{\lambda^6}\right)^{1/5}\mathrm{Ro}^{3/5} > (3C_k)^{3/2}\sqrt{2}. \tag{6.68}$$

Evaluating the numerical constants yields roughly

$$\mathrm{Ro} > 100\left(\frac{\lambda}{\Omega}\right)^2. \tag{6.69}$$

Intuitively what this means is that the more the Coriolis force deflects the wind as it travels around the star, the faster the star needs to dissipate the winds in order to prevent bands from forming.

It is now worth examining how to compute the various quantities mentioned in discussing the Rhines formalism. Many of them have simple definitions but are nontrivial to arrive at from the externally specified fluid parameters, and so this is a somewhat tricky procedure.

To begin with then, consider λ. This may be interpreted as the timescale over which a wind dies down due to drag effects. Given that the Rhines cascade uses a quasi two-dimensional flow, the characteristic scale for the associated sheer will be the pressure scale height, and so λ may be estimated as

$$\lambda = \frac{\dot{E}}{E} \approx \frac{\nu_v v_\phi^2/h_s^2}{v_\phi^2} = \frac{\nu_v}{h_s^2}, \tag{6.70}$$

where ν_v is the effective vertical viscosity on length scales of h_s. Note that we neglect the viscosity in the horizontal direction, as this is already accommodated by the formalism of the Rhines arrest.

In the convection zone, $\nu_v = l \max(v_c, v_\phi)$, so

$$\lambda = \frac{\aleph}{h_s} \max(v_c, v_\phi). \tag{6.71}$$

In the radiation zone, on the other hand, $\nu_h = v/k_R$, and so

$$\nu_v = \frac{v_\phi^2 (\alpha + v_\phi/k_R)}{gl\aleph(\nabla_{ad} - \nabla)} = \frac{v_\phi^2 \left(\alpha + \sqrt{v_\phi^3 R/\Omega}\right)}{gl\aleph(\nabla_{ad} - \nabla)}, \tag{6.72}$$

$$\therefore \lambda = \frac{v_\phi^2 \left(\alpha + \sqrt{v_\phi^3 R/\Omega}\right)}{gl^2 h_s (\nabla_{ad} - \nabla)}. \tag{6.73}$$

The next quantity of interest is ε. This is distinct from the ε used in the previous section, for here it is the power driving the wind, rather than the power the wind moves. Neglecting external heat input, in a steady state this will be the power lost by turbulence to drag, which is given by $\dot{E}$. This may be computed as in the previous paragraph. When external heat is included, however, some fraction of it should be counted towards this quantity. As discussed in Chapter 3, much of the external heating goes towards inducing a divergence in the flux. To compute the amount that goes towards ε, we use the same method as before, computing a power balance between the work extracted by the wind and the losses to bottom drag. The work extracted is, as usual,

$$\dot{W} = \frac{v_s^2 v_\phi \Delta T^2}{2\pi R T^2}. \tag{6.74}$$

The power lost is

$$\dot{E} = \lambda E = \varepsilon = \frac{1}{2} v_\phi^2 \lambda, \tag{6.75}$$

where in the second equality we have assumed that the wind is in power equilibrium. Setting $\dot{E}$ equal to $\dot{W}$ yields

$$\frac{1}{2}v_\phi^2\lambda = \frac{v_s^2 v_\phi \Delta T^2}{2\pi R T^2} \tag{6.76}$$

$$\therefore v_\phi\lambda = \frac{v_s^2\Delta T^2}{\pi R T^2}. \tag{6.77}$$

In the radiation zone this means that

$$\frac{v_\phi^3\left(\alpha + \sqrt{v_\phi^3 R/\Omega}\right)}{g l^2 h_s\left(\nabla_{ad} - \nabla\right)} = \frac{v_s^2\Delta T^2}{\pi R T^2}. \tag{6.78}$$

A series expansion of this around $\Delta T/T = 0$ yields

$$v_\phi = \left(\frac{v_s^2\Delta T^2 g l^2 h_s\left(\nabla_{ad} - \nabla\right)}{\pi R T^2\alpha}\right)^{1/3}. \tag{6.79}$$

This may be simplified by noting that

$$\alpha = \frac{k}{\rho c_p} = -\frac{F}{\rho c_p \partial_r T} = \frac{F}{\rho^2 g c_p \partial_P T} = \frac{FP}{\rho^2 g c_p T\nabla_R} = \frac{F h_s}{\rho c_p T\nabla_R} \approx \frac{F h_s}{P\nabla_R}. \tag{6.80}$$

In the thin-shell approximation, we may write $P = \Sigma g$ and find

$$\alpha = \frac{F h_s}{\Sigma g\nabla_R}. \tag{6.81}$$

Substituting this into the equation for v_ϕ yields

$$v_\phi^3 = \frac{v_s^2 \Delta T^2 g l^2 h_s \left(\nabla_{ad} - \nabla\right)}{\pi R T^2 \alpha} \tag{6.82}$$

$$= \frac{v_s^2 \Delta T^2 g^2 \Sigma \nabla_R l^2 h_s \left(\nabla_{ad} - \nabla\right)}{\pi R T^2 F h_s} \tag{6.83}$$

$$= \frac{v_s^2 \Delta T^2 g^2 \Sigma \nabla_R l^2 \left(\nabla_{ad} - \nabla\right)}{\pi R F T^2} \tag{6.84}$$

$$= \frac{v_s^2 \Delta T^2 \aleph^2 P^2 \Sigma \nabla_R \left(\nabla_{ad} - \nabla\right)}{\pi R \rho^2 F T^2} \tag{6.85}$$

$$= \frac{v_s^6 \Delta T^2 \aleph^2 \Sigma \nabla_R \left(\nabla_{ad} - \nabla\right)}{\pi R \gamma^2 F T^2} \tag{6.86}$$

$$= \frac{v_s^6 \Delta T^2 \aleph^2 \Sigma \nabla_R \left(\nabla_{ad} - \nabla_R\right)}{\pi R \gamma^2 F T^2} \tag{6.87}$$

$$\approx \frac{v_s^6 \Delta T^2 \Sigma \nabla_R}{\pi R F T^2}, \tag{6.88}$$

$$\tag{6.89}$$

where in the last line we have dropped some dimensionless constants of order unity. As a result, we may write

$$\lambda = \frac{v_\phi^2 \left(\alpha + \sqrt{v_\phi^3 R/\Omega}\right)}{g l^2 h_s \left(\nabla_{ad} - \nabla\right)} \tag{6.90}$$

$$= \left(\frac{v_s^6 \Delta T^2 \Sigma \nabla_R}{\pi R F T^2}\right)^{2/3} \frac{\left(\alpha + \sqrt{v_\phi^3 R/\Omega}\right)}{g l^2 h_s \left(\nabla_{ad} - \nabla\right)} \tag{6.91}$$

$$\approx \left(\frac{v_s^6 \Delta T^2 \Sigma \nabla_R}{\pi R F T^2}\right)^{2/3} \frac{\left(\alpha + \sqrt{v_\phi^3 R/\Omega}\right)}{g h_s^3} \tag{6.92}$$

$$\approx v_s^2 \left(\frac{\Delta T^2 \Sigma \nabla_R}{\pi R F T^2}\right)^{2/3} \frac{\left(\alpha + \sqrt{v_\phi^3 R/\Omega}\right)}{h_s^2} \tag{6.93}$$

$$\approx v_s^2 \left(\frac{\Delta T^2 \Sigma \nabla_R}{\pi R F T^2}\right)^{2/3} \frac{\left(\frac{F h_s}{\Sigma g \nabla_R} + \sqrt{\frac{v_s^6 \Delta T^2 \Sigma \nabla_R}{\pi \Omega F T^2}}\right)}{h_s^2}. \tag{6.94}$$

$$\tag{6.95}$$

When $\Delta T/T$ is small, this simplifies to

$$\lambda = \left(\frac{F \Delta T^4}{\pi^2 R^2 \Sigma T^4 \nabla_R}\right)^{1/3}. \tag{6.96}$$

The criterion for the Rhines scale to be in effect is then

$$\mathrm{Ro} > 100\left(\frac{\lambda}{\Omega}\right)^2 \tag{6.97}$$

$$\therefore \frac{v_\phi}{2\pi R\Omega} > 100\left(\frac{F\Delta T^4}{\pi^2 R^2 \Sigma T^4 \nabla_R \Omega^3}\right)^{2/3} \tag{6.98}$$

$$\therefore \frac{1}{2\pi R\Omega}\left(\frac{v_s^6 \Delta T^2 \Sigma \nabla_R}{\pi R F T^2}\right)^{1/3} > 100\left(\frac{F\Delta T^4}{\pi^2 R^2 \Sigma T^4 \nabla_R \Omega^3}\right)^{2/3} \tag{6.99}$$

$$\therefore \frac{1}{8\pi^3 R^3 \Omega^3}\left(\frac{v_s^6 \Delta T^2 \Sigma \nabla_R}{\pi R F T^2}\right) > 10^6 \frac{F^2 \Delta T^8}{\pi^4 R^4 \Sigma^2 T^8 \nabla_R^2 \Omega^6} \tag{6.100}$$

$$\therefore \frac{1}{8\Omega^3}\left(\frac{v_s^6 \Delta T^2 \Sigma \nabla_R}{F T^2}\right) > 10^6 \frac{F^2 \Delta T^8}{\Sigma^2 T^8 \nabla_R^2 \Omega^6} \tag{6.101}$$

$$\therefore \frac{1}{8}\left(\frac{v_s^6 \nabla_R}{F}\right) > 10^6 \frac{F^2 \Delta T^6}{\Sigma^3 T^6 \nabla_R^2 \Omega^3} \tag{6.102}$$

$$\therefore v_s^6 > 10^7 \frac{F^3 \Delta T^6}{\Sigma^3 T^6 \nabla_R^3 \Omega^3} \tag{6.103}$$

$$\therefore v_s^2 > 100 \frac{F \Delta T^2}{\Sigma T^2 \nabla_R \Omega} \tag{6.104}$$

$$\therefore T_4 > 10^{-3} \frac{F \Delta T^2 \Sigma_h}{F_\odot T^2 \Sigma \nabla_R \Omega} \tag{6.105}$$

$$\therefore T_4 > 100 \frac{F \Delta T^2 \Sigma_h}{F_\odot T^2 \Sigma \Omega_{-4}}. \tag{6.106}$$

When it is in effect, the heat transported is

$$\varepsilon' = c_p v_\phi \frac{\Delta T}{\pi R} \approx \frac{1}{\pi R} v_s^2 v_\phi \frac{\Delta T}{T} = v_s^3 \left(\frac{16 v_s^3 \Sigma \nabla_R}{l^4 F}\right)^{1/3} \left(\frac{l}{2\pi R}\right)^{4/3} \left(\frac{\Delta T}{T}\right)^{5/3}. \tag{6.107}$$

Recalling the definition of ∇_R, this becomes

$$\varepsilon' = v_s^3 \left(\frac{16 v_s^3 \Sigma \nabla_R}{l^4 F}\right)^{1/3} \left(\frac{l}{2\pi R}\right)^{4/3} \left(\frac{\Delta T}{T}\right)^{5/3} \tag{6.108}$$

$$= v_s^3 \left(\frac{16 v_s^3 \Sigma 3\kappa L P}{16\pi a c G M T^4 l^4 F}\right)^{1/3} \left(\frac{l}{2\pi R}\right)^{4/3} \left(\frac{\Delta T}{T}\right)^{5/3} \tag{6.109}$$

$$= \frac{v_s^3}{\pi R} \left(\frac{2 v_s^3 \Sigma 3\kappa L P}{16\pi a c G M T^4 l F}\right)^{1/3} \left(\frac{l}{2\pi R}\right)^{1/3} \left(\frac{\Delta T}{T}\right)^{5/3} \tag{6.110}$$

$$= \frac{v_s^3}{\pi R} \left(\frac{2 v_s^3 \Sigma 3\kappa L P}{16\pi a c g R^2 T^4 l F}\right)^{1/3} \left(\frac{l}{2\pi R}\right)^{1/3} \left(\frac{\Delta T}{T}\right)^{5/3} \tag{6.111}$$

$$= \frac{v_s^3}{\pi R} \left(\frac{2 v_s^3 \Sigma 3\kappa 4\pi R^2 P}{16\pi a c g R^2 T^4 l}\right)^{1/3} \left(\frac{l}{2\pi R}\right)^{1/3} \left(\frac{\Delta T}{T}\right)^{5/3} \tag{6.112}$$

$$= \frac{v_s^3}{\pi R} \left(\frac{2 v_s^3 \Sigma 3\kappa P}{4 a c g T^4 l}\right)^{1/3} \left(\frac{l}{2\pi R}\right)^{1/3} \left(\frac{\Delta T}{T}\right)^{5/3} \tag{6.113}$$

$$= \frac{v_s^3}{\pi R} \left(\frac{3 v_s^3 \Sigma \kappa P}{8\sigma g T^4 l}\right)^{1/3} \left(\frac{l}{2\pi R}\right)^{1/3} \left(\frac{\Delta T}{T}\right)^{5/3} \tag{6.114}$$

$$= \frac{v_s^3}{\pi R} \left(\frac{3 v_s \Sigma \kappa P \gamma}{8\sigma T^4 \aleph}\right)^{1/3} \left(\frac{l}{2\pi R}\right)^{1/3} \left(\frac{\Delta T}{T}\right)^{5/3}. \tag{6.115}$$

$$\tag{6.116}$$

When $\Delta T/T$ is large, on the other hand,

$$\frac{v_\phi}{v_s} = \left(\frac{v_s^3 \Delta T^2 \Sigma \nabla_R}{\pi R F T^2}\right)^{1/3} \sim \left(\frac{T_4^{3/2} \Sigma F_\odot R_\odot \Delta T^2}{\Sigma_h F R T^2}\right)^{1/3}, \tag{6.117}$$

so we expect v_ϕ to be of order v_s. Note that if this formula indicates a speed greater than the sound speed we truncate it as usual to the sound speed. Using $v_\phi \sim v_s$, we find

$$\lambda = \frac{v_\phi^2\left(\alpha + \sqrt{v_\phi^3 R/\Omega}\right)}{gl^2 h_s\left(\nabla_{ad} - \nabla\right)} \tag{6.118}$$

$$\approx \frac{v_\phi^2\left(\alpha + \sqrt{v_\phi^3 R/\Omega}\right)}{v_s^2 h_s^2} \tag{6.119}$$

$$\approx \frac{v_s^2\left(\alpha + \sqrt{v_s^3 R/\Omega}\right)}{v_s^2 h_s^2} \tag{6.120}$$

$$\approx h_s^{-2}\left(\alpha + \sqrt{\frac{v_s^3 R}{\Omega}}\right) \tag{6.121}$$

$$\approx h_s^{-2}\left(\frac{F h_s}{P\nabla_R} + \sqrt{\frac{v_s^3 R}{\Omega}}\right) \tag{6.122}$$

$$\approx h_s^{-2}\left(10^9\frac{F h_s \Sigma_h g_\odot}{10^7\mathrm{cm} F_\odot \Sigma g} + 10^1 6 T_4^{3/4}\sqrt{\Omega_{-4}^{-1}\frac{R}{R_\odot}}\right) \tag{6.123}$$

$$\approx \sqrt{\frac{v_s^3 R}{h_s^4 \Omega}}. \tag{6.124}$$

The criterion for the Rhines scaling is then

$$\frac{v_s}{2\pi R\Omega} > 100\frac{v_s^3 R}{h_s^4\Omega^3} \therefore 1 > 200\pi\frac{v_s^2 R^2}{h_s^4\Omega^2} \therefore 1 > 200\pi\frac{g^4 R^2}{v_s^6\Omega^2}. \tag{6.125}$$

As a rough estimate, the right side should be 10^9 or so for a sun-like star with $\Omega = 10^{-4}\mathrm{s}^{-1}$, so this case does not concern us.

We may now perform the same procedure for convecting regions, where

$$v_\phi\frac{\aleph}{h_s}\max\left(v_c, v_\phi\right) = \frac{v_s^2\Delta T^2}{\pi R T^2}. \tag{6.126}$$

To solve this, we first assume $v_c > v_\phi$ and write

$$v_\phi = \frac{h_s v_s^2 \Delta T^2}{v_c \aleph \pi R T^2}. \tag{6.127}$$

If this exceeds v_c, then we instead use

$$v_\phi = \sqrt{\frac{h_s v_s^2\Delta T^2}{\aleph\pi R T^2}}. \tag{6.128}$$

We then have

$$\varepsilon' = \frac{v_\phi c_p \Delta T}{\pi R}. \tag{6.129}$$

Once more λ and ε may be computed from these results. If $v_c > v_\phi$, λ is a constant and ε goes as ΔT^4. Otherwise, λ goes as ΔT and ε goes as ΔT^3.

6.4 Convective Reynold's Stress

In addition to being powered by temperature differentials, circumferential flows may be powered by rotation-induced anisotropy in convecting regions. To model this, we treat convection zones via the mean field theory of Reynolds stress. The Navier-Stokes equation, written with the Reynolds stresses in place, is

$$\rho \partial_t \boldsymbol{v} + \rho \boldsymbol{v} \cdot \boldsymbol{\nabla} \boldsymbol{v} = -\boldsymbol{\nabla} p + \boldsymbol{F} + \boldsymbol{F}_{visc} - \hat{e}_i \partial_j (\rho R_{ij}), \tag{6.130}$$

where there is an implied summation over repeated indices and where R_{ij} are the components of the Reynolds stress. If we take the body force to be gravitational, and further take this to be precisely canceled by the unperturbed pressure, then

$$\rho \partial_t \boldsymbol{v} + \rho \boldsymbol{v} \cdot \boldsymbol{\nabla} \boldsymbol{v} = -\boldsymbol{\nabla} \delta p + \boldsymbol{F}_{visc} - \hat{e}_i \partial_j (\rho R_{ij}). \tag{6.131}$$

If we approximate the velocity as constant then

$$\rho \boldsymbol{v} \cdot \boldsymbol{\nabla} \boldsymbol{v} = -\boldsymbol{\nabla} \delta p + \boldsymbol{F}_{visc} - \hat{e}_i \partial_j (\rho R_{ij}). \tag{6.132}$$

Now suppose that the only non-turbulent velocity is along $\hat{\phi}$. Then

$$\rho v_\phi R^{-1} \partial_\phi \boldsymbol{v} = -\boldsymbol{\nabla} \delta p + \boldsymbol{F}_{visc} - \hat{e}_i \partial_j (\rho R_{ij}). \tag{6.133}$$

This may be further simplified, for $\boldsymbol{F}_{visc}$ will go parallel to $\hat{\phi}$ and opposing $\boldsymbol{v}$ in this case, so

$$\rho v_\phi R^{-1} \partial_\phi \boldsymbol{v} = -\boldsymbol{\nabla} \delta p - \hat{v} F_{visc} - \hat{e}_i \partial_j (\rho R_{ij}). \tag{6.134}$$

We generally expect that only a fraction of the convective energy may be diverted into powering a horizontal wind. As a result, the viscosity is just the convective turbulent viscosity, so

$$\begin{aligned}
\rho v_\phi R^{-1} \partial_\phi \boldsymbol{v} &= -\boldsymbol{\nabla} \delta p - \hat{v} \left(\rho \frac{v_\phi}{l^2} (v_c l) + \rho \frac{v_\phi}{(\xi R)^2} (v_c \min(l, r_{rot})) \right) - \hat{e}_i \partial_j (\rho R_{ij}) && (6.135) \\
&= -\boldsymbol{\nabla} \delta p - \hat{v} \left(\rho v_\phi \tilde{N} + \rho \frac{v_\phi}{(\xi R)^2} (v_c \min(l, r_{rot})) \right) - \hat{e}_i \partial_j (\rho R_{ij}) && (6.136) \\
&= -\boldsymbol{\nabla} \delta p - \hat{v} \rho \tilde{N} v_\phi \left(1 + \frac{l \min(l, r_{rot})}{(\xi R)^2} \right) - \hat{e}_i \partial_j (\rho R_{ij}), && (6.137)
\end{aligned}$$

where ξR is the length scale for shearing within isobars. In the absence of Rhines scaling, we expect ξ to be of order unity and hence the second term in parentheses may be dropped, for $l \ll R$. In the presence of Rhines scaling, $\xi R = k_R^{-1} = \sqrt{R v_\phi / \Omega}$. The second term in parentheses is then

$$\frac{l \min(l, r_{rot})}{(\xi R)^2} = \frac{\Omega l \min(l, r_{rot})}{R v_\phi}. \tag{6.138}$$

As will be argued later, v_ϕ should be of order $\sqrt{\Omega l v_c}$, so we may write

$$\frac{l \min(l, r_{rot})}{(\xi R)^2} = \frac{\min(l, r_{rot})}{R}\sqrt{\frac{\Omega}{\tilde{N}}}. \tag{6.139}$$

The first term is at most 10^{-2}. At the depths of interest, $\tilde{N}$ is never less than 10^{-5}, and in no case do we consider $\Omega > 10^{-4}$, so the second term is at most of order unity. As a result, we may neglect the product of these two and write

$$\rho v_\phi R^{-1} \partial_\phi \boldsymbol{v} = -\boldsymbol{\nabla} \delta p - \hat{v} \rho \tilde{N} v_\phi - \hat{e}_i \partial_j (\rho R_{ij}), \tag{6.140}$$

and hence

$$\rho v_\phi R^{-1} \partial_\phi \boldsymbol{v} = -\boldsymbol{\nabla} \delta p - \hat{\phi} \rho v_\phi \tilde{N} - \hat{e}_i \partial_j (\rho R_{ij}). \tag{6.141}$$

Note that in the bottom friction term we have assumed $v_\phi > 0$. Once more making use of the expected direction of the motion, we find

$$\rho v_\phi R^{-1} \partial_\phi v_\phi = -R^{-1} \partial_\phi \delta p - \rho v_\phi \tilde{N} - \partial_j (\rho R_{\phi,j}). \tag{6.142}$$

Typically we expect band speeds to not vary too much across the system, so $\partial_\phi v_\phi \approx 0$. We may average the equation then over ϕ to find

$$0 = -\rho v_\phi \tilde{N} - \partial_j (\rho R_{\phi,j}). \tag{6.143}$$

This may be written as

$$-\partial_j R_{\phi,j} - R_{\phi,j} \partial_j \ln \rho = v_\phi \tilde{N}. \tag{6.144}$$

If we take θ derivatives to be small and once more average over ϕ we find that only the radial derivatives survive. Thus

$$-\partial_r R_{\phi,r} - R_{\phi,r} \partial_r \ln \rho = v_\phi \tilde{N}. \tag{6.145}$$

We now need an expression R_{ij}. In a rotating system, and to linear order in the inverse of the Rossby number, we have[19]

$$\bar{R}_0 = \frac{2}{c_1 c_6}\left(\frac{c_1}{c_7} + \frac{3c_1 + c_2}{3(c_1 + c_2)}\right) L^2 \tilde{N}^2, \tag{6.146}$$

$$R_{\phi\phi,0} = R_{\theta\theta,0} = \frac{\bar{R}_0}{3}\left(\frac{c_2}{c_1 + c_2}\right), \tag{6.147}$$

$$R_{rr,0} = \frac{\bar{R}_0}{3}\left(\frac{3c_1 + c_2}{c_1 + c_2}\right), \tag{6.148}$$

$$F_{r,0} = \frac{-c_1 \bar{R}_0^{3/2}}{2l\tilde{N}^2}\left(\frac{dT}{dr}\right)^2, \tag{6.149}$$

$$R_{\phi r} = -2l^2\tilde{N}^2 \mathrm{Ro}^{-1} \sin\theta \left(\frac{-F_{z,0} l^{-2} \tilde{N}^{-1} \frac{dr}{dT} + c_6 \frac{\sqrt{\bar{R}_0}}{l^3 \tilde{N}^3}\left(R_{zz,0} - R_{xx,0}\right)}{1 + 2(c_1 + c_2)/c_7 + 2c_2/3c_1}\right). \tag{6.150}$$

where

$$\tilde{N}^2 = v_c^2/l^2, \tag{6.151}$$

$$c_1 = 0.4, \tag{6.152}$$

$$c_2 = 0.6, \tag{6.153}$$

$$c_6 = 1.4, \tag{6.154}$$

$$c_7 = 1.4. \tag{6.155}$$

As a result, we may write

$$R_{\phi r} = -2l^2\tilde{N}^2 \frac{\Omega}{\tilde{N}} \sin\theta \left(\frac{-F_{z,0} l^{-2}\tilde{N}^{-1}\left(\frac{dT}{dr}\right)^{-1} + c_6 l^{-3}\tilde{N}^{-3}\bar{R}_0^{3/2}\left(\frac{1}{c_1+c_2}\right)}{1 + 2(c_1 + c_2)/c_7 + 2c_2/3c_1}\right) \tag{6.156}$$

$$= -2l^2\tilde{N}^2 \frac{\Omega}{\tilde{N}} \sin\theta \left(\frac{\frac{c_1\bar{R}_0^{3/2}}{2l^3\tilde{N}^3} + c_6 l^{-3}\tilde{N}^{-3}\bar{R}_0^{3/2}\left(\frac{1}{c_1+c_2}\right)}{1 + 2(c_1 + c_2)/c_7 + 2c_2/3c_1}\right) \tag{6.157}$$

$$= -2\bar{R}_0^{3/2} \frac{\Omega}{l\tilde{N}^2} \sin\theta \left(\frac{\frac{c_1}{2} + \frac{c_6}{c_1+c_2}}{1 + 2(c_1 + c_2)/c_7 + 2c_2/3c_1}\right) \tag{6.158}$$

$$= -2\left(\frac{2}{c_1 c_6}\left(\frac{c_1}{c_7} + \frac{3c_1 + c_2}{3(c_1 + c_2)}\right)\right)^{3/2} l^2 \Omega \tilde{N} \sin\theta \left(\frac{\frac{c_1}{2} + \frac{c_6}{c_1+c_2}}{1 + 2\frac{c_1+c_2}{c_7} + \frac{2c_2}{3c_1}}\right) \tag{6.159}$$

$$= -5.25 l^2 \Omega \tilde{N} \sin\theta = -5.25 l \Omega v_c \sin\theta. \tag{6.160}$$

[19]Garaud et al., op. cit.

Note that we have made all of the appropriate substitutions required to make this result applicable for compressible systems, including identification of $\tilde{N}$ with the convective turnover frequency and identification of the characteristic length scale with the convective scale of mixing length theory. Note also that by choice of convention in the Navier-Stokes equation we have taken R to have units of velocity squared rather than energy density.

Using our expression for the Reynolds stress in our approximated and averaged Navier-Stokes equation, we may write that

$$5.25\Omega \sin\theta \left(\partial_r \left(l^2 \tilde{N}\right) + l\tilde{N}\right) = v_\phi \tilde{N}, \tag{6.161}$$

where we have taken $\partial_r \ln \rho$ to be roughly an inverse scale height. Dividing through by $\tilde{N}$ yields

$$5.25\Omega \sin\theta \left(l^2 \partial_r \ln \tilde{N} + \partial_r \tilde{l^2} + l\right) = v_\phi. \tag{6.162}$$

The middle term may be evaluated as

$$\partial_r l^2 = 2l\partial_r \frac{p}{\rho g} = -\frac{\rho g}{\rho g} - \frac{p}{\rho g}\partial_r \ln \rho = 2l\frac{1-\gamma}{\gamma}, \tag{6.163}$$

where we have made use of the near adiabaticity of efficient convection. Thus

$$5.25\Omega \sin\theta \left(l^2 \partial_r \ln \tilde{N} + l\left(\frac{2}{\gamma} - 1\right)\right) = v_\phi. \tag{6.164}$$

Using $\gamma \approx 5/3$ this becomes

$$5.25\Omega \sin\theta \left(l^2 \partial_r \ln \tilde{N} + \frac{l}{5}\right) = v_\phi. \tag{6.165}$$

In the stellar models of interest, $\ln \tilde{N}$ increases by about two orders of magnitude over around seven scale heights, and it increases typically in the radially outward direction. Thus we may write the first derivative as roughly $2/7l$, and hence

$$v_\phi \approx 2.6\Omega l \sin\theta. \tag{6.166}$$

In the ionization zone this should increase somewhat, as γ increases there, but otherwise it should be fairly universal.

If we average the square of this over θ we find that the typical scale of the velocity is

$$v_\phi = 1.3\Omega l \approx \Omega l, \tag{6.167}$$

and so

$$\varepsilon = E\lambda = \frac{1}{2}v^2\lambda = \frac{1}{2}\Omega^2 l^2 \tilde{N} = \frac{1}{2}\Omega^2 l v_c. \tag{6.168}$$

Now should the viscosity be due to shearing rather than convection this result must be amended accordingly. This may occur if a combination of a heat engine and this anisotropy are responsible for driving the wind. In this case, $\lambda = v_\phi/l$ and it can be shown that the wind speed goes as

$$v_\phi^2 = v_s^2 \left(\frac{\Delta T}{T}\right)^2 \frac{l}{2\pi R} + v_\phi \Omega l, \tag{6.169}$$

for the force associated with the Reynolds stress goes as Ωl, so the power goes as $v_\phi \Omega l$. The specific form follows because the right side of this equation is just a rescaled version of the power input, and the left side is a similarly rescaled version of the power removed by turbulence. As a result of the above equation for v_ϕ, the contribution to ε of the convective anisotropy depends on the thermal driving, for

$$\varepsilon_{anis} = \frac{1}{2}v_\phi^3 l^{-1} - \frac{1}{2}v_{\phi,0}^3 l^{-1} = \frac{v_\phi^3 - v_{\phi,0}^3}{2l}, \tag{6.170}$$

where $v_{\phi,0}$ is the solution in the absence of convective anisotropy. As v_ϕ has a nontrivial and non-polynomial dependence on Ωl, this expression does not reduce to something independent of $v_{\phi,0}$. The problems are coupled, therefore, with thermal driving diminishing the significance of convective anisotropy.

Finally, note that the convective Reynolds stress produces in the low thermal anisotropy regime a wind speed of roughly Ωl. This leads to transport of the form

$$\varepsilon' = \Omega l c_p \frac{\Delta T}{\pi R} = \mathrm{Ro}_s^{-1} \frac{v_s^3}{\pi R}\left(\frac{l}{2\pi R}\right), \tag{6.171}$$

where Ro_s is the sonic Rossby number.

6.5 Summary of Results

Our analysis of large Rossby number transport suggests that all of the transport expressions may be written in the same general form. Neglecting convective Reynolds stresses and working in the limit of small $\Delta T/T$, we may write

$$\varepsilon' = y\frac{v_s^3}{\pi R}\left(\frac{\Delta T}{T}\right)^q \left(\frac{l}{2\pi R}\right)^a \mathrm{Ro}_s^b. \tag{6.172}$$

This may also be put in the form

$$\varepsilon' = y' T_4^{3/2} \left(\frac{R_\odot}{R}\right) \left(\frac{\Delta T}{T}\right)^q \left(\frac{10^4 l}{2\pi R}\right)^a \mathrm{Ro}_s^b \left(\frac{F_\odot}{\Sigma_h}\right). \tag{6.173}$$

The dimensionless quantities y, y', q, a, b are given in table 6.1. Note that in computing y', we have used the following relations (and all approximations which accompany them):

$$F = \rho v_c^3 \tag{6.174}$$

$$P = g\Sigma \tag{6.175}$$

Case	y	y'	q	a	b
Radiative $v > 2\pi\Omega R$	1	10	2	0	0
Radiative $v < 2\pi\Omega R$	$\frac{1}{4\pi}$	1	5	0	3
Radiative Rhines	$\left(\frac{3v_s\Sigma\kappa P}{8\sigma T^4}\right)^{1/3}$	$\left(\frac{\kappa_1 M R_\odot^2 \Sigma}{M_\odot R^2 \Sigma_h T_4^{7/2}}\right)^{1/3}$	$\frac{5}{3}$	$\frac{1}{3}$	0
Convective $v > 2\pi\Omega R, v_c$	$\pi\left(\frac{v_s}{v_c}\right)$	$10^{-2} T_4^{1/2}\left(\frac{F\Sigma_h}{F_\odot \Sigma}\right)^{-1/3}$	3	1	0
Convective $v_c > v > 2\pi\Omega R$	1	10^{-1}	2	$\frac{1}{2}$	0
Convective $2\pi\Omega R > v > v_c$	$\frac{1}{4\pi}$	1	5	0	3
Convective $v < 2\pi\Omega R, v_c$	$2\pi\frac{v_c}{v_s}\min\left(1, \frac{v_c}{\Omega l}\right)$	$10^{-3}\left(\frac{F\Sigma_h \min\left(1, \frac{v_c^3}{\Omega^3 l^3}\right)}{F_\odot \Sigma T_4^{3/2}}\right)^{1/3}$	1	1	0
Convective Rhines, $v > v_c$	$\sqrt{2}$	10^{-1}	2	$\frac{1}{2}$	0
Convective Rhines, $v < v_c$	$2\frac{v_s}{v_c}$	$10^{-2}\left(\frac{F\Sigma_h}{F_\odot \Sigma T_4^{3/2}}\right)^{-1/3}$	3	1	0
Convective Reynolds	$\frac{2\pi R\Omega}{v_s}$	$10^{-3}\frac{R\Omega_{-4}}{R_\odot T_4^{1/2}}$	1	1	0

Table 6.1: Computed parameterization of circumferential heat transport by winds. The first column specifies what case is under consideration. All possible cases are enumerated here. The remaining columns specify y, a prefactor on the transport as well as q, a, b, the exponents on $\Delta T/T$, $l/2\pi R$, and Ro respectively. Note that factors of γ and $\aleph$ have been neglected in assembling this table.

The quantity y' has a clear physical interpretation: y' is the fraction of a solar luminosity which, up to powers of the Rossby number and temperature anisotropy, may be moved from one side of the sun-like star to another over a change in depth of Σ_h. We immediately see that radiative stars are orders of magnitude more efficient at transporting heat circumferentially, particularly when the Rhines cascade is relevant. This is a result of the larger turbulent viscosity associated with convection in most cases. Additionally, it is clear that stars with low Rossby number are less efficient at this task than those with high Rossby number. This is because, as the Rossby number is lowered, the problem transitions from being one of ballistic transport to being one of diffusion. The former is much more efficient than the latter, just as a directed walk moves away from its origin faster than a random walk.

Now recall that

$$v = \frac{\pi R}{c_p \Delta T}\varepsilon' = \frac{\varepsilon'}{v_s^2}\pi R \left(\frac{\Delta T}{T}\right)^{-1}. \tag{6.176}$$

This may be written as

$$v = v_s 10^{-1} y' \left(\frac{\Delta T}{T}\right)^{q-1} \mathrm{Ro}_s^b. \tag{6.177}$$

Recalling that the Mach number is expected to be at most one, a good approximation is to use the form in Eq. (6.173) until

$$\left(\frac{\Delta T}{T}\right)_c = \left(\frac{10}{y'\mathrm{Ro}_s^b}\right)^{\frac{1}{q-1}}, \tag{6.178}$$

at which point the wind reaches the sound speed and ceases to grow with increasing temperature anisotropy. Table 6.2 lists the critical anisotropy values at which this occurs. Note that not all cases appear in the table, for v_c is generally quite subsonic, so $v = v_s$ implies that $v > v_c$. Additionally, the Reynolds stress case only occurs when $\Delta T/T$ is small, and even in the fastest-rotating cases of interest we have argued that the Rossby number is at least unity, so the low-Rossby number cases have been omitted.

Case	$(\Delta T/T)_c$
Radiative $v > 2\pi\Omega R$	1
Radiative Rhines	$30\left(\frac{\kappa_1 M R_\odot^2 \Sigma}{M_\odot R^2 \Sigma_h T_4^{7/2}}\right)^{-1/2}$
Convective $v > 2\pi\Omega R, v_c$	$30T_4^{-1/4}\left(\frac{F\Sigma_h}{F_\odot \Sigma}\right)^{1/6}$
Convective Rhines, $v > v_c$	10^2

Table 6.2: Critical thermal anisotropy values are listed for each case of interest. Note that factors of γ and $\aleph$ have been neglected in assembling this table.

References

Atkinson, D. H., J. B. Pollack, and A. Seiff. “The Galileo probe Doppler wind experiment: Measurement of the deep zonal winds on Jupiter”. In: *Journal of Geophysical Research* 103 (Sept. 1998), pp. 22911–22928. DOI: 10.1029/98JE00060 (cit. on p. 80).

Danilov, S. and D. Gurarie. “Scaling, spectra and zonal jets in beta-plane turbulence”. In: *Physics of Fluids* 16 (July 2004), pp. 2592–2603. DOI: 10.1063/1.1752928 (cit. on p. 80).

Danilov, Sergey and David Gurarie. “Rhines scale and spectra of the β-plane turbulence with bottom drag”. In: *Phys. Rev. E* 65 (6 June 2002), p. 067301. DOI: 10.1103/PhysRevE.65.067301. URL: http://link.aps.org/doi/10.1103/PhysRevE.65.067301 (cit. on p. 80).

Galperin, Boris, Semion Sukoriansky, and Huei-Ping Huang. “Universal n-5 spectrum of zonal flows on giant planets”. In: *Physics of Fluids (1994-present)* 13.6 (2001), pp. 1545–1548. DOI: http://dx.doi.org/10.1063/1.1373684. URL: http://scitation.aip.org/content/aip/journal/pof2/13/6/10.1063/1.1373684 (cit. on p. 79).

Garaud, P. et al. “A model of the entropy flux and Reynolds stress in turbulent convection”. In: *Monthly Notices of the Royal Astronomical Society* 407 (Oct. 2010), pp. 2451–2467. DOI: 10.1111/j.1365-2966.2010.17066.x. arXiv: 1004.3239 [astro-ph.SR] (cit. on pp. 91, 102).

Hathaway, D. H., L. Upton, and O. Colegrove. “Giant Convection Cells Found on the Sun”. In: *ArXiv e-prints* (Jan. 2014). arXiv: 1401.0551 [astro-ph.SR] (cit. on p. 92).

Köhler, H. “Differential Rotation Caused by Anisotropic Turbulent Viscosity”. In: *Solar Physics* 13 (July 1970), pp. 3–18. DOI: 10.1007/BF00963937 (cit. on p. 91).

Lesaffre, Pierre et al. “A two-dimensional mixing length theory of convective transport”. In: *Monthly Notices of the Royal Astronomical Society* (2013). DOI: 10.1093/mnras/stt317. eprint: http://mnras.oxfordjournals.org/content/early/2013/03/20/mnras.stt317.full.pdf+html. URL: http://mnras.oxfordjournals.org/content/early/2013/03/20/mnras.stt317.abstract (cit. on p. 91).

Nguyen Duc, J.M., Ph. Caperan, and J. Sommeria. “An Experimental Study of the Inverse Cascade of Energy in Two-Dimensional Turbulence”. English. In: *Advances in Turbulence*. Ed. by Geneviève Comte-Bellot and Jean Mathieu. Springer Berlin Heidelberg, 1987, pp. 265–268. ISBN: 978-3-642-83047-1. DOI: 10.1007/978-3-

642-83045-7_30. URL: http://dx.doi.org/10.1007/978-3-642-83045-7_30 (cit. on p. 80).

Rhines, Peter B. "Waves and turbulence on a beta-plane". In: *Journal of Fluid Mechanics* 69 (03 June 1975), pp. 417–443. ISSN: 1469-7645. DOI: 10.1017/S0022112075001504. URL: http://journals.cambridge.org/article_S0022112075001504 (cit. on p. 79).

Stevens, Richard J.A.M., Herman J.H. Clercx, and Detlef Lohse. "Heat transport and flow structure in rotating RayleighâBÃ©nard convection". In: *European Journal of Mechanics - B/Fluids* 40 (2013). Fascinating Fluid Mechanics: 100-Year Anniversary of the Institute of Aerodynamics, {RWTH} Aachen University, pp. 41–49. ISSN: 0997-7546. DOI: http://dx.doi.org/10.1016/j.euromechflu.2013.01.004. URL: http://www.sciencedirect.com/science/article/pii/S0997754613000058 (cit. on p. 91).

Sukoriansky, Seimion, Nadejda Dikovskaya, and Boris Galperin. "On the Arrest of Inverse Energy Cascade and the Rhines Scale". In: *Journal of the Atmospheric Sciences* 64 (2006). URL: http://journals.ametsoc.org/doi/abs/10.1175/JAS4013.1 (cit. on pp. 80–82).

Sukoriansky, Semion, Boris Galperin, and Nadejda Dikovskaya. "Universal Spectrum of Two-Dimensional Turbulence on a Rotating Sphere and Some Basic Features of Atmospheric Circulation on Giant Planets". In: *Phys. Rev. Lett.* 89 (12 Aug. 2002), p. 124501. DOI: 10.1103/PhysRevLett.89.124501. URL: http://link.aps.org/doi/10.1103/PhysRevLett.89.124501 (cit. on pp. 79–81).

Verhoeven, J. and S. Stellmach. "The compressional beta effect: A source of zonal winds in planets?" In: *Icarus* 237 (July 2014), pp. 143–158. DOI: 10.1016/j.icarus.2014.04.019. arXiv: 1404.6940 [astro-ph.EP] (cit. on p. 80).

7

Higher Dimensional Models with Transport

... très souvent les lois particulières déduites par les physiciens d'un grand nombre d'observations ne sont pas rigoureuses, mais approchées.
... very often the laws derived by physicists from a large number of observations are not rigorous, but approximate.

– Augustin Louis Cauchy

In this chapter we will put all of the pieces other than time dependence together. The addition of time is left for the next chapter, and so for the moment we maintain the steady-state approximation.

For simplicity, suppose that we represent a star by two temperature profiles, one for the hot side and one for the cold. This may be understood as representing the amplitude of the lowest order spherical harmonic which is symmetric about the line connecting the pulsar and its companion star. We refer to the hot side temperature as T_h, and the cold side temperature as T_c. The subscripts h and c will be attached to other quantities as needed to describe the same distinction. Quantities lacking subscripts are taken to be averaged between the two sides.

In this context the quantity ΔT discussed previously is the difference between the two temperatures at the same pressure. In general, we define

$$\Delta A \equiv A_h - A_c, \tag{7.1}$$

where both quantities on the right are evaluated at the same pressure. The isobaric condition is required by our usage of ΔT as the temperature difference experienced by winds moving around the star.

Note that we will neglect gravity modes as a means of energy transfer, as they are only excitable by convective zones and only transferrable over long distances through radiative zones, leaving only the narrow interfaces between these regions as conduits[1]. As a result, they carry relatively little flux compared to the thermal anisotropies of interest[2].

7.1 Radiative Stars

If we take k to be a scalar, neglect winds, and assume that all of one side of the companion experiences heating while the entirety of the other side does not, we know from Chapter 3 that somewhere between 1/6 and 1/2 of the input flux exits on the cold side. The remainder of the input flux exits on the hot side. The assumption that k is a scalar is always valid in radiative stars, and the assumption regarding the geometry of heating is well justified per Chapter 1, so the key assumption which fails, then, is the neglecting of wind. Given that the effect of circumferential wind in a star is to make the flux divergence more isotropic, we expect that there will be a column density at which the wind achieves this, and beyond which the star is isotropic. As a result, we do not expect that such a large fraction of the flux will generically escape to the cold side.

To understand this more thoroughly, note that the flux divergence differs between the two sides of the star as

$$\nabla \cdot \boldsymbol{F}_h = \rho \left(\varepsilon - \varepsilon'_{wind}\right), \tag{7.2}$$
$$\nabla \cdot \boldsymbol{F}_c = \rho \varepsilon'_{wind}, \tag{7.3}$$

where ε is the usual input heat. As we are treating the star as being two one-dimensional stars stuck together, we may also write this as

$$\partial_r F_h = \rho \left(\varepsilon - \varepsilon'_{wind}\right), \tag{7.4}$$
$$\partial_r F_c = \rho \varepsilon'_{wind}, \tag{7.5}$$

[1] Y. Wu and P. Goldreich. "Gravity Modes in ZZ Ceti Stars. IV. Amplitude Saturation by Parametric Instability". In: *The Astrophysical Journal* 546 (Jan. 2001), pp. 469–483. DOI: `10.1086/318234`. eprint: `astro-ph/0003163`; C. C. Mei and T. Y.-t. Wu. "Gravity Waves due to a Point Disturbance in a Plane Free Surface Flow of Stratified Fluids". In: *Physics of Fluids* 7 (Aug. 1964), pp. 1117–1133. DOI: `10.1063/1.1711351`; A. J. Brickhill. "The pulsations of ZZ Ceti stars. III - The driving mechanism". In: *Monthly Notices of the Royal Astronomical Society* 251 (Aug. 1991), pp. 673–680.

[2] J. H. Shiode et al. "The observational signatures of convectively excited gravity modes in main-sequence stars". In: *Monthly Notices of the Royal Astronomical Society* 430 (Apr. 2013), pp. 1736–1745. DOI: `10.1093/mnras/sts719`. arXiv: `1210.5525 [astro-ph.SR]`.

Switching to column density as the independent variable, this becomes

$$\partial_\Sigma F_h = -\left(\varepsilon - \varepsilon'_{wind}\right), \tag{7.6}$$
$$\partial_\Sigma F_c = -\varepsilon'_{wind}, \tag{7.7}$$

Using the radiative equilibrium relation, we get

$$F = -k\partial_r T = -\frac{4acT^3}{\kappa\rho}\partial_r T = \frac{4acT^3}{\kappa}\partial_\Sigma T = \frac{ac}{\kappa}\partial_\Sigma T^4. \tag{7.8}$$

Now for $T > 10^4$K, the key regime of interest for radiative stars, κ doesn't vary much with T or ρ except at unphysically high densities[3]. As a result, we may write

$$\partial_\Sigma F_h = -\left(\varepsilon - \varepsilon'_{wind}\right) = ac\kappa^{-1}\partial^2_\Sigma T^4_h, \tag{7.9}$$
$$\partial_\Sigma F_c = -\varepsilon'_{wind} = ac\kappa^{-1}\partial^2_\Sigma T^4_c. \tag{7.10}$$

Note that we have made an additional approximation in writing the differential equation governing the flux, for we have neglected the heat moved by circumferential radiative transport. To justify this, note that the circumferential transport by radiation should have

$$L_c = 2\pi R dz k\frac{\Delta T}{\pi R} = 2dzk\Delta T \therefore \varepsilon'_{rad} = \frac{2kdz\Delta T}{2\pi R^2 dz\rho} = \frac{k\Delta T}{\rho\pi R^2} \approx \left(\frac{l}{R}\right)\frac{fF}{\rho\pi R}, \tag{7.11}$$

where $f \equiv \Delta T/T$. Taking $F \sim 10^{12}$erg/cm^2/s, $R \sim 10^{10}$cm, $l \sim 10^7$cm, and $v_s \sim 10^7$cm/s, we find that $\varepsilon'_{wind} \sim 10^8 f^2$erg/g while $\varepsilon'_{rad} \sim 10^{-1} f$erg/g. As the wind carries far more heat than the circumferential transport, we are justified in neglecting the latter.

In all radiative models considered, regardless of the Rossby number, we found that for $\Delta T/T < 1$,

$$\varepsilon' = y' T_4^{3/2}\left(\frac{R_\odot}{R}\right)\left(\frac{\Delta T}{T}\right)^q\left(\frac{10^4 l}{2\pi R}\right)^a \mathrm{Ro}_s^b\left(\frac{F_\odot}{\Sigma_h}\right). \tag{7.12}$$

This is just Eq. (6.173). The dimensionless quantities y', q, a, b may be found in table 6.1. Up to minor corrections of order unity, this form should hold until the critical temperature anisotropy is reached. The values associated with this are given in table 6.2.

[3]We are really comparing $4\ln T$ to κ when we say that the latter doesn't vary significantly.

Using these results, we find that the anisotropy of the flux at the star's surface is

$$\Delta F = F_e - 2\int_0^{\Sigma_h} \varepsilon'_{wind} d\Sigma. \tag{7.13}$$

We only integrate to Σ_h because, as we showed in our one-dimensional model, the temperature difference induced by the flux drops off exponentially below that depth. Now from our one-dimensional simulations, we know that $\Delta T/T$ is roughly a constant over the range $\Sigma = 0$ to $\Sigma = \Sigma_h$, changing only by a factor of two or so. As a result, we may estimate for low input luminosities that

$$\frac{\Delta T}{T} \sim \frac{\Delta F}{4F} = \frac{\Delta F}{2F_e + 4F_i} \approx \frac{\Delta F}{4F_i}, \tag{7.14}$$

and estimate the integral as

$$\Delta F = F_e - 2\int_0^{\Sigma} {}_h\varepsilon'_{wind} d\Sigma \tag{7.15}$$

$$\approx F_e - 2\Sigma_h \varepsilon'_{wind} \tag{7.16}$$

$$\approx F_e - 2\Sigma_h y' T_4^{3/2} \left(\frac{R_\odot}{R}\right) \left(\frac{\Delta T}{T}\right)^q \left(\frac{10^4 l}{2\pi R}\right)^a \mathrm{Ro}_s^b \left(\frac{F_\odot}{\Sigma_h}\right) \tag{7.17}$$

$$\approx F_e - 2y' T_4^{3/2} \left(\frac{R_\odot}{R}\right) \left(\frac{\Delta T}{T}\right)^q \left(\frac{10^4 l}{2\pi R}\right)^a \mathrm{Ro}_s^b F_\odot \tag{7.18}$$

$$\approx F_e - 2y' T_4^{3/2} \left(\frac{R_\odot}{R}\right) \left(\frac{\Delta T}{T}\right)^q \left(\frac{10^4 l}{2\pi R}\right)^a \mathrm{Ro}_s^b F_\odot. \tag{7.19}$$

Now in estimating the integral we should multiply the wind solution by a few to accommodate the fact that T typically varies by around a factor of 5 over the integration regime. This allows us to use the surface values for thermodynamic quantities later on. Thus

$$\frac{\Delta F}{F_i} = \frac{F_e}{F_i} - 5y' T_4^{3/2} \left(\frac{R_\odot}{R}\right) \left(\frac{\Delta T}{T}\right)^q \left(\frac{10^4 l}{2\pi R}\right)^a \mathrm{Ro}_s^b \frac{F_\odot}{F_i}. \tag{7.20}$$

This may also be written as

$$u = r - tu^q, \tag{7.21}$$

where $r, t > 0$, $r < 1$. Here r is the ratio of external to intrinsic illumination and t is a dimensionless parameter giving the efficacy of the winds in transporting heat relative to the intrinsic flux. In general we may solve this numerically, but it is also worth examining the behavior of the solution in various limits. For $r \ll t$, a perturbative expansion may be used to find

$$u \approx r - tr^q. \tag{7.22}$$

Physically, this means that the anisotropy is just the maximum allowed minus a small contribution due to the action of winds. For $t \ll r$, we may neglect the linear term in u to find

$$u \approx \left(\frac{r}{t}\right)^{\frac{1}{q}}. \tag{7.23}$$

In this limit the dominant effect is that of the wind, and the result is just a balance reflecting the fact that the wind needs some anisotropy to function. Except for small y', this last limit is generally not accessible while maintaining the small anisotropy approximation. As a result, we generally expect to be in the former limit with radiative stars, and only expect to be in the latter in convective stars with just the right amount of external illumination.

Now suppose that $\Delta T/T$ is large relative to the critical value. Once more we write

$$\Delta F = F_e - 2\int_0^{\Sigma_h} \varepsilon'_{wind} d\Sigma \sim F_e - 2\Sigma_h \varepsilon'_{wind}. \tag{7.24}$$

Here, $\Delta T/T$ corresponds more closely to $(\Delta F/\sigma)^{1/4}T^{-1}$ than to $\Delta F/4F$, for the critical $\Delta T/T$ is at least unity, so

$$\varepsilon'_{wind} = \frac{v_s^3}{\pi R}\left(\frac{\Delta T}{T}\right), \tag{7.25}$$

and hence

$$\Delta F = F_e - \frac{2\Sigma_h}{\pi R T} v_s^3 \left(\frac{\Delta F}{\sigma}\right)^{1/4} = F_e - 10 F_\odot T_4^{1/2}\left(\frac{R_\odot}{R}\right)\left(\frac{\Delta F}{F_\odot}\right)^{1/4}. \tag{7.26}$$

Performing the adjustment to allow us to use all quantities near the surface, we get

$$\Delta F = F_e - 20 F_\odot T_4^{1/2}\left(\frac{R_\odot}{R}\right)\left(\frac{\Delta F}{F_\odot}\right)^{1/4}. \tag{7.27}$$

Now in this regime, the quantity of interest really should be $\Delta F/F_e$, not $\Delta F/F_i$. Casting the equation into this form gives

$$\frac{\Delta F}{F_e} = 1 - 20 F_\odot T_4^{1/2}\left(\frac{R_\odot}{R}\right)\left(\frac{\Delta F}{F_e}\right)^{1/4}\left(\frac{F_e}{F_\odot}\right)^{-3/4}. \tag{7.28}$$

Recalling that the temperature goes as $F^{1/4}$, and that the flux should be of order F_e, we expect that

$$\frac{\Delta F}{F_e} = 1 - 20\left(\frac{R_\odot}{R}\right)\left(\frac{F_e}{F_\odot}\right)^{-5/8}\left(\frac{\Delta F}{F_e}\right)^{1/4}. \tag{7.29}$$

This equation may be solved numerically as a function of the coefficient of the second term. At very large F_e, the anisotropy is once more near unity. As F_e is lowered, a perturbative expansion shows that the anisotropy goes as

$$\frac{\Delta F}{F_e} \sim 1 - 20\left(\frac{R_\odot}{R}\right)\left(\frac{F_\odot}{F_e}\right)^{5/8}. \tag{7.30}$$

At small F_e relative to $20^{8/5}F_\odot \sim 100F_\odot$, the solution goes as

$$\frac{\Delta F}{F_e} \sim 10^{-5}\left(\frac{R}{R_\odot}\right)^{4}\left(\frac{F_e}{F_\odot}\right)^{5/2}. \tag{7.31}$$

7.2 Convective Stars

We now turn to the case of circumferential heat transport in fully convective stars. Suppose first that the star has an active nuclear-burning core. By our arguments in Chapter **??** convection will continue, but it will carry less heat to the surface. If $L_e < L_i/2$, the reduction in heat carried from the core to the surface will be L_e, and the surface temperature will not change, for the external illumination makes up the difference. Otherwise the reduction will be $L_i/2$, and the surface temperature will change on the illuminated side to match L_e. [4]. In either case, the reduction in heat transport results in an increase in the temperature of the core, and hence an increase in the intrinsic luminosity of the star. This increase will generally raise L_i by an amount comparable to L_e. As this change occurs at the core, the resulting changes in stellar structure should be isotropic. The only way for this to not be the case is if the core heats anisotropically and therefore loses heat preferentially to one side. To show that this is not the case, consider just the circumferential transport due to convection-driven turbulent diffusion. As it will be quite slow near the core, we take the Rossby and Mach numbers to be small. Matching the wind transport with the

[4] The factor of two in the comparison of L_e to L_i is of geometric origin: it reflects the fact that the external illumination only comes in on one side. In reality the factor should not be precisely 2, but this is accurate to the degree of precision present in our models.

flux anisotropy yields

$$\varepsilon = \frac{v_c l v_s^2 \Delta T}{\pi R^2 T} = \frac{\min(L_e, L_i/2)}{2\pi R^2 \rho} \tag{7.32}$$

$$\therefore \frac{v_c l v_s^2 \Delta T}{T} = \frac{\min(L_e, L_i/2)}{2\rho} \tag{7.33}$$

$$\therefore \frac{v_c l \Delta T}{T} \approx \frac{\min(L_e, L_i/2)}{2P} \tag{7.34}$$

$$\therefore \frac{(F_i/\rho)^{1/3} l \Delta T}{T} \approx \frac{\min(L_e, L_i/2)}{2P} \tag{7.35}$$

$$\therefore \frac{(F_i v_s^2/P)^{1/3} l \Delta T}{T} \approx \frac{\min(L_e, L_i/2)}{2P} \tag{7.36}$$

$$\therefore \frac{(F_i v_s^2)^{1/3} l \Delta T}{T} \approx \frac{\min(L_e, L_i/2)}{2P^{2/3}} \tag{7.37}$$

$$\therefore \frac{\Delta T}{T} \approx \frac{\min(L_e, L_i/2)}{2(F_i v_s^2)^(1/3) l P^{2/3}}. \tag{7.38}$$

Here we have made use of the usual result that $F_{conv} \sim \rho v_c^3$. At these depths, $T \sim 10^6$K, so $v_s^2 \sim 10^7$cm/s. Additionally, $l \sim R$ here so $l \sim 10^{11}$cm. We may estimate the pressure as $P \sim GM^2/R^4 \sim 10^{17}\mathrm{erg/cm}^3$. Finally, we estimate that $F_i = L_i/(4\pi R_{core}^2) \sim 100L_i/(4\pi R^2) \sim 10^{-21}L_i$. Thus the temperature difference is expected to be

$$\frac{\Delta T}{T} \sim \frac{\max(L_e, L_i/2)}{10^{20} L_i}. \tag{7.39}$$

This is minuscule for any conceivable flux anisotropy, confirming our assumptions and yielding an isotropic star. All of our conclusions about stars of this type from the one-dimensional analysis therefore hold in the steady-state. Of course in the transient case the star can still be anisotropic. As we will see, the transient response of nuclear burning stars is the same as the steady-state response for non-burning stars.

Now suppose that the star is not nuclear burning. The same arguments regarding lowering heat transport from the core apply, but now the core simply responds to different heat transport by matching it. As a result, if $L_e < L_i/2$, there should be no visible changes: the star will cool more slowly, but the surface flux will remain the same and the star will remain isotropic. On the other hand, if $L_e > L_i/2$, the star may be isotropic. This is because the heating cannot run uphill: we cannot put heat in at one temperature and have the energy move towards higher temperatures. As a result, the surface temperature will necessarily rise in the absence of circumferential transport to match the flux associated with L_e. This requires a shallower thermal gradient than convection can support, and so will result in radiative transport for at least some of the range $\Sigma < \Sigma_h$. As we saw in table 6.1, radiative zones are orders of magnitude more efficient than convection zones at transporting heat circumferentially. This means that the limiting factor is the distance that the heat has to traverse in the convection zone on the cool side.

Consider a wind being pushed from one side to the other by a thermal gradient. When this wind reaches the convecting regions, it encounters an increase in resistance, and so slows down. This leads to an accumulation of hot material on the interface between the radiative and convective regions, which will shut down convection in a larger region than that covered by the external heating. This will continue until there is insufficient flux being transported to accommodate a larger radiative zone. We may calculate the area of the new radiative zone roughly as

$$A_{rad} = 2\pi R^2 \left(1 + \min\left(1, \frac{4\pi R^2 \Sigma_h \varepsilon'_{wind}}{L_i}\right)\right), \tag{7.40}$$

where ε'_{wind} is to be calculated using the y' values for radiation, not convection. Within this zone, the temperature and flux anisotropies may be computed as before. Inside the remaining convection zone, the flux is just F_i. In principle one might multiply y' by the ratio of the linear dimension of the radiative transport regime to $2\pi R$, but this correction is a small factor of order unity in all cases, and therefore does not justify the complexity associated with performing a self-consistency calculation for the area of the radiative zone.

7.3 Crossover Behavior

The final case to consider is that where the star is convective for $\Sigma < \Sigma_c$ and radiative otherwise. This case is like the nuclear burning convective case, in that there is an intrinsic flux which can be bottled up. On the other hand, the exponential suppression of changes in thermal structure characteristic of radiative zones means that we generally do not have the ability to change the core temperature of these stars. As a result, the problem of determining whether or not the thermal structure is strongly anisotropic is actually somewhat nontrivial.

To begin with, suppose that the thermal anisotropies are small enough that all winds are subsonic. Initially, the external illumination will not alter the size of the convection zone. All that changes is that the flux carried by the convection zone decreases. As there is no significant heating in this region, the flux differential will be preserved down to the base of the convection zone. When it reaches the radiation zone, it will cause changes in thermal structure which will damp exponentially in Σ. As a result, the core will be unchanged, so the intrinsic flux will still emerge. This means that the surface temperature must be sufficient to accommodate the increased flux. As the convection zone requires that specific entropy be constant, the fractional change in temperature which results will be the same throughout the zone. This temperature differential will drive a wind which attempts to equalize the flux between the two sides of the star. In equilibrium, this provides the self-consistency relation

$$4\frac{\Delta T}{T} = \frac{F_e - \int_0^{\Sigma_c} \varepsilon'_{wind} d\Sigma}{F_i} \tag{7.41}$$

$$= \frac{F_e}{F_i} - \left(\frac{F_\odot}{F_i}\right)\left(\frac{\Delta T}{T}\right)^q \int_0^{\Sigma_c/\Sigma_h} y' T_4^{3/2} \left(\frac{R_\odot}{R}\right)\left(\frac{10^4 l}{2\pi R}\right)^a \mathrm{Ro}_s^b dx, \tag{7.42}$$

where

$$x \equiv \frac{\Sigma}{\Sigma_h}. \tag{7.43}$$

There are several ways to simplify the self-consistency relation. To begin with, we may neglect the variation in R, as this is of order unity across any integration range which does not reach the core. This allows us to write

$$4\frac{\Delta T}{T} = \frac{F_e}{F_i} - \left(\frac{\Delta T}{T}\right)^q \left(\frac{10^4 l}{2\pi R}\right)^a \left(\frac{F_\odot}{F_i}\right)\left(\frac{R_\odot}{R}\right) \int_0^{\Sigma_c/\Sigma_h} y' T_4^{3/2} \mathrm{Ro}_s^b dx. \tag{7.44}$$

Recalling that we may write the sonic Rossby number as

$$\mathrm{Re}_s = \frac{v_s}{2\pi R\Omega}, \tag{7.45}$$

we find that

$$4\frac{\Delta T}{T} = \frac{F_e}{F_i} - 10^{-1}\left(\frac{F_\odot}{F_i}\right)\left(\frac{R_\odot}{R}\right)^{1+b} \Omega_{-4}^{-b} \int_0^{\Sigma_c/\Sigma_h} y' T_4^{3/2+b} dx \left(\frac{\Delta T}{T}\right)^q \left(\frac{10^4 l}{2\pi R}\right)^a. \tag{7.46}$$

Note that in convection zones y' may be put in the form

$$y' = 10^{w_1}\left(\frac{R}{R_\odot}\right)^{w_2}\left(\frac{F}{F_\odot}\right)^{w_3}\left(\frac{\Sigma}{\Sigma_h}\right)^{w_4} T_4^{w_5}\Omega^{w_6}, \tag{7.47}$$

where w_i are constants. The one case which this doesn't handle is that with $v > 2\pi\Omega R, v_c$. There some of the powers w_i must be modified when $\Omega l = v_c$. This introduces a variation of up to ± 0.5 in the exponents here, and we will find such variation to be unimportant. As a result, we may write

$$y' = y_0 x^w, \tag{7.48}$$

where $w = w_4 + w_5$ is in the range $[-1/2, 1]$ and y_0 is the value of y' at $\Sigma = \Sigma_h$. Additionally, we may substitute $T_0(P/P_0)^{1+1/\gamma}$ for T. Though the thin-atmosphere approximation is not guaranteed to hold in all regions of interest, we make errors only of order unity by using it so we further substitute $P = \Sigma g$. This yields

$$4\frac{\Delta T}{T} = \frac{F_e}{F_i} - y_0 10^{-1}\left(\frac{F_\odot}{F_i}\right)\left(\frac{R_\odot}{R}\right)^{1+b}\Omega_{-4}^{-b}\left(\frac{\Sigma_c}{\Sigma_h}\right)^{(3/2+b)(1+1/\gamma)+w+1} T_{4,0}\left(\frac{\Delta T}{T}\right)^q\left(\frac{10^4 l}{2\pi R}\right)^a, \tag{7.49}$$

where $T_{4,0}$ is the temperature at the heating depth, and where we have dropped the order unity factors produced by the integration process. This may be approximated as

$$4\frac{\Delta T}{T} = \frac{F_e}{F_i} - 10^{[-3.5,0]}\Omega_{-4}^{-b}\left(\frac{F_\odot}{F_i}\right)\left(\frac{R_\odot}{R}\right)^{1+b}\left(\frac{\Sigma_c}{\Sigma_h}\right)^3\left(\frac{\Delta T}{T}\right)^q\left(\frac{10^4 l}{2\pi R}\right)^a. \tag{7.50}$$

In the cases of interest, $\Sigma_c \gg \Sigma_h$, for otherwise our arguments in the one-dimensional model indicate that the convection zone will disappear just from the required surface temperature changes. As a result of this and the other prefactors either being large or near unity, there is some positive n for which we may write

$$4\frac{\Delta T}{T} = \frac{F_e}{F_i} - 10^n\left(\frac{\Delta T}{T}\right)^q. \tag{7.51}$$

When $q = 1$ the solution is roughly

$$4\frac{\Delta T}{T} \sim \frac{F_e}{F_i 10^n}. \tag{7.52}$$

When $q > 1$ there is a competition between the linear and nonlinear terms. The two terms are roughly equal when

$$\frac{F_e}{F_i} \sim 10^{-\frac{n}{q-1}}. \tag{7.53}$$

For larger fluxes, the nonlinear term dominates and

$$\frac{\Delta T}{T} = \left(\frac{F_e}{4F_i 10^n}\right)^{1/q}. \tag{7.54}$$

For smaller ones, the linear term dominates and

$$\frac{\Delta T}{T} = \frac{F_e}{4F_i}. \tag{7.55}$$

Note that n goes roughly as $3\log \Sigma_c/\Sigma_h$, so in all cases with very deep convection zones we reproduce our result of high isotropy.

Note that in assuming that radial lines are isentropes, we are requiring that the characteristic timescale of convection be shorter than that of the winds[5]. If this fails, then the winds may circle the star without coming into local equilibrium with any radial lines, and hence a better approximation is that surfaces of fixed r are isentropes. This case is not, however, physically realistic. To see this, first note that for the criterion to assume radial isentropes is

$$\frac{l}{v_c} < \frac{2\pi R}{v}. \tag{7.56}$$

Rearranging gives

$$v/v_c < 2\pi R/l. \tag{7.57}$$

This is roughly

$$v/v_c < 10^3(\Sigma/\Sigma_h)^(-1-1/\gamma). \tag{7.58}$$

Now

$$v_c \sim 10^5(F/F_\odot)^{1/3}(\Sigma/\Sigma_h)^{1/3\gamma}, \tag{7.59}$$

so

$$v < 10^8(F/F_\odot)^{1/3}(\Sigma/\Sigma_h)^{-1-2/3\gamma}. \tag{7.60}$$

For the stars of interest, the first factor is generally of order 1/3, and the sound speed is roughly 10^6cm/s even at large depths, so subsonic violation of this criterion only becomes possible at $\Sigma \sim 30\Sigma_h$. Now the critical thermal anisotropy to get sonic winds in a convection zone is

$$\frac{\Delta T}{T} \sim 30T_4^{-1/4}\left(\frac{F\Sigma_h}{F_\odot\Sigma}\right)^{1/6}. \tag{7.61}$$

[5]The assumption takes this form in regions of high convective efficiency. Were this not to hold, we would need to consider the timescale for material coming into radiative equilibrium as well. Fortunately only a small portion of each convection zone exhibits inefficient convection, as was discussed in Chapter 2, so we need not deal with the inefficient limit.

As the anisotropy is damped into the star by the winds, we may take this as a lower bound on the anisotropy above the point where the radial isentrope assumption fails, so the flux transported is

$$\varepsilon'_{wind} = \frac{v_s c_p \Delta T}{\pi R} \tag{7.62}$$

$$= \frac{v_s^3 \Delta T}{\pi R T} \tag{7.63}$$

$$\geq 30 \frac{v_s^3}{\pi R} T_4^{-1/4} \left(\frac{F\Sigma_h}{F_\odot \Sigma}\right)^{1/6} \tag{7.64}$$

$$= 10^{10} T_4^{5/4} \left(\frac{F\Sigma_h}{F_\odot \Sigma}\right)^{1/6} \text{erg/g/s} \tag{7.65}$$

$$= 2 \times 10^2 \frac{F_\odot}{\Sigma_h} T_4^{5/4} \left(\frac{F\Sigma_h}{F_\odot \Sigma}\right)^{1/6}. \tag{7.66}$$

Integrating this gives

$$F_{wind} = \int_0^{30\Sigma_h} d\Sigma \varepsilon'_{wind} \tag{7.67}$$

$$\geq \int_0^{30\Sigma_h} d\Sigma 2 \times 10^2 \frac{F_\odot}{\Sigma_h} T_4^{5/4} \left(\frac{F\Sigma_h}{F_\odot \Sigma}\right)^{1/6} \tag{7.68}$$

$$= \int_0^{30} dx 2 \times 10^2 F_\odot T_4^{5/4} \left(\frac{F}{F_\odot x}\right)^{1/6} \tag{7.69}$$

$$= 2 \times 10^2 T_{4,0} F_\odot^{5/6} F^{1/6} \int_0^{30} dx x^{\frac{5}{4}(1+1/\gamma)-\frac{1}{6}} \tag{7.70}$$

$$\sim 2 \times 10^2 T_{4,0} F_\odot^{5/6} F^{1/6} \frac{30^3}{3} \tag{7.71}$$

$$\sim 2 \times 10^6 T_{4,0} F_\odot^{5/6} F^{1/6} \tag{7.72}$$

$$\sim 2 \times 10^6 T_{4,0} F_\odot. \tag{7.73}$$

As this lower bound is well in excess of the Eddington luminosity for any convective star, an anisotropy in the flux that large would ablate the star to nothing on short timescales, and is therefore not a case of interest.

Now if $\Delta T/T$ approaches or exceeds unity, then we must instead write

$$\frac{\Delta F}{F_i} = \frac{F_e}{F_i} - 10^n \left(\frac{\Delta T}{T}\right)^q. \tag{7.74}$$

Recalling that $\Delta F \sim \sigma(\Delta T)^4$ in this case,

$$\frac{\Delta F}{F_i} = \frac{F_e}{F_i} - 10^n \left(\frac{\Delta F}{F_i}\right)^{q/4} \left(\frac{T_i}{T}\right)^q . \tag{7.75}$$

As the flux has raised the mean temperature by approximately $(F_e/F_i + 1)^{1/4}$,

$$\frac{\Delta F}{F_i} = \frac{F_e}{F_i} - 10^n \left(\frac{\Delta F}{F_i}\right)^{q/4} \left(\frac{F_e}{F_i} + 1\right)^{q/4} . \tag{7.76}$$

As F_e must be large relative to F_i to bring about a change of this magnitude, the factor of unity at the end may be removed, giving

$$\frac{\Delta F}{F_i} = \frac{F_e}{F_i} - 10^n \left(\frac{\Delta F}{F_i}\right)^{q/4} \left(\frac{F_e}{F_i}\right)^{q/4} . \tag{7.77}$$

The nature of the solutions is the same as the nature of the solutions in the previous section, just with

$$q \to \frac{q}{4} \tag{7.78}$$

$$n \to n + \frac{q}{4} \log \frac{F_e}{F_i} \tag{7.79}$$

$$\frac{\Delta T}{T} \to \frac{\Delta F}{F_i}. \tag{7.80}$$

As in the previous section, it is now more appropriate to speak of the flux anisotropy as $\Delta F/F_e$, so

$$\frac{\Delta F}{F_e} = 1 - 10^n \left(\frac{\Delta F}{F_e}\right)^{q/4} \left(\frac{F_e}{F_i}\right)^{q/2-1} . \tag{7.81}$$

For external luminosities, we require

$$\frac{\Delta F}{F_e} = 10^{-\frac{4n}{q}} \left(\frac{4-2q}{q}\right), \tag{7.82}$$

while for large external luminosities we have

$$\frac{\Delta F}{F_i} = \frac{F_e}{F_i} - 10^n \left(\frac{F_e}{F_i}\right)^{q/4} . \tag{7.83}$$

Here large and small are of course referenced to $10^{4n/q} F_i$.

Finally, if the thermal and flux anisotropies are large, the wind is sonic and we expect $y' = 10$, $q = 1$, $a = 0$, and $b = 0$. This greatly increases the efficiency of circumferential transport, and results in n increasing by an additive factor somewhere between 1 and 4. This pushes us further into the regime where our assumption that $a > 0$ holds, and the remainder of the above analysis is unchanged.

It is worth noting that in all of the cases above, we saw no transition from convective to radiative behavior. This is because increasing the requisite flux does not force this transition. Rather, it is increasing the flux while at the same time insisting that the ratio of the temperature at the base of the convection zone to that at the top of the convection zone remain invariant. Of course if Σ_c is small, then increasing the luminosity results in shrinking the convection zone appreciably in relative terms. This can, as in the case of our one-dimensional model of the sun, cause the convection zone to disappear.

References

Brickhill, A. J. “The pulsations of ZZ Ceti stars. III - The driving mechanism”. In: *Monthly Notices of the Royal Astronomical Society* 251 (Aug. 1991), pp. 673–680 (cit. on p. 111).

Mei, C. C. and T. Y.-t. Wu. “Gravity Waves due to a Point Disturbance in a Plane Free Surface Flow of Stratified Fluids”. In: *Physics of Fluids* 7 (Aug. 1964), pp. 1117–1133. DOI: `10.1063/1.1711351` (cit. on p. 111).

Shiode, J. H. et al. “The observational signatures of convectively excited gravity modes in main-sequence stars”. In: *Monthly Notices of the Royal Astronomical Society* 430 (Apr. 2013), pp. 1736–1745. DOI: `10.1093/mnras/sts719`. arXiv: `1210.5525 [astro-ph.SR]` (cit. on p. 111).

Wu, Y. and P. Goldreich. “Gravity Modes in ZZ Ceti Stars. IV. Amplitude Saturation by Parametric Instability”. In: *The Astrophysical Journal* 546 (Jan. 2001), pp. 469–483. DOI: `10.1086/318234`. eprint: `astro-ph/0003163` (cit. on p. 111).

8

Time Dependence

It is all a matter of time scale. An event that would be unthinkable in a hundred years may be inevitable in a hundred million.

– Carl Sagan

The results of our one-dimensional model indicate that there are two modes of behavior for stars in the presence of external illumination, and that stars pick one or the other on the basis of being predominantly radiative or convective. In this chapter we will analyze these behaviors in the transient case through a combination of numerics and analytics. We begin by describing the numerical methods used, and then proceed to introduce the cases of fully radiative, fully convective, and mixed radiation-convection stars.

8.1 Assumptions and Computational Methods

The time-dependent portion of Acorn represents a compromise between the simplicity of time-independent codes like Gob and the complexity of modern time-dependent codes like MESA. The equation of state used is the same one present in Gob and in the time-independent portion of Acorn, incorporating at leading order various ionization effects as well as radiation pressure. The opacity is the same as that used in Acorn, a mix of the OPAL[1] and Ferguson[2] tables. The thin shell approximation is used everywhere, and only envelope evolution is considered. Hydrostatic equilibrium

[1] C. A. Iglesias and F. J. Rogers. "Updated Opal Opacities". In: *The Astrophysical Journal* 464 (June 1996), p. 943. DOI: 10.1086/177381.

[2] Jason W. Ferguson et al. "Low-Temperature Opacities". In: *The Astrophysical Journal* 623.1 (2005), p. 585. URL: http://stacks.iop.org/0004-637X/623/i=1/a=585.

is assumed at all times. Finally, it is assumed that convection adjusts to the changing flux being carried faster than the thermal adjustment timescale of the envelope, and hence that it may be assumed that the convective gradient is the gradient required to carry the appropriate flux in steady-state. This last assumption will be justified later on.

Assuming hydrostatic equilibrium only, the time-dependent equations of stellar structure are[3]

$$\frac{\partial r}{\partial m} = -\frac{1}{4\pi r^2 \rho}, \tag{8.1}$$

$$\frac{\partial P}{\partial m} = \frac{Gm}{4\pi r^2}, \tag{8.2}$$

$$\frac{\partial L}{\partial m} = -\varepsilon + c_p \frac{\partial T}{\partial t} - \frac{\delta}{\rho}\frac{\partial P}{\partial t}, \tag{8.3}$$

$$\frac{\partial T}{\partial m} = \frac{GmT}{4\pi r^4 P}\nabla, \tag{8.4}$$

where ε is the power per unit mass being deposited by external illumination, and the signs have been chosen such that the mass coordinate is the mass above the point in question. Note that we include the equation governing r for purposes of tracking how r changes as the other quantities vary, but we do not allow it to produce feedback with the other equations. Note also that the time derivatives are to be taken at fixed mass, not at fixed spatial coordinate. Now the condition of hydrostatic equilibrium means that $\frac{\partial P}{\partial t} = 0$, so we may drop this term.

We now make the substitution

$$P = \frac{mg}{4\pi r^2}, \tag{8.5}$$

in accordance with the thin-shell approximation. This, combined with the previous arguments regarding time derivatives, allows us to eliminate P and write

$$P = \frac{mg}{4\pi r^2}, \tag{8.6}$$

$$\frac{\partial r}{\partial m} = -\frac{1}{4\pi r^2 \rho}, \tag{8.7}$$

$$\frac{\partial L}{\partial m} = -\varepsilon + c_p \frac{\partial T}{\partial t}, \tag{8.8}$$

$$\frac{\partial T}{\partial m} = \frac{T}{m}\nabla. \tag{8.9}$$

[3]Rudolf Kippenhahn, Alfred Weigert, and Achim Weiss. *Stellar Structure and Evolution*. Springer, 2012. ISBN: 978-3-642-30304-3.

In order to fully specify the system, we must of course specify boundary conditions. For the $t = 0$ boundary, we specify that $\varepsilon = 0$ and that $\partial_t T = 0$. When the mass coordinate equals the envelope mass, i.e. $m = M_e$, we choose to hold T constant. Physically this choice simply means that we must only consider timescales shorter than the thermal timescale of the envelope, given by

$$t_e = \frac{c_p T(M_e) M_e}{L_{in}} \approx 7 \times 10^{12} \mathrm{s} T_5 \frac{M_e L_\odot}{M_\odot L}. \tag{8.10}$$

The envelope mass was generally chosen to optimize convergence of the time-stepping code and to stay carefully within the realm of validity of the opacity and equation of state microphysics. As a result, typical values were $3 \times 10^{-3} M$. Typical envelope-base temperatures are $T \approx 10^5$K, and generally $\frac{ML_\odot}{M_\odot L} \approx 1$, so the timescales the code may investigate with this boundary condition are those shorter than 2×10^9s, which should be long enough to see the transient effects of interest. Note that in considering ∇ to respond immediately, we are also imposing a minimum timescale over which the results may be taken seriously. This timescale is given roughly by the convective turnover time, l/v_c, or around 10^6s at the base of the envelope and 10^3s where convection begins. As a result, time steps will usually be chosen at 10^6s.

The remaining boundary condition we use to set

$$4\pi r^2 \sigma T^4 = wL, \tag{8.11}$$

where all quantities are evaluated at the mass corresponding to $\tau = 2/3$ and w is a fudge factor obtained from the steady state evolution which makes this relation true at $t = 0$. Note that this means that we only track the mass in the star at $\tau > 2/3$. This helps with numerical stability, as it reduces the range of densities to consider, which drastically improves the condition number of the linear algebra problems solved in the time-stepping process.

In typical simulations, w was found to be roughly 0.5. This is not a matter of a misplaced factor of two in the surface temperature determination. Rather, it is due to well-documented approximations made in Gob's, and hence Acorn's, method for computing the effects of radiation dilution in the photosphere[4]. It is clear that these boundary conditions are sufficient, for L and T are the only variables involved, all others being determined by either the approximations made or the equation of state, and we now have two first order differential equations with one boundary condition each in one dimension.

[4] B. Paczyński. "Envelopes of Red Supergiants". In: *Acta Astronomica* 19 (1969), p. 1.

For the starting state, we use the steady state solution. This additionally defines the mass grid used to discretize the problem. Note that this produces $N+1$ points for L and N points for T, such that the temperature is defined only between pairs of points at which the luminosity is defined. For the sake of writing down the discretization, let there be $2N+1$ points in the mass grid numbered 0 through $2N$. Define L on all even-numbered points and all other quantities on the odd-numbered points. The equations of interest are then:

$$\partial_t \rho_{2i+1} = \frac{\partial \rho_{2i+1}}{\partial T}|_P \partial_t T_{2i+1} \tag{8.12}$$

$$(i \neq N)\partial_t T_{2i+1} = \frac{1}{c_{p(2i+1)}}\left[\epsilon_{2i+1} - \frac{L_{2i+2} - L_{2i}}{m_{2i+2} - m_{2i}} - c_{p(2i+1)}\frac{v_{\phi(2i+1)}}{R}\partial_\phi T_{(2i+1)}\right] \tag{8.13}$$

$$(i \neq 0)\frac{T_{2i+1} - T_{2i-1}}{m_{2i+1} - m_{2i-1}} = \nabla_{2i+1}\frac{T_{2i+1}}{m_{2i+1}} \tag{8.14}$$

$$\partial_t T_{2N-1} = 0 \tag{8.15}$$

$$\partial_t L_0 = 16 w \pi R^2 \sigma T_1^3 \partial_t T_1 \tag{8.16}$$

Note that the boundary conditions are enforced in differential form. In addition, note that our use of asymmetric differences in places should not matter in the limit of large N.

The equations complete and discretized, we turn to the method of solution. For numerical stability the backwards Euler method was used, such that all time derivatives were written in the form

$$\partial_t A(t) = \frac{A(t+dt) - A(t)}{dt}. \tag{8.17}$$

Thus the equations solved were of the form

$$\boldsymbol{f}(t+dt) = \boldsymbol{f}(t) + dt\frac{d\boldsymbol{f}}{dt}|_{t=t+dt}. \tag{8.18}$$

This method is particularly appropriate given the stiff nature of ∇ in convection zones, a fact that will be discussed at length later on. As the backwards Euler method is an implicit integrator, it requires knowledge of all relevant derivatives evaluated in the future. To solve for these self-consistently, a damped version of Newton's method was implemented. The Jacobian was constructed analytically, with the exception of parts involving ∇, which were computed numerically. This then allowed for an iterative solution of the form

$$\boldsymbol{f}^{i+1}(t+dt) = \boldsymbol{f}^i(t+dt) + \lambda\boldsymbol{\delta}, \tag{8.19}$$

where λ is an adaptively chosen damping parameter beginning at 0.3 for $i = 0$ and then reduced geometrically whenever slow convergence was indicated. Here $\boldsymbol{\delta}$ is the solution to the equation

$$\hat{J}\boldsymbol{\delta} = -\boldsymbol{b}, \tag{8.20}$$

where $\boldsymbol{b}$ is a vector formed by subtracting the right side of each of the discretized equations from the left and $\hat{J}$ is the operator formed from the derivatives of $\boldsymbol{b}$'s components with respect to the entries in $\boldsymbol{f}$. The latter is fortunately sparse, and so the equation does not require an explicit matrix inversion and hence is fast to solve. The above procedure is iterated in the code until the error, as measured by $\boldsymbol{b}$, falls below a critical threshold, usually defined as 10^{-4} relative to $\boldsymbol{f}$. Given a desired time-step, this procedure was attempted first for the full step. If the solution proves numerically unstable, the step is divided in two and attempted again. This is done recursively until the full requested step has completed or until a certain number of failures are reached, at which point an error is generated and the program exits.

It is finally worth noting that an initial settling period is allowed, generally twenty time-steps, over which any deviations due to numerical imprecision in the steady state solution are worked out and allowed to come to equilibrium. This generally results in the luminosity of the star shifting by as much as several percent.

8.2 Fully Radiative Stars

The first model of interest is that of a completely radiative star, such that we may verify our claim that such stars are only heated significantly at depths above the heating one. Figure 8.1 shows the time evolution of just such a star, with $M = M_\odot, R = R_\odot, L = 100L_\odot$. From the figure it is clear that the change in temperature does indeed drop off exponentially for $\Sigma = \Sigma_h$, as predicted. Additionally, the value of $\Delta T/T$ at the surface, roughly 0.19, matches our expectation of

$$\frac{\Delta T}{T_0} = \frac{L_f^{1/4} - L_i^{1/4}}{L_i^{1/4}} = \left(\frac{L_f}{L_i}\right)^{1/4} - 1 = 2^{1/4} - 1 = 0.19. \tag{8.21}$$

To verify that the star was indeed in equilibrium at the end of this simulation, the same scenario was run again with twice the total time interval, such that the final 10^8s had constant luminosity. The results of this are shown in figure 8.2. The good agreement between the two simulations indicates that the star is indeed in equilibrium at the end of the first one.

Now in many cases we are actually interested in the case where the star is initially illuminated from without and that illumination is turned off. The results of simulating

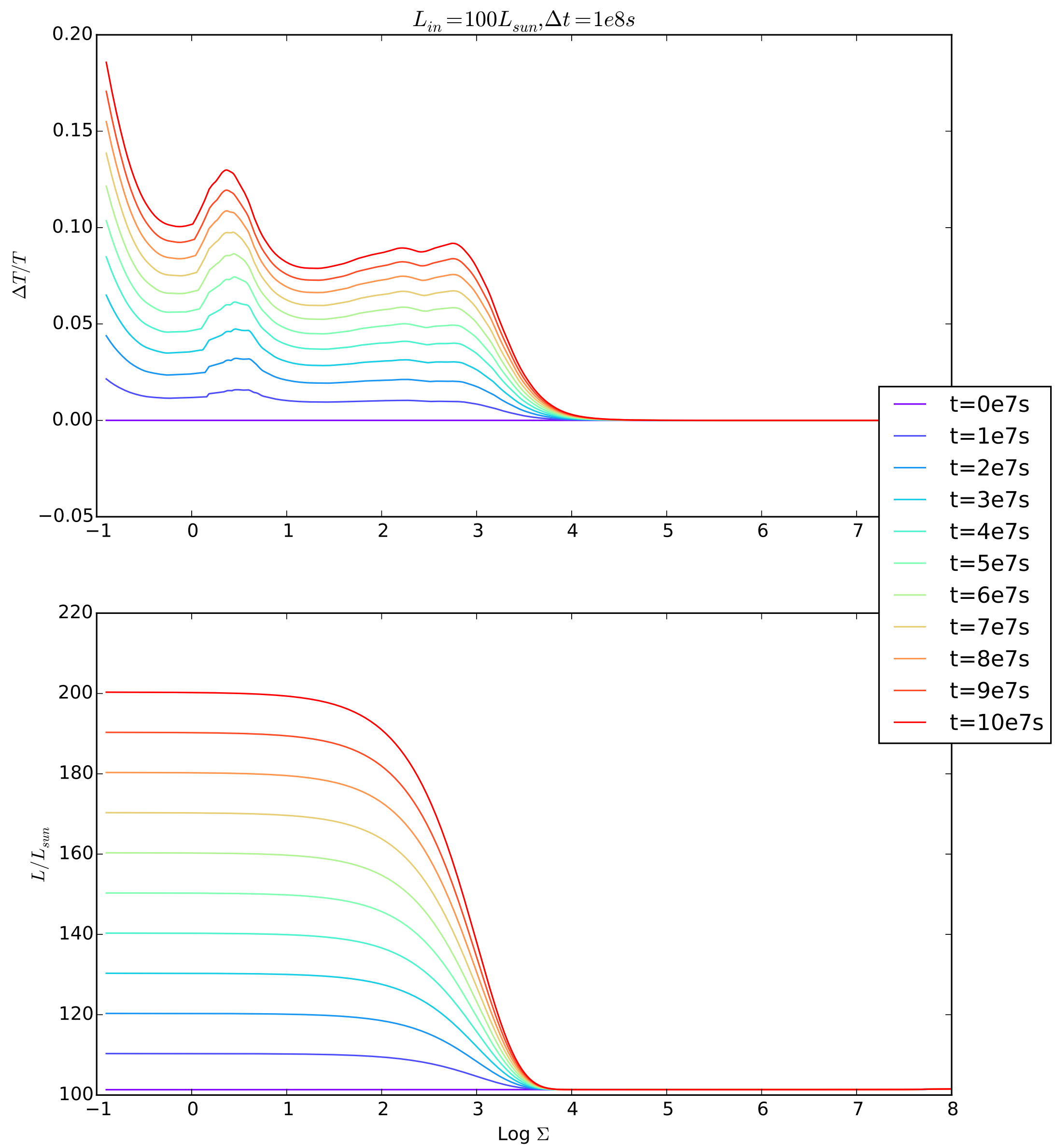

Figure 8.1: $\Delta T/T_0$ (top) and $L/L_\odot$ (bottom) versus $\log\Sigma$ (in g/cm^2) for a star of mass $M_\odot$, radius $R_\odot$, and luminosity $100L_\odot$. The external heat was put in at $\Sigma = 10^3$g/cm^2 and linearly increased from zero to $100L_\odot$ over the course of 10^8s, which is where the simulation ends. Color represents time, with the simulation beginning at violet and ending with red.

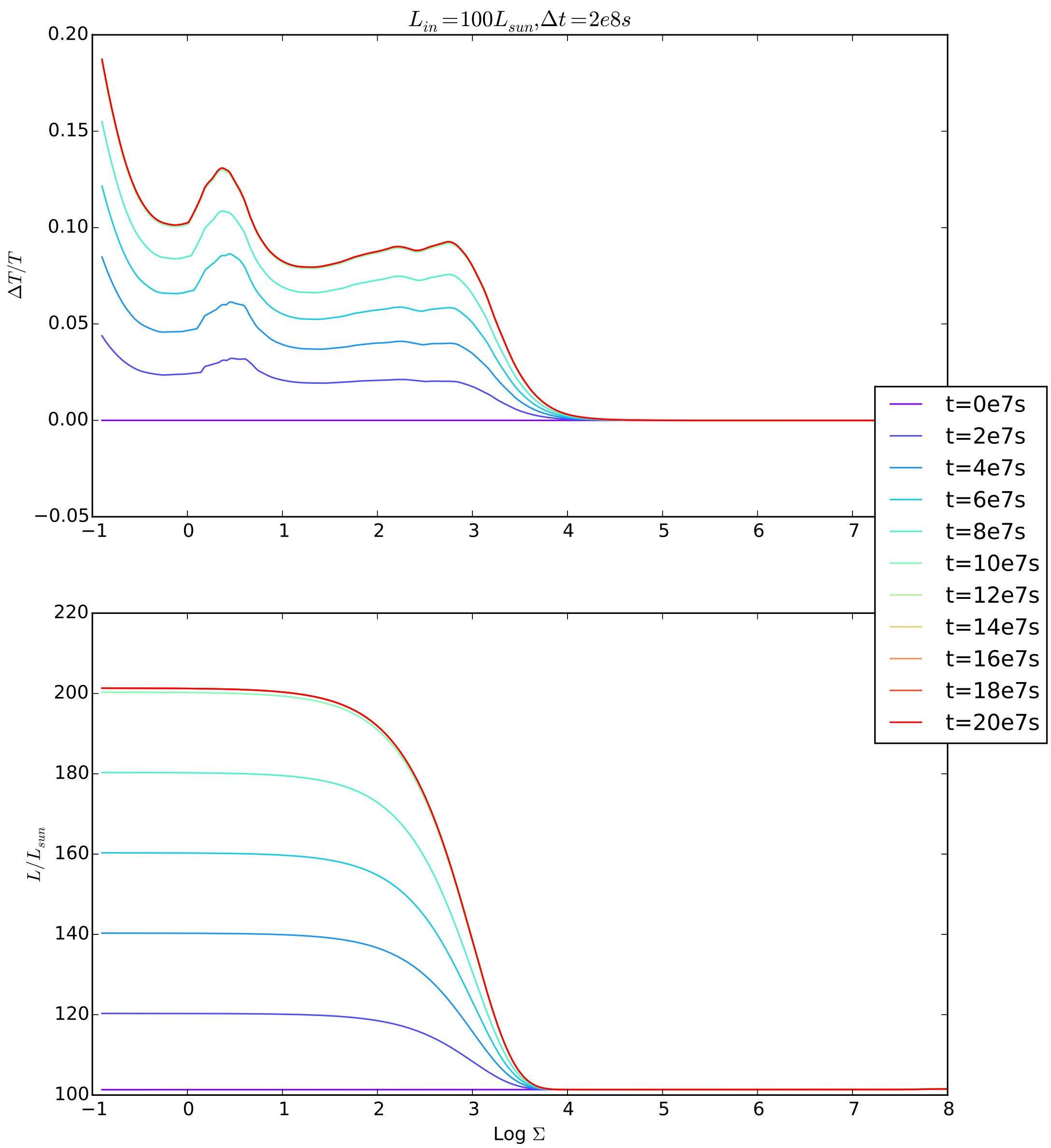

Figure 8.2: $\Delta T/T_0$ (top) and $L/L_\odot$ (bottom) versus $\log \Sigma$ (in g/cm^2) for a star of mass $M_\odot$, radius $R_\odot$, and luminosity $100L_\odot$. The external heat was put in at $\Sigma = 10^3$g/cm^2 and linearly increased from zero to $100L_\odot$ over the course of 10^8s, after which the simulation continued for another 10^8s to allow for equilibration. Color represents time, with the simulation beginning at violet and ending with red.

this scenario on the same radiative star as before are shown in figure 8.3. The trend is just the same as before, with the temperature falling by the same amount it initially rose, and the luminosity falling everywhere back down to the internally generated value.

These results confirm that radiative stars exponentially damp temperature differences as a function of depth. Additionally, the quick response of radiative stars to changes in external illumination mean that they track the present-day properties of the pulsar wind. This, combined with possible anisotropies in their thermal profiles, means that they may still be useful for exploring the environments pulsars produce.

8.3 Fully Convective Stars

We now turn to fully convective stars. Figure 8.4 shows a fully convective star with $M = 0.3M_{\odot}, L_{in} = 0.1L_{\odot}, R = 2.65R_{\odot}$. The star was initially subjected to external illumination equal to its intrinsic illumination, and this was then turned off over the course of 10^8s. To verify that the final state is indeed an equilibrium solution, this scenario was then run for an additional 10^8s, with the results shown in figure 8.5. The good agreement between these two figures indicates that 10^8s suffices to compute an equilibrium, though the question of what is meant by equilibrium is actually quite subtle in this case. As specified in the differential equations being solved, the solution is in equilibrium. That is, all time derivatives are zero within the envelope. This does not, however, mean that the solution describes an equilibrium scenario for the star in question. This is because the luminosity at the lower boundary has adjusted up to match the initial outer boundary luminosity. As a result heat is exiting the star below this envelope faster than it is being produced by nuclear burning. This effect is also seen in cases with much higher external luminosities, as shown in figure 8.6, where $L_e = L_{\odot}$. To understand this, we must examine in more detail the structure of ∇ as a function of L.

In radiative zones, $\nabla \propto L$, and so both $\ln T$ and L adjust to similar degrees to changing circumstances. In convective regions, on the other hand, ∇ is nearly independent of L, and so the equations become stiff in $\ln T$ relative to L. In the case of a fully convective envelope, then, to a good approximation, T may be treated as fixed, while L is allowed to vary. The surface temperature sets the outer boundary condition on L, and so this leads to L rising in the interior to meet the outgoing flux at the surface, rather than the surface flux falling to match that of the interior.

The process outlined above cannot happen instantaneously. Rather, the timescale

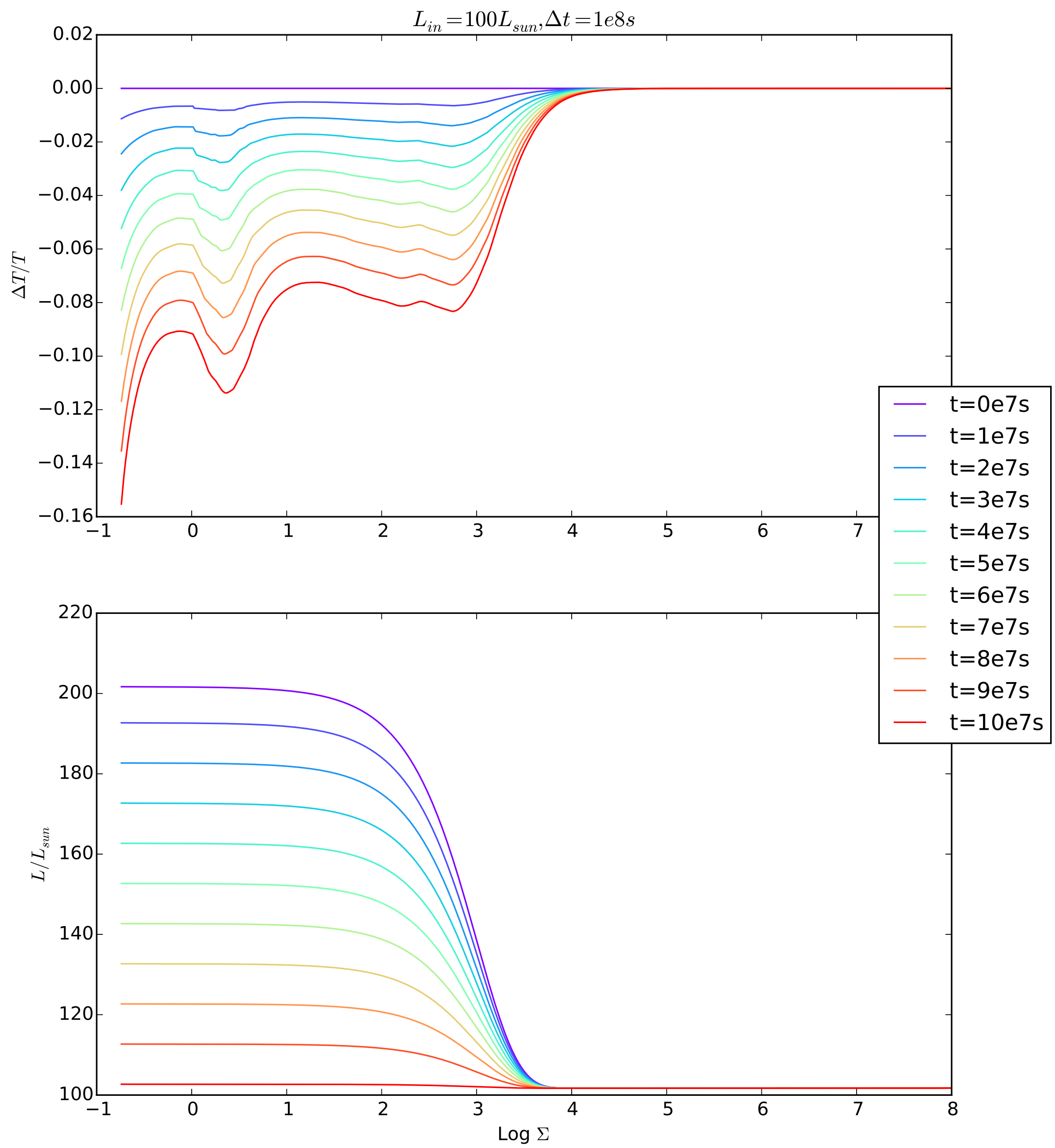

Figure 8.3: $\Delta T/T_0$ (top) and $L/L_\odot$ (bottom) versus $\log\Sigma$ (in g/cm^2) for a star of mass $M_\odot$, radius $R_\odot$, and luminosity $100L_\odot$. The external heat was put in at $\Sigma = 10^3$g/cm^2 and linearly decreased from $100L_\odot$ to zero over the course of 10^8s. Color represents time, with the simulation beginning at violet and ending with red.

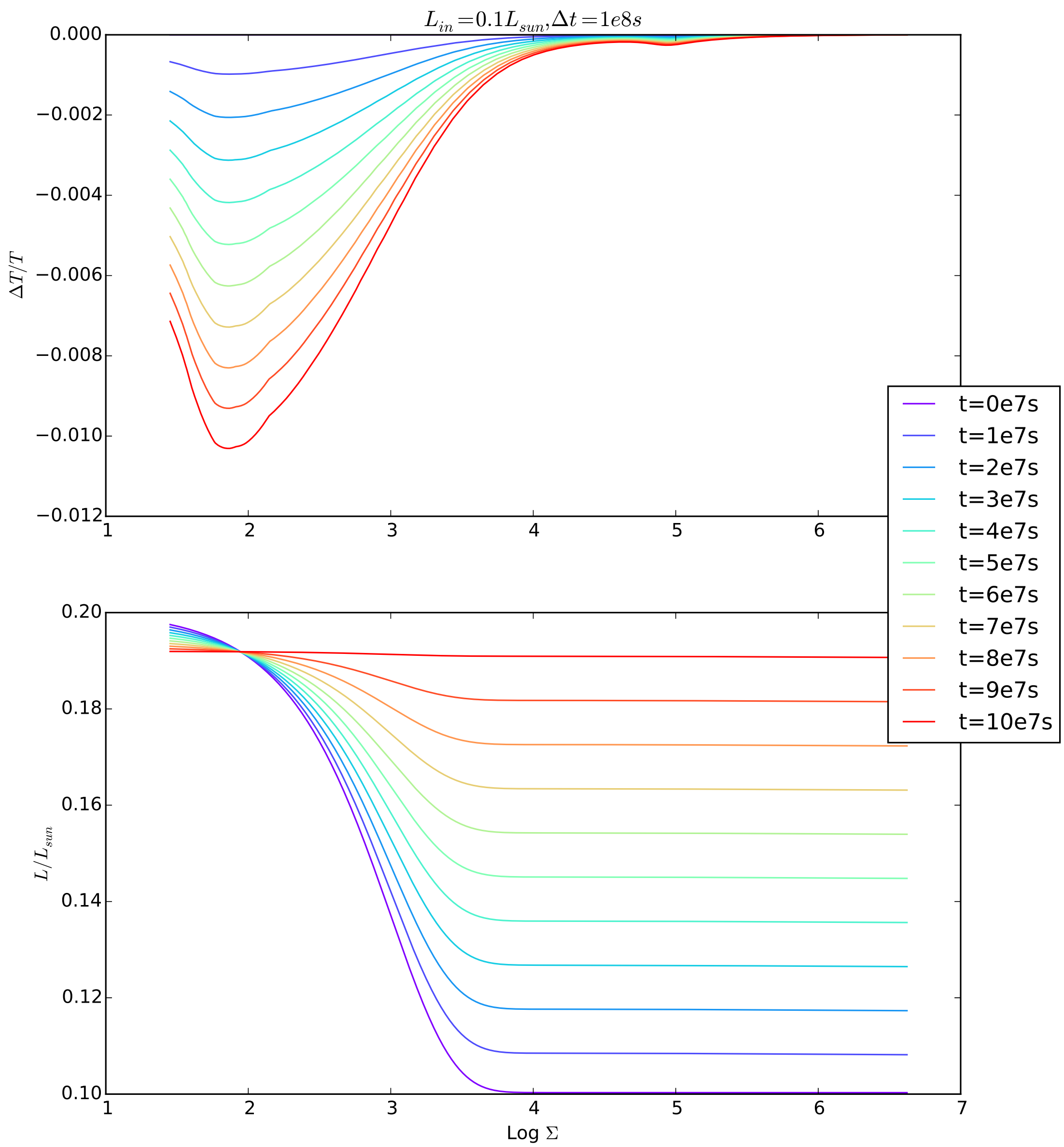

Figure 8.4: $\Delta T/T_0$ (top) and $L/L_\odot$ (bottom) versus $\log \Sigma$ (in g/cm^2) for a star of mass $0.3M_\odot$, radius $2.65R_\odot$, and luminosity $0.1L_\odot$. The external heat was put in at $\Sigma = 10^3$g/cm^2 and linearly decreased from $0.1L_\odot$ to zero over the course of 10^8s. Color represents time, with the simulation beginning at violet and ending with red.

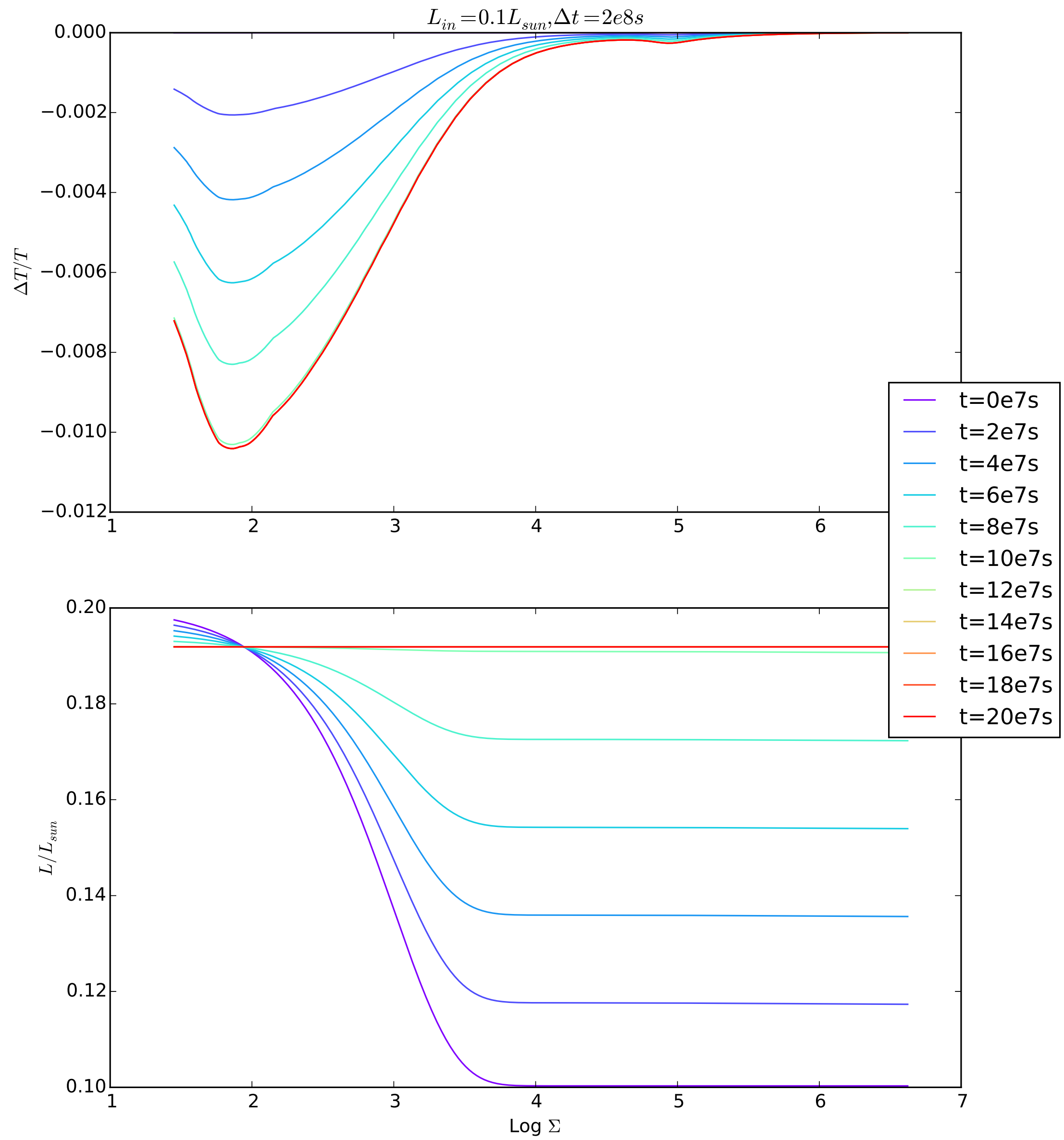

Figure 8.5: $\Delta T/T_0$ (top) and $L/L_\odot$ (bottom) versus $\log\Sigma$ (in g/cm^2) for a star of mass $0.3M_\odot$, radius $2.65R_\odot$, and luminosity $0.1L_\odot$. The external heat was put in at $\Sigma = 10^3$g/cm^2 and linearly decreased from $0.1L_\odot$ to zero over the course of 10^8s. The simulation was then run for an additional 10^8s with no external heating. Color represents time, with the simulation beginning at violet and ending with red.

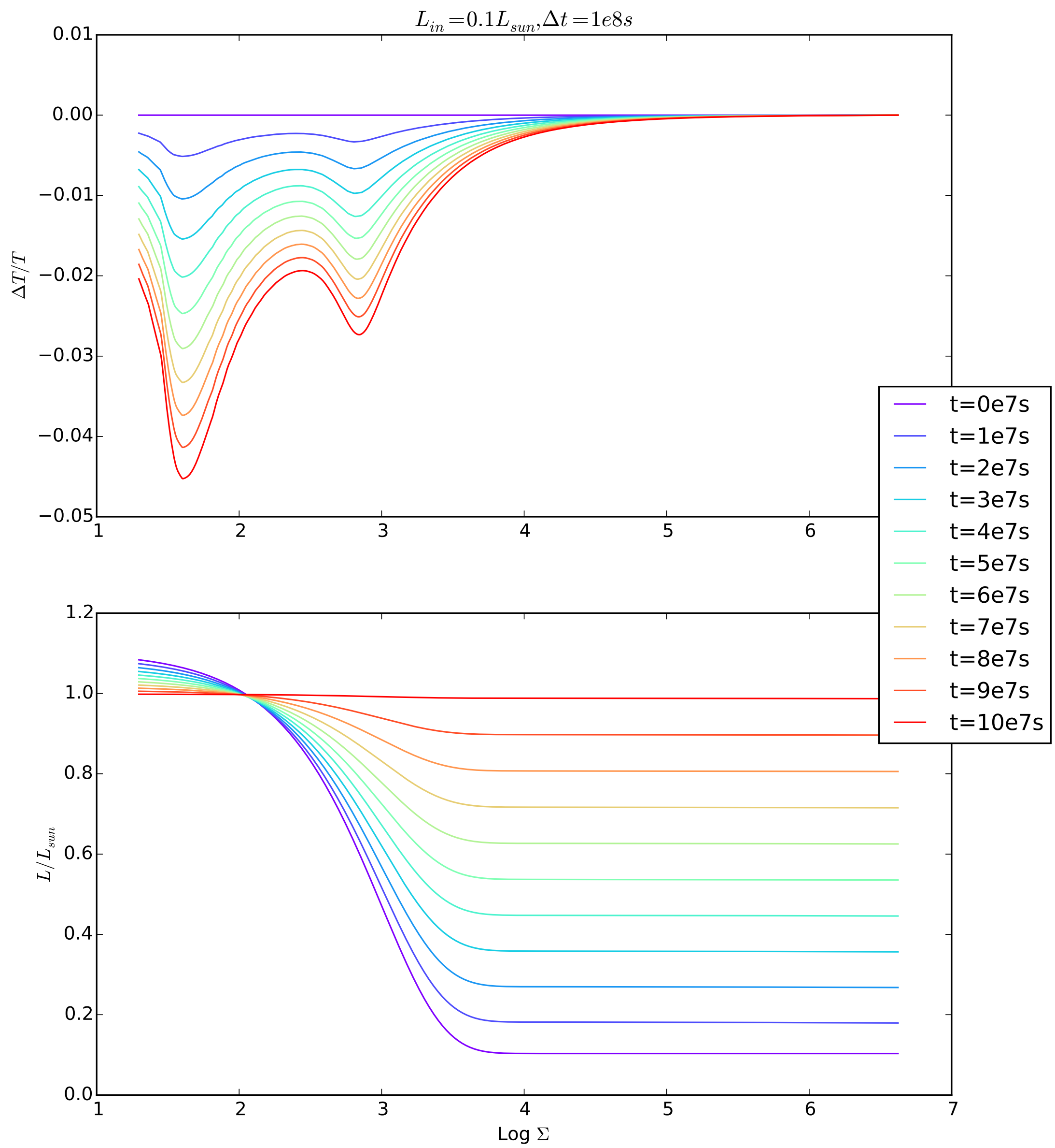

Figure 8.6: $\Delta T/T_0$ (top) and $L/L_\odot$ (bottom) versus $\log\Sigma$ (in g/cm^2) for a star of mass $0.3M_\odot$, radius $2.65R_\odot$, and luminosity $0.1L_\odot$. The external heat was put in at $\Sigma = 10^3$g/cm^2 and linearly decreased from $L_\odot$ to zero over the course of 10^8s. The simulation was then run for an additional 10^8s with no external heating. Color represents time, with the simulation beginning at violet and ending with red.

of adjustment for L in a convection cell is set by the convective turnover time l/v_c[5], and so what occurs is that the temperature adjusts due to the nonzero slope of L in m for a time l/v_c, after which the flux has uniformly risen to match the outer boundary condition. At this point and in this region, the flux ceases to vary, and hence $\partial_t T$ falls to zero. The expected change in T is then expected to be roughly

$$\delta T \approx \partial_t T \delta t \approx \frac{\Delta L}{c_p \delta m} \frac{\delta z}{v_c} = \frac{\Delta L}{4\pi r^2 \rho c_p v_c}, \tag{8.22}$$

where δm and δz refer to the mass and thickness of a spherical shell of material, and ΔL is the change in luminosity, which should be equal to the external luminosity. Now the convective flux may be written as

$$F_c \approx \rho v_c^3 \approx \frac{L_{in}}{4\pi r^2}, \tag{8.23}$$

so

$$\delta T \approx \frac{L_e}{4\pi r^2 \rho c_p} \left(\frac{L_{in}}{4\pi r^2 \rho} \right)^{-1/3} = \frac{1}{c_p} \left(\frac{L_e}{4\pi r^2 \rho} \right)^{2/3} \left(\frac{L_e}{L_{in}} \right)^{1/3}. \tag{8.24}$$

This may also be written as

$$\delta \ln T \approx \frac{\delta T}{T} \approx \frac{v_c^2}{v_s^2} \left(\frac{L_e}{L_{in}} \right). \tag{8.25}$$

Near the surface of a fully convective star, we usually have $v_c \approx v_s/10$, so for $L_e = L_{in}$ we expect $\delta T/T \approx 10^{-2}$. Furthermore, at higher pressures the sound speed rises relative to the convection speed, and so the difference drops off. This may be understood as following from the above result that $\delta T \propto \rho^{-2/3}$. The endpoint of this process occurs when the moving "wavefront" of the flux change reaches the nuclear burning regime. At this stage the temperature will drop significantly more, for there is nowhere else for the wavefront to go.

To understand what happens next, we first remark that the convection zone will adjust to maintain an adiabatic gradient on a timescale set by the convective turnover rate. As a result, the timescale for the entire star to adjust to maintain this gradient is

$$\tau_{adj} = \int \frac{dr}{v_c} = \int \frac{1}{\rho v_c} d\Sigma \approx \int \rho^{-1} \left(\frac{F}{\rho} \right)^{-1/3} d\Sigma = F^{-1/3} \int \rho^{-2/3} d\Sigma, \tag{8.26}$$

[5]Recall that this is why Acorn only takes time-steps which are at least $\max(l/v_c)$ in size.

where the integral is taken over the entire star. In a convective atmosphere, $P \propto \rho^\gamma$, so $\rho \propto P^{1/\gamma}$. If we make the thin atmosphere approximation throughout the star, just to gain an order-of-magnitude estimate, then $P = g\Sigma$, and so

$$\tau_{adj} \approx g^{-1}F^{-1/3}\int \rho^{-2/3}dP = g^{-1}F^{-1/3}\rho_0^{-2/3}\int\left(\frac{P}{P_0}\right)^{-2/3\gamma}dP \tag{8.27}$$

$$= \frac{1}{1-\frac{2}{3\gamma}}g^{-1}F^{-1/3}\rho_0^{-2/3}P_0^{2/3\gamma}\left(P_f^{1-2/3\gamma}-P_0^{1-2/3\gamma}\right). \tag{8.28}$$

Now γ is typically 5/3 outside of the ionization zone, so $2/3\gamma$=2/5, and hence

$$\tau_{adj} \approx \frac{5P_0^{2/5}}{3gF^{1/3}\rho_0^{2/3}}\left(P_f^{3/5}-P_0^{3/5}\right) \approx \frac{5P_0^{2/5}P_f^{3/5}}{3gF^{1/3}\rho_0^{2/3}} = \frac{5v_{s,0}^2}{3\gamma g v_{c,0}}\left(\frac{P_f}{P_0}\right)^{3/5} = \frac{v_{s,0}^2}{g v_{c,0}}\left(\frac{P_f}{P_0}\right)^{3/5}, \tag{8.29}$$

where we have made the approximation that the core pressure vastly exceeds the pressure at the top of the convection zone. Now $v_{c,0}$ is typically around $v_{s,0}/10$, and $v_{s,0}$ is typically around 10^6cm/s ≈ 100sg, so the prefactor is around 10^3s. Typically $P_0 \sim 10^5$erg/cm^3, and $P_f \sim gM/(4\pi R^2) \sim 10^{15}$erg/cm^3 for the sun, so the overall timescale is around $10^{3+6} = 10^9$s, scaling roughly as $M^{6/5}R^{-12/5}$. For the fully convective star considered in simulation, $M = 0.3M_\odot$ and $R = 2.65R_\odot$, so this timescale is smaller by a factor of 25, giving around 4×10^7s, or roughly a year.

On the other hand, the core adjusts its temperature in time

$$\tau_{core} = \frac{m_{core}c_pT_{core}}{L_e} = f_M\frac{L_{in}}{L_e}\tau_K = f_M\frac{GM^2}{2RL_e}, \tag{8.30}$$

where $f_M \approx 1/10$ is the fraction of the star's mass in the core and τ_K is the Kelvin timescale for the star. This is typically of order ten million years, and so if $L_e = L_{in}$ the core's adjustment timescale is of order a million years. As this is much shorter than the timescale required to maintain adiabaticity, the star may be approximated as being adiabatic at all times after the cooling wavefront reaches the core.

8.4 Mixed Stars

For stars with a convection zone above a radiative region, there are two considerations which our steady-state analysis leads us to expect to differ from the fully convective case. First, any bloating effects are limited to the convection zone, and so the extent of bloating is decreased proportional to the size of the zone. Additionally, the nuclear burning of the core is unchanged by the addition or removal of external illumination in these stars, meaning that the bloating effect is further decreased by the amount given in figure 2.7.

To investigate these effects in the transient case, we first simulated a sun-type star initially illuminated by $L_e = L_\odot$ and watched as the illumination was turned off. The results of this are shown in figure 8.7. The key feature we see here is that the luminosity sits fixed near the initial steady-state value at the surface, and that the main effect of time evolution is to push the transition between this value and the nuclear-burning value deeper into the star. The depth at which this occurs is between $\Sigma = 10^4\text{g/cm}^2$ and $\Sigma = 10^5\text{g/cm}^2$, just slightly deeper than the point in our steady-state calculations where the radiative-convective transition arises in illuminated equilibrium in this sort of star. This feature is not unique to stars of $M = M_\odot$. Figure 8.8 shows a star of the form examined in the preceding section, but with $L_e = 10L_\odot$. This star exhibits a similar transition between radiative and convective heat transport in the steady state and hence exhibits a similar transient adjustment process. The story behind the evolution of stars such as these is then that the external illumination shuts off convection beyond a certain depth. When the illumination is removed, that radiative region dampens the resulting change in temperature exponentially into the star, while the convective region maintains a luminosity close to the initial steady-state value. This is precisely what we see, but we can further test this notion by examining the star on longer timescales. If this story is correct, the star will slowly turn the radiative zone back into a convection zone, and in the process the luminosity profile will settle down to have $L = L_\odot$ everywhere.

To determine if this is the case, the simulation was run for another 10^8s and found indeed to be out of equilibrium, a feature not seen in any of the previous scenarios considered. The results of the longer simulation are shown in figure 8.9. Note that as the luminosity transition region pushes deeper into the star, the magnitude of the transition falls. Over even longer timescales, the equilibration continues but slows down somewhat, as shown in figure 8.10. The adjustment time for this process is on the order of the thermal timescale for the entire region in which the mode of heat transport shifted from being convective to being radiative, perhaps decreased by a factor of 10 to account for the relatively small temperature changes required to do this at high Σ. As a result, the full adjustment process requires timescales beyond the realm of validity of our lower boundary condition on T. Fortunately all that matters for our purposes are the trend and timescale involved, which are clearly seen in the simulations which are accessible.

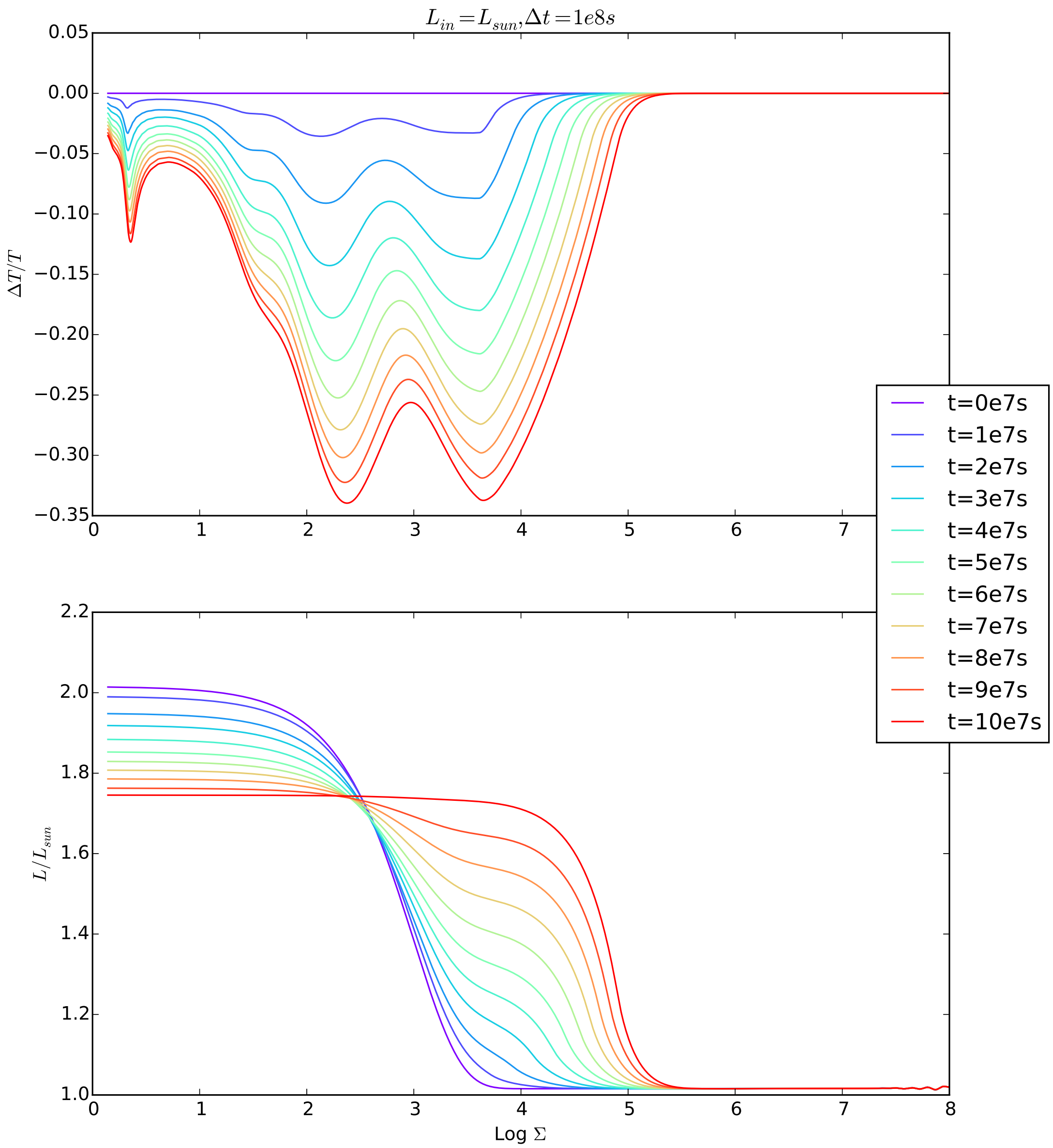

Figure 8.7: $\Delta T/T_0$ (top) and $L/L_\odot$ (bottom) versus $\log \Sigma$ (in g/cm^2) for a star of mass $M_\odot$, radius $R_\odot$, and luminosity $L_\odot$. The external heat was put in at $\Sigma = 10^3$g/cm^2 and linearly decreased from $L_\odot$ to zero over the course of 10^8s. Color represents time, with the simulation beginning at violet and ending with red.

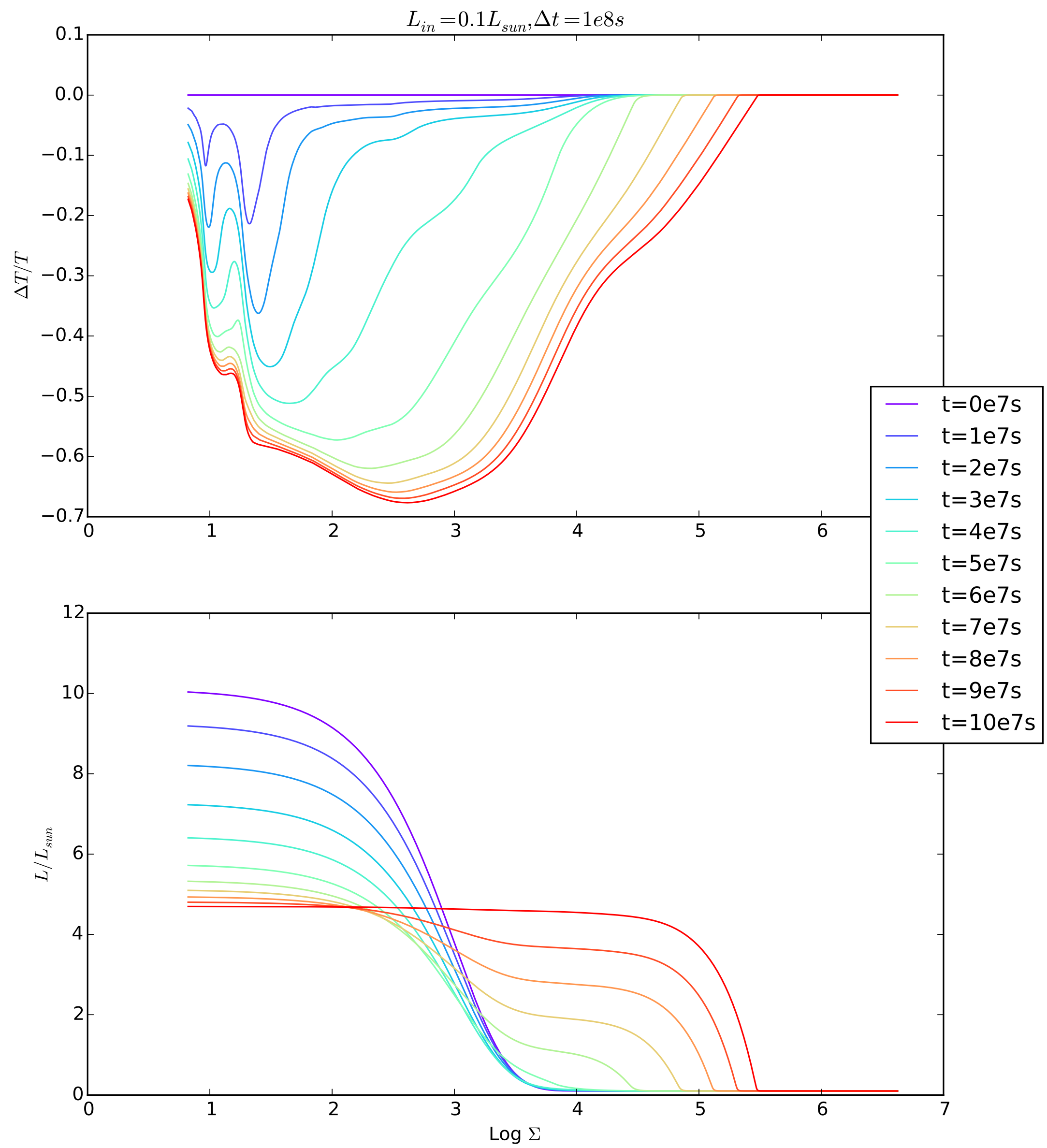

Figure 8.8: $\Delta T/T_0$ (top) and $L/L_\odot$ (bottom) versus $\log \Sigma$ (in g/cm^2) for a star of mass $0.3M_\odot$, radius $2.65R_\odot$, and luminosity $0.1L_\odot$. The external heat was put in at $\Sigma = 10^3$g/cm^2 and linearly decreased from $10L_\odot$ to zero over the course of 10^8s. The simulation was then run for an additional 10^8s with no external heating. Color represents time, with the simulation beginning at violet and ending with red.

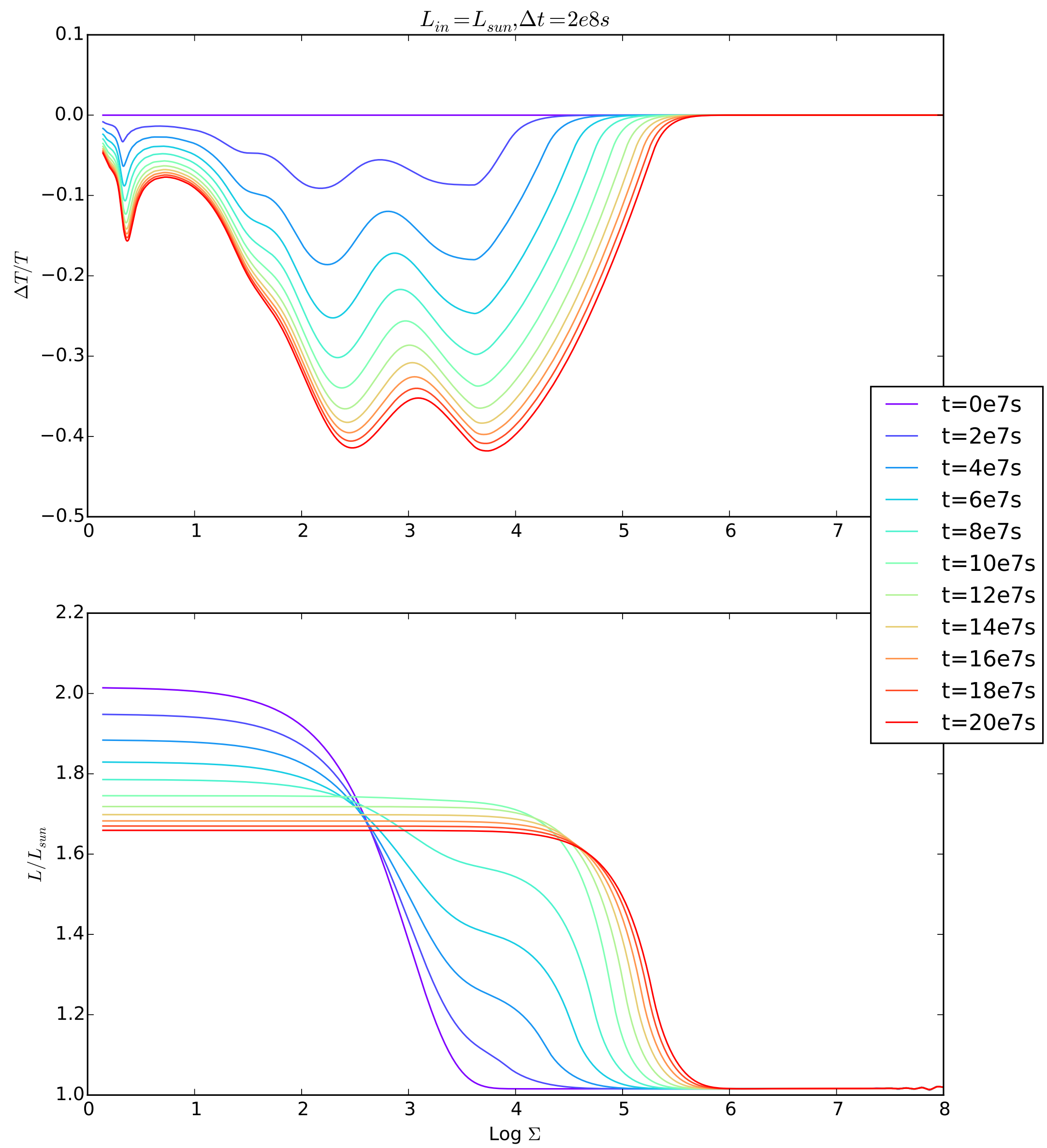

Figure 8.9: $\Delta T/T_0$ (top) and $L/L_\odot$ (bottom) versus $\log \Sigma$ (in g/cm^2) for a star of mass $M_\odot$, radius $R_\odot$, and luminosity $L_\odot$. The external heat was put in at $\Sigma = 10^3$g/cm^2 and linearly decreased from $L_\odot$ to zero over the course of 10^8s. It was then run for another 10^8s at that value. Color represents time, with the simulation beginning at violet and ending with red.

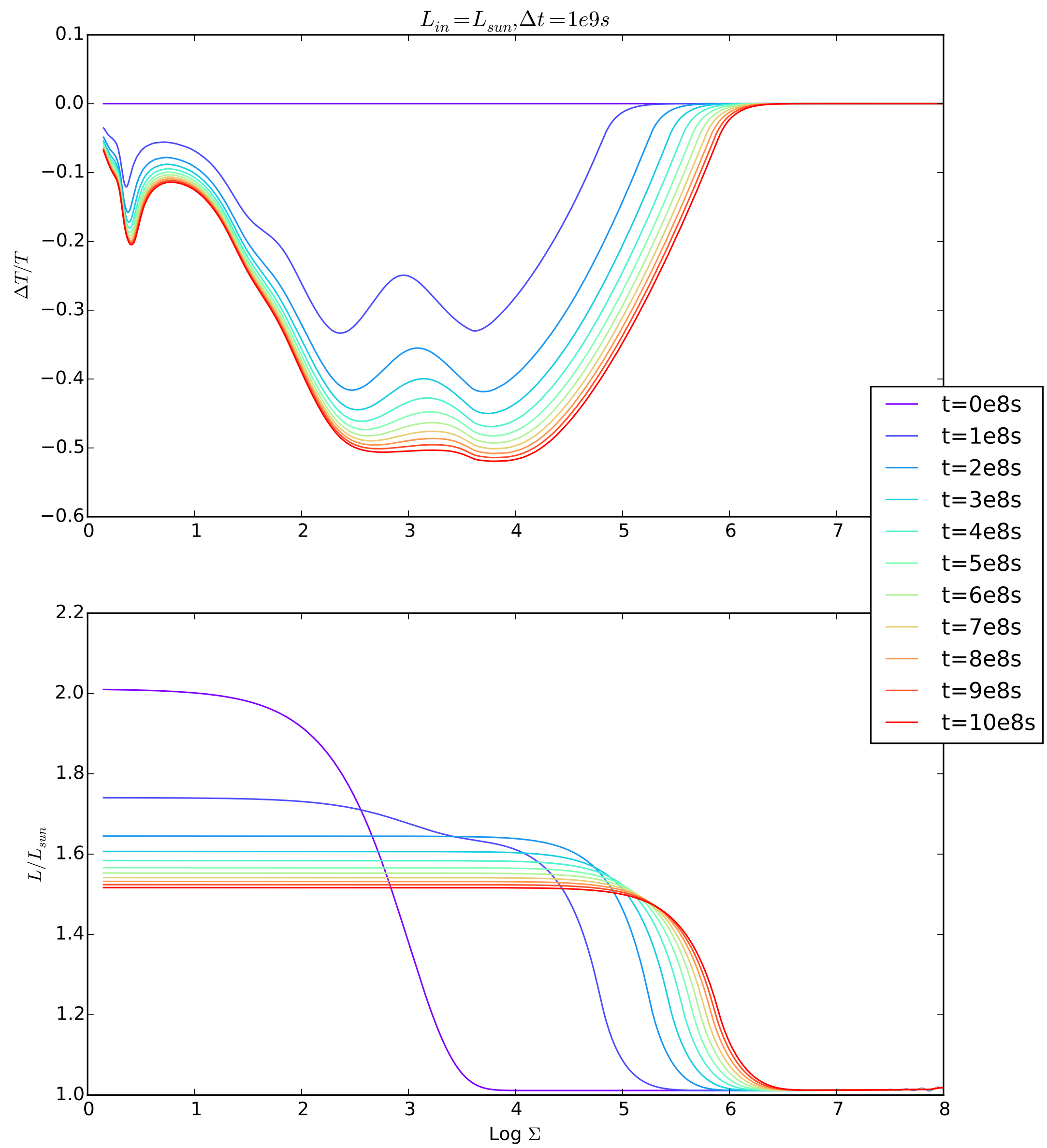

Figure 8.10: $\Delta T/T_0$ (top) and $L/L_\odot$ (bottom) versus $\log \Sigma$ (in g/cm^2) for a star of mass $M_\odot$, radius $R_\odot$, and luminosity $L_\odot$. The external heat was put in at $\Sigma = 10^3$g/cm^2 and immediately decreased from $L_\odot$ to zero over the course of 10^8s before being run for another 10^9s. Color represents time, with the simulation beginning at violet and ending with red.

Part II

Applications in Astronomy

9

X-Ray Binaries

You know, you blow up one sun and suddenly everyone expects you to walk on water.

– Lt Col. Samantha Carter, Stargate SG-1 Season 8 Episode 17

The results presented thus far have been general, in the sense that while there were motivating examples of phenomena of interest, many avenues were pursued to provide a picture of the phenomenology of pulsar-companion systems. We are now interested in examining the specific case in which the pulsar interacts with its companion to produce transient X-ray emissions. This case has long been studied[1], though conclusions have proven scarce. In addition, while in previous chapters the companion was a passive agent, here we will consider the role it plays in influencing its own fate. The first section deals with the isotropic illumination case, while the second discusses the effects of anisotropy.

9.1 Accretion rate

The initial heating of the star causes it to expand at some rate $\dot{R}$. This rate is everywhere the same in the atmosphere due to the expansion being driven by deep heating, as discussed earlier. As the atmosphere of the star falls off exponentially

[1] J. C. Brown and C. B. Boyle. "An exploratory eccentric orbit 'Roche lobe' overflow model for recurrent X-ray transients". In: *Astronomy and Astrophysics* 141 (Dec. 1984), pp. 369–375; H. Ritter, Z.-Y. Zhang, and U. Kolb. "Irradiation and mass transfer in low-mass compact binaries". In: *Astronomy and Astrophysics* 360 (Aug. 2000), p. 969. eprint: `astro-ph/0005480`; A. R. King et al. "Mass Transfer Cycles in Close Binaries with Evolved Companions". In: *The Astrophysical Journal* 482 (June 1997), pp. 919–928. eprint: `astro-ph/9701206`.

in the radial coordinate above the photosphere, no significant accretion is expected until this region approaches the Roche lobe radius R_b. The accretion rate is expected to be[2]

$$\dot{M} = \sqrt{2\pi} R h_s v_s \rho(R_b). \tag{9.1}$$

Here $h_s \approx R v_s^2 / v_0^2$, where v_0 is the orbital velocity of the star. This is due to the fact that in the vicinity of the Roche lobe, the pressure profile is set by orbital parameters rather than the thermal structure of the star. As a result, we may write

$$\dot{M} \approx \sqrt{2\pi} R^2 v_0^{-2} v_s^3 \rho(R_b). \tag{9.2}$$

If the accretion rate is low[3], it typically means that ρ is low at R_b, the Roche radius, and hence that we are in the upper portion of the atmosphere. This allows us to make use of $\rho \propto \exp(-r/h_s)$ and write

$$\dot{M} \approx \sqrt{2\pi} R^2 v_0^{-2} v_s^3 \rho_0 \exp\left(\frac{r v_0^2}{R v_s^2}\right) = \sqrt{2\pi} \Omega^{-2} v_s^3 \rho_0 \exp\left(\frac{r R_0^2 \Omega^2}{R v_s^2}\right), \tag{9.3}$$

where ρ_0 is chosen to make this relation true and r is a Lagrangian quantity. For the accretion to be significant we must have $R \approx R_b$, for $R, R_b \gg h_s$ because $v_0 \approx 10^7 \text{cm/s} \gg 10^5 \text{cm/s} \approx v_s$. Thus

$$\dot{M} \approx \sqrt{2\pi} \Omega^{-2} v_s^3 \rho_0 \exp\left(\frac{r R_0^2 \Omega^2}{R_b v_s^2}\right). \tag{9.4}$$

In Part 1, we found that only stars with deep convection can swell to the point where $R \sim R_b$, so we restrict ourselves to stars of this form. As a result, $M < 1.2 M_\odot$. Using $M_p \approx 2 M_\odot$, we may approximate[4]

$$R_b \approx 0.46 R_0 \left(\frac{M}{M + M_p}\right)^{1/3}, \tag{9.5}$$

yielding

$$\dot{M} \approx \sqrt{2\pi} \Omega^{-2} v_s^3 \rho_0 \exp\left(\frac{2 r R_0 \Omega^2 (M + M_p)^{2/3}}{M^{2/3} v_s^2}\right), \tag{9.6}$$

[2] Brown and Boyle, op. cit.

[3] Using Eq. (9.2), we find that $\dot{M} \sim 10^{24} \rho \text{cm}^3/\text{s}$. Based on the data in Appendix E, the exponential atmosphere assumption holds at least up to $\rho \sim 10^{-8} \text{g/cm}^3$, so we are safe making this assumption if $\dot{M} < 10^{16} \text{g/s}$. As will become clear subsequently, this is much larger than the typical values we will encounter.

[4] B. Paczyński. "Evolutionary Processes in Close Binary Systems". In: *Annual Review of Astronomy and Astrophysics* 9 (1971), p. 183. DOI: 10.1146/annurev.aa.09.090171.001151.

where

$$R_0 = \left(\frac{G(M+M_p)}{\Omega^2}\right)^{1/3}. \tag{9.7}$$

Typical atmospheric temperatures are such that $\mu = m_p$, so $\gamma = 5/3$ and

$$v_s^2 = \frac{5k_BT}{3m_p}. \tag{9.8}$$

Thus we can compute all of the quantities in the exponential.

Now we haven't yet fixed r or ρ_0, and so we actually have the freedom to absorb any constants we wish. Furthermore, relative to the exponential the dependence on T is negligible, so we may let $T \to T_0$ for some reference photospheric temperature T_0 and absorb it as well. Thus we will write instead

$$\dot{M} \approx \exp\left(\frac{2rR_0\Omega^2(M+M_p)^{2/3}}{M^{2/3}v_s^2}\right). \tag{9.9}$$

We now no longer have the freedom to pick the zero-point of r. Rather, it is uniquely determined given $\dot{M}$ at some time. Without solving for it, though, we may write

$$\ddot{M} = \frac{2R_0\Omega^2(M+M_p)^{2/3}}{M^{2/3}v_s^2}\dot{r}\dot{M}. \tag{9.10}$$

Using $\dot{r} = \dot{R}$ and dividing through by $\dot{M}$ yields

$$\partial_t \ln \dot{M} = \frac{2rR_0\Omega^2(M+M_p)^{2/3}}{M^{2/3}v_s^2}\dot{R}. \tag{9.11}$$

This equation is independent of the zero-point of r, for r no longer appears anywhere in it. Given $\ln \dot{M}$ at some point in time, we may use this relation to determine it at any subsequent point so long as we know $\dot{R}$.

9.2 Pre-Roche Expansion

Recall that the radius of the star obeys

$$\frac{dr}{dm} = \frac{1}{4\pi r^2\rho}. \tag{9.12}$$

This may also be written as

$$\frac{dr^3}{dm} = \frac{3}{4\pi\rho}. \tag{9.13}$$

Differentiating with respect to time gives

$$\frac{d}{dm}\left(\frac{dr^3}{dt}\right) = \frac{-3}{4\pi\rho}\left(\frac{d\ln\rho}{dt}\right) = -\frac{dr^3}{dm}\left(\frac{d\ln\rho}{dt}\right). \tag{9.14}$$

At fixed pressure, $d\ln\rho = -d\ln T$, neglecting the small space occupied by the ionization zone, so

$$\frac{d\ln\rho}{dt} = -\frac{d\ln T}{dt}. \tag{9.15}$$

As a result,

$$\frac{d}{dm}\left(\frac{dr^3}{dt}\right) = \frac{dr^3}{dm}\frac{d\ln T}{dt}, \tag{9.16}$$

and hence

$$\frac{dR^3}{dt} = R^3\frac{d\ln T}{dt}. \tag{9.17}$$

Note that we have assumed here that the majority of the star, as measured by the radial coordinate cubed, is convective. This is equivalent to assuming that the majority of the volume of the star is convective. This must be true in order for us to get the expansion of interest, and so may be thought of as a condition on the star, rather than an assumption to be tested later on. Though in equilibrium many stars become fully radiative, as we found in Chapter 2, during the initial expansion the star remains convective for quite a while. For many systems the equilibrium state is never reached, as the Roche lobe overflows well before this occurs, and so we may safely assume that a substantial convection zone remains.

Now the convective turnover timescale of the star is given by Eq. (8.29) as

$$\tau_{adj} = \frac{v_{s,0}^2}{g v_{c,0}}\left(\frac{P_f}{P_0}\right)^{3/5}, \tag{9.18}$$

where $v_{c,0}$ is the convection speed near the top of the efficient convection region (i.e. where $\Gamma \sim 10$), $v_{s,0}$ is the sound speed at the same location, P_0 is the pressure at the same location, and P_f is the pressure at the base of the convection zone. The thermal adjustment time, on the other hand, is

$$\tau'_{adj} = \frac{\int_{conv} c_p T dm}{(L_i + L_e - L_{\rm surface})} \tag{9.19}$$

$$= \frac{\int_{conv} c_p T 4\pi r^2 dp}{g\,(L_i + L_e - L_{\rm surface})} \tag{9.20}$$

$$\approx \frac{4\pi R^2 c_p T_0 P_0 \,(P_f/P_0)^{\nabla_{ad}+1}}{g(\nabla_{ad}+1)\,(L_i + L_e - L_{\rm surface})} \tag{9.21}$$

$$= \frac{4\pi R^2 v_{s,0}^2 P_0 \,(P_f/P_0)^{\nabla_{ad}+1}}{g\gamma(\nabla_{ad}+1)\,(L_i + L_e - L_{\rm surface})} \tag{9.22}$$

$$= \frac{4\pi R^2 \tau_{adj} v_{c,0} P_0 \,(P_f/P_0)^{\nabla_{ad}+2/5}}{\gamma(\nabla_{ad}+1)\,(L_i + L_e - L_{\rm surface})} \tag{9.23}$$

$$= \frac{4\pi R^2 \tau_{adj} v_{c,0} P_0 \,(P_f/P_0)^{\nabla_{ad}+2/5}}{\gamma(\nabla_{ad}+1)\,(L_i + L_e - L_{\rm surface})} \tag{9.24}$$

$$\therefore \frac{\tau'_{adj}}{\tau_{adj}} \approx \frac{4\pi R^2 P_0 v_{c,0} \,(P_f/P_0)^{\nabla_{ad}+2/5}}{\gamma(\nabla_{ad}+1)\,(L_i + L_e - L_{\rm surface})}. \tag{9.25}$$

Note that we have made use of the fact that the heat being bottled up is $L_i + L_e - L_{\rm surface}$, where L_i is a time-dependent quantity in the case that the core is heated. This is the isotropic expression, as we are assuming deep convection. Now $R \sim 10^{11}$cm, $v_{c,0}$ is generally between 10^4cm/s and 10^5cm/s, $P_0 \sim 10^5$erg/cm^3, $L_i < 10^{35}$erg/s, so this ratio is at least

$$\frac{\tau'_{adj}}{\tau_{adj}} = 10^{-7}\,(P_f/P_0)^{\nabla_{ad}+2/5} \sim 10^{-7}\,(P_f/P_0)^{4/5}\,. \tag{9.26}$$

As long as $P_f > 10^8 P_0$ the thermal adjustment time is greater than the convective adjustment time, and we may take the convective gradient to hold everywhere. This will always be the case in the stars of interest: if it does not hold, a substantial fraction of the convection zone will disappear when the heating is introduced, as discussed in Chapter 2.

Our result involving R^3 may now be cast as a result involving R, giving

$$\dot{R} = \frac{R}{3}\frac{d\ln T}{dt}. \tag{9.27}$$

Now the characteristic timescale defined by $d\ln T/dt$ is just τ'_{adj}, so

$$\dot{R} = \frac{R}{3}\frac{d\ln T}{dt} = \frac{R}{3\tau'_{adj}} = \frac{g\gamma(\nabla_{ad}+1)\,(L_i + L_e - L_{\rm surface})}{12\pi R v_{s,0}^2 P_0\,(P_f/P_0)^{\nabla_{ad}+1}}. \tag{9.28}$$

Note that we have neglected the gravitational potential energy associated with the change in radius. By the virial theorem, we expect that the fraction of the input energy which goes into changing the gravitational potential is half that which goes into changing the temperature. As this is an order unity correction we are justified in neglecting it.

Now there are three possible cases. First, the Roche radius may exceed the maximum possible radius the star can expand to. In this case no accretion is observed. Second, the Roche radius may be smaller than the main sequence radius of the star. In this case we expect the star to cataclysmically accrete onto the companion. This possibility has been extensively studied elsewhere and is not the focus of this text. Finally, the Roche radius may lie between the main sequence radius of the companion and the maximum possible radius the companion can expand to. It is this final case which is of interest in this chapter.

To examine the case of interest, we need to compute the maximum possible post-expansion companion radius. Formally, the problem of interest is to determine the maximum R consistent with the constraint that $R = R_b$ and with the incident external illumination L_e. To do this, we must first determine the depth of the base of the convection zone. In the region deeper than the ionization zone, the Kramer opacities are valid and we may write

$$\kappa = \beta P T^{-4.5}, \tag{9.29}$$

where β is a constant independent of pressure or temperature. As we are interested in the expansion of the entire star, we may focus on this region and neglect effects near the surface. The base of the convection zone is the location where

$$\nabla_{ad} = \nabla_{rad}. \tag{9.30}$$

Solving this with the known form of ∇_{rad} gives

$$T^{9.5} = \frac{3\beta P^2 L}{16\pi acGM\nabla_{ad}}. \tag{9.31}$$

As we are working deep in the star, ∇_{ad} is a constant, and so we know that there is only one solution. Now at any given pressure in the convection zone,

$$T = T_0 \left(\frac{P}{P_0}\right)^{\nabla_{ad}}, \tag{9.32}$$

where T_0 and P_0 are just the temperature and pressure at some reference position in the convection zone. Using this we may solve for the base of the convection zone as

$$P_f = P_0 \left(\frac{\nabla_{rad}(P = P_0)}{\nabla_{ad}}\right)^{\frac{1}{9.5\nabla_{ad}-2}}. \tag{9.33}$$

Using $\nabla_{ad} = 0.4$, the exponent may be evaluated as 0.56. Thus

$$P_f = P_0 \left(\frac{\nabla_{rad}(P = P_0)}{\nabla_{ad}} \right)^{0.56} . \tag{9.34}$$

What this means is that we may compute a stellar envelope down to some position deeper than the ionization zone and determine the position of the base of the convection zone from local thermodynamic quantities in the envelope. This means that if the computed P_f is smaller than P_0, we know that the envelope is radiative through the reference pressure. We will pick P_0 as shallow as possible while remaining deeper than the ionization zone, such that this allows us to classify the entire envelope minus the portion very close to the surface. In practice this amounts to picking a test P_0 above the ionization zone, and then increasing it geometrically until a well-converged envelope matching the self-consistency conditions is achieved.

Using our knowledge of P_f, along with our equations giving $\dot{R}$ in terms of it, we may compute the radius of a star as a function of its main sequence and current P_f values. This is just given by

$$R(P_f') = R(P_f) \max\left(1, \frac{P_f}{P_f'}\right)^{\frac{2}{3*9.5}} , \tag{9.35}$$

where we have once more made use of Kramer's opacities in the deep stellar interior. We see that this provides a self-consistency relation which must be evaluated numerically. To solve this, an add-on to the core Acorn code was developed. The full code is shown in Appendix B.2. It begins by computing for a given star and a given pulsar luminosity the maximum radius the star may achieve through thermal expansion. This accounts for the fact that the orbital position is not independent of the Roche radius, as well as the fact that the incident flux is not independent of the orbital position. A shooting method is used in these computations, where a guess of P_f' is used to compute a new value of it. The resulting radius is averaged with that of the previous guess, and used as input for the next iteration. Convergence is achieved when the radius changes by less than $10^{-3}R_\odot$ per iteration. To determine the surface luminosity of stars with radii between the main sequence radius and the maximum radius, binary search is used. The algorithm tracks a lower and upper bound on the luminosity, initially between L_e and $L_e + L_i$. Given such an interval, the radius resulting from the midpoint luminosity is computed. If this is larger than the desired radius, the upper bound on the interval is set to the midpoint. Likewise if it is smaller than the desired radius, the lower bound is set to the midpoint. The algorithm converges when the computed radius minus the main sequence radius is within one part in one thousand of the desired difference.

Putting all of this together, we can compute the characteristic timescale $\tau_{\text{exp}} = h_s/\dot{R}$ over which $\dot{M}$ increases by a factor of e. A plot of this is shown in figure 9.1. Note that low mass stars have a much easier time expanding, both because they have lower thermal content and because they both can be and have to be much closer to the pulsar to satisfy the expansion criteria.

9.3 Post-Roche Accretion

From the previous section, we know that the characteristic increase timescale τ_{exp} for $\dot{M}$ is of order of a century for most stars. This exponential increase in $\dot{M}$ clearly cannot continue indefinitely. There are three processes which may interrupt it. First, the star could continue expanding until it all overflows the Roche lobe. This is unlikely given that long before that happens the pulsar's radiation will be blocked by the accreting material. This is the second possibility: the accreting material can prevent the heating from continuing, putting an upper limit on $\dot{M}$. Finally, the star can reach a balance where the amount of heat being removed by the accreting material equals the input heat.

Ignoring the first possibility, we turn to the second. Let r be distance from the pulsar. The pressure exerted by the pulsar wind is

$$P_w = \frac{L_p}{4\pi r^2 c}. \tag{9.36}$$

The pressure exerted by the accreting material is given roughly by ρv_r^2, where v_r is the radial velocity. If we assume that the accreting material spreads out in all directions by the time it reaches the pulsar, then

$$\dot{M} = 4\pi r^2 \rho v. \tag{9.37}$$

Now v should be roughly the free-fall velocity onto the pulsar, given by

$$v \sim \frac{GM_p}{r}, \tag{9.38}$$

so assuming spherical accretion yields

$$P_{acc} = \frac{\dot{M}\sqrt{GM_p}}{4\pi r^{5/2}}. \tag{9.39}$$

Equating this with the pulsar wind pressure, we find

$$r_{eq} = \frac{GM_p c^2}{L_p^2}\dot{M}^2. \tag{9.40}$$

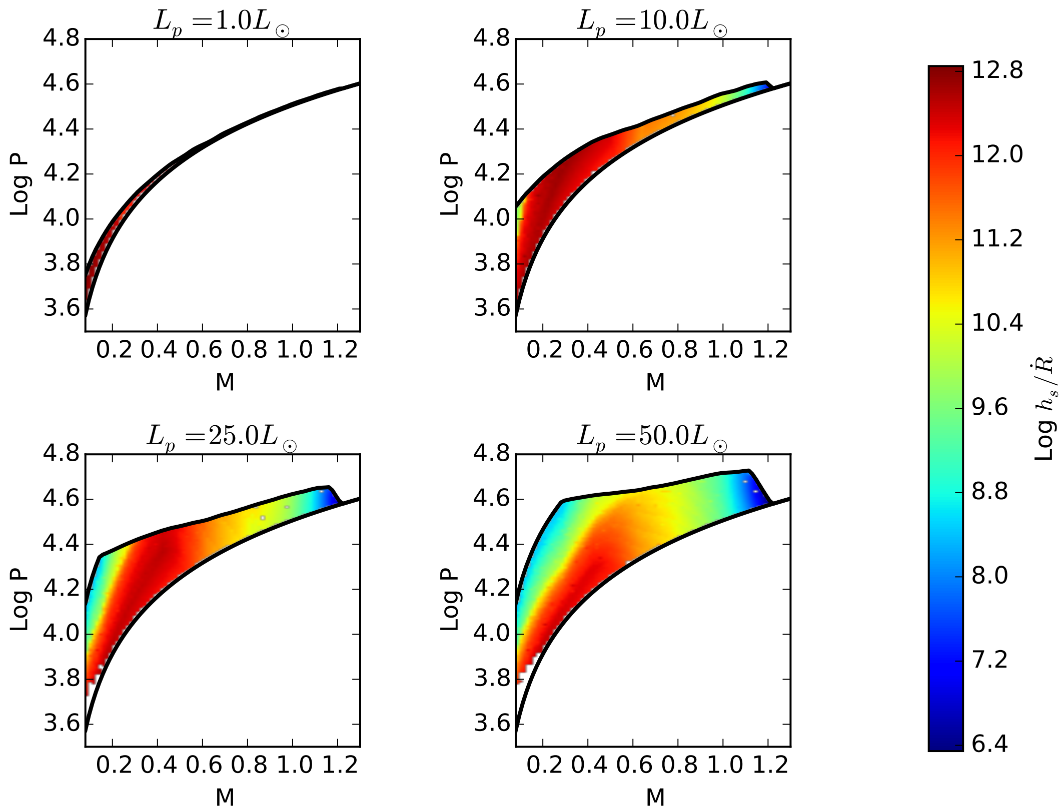

Figure 9.1: The vertical axis is $\log \mathcal{P}$ in seconds, the horizontal axis is the companion mass M in solar masses, and the color represents the log of the expansion timescale $h_s/\dot{R}$ in seconds. The four different plots correspond to four different pulsar luminosities.

If this radius falls within the Pulsar's light cylinder it will bury the magnetic field[5]. This occurs when

$$\dot{M}_c = \frac{L_p}{\sqrt{\omega G M_p c}} = 5 \times 10^{13} \mathcal{P}_{p,-3}^{1/2} \frac{L_p}{L_\odot} \mathrm{g/s}, \tag{9.41}$$

where $\mathcal{P}_{p,-3}$ is the pulsar period measured in milliseconds. We may compute the thermal energy lost when this mass leaves the star at $\sim 10^4$K. The result is roughly $3 \times 10^{-8} L_p$. As the input heat is expected to be only a few orders of magnitude below L_p, this effect is negligible. Thus we expect the limiting factor in the accretion process to be that the heat coming from the pulsar is blocked above a certain $\dot{M}$.

Now at the accretion rate $\dot{M}_c$ we may estimate the structure of the accretion disk which forms. The accretion luminosity is

$$L_{\mathrm{acc}} = \frac{G M_p \dot{M}}{R_0/2}. \tag{9.42}$$

We may equate this with the heat flux of the disk as a black body, giving

$$T = \left(\frac{G M_p \dot{M}}{\pi R_0^3 \sigma} \right)^{1/4}. \tag{9.43}$$

If the disk is optically thin, then the temperature gradient in the vertical direction is negligible. We will assume that this is the case, and later demonstrate its consistency in the regimes of interest. The remaining structural equations which must be solved

[5]There is some evidence that the actual radius to compare to is smaller than the light cylinder radius by a factor of 20 or so (Unal Ertan. "Inner disk radius, accretion and the propeller effect in the spin-down phase of neutron stars". In: []. eprint: `http://arxiv.org/pdf/1504.03996v1.pdf`). As this work is only suggestive, we proceed with the currently accepted model. If it turns out that a smaller radius is necessary, the critical accretion rates and associated luminosities will be reduced, which would mean a higher disk timescale and hence more type 1 cycles, as will be explained in subsequent sections. If the increase in timescale is sufficient, it could even allow asteroids and other similar objects to form in the disk, providing an explanation for some of the timing noise in pulsars with known companions.

are[6]

$$h_s = \frac{v_s R_0^{3/2}}{\sqrt{GM_p}} \tag{9.44}$$

$$v_s^2 = \frac{P}{\rho} \tag{9.45}$$

$$\alpha v_s h_s \Sigma = \frac{\dot{M}}{3\pi} f, \tag{9.46}$$

where α is a dimensionless parameter less than unity relating the viscosity of the disk to the product of h_s and v_s, and f is a dimensionless parameter equal to $(1 - \sqrt{R_{\text{inner}}/R_0})^{1/4} \approx 1$. Solving for Σ yields

$$\Sigma \approx \frac{2\dot{M} m_p}{3\alpha k_B T \mathcal{P}} \sqrt{\frac{M}{2+M}}, \tag{9.47}$$

where M is measured in solar masses. Plugging in $\dot{M} = 10^{13}$g/s, $\mathcal{P} \sim 10^4$s, and $\alpha > 10^{-2}$ yields $\Sigma < 2$g/cm^2. Low-temperature opacities tend towards ~ 1cm^2/g, so for this $\dot{M}$ the optically-thin assumption is valid. The worst case scenario for this assumption while still keeping $\dot{M}$ sub-critical occurs when $T \sim 10^3$K. For hotter disks, the opacity drops off by several orders of magnitude[7]. When T is 10^3K, Σ is between 0.2g/cm^2 and 20g/cm^2, depending on the chosen value of α. Here τ can be as great as 10, so taking the system to be optically thin is perhaps not a good assumption. On the other hand, the ratio of the disk interior temperature to the surface temperature goes as the optical depth to the one-fourth power, and this ratio is the resulting error in the scale height and squared sound speed, so even an optical depth of 10 does not incur error in Σ greater than the existing error due to the uncertainty in α. Thus we will proceed with the optically-thin assumption.

Now the radial velocity of the accreting material is determined by the timescale over which viscosity dissipates angular momentum. This is given by[8]

$$\tau_{\text{disk}} = \frac{R_0^2}{\nu} = \frac{R_0^2}{\alpha h_s v_0} = \frac{R_0}{\alpha}\sqrt{\frac{m_p}{k_B T}} \sim 3 \times 10^5 \text{s} R_0^{5/8} \dot{M}_{13.7}^{-1/8}, \tag{9.48}$$

[6] T. Padmanabhan. *Theoretical Astrophysics*. Vol. 2. ISBN: 978-0521566315. Cambridge University Press, 2001. Chap. 6.

[7] Jason W. Ferguson et al. "Low-Temperature Opacities". In: *The Astrophysical Journal* 623.1 (2005), p. 585. URL: `http://stacks.iop.org/0004-637X/623/i=1/a=585`.

[8] D. Lynden-Bell and J. E. Pringle. "The evolution of viscous discs and the origin of the nebular variables." In: *Monthly Notices of the Royal Astronomical Society* 168 (Sept. 1974), pp. 603–637.

where R_0 is measured in solar radii. At the critical accretion rate, this is

$$\tau_{\rm disk,c} = 3 \times 10^5 {\rm s} L_p^{-1/8} \mathcal{P}_{p,-3}^{-1/16} R_0^{5/8}, \tag{9.49}$$

where L_p is measured in solar luminosities, R_0 is in solar radii, and $\mathcal{P}$ is measured in seconds. This timescale may be viewed as the time over which material falling onto the outer edge of the disk travels to the inner edge when the accretion rate is near the critical value. We see that in most cases this is quite short, only of order one hundred orbits.

It is extremely important to note in this analysis that the pulsar field only turns off when the mass loss rate **on the inner edge of the disk** reaches the critical value. In the event that the disk forms quickly relative to $\tau_{\rm exp}$, this $\dot{M}$ is the same as the $\dot{M}$ which fell onto the disk a time $\tau_{\rm disk}$ earlier, so there is a time delay associated with waiting for the material to reach the pulsar. This has two key impacts on our system. First, it introduces the possibility of limit-cycles by building in a characteristic delay timescale, and second it allows the mass loss rate to continue to grow after $\dot{M}_c$ has been reached at the companion. When the disk timescale is not too much longer than the expansion timescale, the typical overshoot in mass loss associated with this delay is

$$\Delta \ln \dot{M} = \frac{\tau_{\rm disk}}{\tau_{\rm exp}}. \tag{9.50}$$

We can plot this using our numerical results for $\tau_{\rm exp}$. In figure 9.2 we have done this for a variety of L_p values with $\mathcal{P}_p = 10^{-3}$s. Examining the figure, we see in all cases that the growth is negligible, so the limit-cycle possibility is the key impact of the disk clearing time.

Of course, in the event that the disk forms slowly, the disk forming time may become the relevant parameter. In this case, we expect

$$\Delta \ln \dot{M} = \frac{\tau_{\rm spread}}{\tau_{\rm exp}}, \tag{9.51}$$

where $\tau_{\rm spread}$ is the time the disk takes to form and spread once the companion star overflows the Roche radius. We will consider this timescale in more detail in later sections.

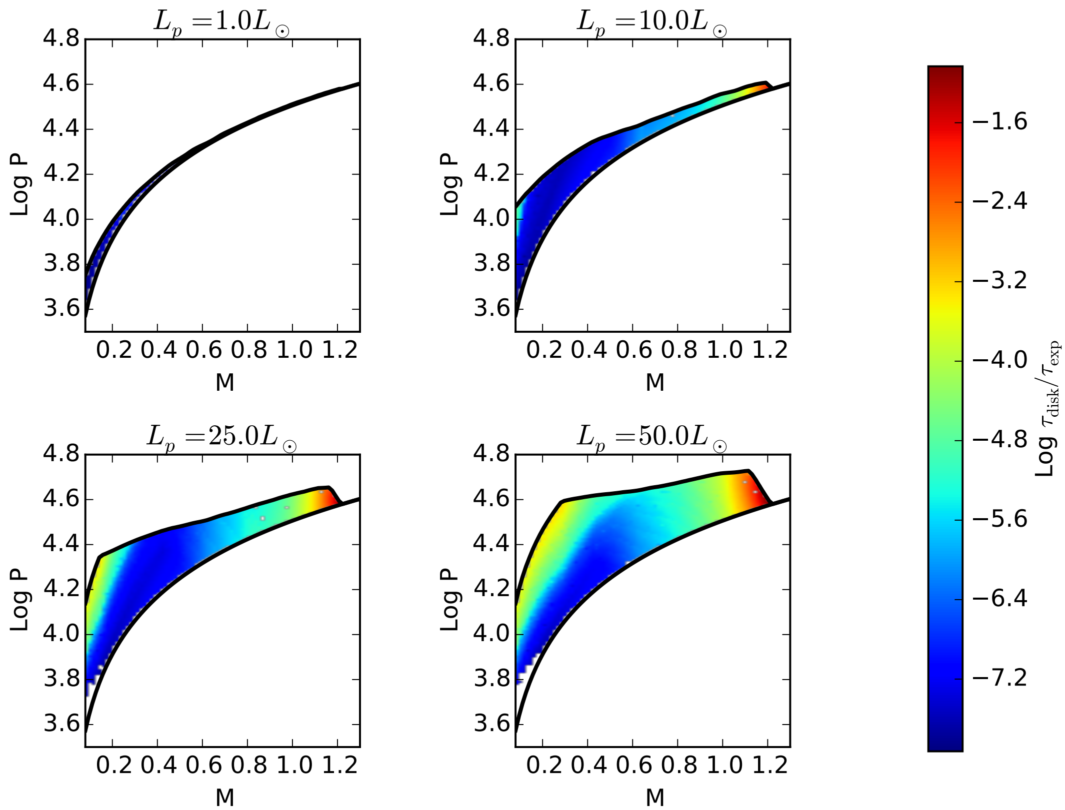

Figure 9.2: The vertical axis is $\log \mathcal{P}$ in seconds, the horizontal axis is the companion mass M in solar masses, and the color represents the log of $\tau_{\rm disk}/\tau_{\rm exp}$. The four plots correspond to different pulsar luminosities.

9.4 Critical Accretion Dynamics

Once the accretion rate reaches the critical rate, the heating stops on a very short timescale[9]. At this point, the short time dynamics of the star are important. The envelope has some momentum, as $\dot{R}$ was 2×10^{-3}cm/s prior to the heating ceasing. This will continue at a minimum until a wave traveling at the sound speed traverses the star, which takes time $R/v_s \sim 10^5$s. More importantly, the deep convective and shallow regions have characteristic adjustment timescales which exceed this.

As discussed in Chapters 2 and 8, the convection zone cannot adjust on timescales shorter than the eddy turnover time. This was determined in Chapter 2 to be

$$\tau_{\text{eddy}} \sim \frac{v_{s,0}^2}{g v_{c,0}} \left(\frac{P_f}{P_0}\right)^{3/5} \tag{9.52}$$

$$= \frac{v_{s,0}^2}{g v_{c,0}} \left(\frac{P_f}{P_c}\right)^{3/5} \left(\frac{P_c}{P_0}\right)^{3/5} \tag{9.53}$$

$$= 5 \times 10^8 \frac{M^{1/5} T_{0,4}}{R^{2/5} P_{0,5}^{3/5} v_{c,0,5}} \min\left(1, \frac{1}{2} M^{-4/5}\right), \tag{9.54}$$

where P_9 is the pressure at the top of the convection zone, T_0 is the corresponding temperature, $v_{c,0}$ is the convection speed at the top of the efficient portion of the convection zone, and M and R are measured in solar units. This sets a lower bound on the adjustment timescale for the convection zone. In the event that this is longer than the thermal adjustment timescale, then eddy turnover is the limiting factor and we expect this to be the relevant timescale. If, on the other hand, adjusting the thermal profile to match the new flux profile takes longer, then the time that takes is the relevant timescale.

To quantify the thermal adjustment timescale, we first compute $\partial_L \nabla$. Note that the thermal gradient needs very little correction, as ∇ is very nearly independent of L. Making use of the mixing length theory from Gob[10], we may write

$$\nabla = \nabla_{ad} + (\nabla_{rad} - \nabla_{ad})\, y(y + V), \tag{9.55}$$

$$\frac{2A}{V} y^3 + y^2 + V y - 1 = 0, \tag{9.56}$$

[9] Naively one might expect this to be R_0/c, typically of order one second. There are, however, geometric factors involved which adjust on the star's orbital period, so a few hours is probably a better estimate.

[10] B. Paczyński. "Envelopes of Red Supergiants". In: *Acta Astronomica* 19 (1969), p. 1.

and

$$V = \frac{1}{\gamma_0 \sqrt{C\left(\nabla_{rad} - \nabla_{ad}\right)}}, \tag{9.57}$$

where A, C, γ_0, and ∇_{ad} are parameters independent of L and where V is typically within an order of magnitude of unity. Implicit differentiation of the second equation yields

$$\frac{6A}{V} y^2 \partial_L y - \frac{2A}{V^2} y^3 \partial_L V + 2y\partial_L y + y\partial_L V + V\partial_L y = 0, \tag{9.58}$$

and hence

$$\partial_L y = \frac{\frac{2A}{V^2} y^3 \partial_L V + y\partial_L V}{V + 2y + \frac{6A}{V} y^2} = -\left(\frac{V}{2(\nabla_{rad} - \nabla_{ad})}\right) \frac{\frac{2A}{V^2} y^3 + y}{V + 2y + \frac{6A}{V} y^2} \partial_L \nabla_{rad}. \tag{9.59}$$

This may be used to compute $\partial_L \nabla$ as

$$\partial_L \nabla = y(y+V)\partial_L \nabla_{rad} + (\nabla_{rad} - \nabla_{ad}) 2y\partial_L y + (\nabla_{rad} - \nabla_{ad})\left(V\partial_L y + y\partial_L V\right) \tag{9.60}$$

$$= \left(y(y+V) - \frac{\frac{2A}{V^2} y^3 + y}{V + 2y + \frac{6A}{V} y^2}\left[Vy + \frac{V^2}{2}\right] - \frac{yV}{2}\right) \partial_L \nabla_{rad} \tag{9.61}$$

$$= \left(\frac{y^2 (V+2y)(V+2Ay)}{V^2 + 2Vy + 6Ay^2}\right) \partial_L \nabla_{rad}. \tag{9.62}$$

Now $(\nabla_{rad} - \nabla_{ad}) y(y+V)$ is a measure of the superadiabaticity of the convection. Denote this by P. Then in efficient convection we expect $P \ll 1$, and hence $y(y+V) \ll 1$, as $\nabla_{rad} - \nabla_{ad}$ is typically at least of order 0.1 in convection zones. Thus $y \ll 1$, so

$$\partial_{\ln L} \ln \nabla \sim y^2 \partial_{\ln L} \ln \nabla_{rad}. \tag{9.63}$$

We can relate y to v_c as[11]

$$v_c = y v_s \sqrt{\frac{\nabla_{rad} - \nabla_{ad}}{8}} \sim \frac{1}{3} y v_s \nabla_{rad}^{1/2}. \tag{9.64}$$

The ratio of the time dt over which the thermal structure in a layer adjusts to the thickness dr of the layer is

$$v_{adj} = \frac{F_e}{\rho c_p T \Delta\left(\nabla_{ad}\right)} = \frac{F_i}{\rho c_p T y^2 \nabla_{rad}} = \frac{v_c^3}{v_s^2 y^2 \nabla_{rad}} = \frac{1}{30} y v_s \nabla_{rad}^{1/2} = \frac{v_c}{10}. \tag{9.65}$$

[11] Ibid.

whereas the corresponding rate for eddy adjustment is just v_c. Thus the true timescale over which the convection zone "notices" that the heating has been turned off is ten times the eddy timescale. The change in temperature is just

$$\Delta T = \frac{\Delta L}{4\pi R^2 \rho v_{adj} c_p}. \tag{9.66}$$

The resulting rate at which R changes is

$$\dot{R} = v_{adj}\frac{\Delta T}{T} = \frac{\Delta L}{4\pi R^2 \rho c_p T} = \frac{\Delta L}{10\pi R^2 P}, \tag{9.67}$$

where here ρ is evaluated at the location of the advancing flux adjustment wave and ΔL is $L_e + L_i - L_{\text{surface}}$. Using $P \sim \exp(v_{adj} t/l)$, we may write

$$\dot{R} = v_{adj}\frac{\Delta T}{T} = \frac{\Delta L e^{-v_c t/10}}{4\pi R^2 P_0}, \tag{9.68}$$

where P_0 is the pressure at the shallowest point in the convection zone above the ionization zone. When the adjustment wave reaches the base of the convection zone, $\dot{R}$ approaches the negative of the expansion rate.

We now turn to the shallow case. When the external illumination is turned off the upper envelope temperature drops due to $\partial_m L - \varepsilon$ being nonzero in the heating zone. Simultaneously, the convection zone adjusts to provide the flux needed to match the surface temperature. The boundary condition which reconciles these two is that the convection zone maintains an adiabatic gradient, and so deeper than the ionization zone its temperature must be effectively unchanged. The code we have used to compute the various expansion plots shown previously has a module which computes this process, once more using binary search. Here the objective is to minimize the deviation in the convection zone temperature in the parts deeper than the ionization zone from the heated value, and the free parameter is the surface temperature. The resulting stellar structure allows us to compute the extent of the fast contraction, occurring on a thermal timescale for the heating zone, for each heated stellar model. The results of this calculation are shown in figure 9.3. Note that this contraction does not just occur on the day side of the star. In cases where substantial bloating has occurred, the flux profile has been altered by winds, so turning off the illumination does precisely what would be expected from these calculations. The characteristic timescale for adjustment of the day-side surface region is just

$$\tau_{rad} \sim \frac{4\pi R^2 \Sigma_h c_p T}{\Delta L} = \frac{L_i}{\Delta L}\left(\frac{\Sigma_h c_p}{T^3 \sigma}\right) = 10^4 \frac{L_i}{(T/T_\odot)^3 \Delta L}\text{s}. \tag{9.69}$$

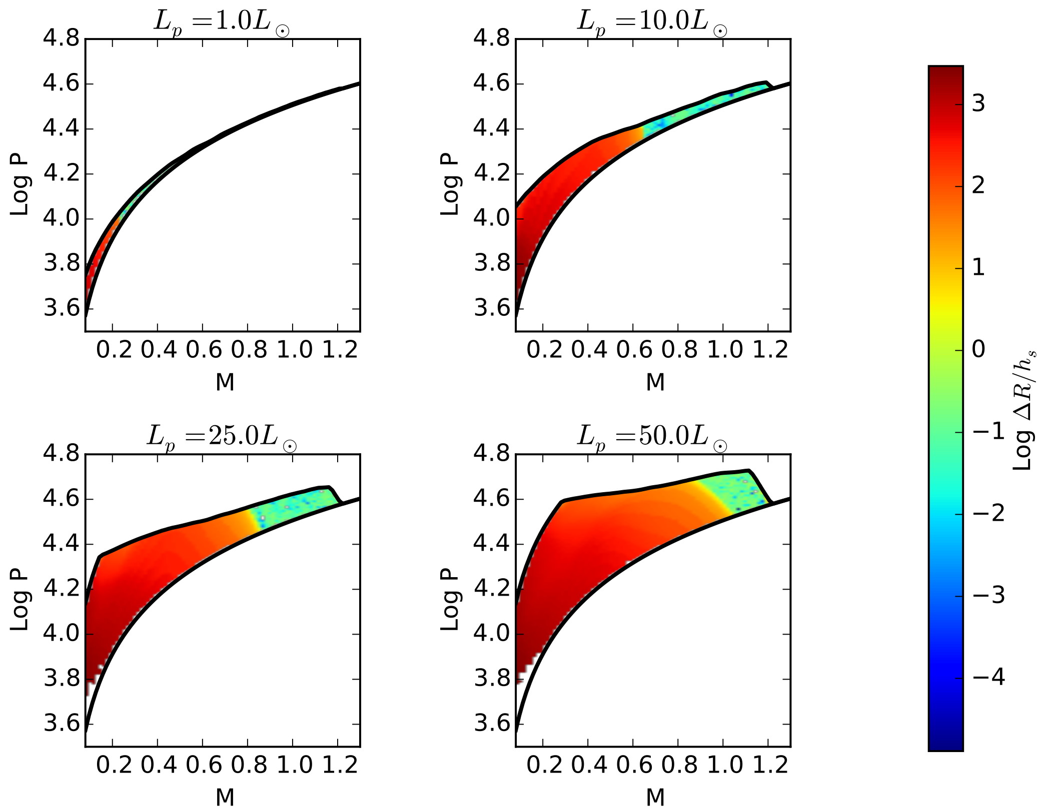

Figure 9.3: The vertical axis is $\log \mathcal{P}$ in seconds, the horizontal axis is the companion mass M in solar masses, and the color represents the log of the ratio of the quick contraction length to the scale height. The four plots correspond to different pulsar luminosities.

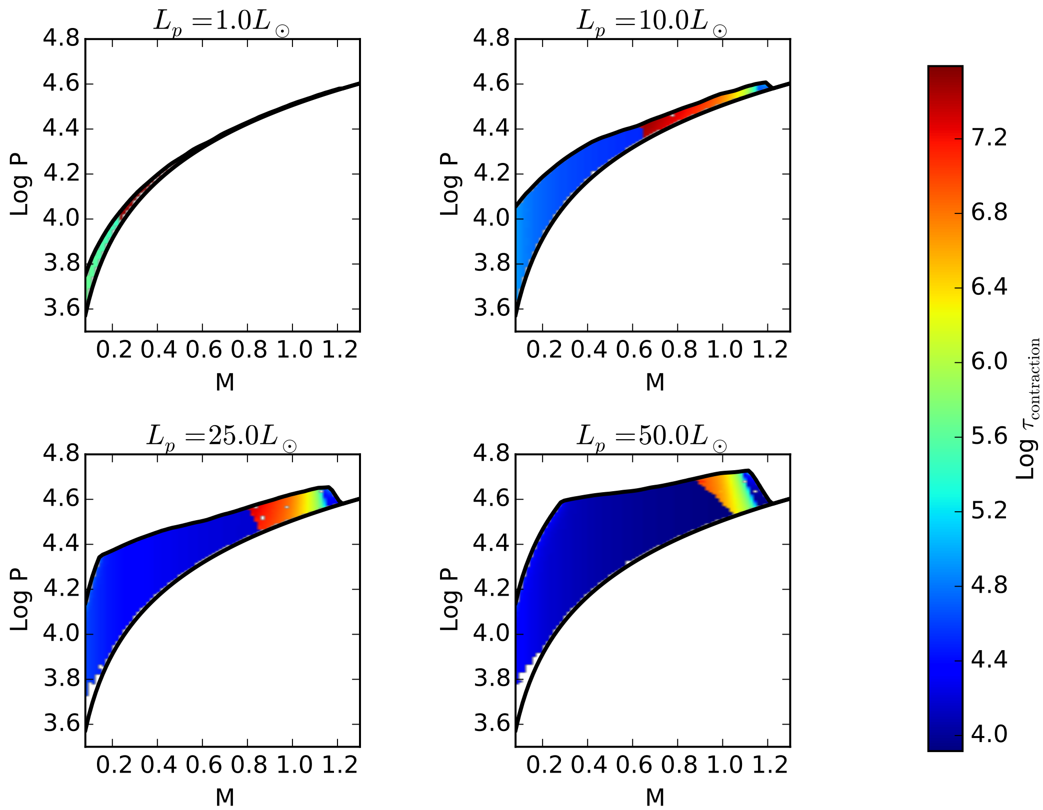

Figure 9.4: The vertical axis is $\log \mathcal{P}$ in seconds, the horizontal axis is the companion mass M in solar masses, and the color represents the log of the contraction timescale. The four plots correspond to different pulsar luminosities.

Now only the irradiated side can adjust this quickly: the other side, if radiative, will adjust on the wind timescale, typically an order of magnitude longer than the sound speed timescale. Thus 10^6s is an upper bound on the timescale associated with radiative envelope adjustments. This is much faster than the eddy or convective thermal timescale, both at least four orders of magnitude larger, and so this will be the dominant timescale where applicable.

Putting it all together, we may compute the expected timescale over which the accretion rate drops by a factor of ten when the heating turns off. This is shown in figure 9.4. We see that for most stars, the time is quite short. For those which have the least sudden contraction, the timescale is longest, as expected. The divide is primarily one of mass, indicating that companion mass is the primary determining factor in the accretion response of the companion.

One thing worth noting is that the computed contraction timescales are, to leading order, the same as the expected expansion timescales if the pulsar is turned off and then back on. The ratio of the disk time to the contraction time can then provide a measure of $\dot{M}$ overshoot, and is shown in figure 9.5.

9.5 Limit Cycles

Having now characterized the initial heating, post-Roche processes, and accretion disk dynamics, we now turn to the possibility of a limit cycle. The general picture is this:

1. The initial heat goes on until the star overflows its Roche-lobe.
2. The resulting accretion builds up a disk.
3. When $\dot{M} = \dot{M}_c$ at the inside of the disk, a time τ_{disk} after $\dot{M}$ on the star reaches this value, the pulsar shuts off.
4. The accretion turns off as the companion cools.
5. The accretion disk clears after time τ_{disk}, after which the pulsar turns back on.
6. Accretion begins rapidly, as the radiative zone expands once more and begins to build a disk.
7. Time τ_{disk} later, the material reaches the pulsar and it turns off. The process then repeats.

There are four timescales which are potentially of interest for these cycles:

1. τ_{disk} - The time over which the equilibrium disk adjusts to perturbations.
2. τ_{spread} - The time over which a disk forms and spreads to the pulsar.
3. τ_{M} - The timescale over which $\dot{M}$ changes by a factor of e prior to the limit cycle. Note that this is the same as τ_{exp}.
4. $\tau_{\text{M,L}}$ - The timescale over which $\dot{M}$ changes by a factor of e inside the limit cycle. Note that this is what we have previously been calling $\tau_{\text{contraction}}$, as the

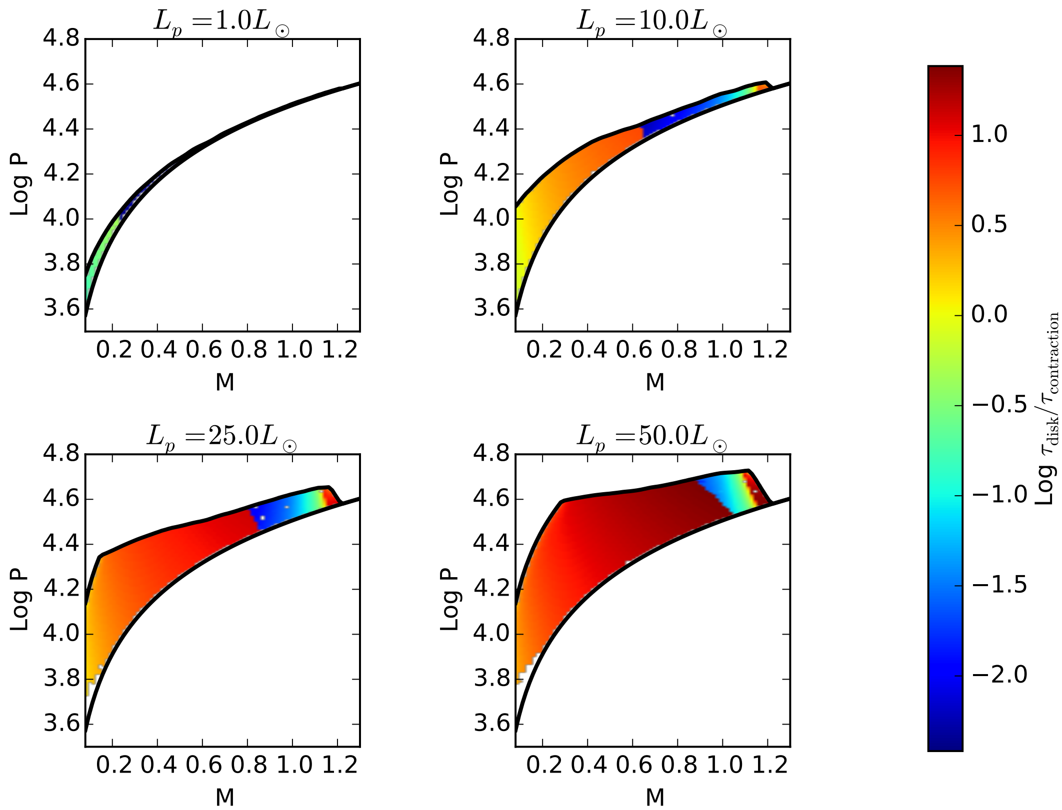

Figure 9.5: The vertical axis is $\log \mathcal{P}$ in seconds, the horizontal axis is the companion mass M in solar masses, and the color represents the log of the ratio of the critical disk viscous timescale to the contraction timescale. The four plots correspond to different pulsar luminosities.

corresponding timescale for expansion when the pulsar turns on is the same to leading order[12].

To investigate the properties of these limit cycles, we begin by computing τ_{spread}, as it is the only timescale of interest which we have not determined. To that end, suppose that we have a disk with inner radius R_i and outer radius equal to the companion orbital radius R_0. The area of the disk is then

$$A = \pi \left(R_0^2 - R_i^2\right), \tag{9.70}$$

and the accretion luminosity is

$$L_a = \frac{GM_p\dot{M}}{R_a}, \tag{9.71}$$

where

$$R_a \equiv \frac{R_0 + R_i}{2} \tag{9.72}$$

is the mean radius. If the disk thermally equilibrates on timescales short relative to τ_{spread}, as we will verify is the case, then

$$T = \left(\frac{L_a}{2A\sigma}\right)^{1/4}. \tag{9.73}$$

We will later verify that Σ monotonically approaches its equilibrium value, such that our prior calculations showing that the surface and interior temperatures of equilibrium disks applies here as well. Assuming this for the moment, we find that the viscous timescale for the disk is

$$\tau_{\mathrm{visc}} = \frac{R_0^2}{\nu} = \frac{3\pi R_0^2 v_s \Sigma}{\dot{M} f v_0}, \tag{9.74}$$

where v_0 is mean orbital speed, v_s is the mean sound speed, Σ is the mean column density, and f is given by

$$f \equiv \left(1 - \sqrt{\frac{R_i}{R_0}}\right)^{1/4}. \tag{9.75}$$

In the limit where $R_0 - R_i \ll R_0$, we may write

$$R_0 - R_i = \varepsilon R_0. \tag{9.76}$$

[12] There is a small discrepancy due to the changed thermal properties of the star, but this is irrelevant at the level of estimation being used here.

In this regime,

$$f = \left(\frac{\varepsilon}{2}\right)^{1/4} \tag{9.77}$$

$$A = 2\pi R_0^2 \varepsilon \tag{9.78}$$

$$\frac{v_s}{v_{s,0}} = \left(\frac{A}{A_0}\right)^{-1/8} = (2\varepsilon)^{-1/8}, \tag{9.79}$$

where $v_{s,0}$ is the equilibrium mean sound speed and v_s is the instantaneous mean sound speed. Using these approximations, as well as our expression in Eq. (9.48) for $\tau_{\rm disk}$, we may expand $\tau_{\rm visc}$ as

$$\tau_{\rm visc} = \frac{1}{2^{3+1/8}} \tau_{\rm disk} \varepsilon^{-11/8}, \tag{9.80}$$

where $\tau_{\rm disk}$ is the timescale for the equilibrium disk at this $\dot{M}$. Note that in performing this expansion, we made use of the fact that the mean orbital radius and mean sound speed both depend on ε. The differential equation for the evolution of ε is therefore

$$\partial_t \varepsilon = 2^{3+1/8} \tau_{\rm disk}^{-1} \varepsilon^{11/8}, \tag{9.81}$$

and hence

$$\varepsilon = \left(\varepsilon_0^{-3/8} - 3 \times 2^{1/8} \frac{t}{\tau_{\rm disk}}\right)^{-8/3}. \tag{9.82}$$

Setting this equal to unity, we see that

$$\frac{\tau_{\rm spread}}{\tau_{\rm disk}} = \frac{\varepsilon_0^{-3/8} - 1}{3 \times 2^{1/8}}. \tag{9.83}$$

This method of solution is justified by the fact that $\tau_{\rm visc}$ diverges at small ε, and hence we may focus on the time spent in that regime. Now typically we expect ε_0, which measures the initial disk width in units of R_0, to be comparable to the atmospheric scale height of the companion. This is given by $R_b v_s^2 / v_0^2$, so

$$\varepsilon_0 = \frac{R_b}{R_0} \left(\frac{v_s}{v_0}\right)^2 = 0.46 \left(\frac{M}{M + M_p}\right)^{1/3} \left(\frac{v_s}{v_0}\right)^2. \tag{9.84}$$

For an order of magnitude estimate, we note that $M \sim M_\odot$, $M_p \approx 2M_\odot$, and $v_s \sim v_0/10$, giving $\varepsilon_0 \sim 1/300$. As a result, we may write simply

$$\frac{\tau_{\rm spread}}{\tau_{\rm disk}} \approx \frac{2}{5} \left[\left(\frac{M}{M + M_p}\right)^{1/3} \left(\frac{v_s}{v_0}\right)^2\right]^{-3/8}. \tag{9.85}$$

This tells us that the spreading time always exceeds the equilibrium disk viscous time. The factor by which this occurs is typically of order a few, and so does not change the conclusion that the accretion rate does not change substantially from the critical value before the heating turns off.

To tie up loose ends, we now must verify some assumptions. First, consider the question of the monotonicity of Σ. We may write

$$\dot{\Sigma} = \frac{\partial}{\partial t}\left(\frac{M_a}{A}\right) = \frac{\dot{M}}{A} - \frac{M_a \dot{A}}{A^2} = \Sigma\left(\partial_t \ln M_a - \partial_t \ln A\right), \tag{9.86}$$

where M_a is the disk mass. Now initially $\partial_t \ln A$ is roughly $\tau_{\text{spread}}^{-1}$ and $\partial_t \ln M_a$ is infinite. Thus $\dot{\Sigma}$ begins positive. Now M_a increases monotonically, so $\partial_t \ln M_a$ decreases monotonically if $\dot{M}$ is fixed. This decrease ends with a sharp drop to zero, coinciding with the time when the increase in A ends, as then the steady-state is achieved. Right before that time, $M_a = \dot{M}\tau_{\text{spread}}$, so at all times before this $\partial_t \ln M_a \geq \tau_{\text{spread}}^{-1}$. As a result, Σ is monotonically increasing in time prior to equilibrium being established.

Next consider the question of thermal equilibration. The relevant dimensionless quantity of interest is $M_a c_p \partial_t T / L_a$, where the time derivative is computed assuming thermal equilibrium. If the magnitude of this is less than unity then it is valid to assume thermal equilibrium. The rate at which T changes is given by

$$\partial_t T = -\frac{1}{4} T \partial_t \ln A = -\frac{T}{4\tau_{\text{spread}}}. \tag{9.87}$$

As a result, our dimensionless quantity is roughly $M_a v_s^2 / 4L_a$. The numerator is maximized in equilibrium, where $M_a = \dot{M}\tau_{\text{spread}}$, for $v_s^2 \propto T \propto A^{-1/4}$, whereas $M_a = \Sigma A$ scales at least as A, as Σ increases monotonically in A. The denominator is maximized initially, as $L_a \propto R_a^{-1}$, so we may upper bound the quantity of interest by

$$\frac{\tau_{\text{spread}} v_s^2 R_0}{4GM_p}. \tag{9.88}$$

For an order of magnitude estimate, $R_0 \sim 10^{11}$cm, $v_s^2 \leq 3\times 10^{10}\text{cm}^2/\text{s}^2$, $M_p \sim 4\times 10^{34}$g, $4G \sim 3 \times 10^{-7}\text{cm}^3/\text{g}/\text{s}^2$, so this quantity is at most $3 \times 10^{-7}\tau_{\text{spread}}\text{s}^{-1}$. From the last section, we know that $\tau_{\text{disk}} \sim 3 \times 10^5$s, so really we are interested in the quantity

$$\frac{2}{50}\left[\left(\frac{M}{M+M_p}\right)^{1/3}\left(\frac{v_s}{v_0}\right)^2\right]^{-3/8}. \tag{9.89}$$

We may determine the maximum value of v_0/v_s by setting this equal to unity, giving a ratio of 2000. Typically v_0/v_s is at most 100, so we are safe in assuming thermal equilibrium.

Having determined that the spreading time exceeds the equilibrium viscous time, and having satisfied our various assumptions, we note that there are three possible limit cycle cases to consider:

1. $\tau_{\text{spread}} > \tau_{\text{disk}} > \tau_{\text{M,L}}$
2. $\tau_{\text{spread}} > \tau_{\text{M,L}} > \tau_{\text{disk}}$
3. $\tau_{\text{M,L}} > \tau_{\text{spread}} > \tau_{\text{disk}}$

We have not included τ_{M} in these orderings because it is only relevant in determining how long the cycle takes to begin, and because it is typically much larger than the other three timescales.

Examining the timescales involved, we may classify regions of phase space into the different kinds of limit cycle. This is done in figure 9.6. The first thing to note about this plot is that as the pulsar luminosity increases, the low mass companions lose the possibility of a type 2 cycle. This results from the adjustment of the upper radiative zone increasing with L_p, thereby reducing $\tau_{\text{M,L}}$. That the type 2 cycles also disappear as we go to higher M at fixed L_p results from the deepening of the upper radiative layer as we approach the main sequence line.

The transition from type 1 to type 3 around $0.6M_{\odot}$ is due to the shrinkage and eventual disappearance of the heating-induced radiative zone. The radiative-convective transition is set by the condition that $\nabla_{ad} = \nabla_{rad}$. In the upper layers of the star, this requires that the escaping luminosity be $L_{esc} \ll L_{in}$, which makes the transition quite sharp. Additionally, the transition depends on the microphysics of opacity and ionization. These phenomena are often exponentially dependent on the thermal structure of the outer layers of the star, which further sharpens the change.

The transition from type 3 to type 2, and eventually to type 1 as M increases is just due to the convection zone shrinking, which reduces $\tau_{\text{M,L}}$ by reducing the relevant thermal mass. The thermal mass goes roughly as the convective base pressure P_f to the three-fifths power[13]. If we hold the period fixed, then to a good approximation R is fixed. As a result, the thermal mass just scales as $M^{6/5}$. We expect that $\tau_{\text{M,L}}$ will be proportional to this. At the same time, the scale height is increasing, which counteracts this effect. We may compute the scaling as

$$h_s = R_0 \frac{{v_s^2}^2}{v_0} \sim v_s^2 \propto T \propto \frac{L^{1/4}}{R^{1/2}} \propto \frac{M^{2.3/4}}{M^{0.9/2}} \propto M^{0.13}. \tag{9.90}$$

[13]This is set by the adiabatic constant γ.

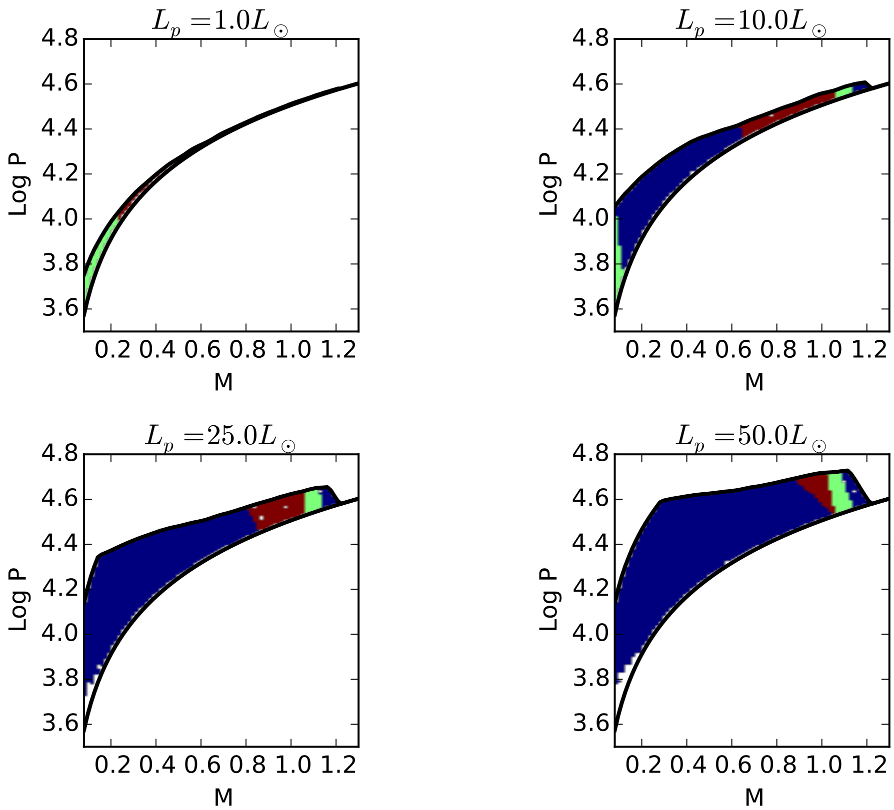

Figure 9.6: The vertical axis is $\log \mathcal{P}$ in seconds, the horizontal axis is the companion mass M in solar masses, and the color represents the type of limit cycle. Blue is type 1, Green is type 2, Maroon is type 3. The four plots correspond to different pulsar luminosities.

As this is a much lower power of M, we expect that $\tau_{\mathrm{M,L}} \propto h_s/M^{6/5}$ will decrease as we move to higher mass.

Having established which kind of cycle occurs in which regime, it is worth contrasting the various kinds of cycles. The first case corresponds to the fast expansion case. Based on figure 9.2, this case matters in a fairly wide regime. Here the limit cycle time is set by $2\tau_{\mathrm{spread}} + 2\tau_{\mathrm{M,L}}$. This may be seen by noting that when accretion begins, it takes time τ_{spread} for material to reach the pulsar. It then takes time $\tau_{\mathrm{M,L}}$ for the accretion rate at the pulsar to reach the critical value, assuming that in the previous cycle it reached the critical value. It then takes time $\tau_{\mathrm{M,L}}$ for the accretion to halt. Finally, it takes time τ_{spread} for the disk to clear, allowing the process to begin again. The reason τ_{spread} is relevant here is that the disk is never near equilibrium at any stage of the process. Given the orderings of timescales, we make at most a factor of two error by writing the full timescale as $2\tau_{\mathrm{spread}}$. Naively, one might expect the corresponding overshoot in $\dot{M}$ to be $\exp\left(\tau_{\mathrm{spread}}/\tau_{\mathrm{M,L}}\right)$. In practice this is not the case. To see why, note that τ_{spread} and τ_{disk} both decrease with T, the latter as $T^{-1/2}$ and the former as $T^{-7/8}$. As a result, as T increases, the disk spreads faster, and so when τ_{spread} is considerably larger than $\tau_{\mathrm{M,L}}$, the increase in $\dot{M}$ will be that required to set the relevant timescale connecting the outer and inner portions of the disk to $\tau_{\mathrm{M,L}}$. As that timescale is τ_{spread} in this case, and as $T \propto \dot{M}^{1/4}$ and $\tau_{\mathrm{spread}} \propto \dot{M}^{-1}$, we see that $\dot{M}$ will increase by a factor of $\left(\tau_{\mathrm{spread}}/\tau_{\mathrm{M,L}}\right)^{15/8}$ over the critical value. This typically involves just a few extra scale heights of motion, and so we do not expect the timescale $\tau_{\mathrm{M,L}}$ to be off by too much from the actual timescale over which the mass loss rate adjusts, and at any rate the limit cycle timescale is dominated by τ_{spread}, so any corrections to the adjustment timescale effect are not relevant.

Now consider the second case. Here the limit cycle time is set by $\tau_{\mathrm{spread}} + \tau_{\mathrm{disk}} + 2\tau_{\mathrm{M,L}}$. This may be seen by noting that when accretion begins, it takes time τ_{spread} for material to reach the pulsar. It then takes time $\tau_{\mathrm{M,L}}$ for the accretion rate at the pulsar to reach the critical value, assuming that in the previous cycle it reached the critical value. It then takes time $\tau_{\mathrm{M,L}}$ for the accretion to halt. Finally, it takes time τ_{disk} for the disk to clear, allowing the process to begin again. To good approximation, given this ordering, we may simply say that the limit cycle takes time τ_{spread}, and thereby incur error of at most a factor of two given the large disparity between τ_{spread} and τ_{disk}. The overshoot is given by the same expression as in the first case, for once more the disk is out of equilibrium the entire time.

In the third case, the expansion is slow, and so the spreading time is irrelevant to the overshoot. The limit cycle time is once more set by $\tau_{\mathrm{spread}} + \tau_{\mathrm{disk}} + 2\tau_{\mathrm{M,L}}$. Given the ordering of timescales, we may approximate this as $2\tau_{\mathrm{M,L}}$, and thereby at most a 50% error. The overshoot in $\dot{M}$ is $\exp\left(\tau_{\mathrm{disk}}/\tau_{\mathrm{M,L}}\right)$, for now τ_{disk} is the timescale mediating the delay between the companion and the accretion onto the pulsar.

In summary, then, we expect that there are three kinds of accretion disk limit cycles which are unique to these illuminated companion systems. These cycles are characterized by the relative orderings of the companion atmospheric timescale, the critical accretion disk formation timescale, and the equilibrium critical accretion disk viscous timescale. The cycles range in timescale from days to years, with on-off times typically measured in days. The key difference between the cycles is generally the process modulating them, either atmospheric effects or disk dynamics, as well as the scales of these effects. The luminosity of the accretion disk in each case is given approximately by the accretion luminosity of the mid-disk ring, and corresponds to a mass loss rate on the order of $10^{14\pm1}$g/s. This puts the accretion disk radiation somewhere between the IR and soft X-Ray bands, depending on the precise system parameters. The luminosity of the accreting material at the pulsar is therefore of order $10^{35\pm1}$erg/s. This radiation is expected to be mostly X-Rays, as is typical of accreting magnetic neutron stars.

References

Brown, J. C. and C. B. Boyle. "An exploratory eccentric orbit 'Roche lobe' overflow model for recurrent X-ray transients". In: *Astronomy and Astrophysics* 141 (Dec. 1984), pp. 369–375 (cit. on pp. 145, 146).

Ferguson, Jason W. et al. "Low-Temperature Opacities". In: *The Astrophysical Journal* 623.1 (2005), p. 585. URL: `http://stacks.iop.org/0004-637X/623/i=1/a=585` (cit. on p. 155).

King, A. R. et al. "Mass Transfer Cycles in Close Binaries with Evolved Companions". In: *The Astrophysical Journal* 482 (June 1997), pp. 919–928. eprint: `astro-ph/9701206` (cit. on p. 145).

Lynden-Bell, D. and J. E. Pringle. "The evolution of viscous discs and the origin of the nebular variables." In: *Monthly Notices of the Royal Astronomical Society* 168 (Sept. 1974), pp. 603–637 (cit. on p. 155).

Paczyński, B. "Envelopes of Red Supergiants". In: *Acta Astronomica* 19 (1969), p. 1 (cit. on pp. 158, 159).

— "Evolutionary Processes in Close Binary Systems". In: *Annual Review of Astronomy and Astrophysics* 9 (1971), p. 183. DOI: `10.1146/annurev.aa.09.090171.001151` (cit. on p. 146).

Padmanabhan, T. *Theoretical Astrophysics*. Vol. 2. ISBN: 978-0521566315. Cambridge University Press, 2001. Chap. 6 (cit. on p. 155).

Ritter, H., Z.-Y. Zhang, and U. Kolb. "Irradiation and mass transfer in low-mass compact binaries". In: *Astronomy and Astrophysics* 360 (Aug. 2000), p. 969. eprint: `astro-ph/0005480` (cit. on p. 145).

Unal Ertan. "Inner disk radius, accretion and the propeller effect in the spin-down phase of neutron stars". In: (). eprint: `http://arxiv.org/pdf/1504.03996v1.pdf` (cit. on p. 154).

10

Accretion Induced Collapse

... being nine years old, I'm enthusiastic about a lot of things.
– Thomas A. Tombrello[1]

Recently, a number of millisecond pulsars with white dwarf companions and high eccentricities have been discovered[2]. The observed eccentricities exceed the period-eccentricity relations for accreting red giants by several orders of magnitude[3]. It has been proposed that these systems are a result of rotationally delayed accretion induced collapse[4], though this model has difficulty explaining the relatively small magnetic fields these pulsars are observed to have. It has also been proposed that these systems are formed by the spin-up of an accreting neutron star with a circumbinary disk, but the lack of longer period systems of this sort, which support a higher $\dot{M}$, runs counter to this model. Kozai encounters in triple star systems may also explain these systems, but the expected mass distribution of companions after one star is ejected is substantially different than what is observed.

Here we propose a different model for the formation of high eccentricity millisecond pulsar-white dwarf systems. In this model, accretion from a red giant onto a white

[1]Thomas A. Tombrello. *Caltech Oral History*. Dec. 2012. URL: `http://resolver.caltech.edu/CaltechOH:OH_Tombrello_T`.

[2]B. Knispel et al. "Einstein@Home Discovery of a PALFA Millisecond Pulsar in an Eccentric Binary Orbit". In: *ArXiv e-prints* (Apr. 2015). arXiv: `1504.03684 [astro-ph.HE]`.

[3]E. S. Phinney. "Pulsars as Probes of Newtonian Dynamical Systems". In: *Royal Society of London Philosophical Transactions Series A* 341 (Oct. 1992), pp. 39–75. DOI: `10.1098/rsta.1992.0084`.

[4]P. C. C. Freire and T. M. Tauris. "Direct formation of millisecond pulsars from rotationally delayed accretion-induced collapse of massive white dwarfs". In: *Monthly Notices of the Royal Astronomical Society* 438 (Feb. 2014), pp. L86–L90. DOI: `10.1093/mnrasl/slt164`. arXiv: `1311.3478 [astro-ph.SR]`.

dwarf induces the dwarf's collapse into a pulsar. The pulsar wind then irradiates the red giant, forcing it to bloat and lose its upper atmosphere on timescales shorter than the tidal circularization time.

In order for this to occur, the timescale over which the envelope is lost must be short relative to the orbital circularization time, given as[5]

$$\tau_c \sim \left(\frac{R_0}{R}\right)^8 \left(\frac{M_c}{M_p}\right)^2 \left(\frac{M_p}{M_c + M_p}\right) \frac{M_c}{M_{\rm env}} \left(\frac{R^2 M_{\rm env}}{L_i}\right)^{1/3}. \tag{10.1}$$

Letting $M_p \sim 2$ and working in solar units, we find that

$$\tau_c = 7 \times 10^{17}{\rm s} \left(\frac{(M+2)^{1/3}\mathcal{P}_6^{2/3}}{R}\right)^8 \left(\frac{M_c}{2}\right)^2 \left(\frac{2}{M_c + 2}\right) \frac{M_c}{M_{\rm env}} \left(\frac{R^2 M_{\rm env}}{L_i}\right)^{1/3}. \tag{10.2}$$

At the end of the day, we want a white dwarf core left over with mass $\sim 0.25 M_\odot$, so we set $M_c = 0.25$. This yields

$$\tau_c = 2 \times 10^{16}{\rm s}\mathcal{P}_6^{32/3} M_{\rm env}^{-2/3} R^{-22/3} L_i^{-1/3}. \tag{10.3}$$

In order for the red giant to have evolved in at most the age of the universe, we must have $M_c + M_{\rm env} > 1$, and in order to have red giants with a helium flash at all we must have $M_c + M_{\rm env} < 2.5$[6]. Thus $M_{\rm env}$ is within a factor of two of $M_\odot$. As a result, we will write

$$\tau_c = 2 \times 10^{16}{\rm s}\mathcal{P}_6^{32/3} R^{-22/3} L_i^{-1/3}. \tag{10.4}$$

If the envelope will be bloated away, the characteristic timescale for this process to occur is

$$\tau_e = \frac{M_{\rm env} c_p T}{L_e} = 5 \times 10^{12}{\rm s} M R^{-2} \frac{L_i}{L_e}, \tag{10.5}$$

where L_e is the luminosity arriving from the pulsar at the companion. Note that we are assuming that $L_i > L_e$ in this analysis, such that all of the heat arriving at the companion is bottled up by its convective envelope. Further note that this timescale relies on the fact that the scale height is approximately R, and hence we only need to achieve a bloating of a single scale height. Thus

$$\frac{\tau_e}{\tau_c} = 2.5 \times 10^{-4} \mathcal{P}_6^{-32/3} R^{16/3} M L_i^{4/3} L_e^{-1}. \tag{10.6}$$

---

[5]Phinney, op. cit.

[6]Rudolf Kippenhahn, Alfred Weigert, and Achim Weiss. *Stellar Structure and Evolution.* Springer, 2012. ISBN: 978-3-642-30304-3.

Making use of $L_e = L_p R^2/R_0^2 = L_p R^2 (M+2)^{-2/3}\mathcal{P}_4^{-4/3}$, we see that

$$\frac{\tau_e}{\tau_c} = 10^{-1}\mathcal{P}_6^{-28/3} R^{10/3} M(M+2)^{2/3} L_i^{4/3} L_p^{-1}. \tag{10.7}$$

Now we may find L_i by[7]

$$L_i = \frac{10^{5.3}(M_c/M)^6}{1 + 10^{0.4}(M_c/M)^4 + 10^{0.5}(M_c/M)^5} \sim 50M^{-6}. \tag{10.8}$$

Likewise[8],

$$R = \frac{3.7\times 10^3 (M_c/M)^4}{1 + (M_c/M)^3 + 1.75(M_c/M)^4} \sim 14M^{-4}. \tag{10.9}$$

Thus

$$\frac{\tau_e}{\tau_c} = 10^{-4}\left(\frac{\mathcal{P}_6}{2}\right)^{-28/3}\left(\frac{M}{2}\right)^{-20.3}(M+2)^{2/3} L_p^{-1}. \tag{10.10}$$

As a result, for the observed periods of $\sim$ 20days and total masses near $M = 2M_\odot$, the time for the envelope to be swept away, if it is swept away, is well below the orbit circularization time.

Of course in order for this process to occur, the envelope must be lost in much less than the timescale over which the core grows by fusion. Otherwise the envelope will be replenished faster than it is lost. This timescale is given by[9]

$$\frac{dM_c}{dt} \sim \frac{L_i}{0.007c^2} \to \tau_f \sim \frac{0.007M_c c^2}{L_i} \sim 2.5\times 10^{14}\text{s}\left(\frac{M}{2}\right)^{-6}. \tag{10.11}$$

By comparison, the timescale τ_e is

$$\tau_e \sim 5\times 10^{15}\text{s}\left(\frac{M}{2}\right)^{11} L_p^{-1}(M+2)^{2/3}\mathcal{P}_6^{4/3}. \tag{10.12}$$

The timescale ratio is therefore

$$\frac{\tau_e}{\tau_f} = 50\left(\frac{M}{2}\right)^{17} L_p^{-1}(M+2)^{2/3}\left(\frac{\mathcal{P}_6}{2}\right)^{4/3}. \tag{10.13}$$

---

[7] P. C. Joss, S. Rappaport, and W. Lewis. "The core mass-radius relation for giants - A new test of stellar evolution theory". In: *The Astrophysical Journal* 319 (Aug. 1987), pp. 180–187. DOI: 10.1086/165443.

[8] Ibid.

[9] S. Refsdal and A. Weigert. "Shell Source Burning Stars with Highly Condensed Cores". In: *Astronomy and Astrophysics* 6 (July 1970), p. 426.

Define

$$c \equiv \log \frac{L_p}{50(M+2)^{2/3}} \tag{10.14}$$

and

$$d \equiv \log \frac{10^4 L_p}{(M+2)^{2/3}}. \tag{10.15}$$

In order for both timescale ratios to be less than unity, we need to have

$$\log \frac{M}{2} < \frac{21c + 3c}{170} \tag{10.16}$$

$$\frac{-61 \log \frac{M}{2} - 3d}{28} < \log \frac{\mathcal{P}_6}{2} < \frac{-33 \log \frac{M}{2} + 3c}{4}. \tag{10.17}$$

There generically exist solutions to these conditions. For instance, for $L_p = 50$, any mass up to $M \sim 2$ supports solutions, with the period converging to 17days. At $M = 1$, the supported periods range from 50days up to just under a century. Thus the relevant parameter space is not disallowed by these timescale considerations.

The one remaining condition which must be satisfied is that the requisite expansion actually be possible. For $M \sim 2$ and $\mathcal{P}_6 \sim 2$, the Roche radius is $\sim 30R_\odot$. Using a star tracking script included in Appendix B.2, the maximum post-expansion radius was computed for a variety of core and total masses. The ratio of this to $30R_\odot$ is shown in Figure 10.1 From this, we see that for cores above $M_c \sim 0.24M_\odot$, the envelope expands to several times the Roche radius, and hence either blows away or accretes onto the pulsar. In either case, the envelope is gone, and this may be achieved on a timescale shorter than both the circularization time and the fusion growth time.

This process for forming high eccentricity millisecond pulsar-white dwarf systems preserves the initial eccentricity of the system immediately post-accretion induced collapse. This mechanism predicts, as observed, that the pulsars in these systems should appear like typical recycled pulsars in terms of period and magnetic field, as the collapse need not be rotationally supported. It also predicts companion core masses which match the observed white dwarf masses well.

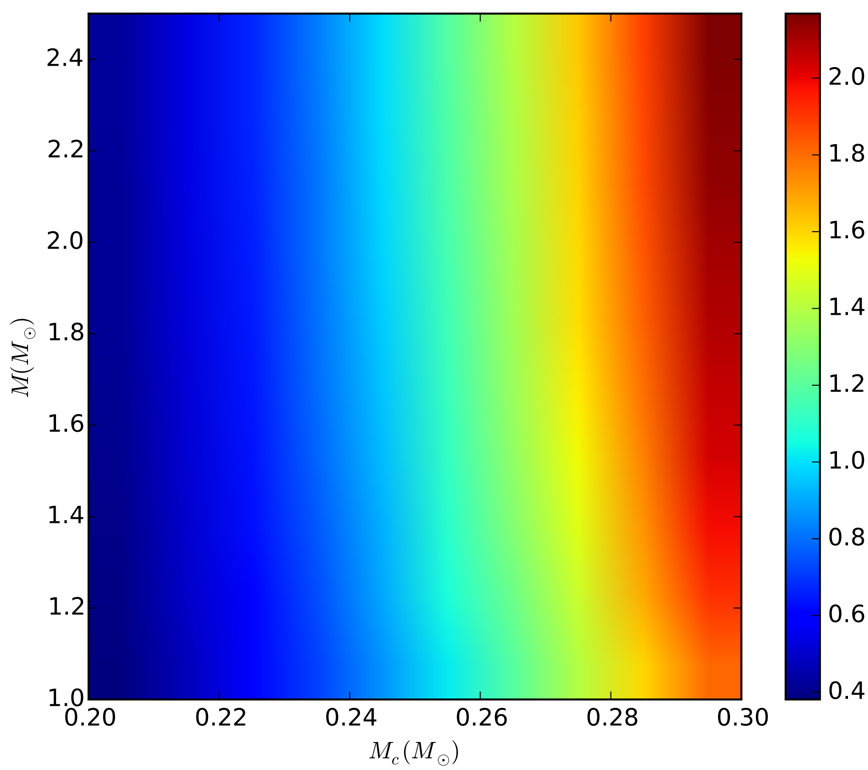

Figure 10.1: The vertical axis is $M/M_\odot$, the horizontal axis is $M_c/M_\odot$, with both axes log-scaled. The color represents the ratio $R_{\max}/30R_\odot$, the denominator being the approximate Roche radius for the period and mass range of interest, and the numerator being the post-expansion radius of the red giant of interest.

References

Freire, P. C. C. and T. M. Tauris. "Direct formation of millisecond pulsars from rotationally delayed accretion-induced collapse of massive white dwarfs". In: *Monthly Notices of the Royal Astronomical Society* 438 (Feb. 2014), pp. L86–L90. DOI: 10.1093/mnrasl/slt164. arXiv: 1311.3478 [astro-ph.SR] (cit. on p. 173).

Joss, P. C., S. Rappaport, and W. Lewis. "The core mass-radius relation for giants - A new test of stellar evolution theory". In: *The Astrophysical Journal* 319 (Aug. 1987), pp. 180–187. DOI: 10.1086/165443 (cit. on p. 175).

Kippenhahn, Rudolf, Alfred Weigert, and Achim Weiss. *Stellar Structure and Evolution*. Springer, 2012. ISBN: 978-3-642-30304-3 (cit. on p. 174).

Knispel, B. et al. "Einstein@Home Discovery of a PALFA Millisecond Pulsar in an Eccentric Binary Orbit". In: *ArXiv e-prints* (Apr. 2015). arXiv: 1504.03684 [astro-ph.HE] (cit. on p. 173).

Phinney, E. S. "Pulsars as Probes of Newtonian Dynamical Systems". In: *Royal Society of London Philosophical Transactions Series A* 341 (Oct. 1992), pp. 39–75. DOI: 10.1098/rsta.1992.0084 (cit. on pp. 173, 174).

Refsdal, S. and A. Weigert. "Shell Source Burning Stars with Highly Condensed Cores". In: *Astronomy and Astrophysics* 6 (July 1970), p. 426 (cit. on p. 175).

Tombrello, Thomas A. *Caltech Oral History*. Dec. 2012. URL: http://resolver.caltech.edu/CaltechOH:OH_Tombrello_T (cit. on p. 173).

11

Spotted Black Widows

The universe is asymmetric and I am persuaded that life, as it is known to us, is a direct result of the asymmetry of the universe or if its indirect consequences.

– Louis Pasteur, Comptes Rendus de l'Acadmie des Sciences

In this chapter we will examine the question of observable thermal anisotropy in pulsar companions. The methods developes here are also of potential interest for exoplanets[1] The objects under consideration will be either radiative or convective for $\Sigma < \Sigma_h$. We need not consider the in-between cases, as the transition in this region between the two modes is sharp, and as whichever mode holds near the base of this region will dominate the heat transfer. Except for at low mass, all stars considered will be on the main sequence. For the deep convective stars, we will consider both main sequence objects and brown dwarfs with negligible intrinsic luminosity.

Throughout this chapter all masses, luminosities, fluxes, and distances will be

[1] A. Roy, J. T. Wright, and S. Sigurð*sson*. "Earthshine on a Young Moon: Explaining the Lunar Farside Highlands". In: *The Astrophysical Journal* 788, L42 (June 2014), p. L42. DOI: 10.1088/2041-8205/788/2/L42. arXiv: 1406.2020 [astro-ph.EP]; V. Parmentier, A. P. Showman, and Y. Lian. "3D mixing in hot Jupiters atmospheres. I. Application to the day/night cold trap in HD 209458b". In: *Astronomy and Astrophysics* 558, A91 (Oct. 2013), A91. DOI: 10.1051/0004-6361/201321132. arXiv: 1301.4522 [astro-ph.EP]; B. Hansen et al. *Day and Night on Hot Jupiters.* Spitzer Proposal. June 2005; A. P. Showman, K. Menou, and J. Y.-K. Cho. "Atmospheric Circulation of Hot Jupiters: A Review of Current Understanding". In: *Extreme Solar Systems.* Ed. by D. Fischer et al. Vol. 398. Astronomical Society of the Pacific Conference Series. 2008, p. 419. arXiv: 0710.2930; T. Kataria et al. "The Atmospheric Circulation of the Hot Jupiter WASP-43b: Comparing Three-Dimensional Models to Spectrophotometric Data". In: *AAS/Division for Planetary Sciences Meeting Abstracts.* Vol. 46. AAS/Division for Planetary Sciences Meeting Abstracts. Nov. 2014, 104.03.

given in solar units. Speeds will be given in cm/s, temperatures in K, and times in seconds. Subscript notation will be used, as usual, to denote an exponent to divide out.

11.1 Setup

Recall from Chapter 7 that

$$\frac{\Delta F}{F_i} = \frac{F_e}{F_i} - 5y' T_4^{3/2} R^{-1} \left(\frac{\Delta T}{T}\right)^q \left(\frac{10^4 l}{2\pi R}\right)^a \mathrm{Ro}_s^b F_i^{-1}, \tag{11.1}$$

where the rightmost term is twice the flux transported by the wind. Once more Ro_s is the sonic Rossby number, l is the convective mixing length, F_e is the flux which impinges on the star averaged over the pulsar-facing (day) side, ΔF is the difference in the flux emerging from the day and night sides, F_i is the intrinsic flux, R is the companion radius, T_4 is the mean surface temperature measured in units of 10^4K, and a, b, q, and y' are dimensionless constants characteristic of the wind pattern of interest, to be determined self-consistently. Actually, as we learned in Chapter 8, this is not quite right on timescales shorter than the star's thermal timescale, as convection zones may absorb some of the external flux. Thus the relation really should be

$$\frac{\Delta F}{F_i} = \frac{F_e - F_{\mathrm{bottle}}}{F_i} - 5y' T_4^{3/2} R^{-1} \left(\frac{\Delta T}{T}\right)^q \left(\frac{10^4 l}{2\pi R}\right)^a \mathrm{Ro}_s^b F_i^{-1}, \tag{11.2}$$

where F_{bottle} is the bottled flux of the convection zone. We may solve this equation if we note that

$$T_4 = 0.3 \left(F_{\mathrm{day}}^{1/4} + F_{\mathrm{night}}^{1/4}\right) \tag{11.3}$$

and

$$\frac{\Delta T}{T} = 2 \frac{F_{\mathrm{day}}^{1/4} - F_{\mathrm{night}}^{1/4}}{F_{\mathrm{day}}^{1/4} + F_{\mathrm{day}}^{1/4}}. \tag{11.4}$$

Note that we do not simplify this last expression yet, as we may need to deal with flux anisotropies which push this relation outside of the linear regime. Further note that because we have been more careful than before in letting T be the average surface temperature, we do not need to deal with the case of supersonic winds: the formalism automatically precludes them. The day and night fluxes are related by

$$F_{\mathrm{day}} - F_{\mathrm{night}} = \Delta F, \tag{11.5}$$

$$F_{\mathrm{day}} + F_{\mathrm{night}} = F_e + 2F_i - F_{\mathrm{bottle}}, \tag{11.6}$$

As this quantity is uniquely determined by the flux carried by the wind, our equation is closed and may in principle be solved.

The first step to a solution is eliminating as many variables as possible. To that end, note that

$$\mathrm{Ro}_s = \frac{v_s}{2\pi R\Omega} \approx 0.012 T_4^{1/2} \mathcal{P}_4 R^{-1}, \tag{11.7}$$

$$\frac{10^4 l}{2\pi R} = \frac{10^4 v_s^2}{2\pi R g} \approx 2 T_4 R M^{-1}, \tag{11.8}$$

$$F_{\mathrm{day}} = F_i + \frac{1}{2}\left(F_e - F_{\mathrm{bottle}} + \Delta F\right), \tag{11.9}$$

$$F_{\mathrm{night}} = F_i + \frac{1}{2}\left(F_e - F_{\mathrm{bottle}} - \Delta F\right), \tag{11.10}$$

$$F_e = \frac{L_p}{2R_0^2}, \tag{11.11}$$

$$\frac{R_0^3}{\mathcal{P}_4^2} = M + 2, \tag{11.12}$$

where R_0 is the orbital radius and is as usual measured in solar units. Note that the final relation here is only a good approximation at low orbital eccentricity. At high eccentricity, it gives the approximate mean distance, the inverse square of which may deviate somewhat from the relevant mean inverse square distance. To order of magnitude, however, this should not matter significantly. Additionally, pulsar-companion systems are not generally expected or observed to have high eccentricities, so we will proceed with this approximation. Making use of these substitutions leaves as variables only F_{bottle}, ΔF, and the various dimensionless constants characteristic of the wind.

We now wish to compute the bottled flux in convective stars. For these objects there are two possibilities: either the flux reaching the convection zone exceeds the intrinsic flux, or it does not. If it does not exceed the intrinsic flux, then the fact that the non-irradiated $\nabla_{rad} \gg \nabla_{ad}$ implies that the star remains convective, and the resulting stiffness of ∇ in L implies that the star's surface temperature goes unchanged except over thermal timescales. As a result, when $F_e < F_i$, the full flux is bottled, giving $F_{\mathrm{bottle}} = F_e$.

In the opposing case, where $F_e > F_i$, the irradiated side of the star should become radiative, as ∇_{rad} becomes negative and hence trivially falls below the always-positive ∇_{ad}. This will once more bottle up heat and lead to swelling, but now some of the excess $F_e - F_i$ may escape, raising the surface temperature on the day side. This may then drive a wind, heating the night side. As discussed in Chapter 7, this wind leads to an increase in the area over which the star bottles heat, such that the bottled heat is

$$F_{\mathrm{bottle}} = \frac{A}{4\pi R^2} F_i. \tag{11.13}$$

The area fraction is given by

$$\frac{A}{4\pi R^2} = \min\left(1, \frac{1}{2}\left(1 + \frac{W}{F_i}\right)\right), \tag{11.14}$$

where W is the flux transported by the winds. This relation, which effectively states that the winds organize to maximize bottling, fundamentally results from the wind moving more easily through radiative zones than through convection zones. Putting all of this together, we see that

$$F_{\mathrm{bottle}} = \min\left(F_e, F_i \min\left(1, \frac{1}{2}\left(1 + \frac{W}{F_i}\right)\right)\right). \tag{11.15}$$

Now we have all relevant quantities except for the wind constants. These may be found in Table 6.1. As the convection zone always has a significantly higher viscosity than the radiation zone, the winds will always move around any residual convection zone. Thus we may focus on the radiative wind cases. There are mercifully only three of these: ballistic, hurricanes, and Rhines. The decision between the first two is made based on the Rossby number. This is a function of the flux anisotropy, of course, and so a solution must be found self-consistently. In cases where the criteria for Rhines scaling are satisfied and where the full area of the star is radiative, this model is used. We require that the full star be radiative for this because Rhines transport works by forming continuous bands around the star.

The driving turbulence in the Rhines case is the primarily horizontal turbulence that the wind itself produces. The condition we derived for this to occur is given by Eq. (6.106) as

$$T_4 > 100F\left(\frac{\Delta T}{T}\right)^2 \Sigma^{-1}\Omega_{-4}^{-1}, \tag{11.16}$$

where F is the mean flux over the surface of the star and column density is measured in units of Σ_h. This relation may also be written as

$$T_4 > 16F\left(\frac{\Delta T}{T}\right)^2 \Sigma^{-1}\mathcal{P}_4. \tag{11.17}$$

Recalling that T_4 here refers to the typical temperature for $\Sigma < \Sigma_h$, we may write $T_4 \sim 0.6F^{1/4}$. This yields

$$1 > 25F^{3/4}\left(\frac{\Delta T}{T}\right)^2 \Sigma^{-1}\mathcal{P}_4. \tag{11.18}$$

The best case scenario for this inequality is when $\Sigma = \Sigma_h$, which gives

$$1 > 25F^{3/4}\left(\frac{\Delta T}{T}\right)^2 \mathcal{P}_4. \tag{11.19}$$

Fortunately we don't need to consider the edge case where the inequality holds for some $\Sigma < \Sigma_h$ but not for all. This is because to leading order the majority of the heat is carried at larger Σ due to v_s and ρ being so much greater. Thus we will ignore the edge case, as the strong depth dependence of heat transport makes the transition between Rhines and non-Rhines transport sharp. Note that κ, the opacity, is required to compute y' for Rhines scaling. In the majority of the heating zone these stars are hot enough to fully ionize, so we may use the Kramer opacity[2]

$$\kappa_1 \sim 4 \times 10^{10}(1+X)(Z+10^{-3})\frac{\rho_0}{T_4^{3.5}}, \tag{11.20}$$

where κ_1 is the opacity measured in units of $10\text{cm}^2/\text{g}$ and where we will generally use $X \sim 1$ and $Z \sim 10^{-2}$. The full expression may be evaluated by making use of the relation

$$\rho = P/v_s^2 = \Sigma g/v_s^2. \tag{11.21}$$

11.2 Main Sequence Solutions

The equations described in the previous section are nonlinear and involve many cases. As a result, a numerical approach was used rather than an analytic one. The complete code used may be found in Appendix D. The space of possible systems was discretized in L_p, $\mathcal{P}$, and M. The discretization in L_p was done with the usual four values of $1, 10, 25, 50L_\odot$, with dense grids in the other quantities. This grid was then expanded to include as a dimension $\Delta F/F_i$. This dimension scales from 0 to F_e/F_i, with 0 prepended to an exponentially spaced grid.

The main sequence scaling laws were used to fill in R and L_i. The specific relations used were[3]

$$L_i = \begin{cases} 2^{4-3.6}M^{3.6} & \text{if } 2 < M < 20 \\ M^4 & \text{if } 0.43 < M < 2 \\ 0.43^{4-2.3}M^{2.3} & \text{if } 0.08 < M < 0.43 \end{cases} \tag{11.22}$$

[2]Bradley W. Carroll. *An Introduction to Modern Astrophysics*. Vol. 1. Addison-Wesley, 1996, p. 274.

[3]Maurizio Salaris and Cassisi Santi. *Evolution of stars and stellar populations*. Vol. 1. ISBN: 0-470-09220-3. John Wiley Sons, 2005, pp. 138–140; O. Demircan and G. Kahraman. "Stellar mass-luminosity and mass-radius relations". In: *Astrophysics and Space Science* 181 (July 1991), pp. 313–322. DOI: 10.1007/BF00639097.

and

$$R = \begin{cases} 2^{0.72-0.57} M^{0.57} & \text{if } 2 < M < 20 \\ M^{0.57} & \text{if } 0.08 < M < 2 \end{cases} \tag{11.23}$$

Masses from $0.08M_\odot$ to $20M_\odot$ were considered, with the lower end chosen due to its role in separating the main sequence from brown dwarfs[4]. Periods ranging from 3×10^3s up to 10^7s were considered. This range was chosen to capture all of the relevant physics after examining several different ranges.

At each point in the grid, the dominant kind of wind transport was computed, and from this the squared violation of the anisotropy relation. As the area fraction depends on W, and W depends on the area fraction through T, an iterative approach was used, treating the area fraction first as 0, computing W, then updating A, then updating W, and so on. This method converges in only a few iterations due to the small allowed range for A.

The wind calculations were handled carefully in these numerics. The number of cases was reduced by smoothly interpolating between ballistic and hurricane winds. This was done because these cases do not precisely match at their boundary as parametrized. The interpolation was done by letting each of a, b, q, and y' vary as $\tanh(\mathrm{Ro})^2$. The tanh function was chosen because an exponential variation is expected. This was squared because Ro depends on $v = |\boldsymbol{v}|$, and the physical constructions depending on a single vector are generally even rather than odd. Note that the Rossby number was computed as

$$\mathrm{Ro} = \frac{v}{2\pi R\Omega}. \tag{11.24}$$

Rhines scaling was examined at each grid point, but never produced self-consistent solutions. This is due to Rhines scaling being more prevalent at low $\mathcal{P}$, but being unable to carry the increased flux associated with the companion being closer to the pulsar.

Note that we must filter for companions with Roche radii exceeding their main sequence radii. This is done by noting that the Roche radius for such stars is[5]

$$R_b = \left(0.38 + 0.2\log\frac{M}{2}\right) R_0 = \left(0.38 + 0.2\log\frac{M}{2}\right)(M+2)^{1/3}\mathcal{P}_4^{2/3}. \tag{11.25}$$

[4] D. J. Stevenson. “The search for brown dwarfs”. In: *Annual Review of Astronomy and Astrophysics* 29 (1991), pp. 163–193. DOI: 10.1146/annurev.aa.29.090191.001115.

[5] B. Paczyński. “Evolutionary Processes in Close Binary Systems”. In: *Annual Review of Astronomy and Astrophysics* 9 (1971), p. 183. DOI: 10.1146/annurev.aa.09.090171.001151; P. P. Eggleton. “Approximations to the radii of Roche lobes”. In: *The Astrophysical Journal* 268 (May 1983), p. 368. DOI: 10.1086/160960.

Below the Roche cutoff we get into murky territory. Radiative stars, as well as some convective ones, are often catastrophically unstable in this regime. Should a case below the Roche cutoff be of interest, nothing precludes applying the methods described here below the cutoff.

Using all of these results, we may finally compute the anisotropy. Figure 11.1 shows the ratio $F_{\text{day}}/F_{\text{night}}$ over the mass and radius range of interest. This decreases as $\mathcal{P}$ increases, for this corresponds to the companion being placed further from the pulsar. It also increases as the pulsar luminosity increases, again in accordance with expectations. Similarly, as the companion mass increases, this ratio decreases. This is because the scaling relations indicate that F_i increases with M, for L_i increases faster than R^2. The maximum anisotropy is quite large, of order several hundred. This is because at low M, F_e may be thousands of times F_i, a difference which significantly exceeds the heat transport capacity of even a sonic wind.

At first glance, it appears that only low-period low-mass convective companions exhibit interesting anisotropy physics, with a small blip near $M = 2$. To dispel this notion, we turn to the quantity $\Delta F/F$, shown in Figure 11.2. In this plot, white regions above the Roche cutoff are those where $\Delta F = 0$ due to complete heat bottling. It is apparent that there are three distinct regions here. First, there is the convective regime on the left where not all of F_e is bottled. This corresponds to the significant anisotropy we saw in Figure 11.1. The size of this region depends on L_p as expected, as it is easier to have unbottled heat with higher values of F_e.

On the right there is the radiative regime where no heat is bottled. The anisotropy is small in this regime cases, peaking at a few percent, just at the edge of what can be observed. Note that the transition between the white region and the radiative one is shown as being infinitely sharp here. This is not quite accurate; there is an exponential transition as the convection zone disappears. This transition is coupled to the timescale of interest; as the convection zone disappears, the timescale over which heat bottling occurs drops, until in the radiative case it reaches the thermal timescale for the heating layer. As a result the precise smearing is not well defined, and the relevant physics is well represented by a sharp boundary.

The data presented thus far say little directly about the effect of winds. The relevant quantities here are the difference between the anisotropy with and without winds. To that end, Figure 11.3 shows the ratio $F_{\text{day}}/(F_i + F_e)$. This is what we expect observation to see. The ratio deviates most from unity near the bottling boundary. This is just a result of the bottled heat being a maximum possible fraction of $F_e + F_i$ at this boundary.

To examine the effect of the wind on the day side separately, we now consider the quantity $W/(F_i + F_e)$. This is shown for the day side in Figure 11.4. Here we

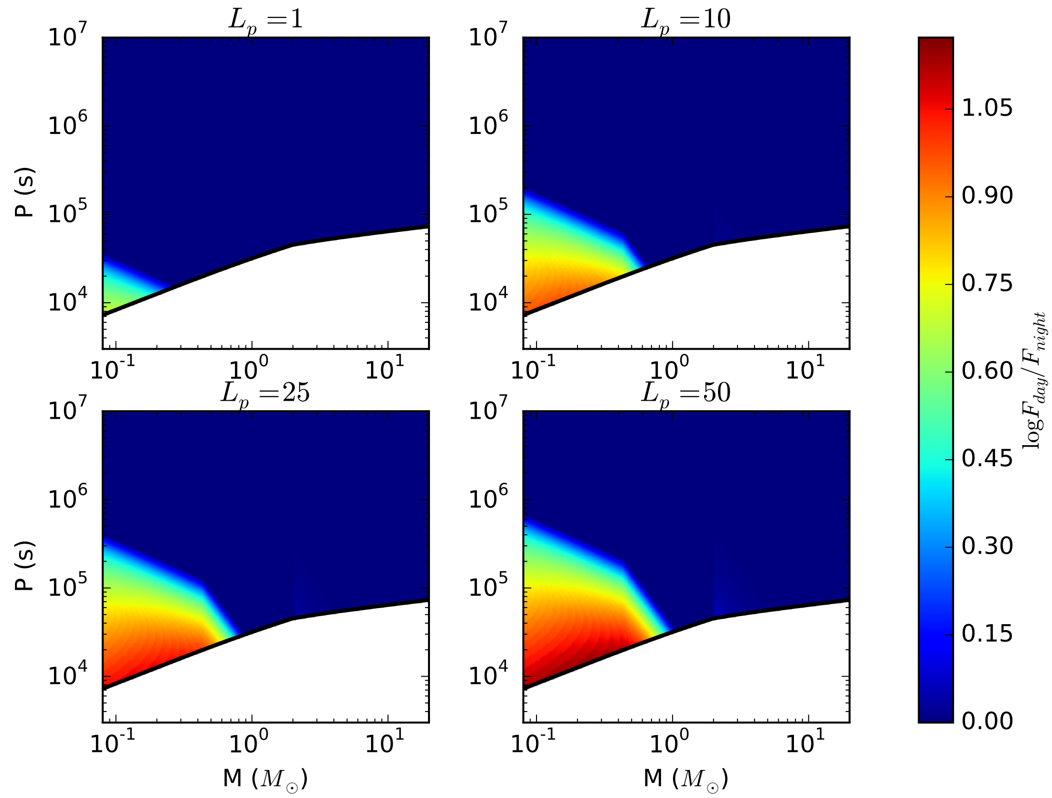

Figure 11.1: The vertical axis is $\mathcal{P}$ in seconds, the horizontal axis is the companion mass in solar masses, with both axes log-scaled. The color represents the log of the day/night flux ratio $\log F_{\rm day}/F_{\rm night}$. The four different plots correspond to four different pulsar luminosities. The black line corresponds to the Roche cutoff.

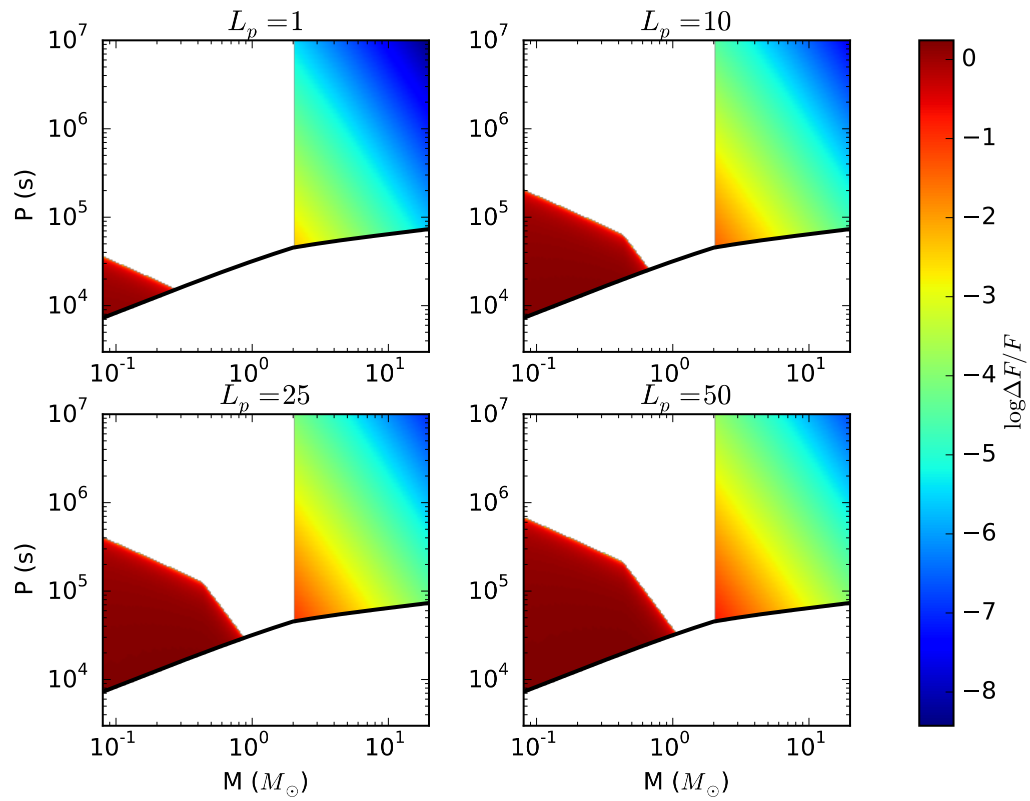

Figure 11.2: The vertical axis is $\mathcal{P}$ in seconds, the horizontal axis is the companion mass in solar masses, with both axes log-scaled. The color represents the log of the day/night flux ratio $\log \Delta F/F$. The four different plots correspond to four different pulsar luminosities. The black line corresponds to the Roche cutoff. The white regions above the Roche cutoff have $\Delta F = 0$ due to heat bottling.

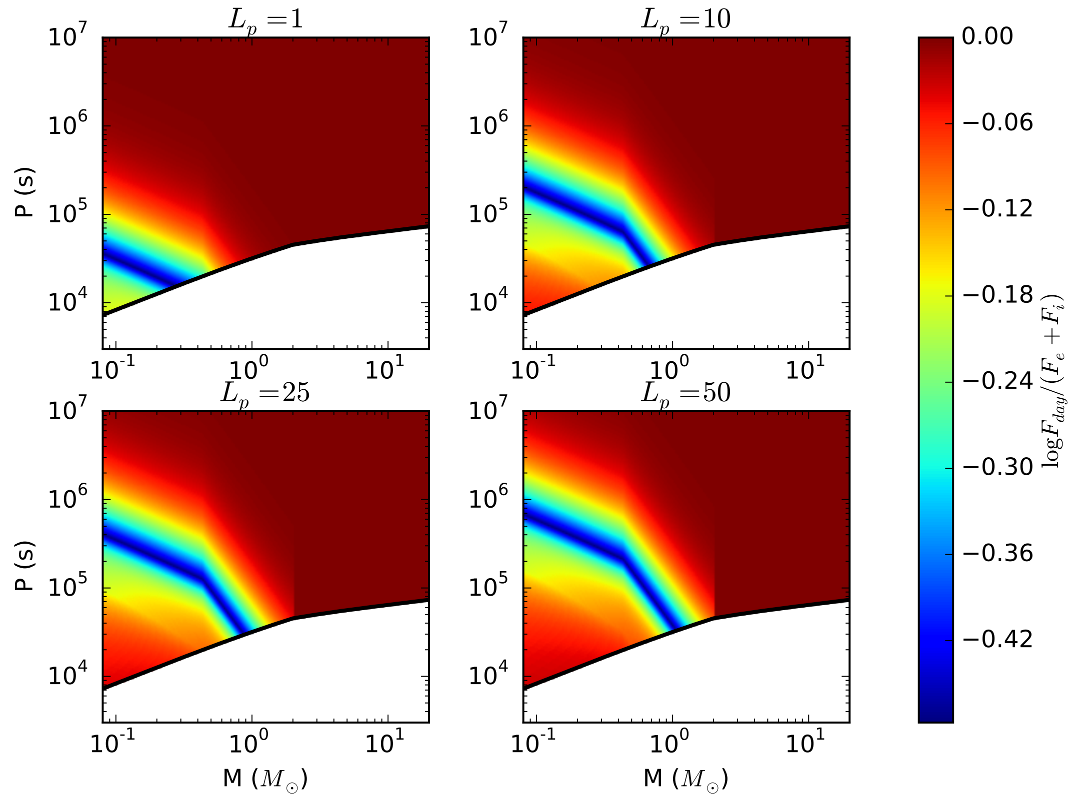

Figure 11.3: The vertical axis is $\mathcal{P}$ in seconds, the horizontal axis is the companion mass in solar masses, with both axes log-scaled. The color represents the log of the day/night flux ratio $\log F_{\rm day}/(F_i + F_e)$. The four different plots correspond to four different pulsar luminosities. The black line corresponds to the Roche cutoff.

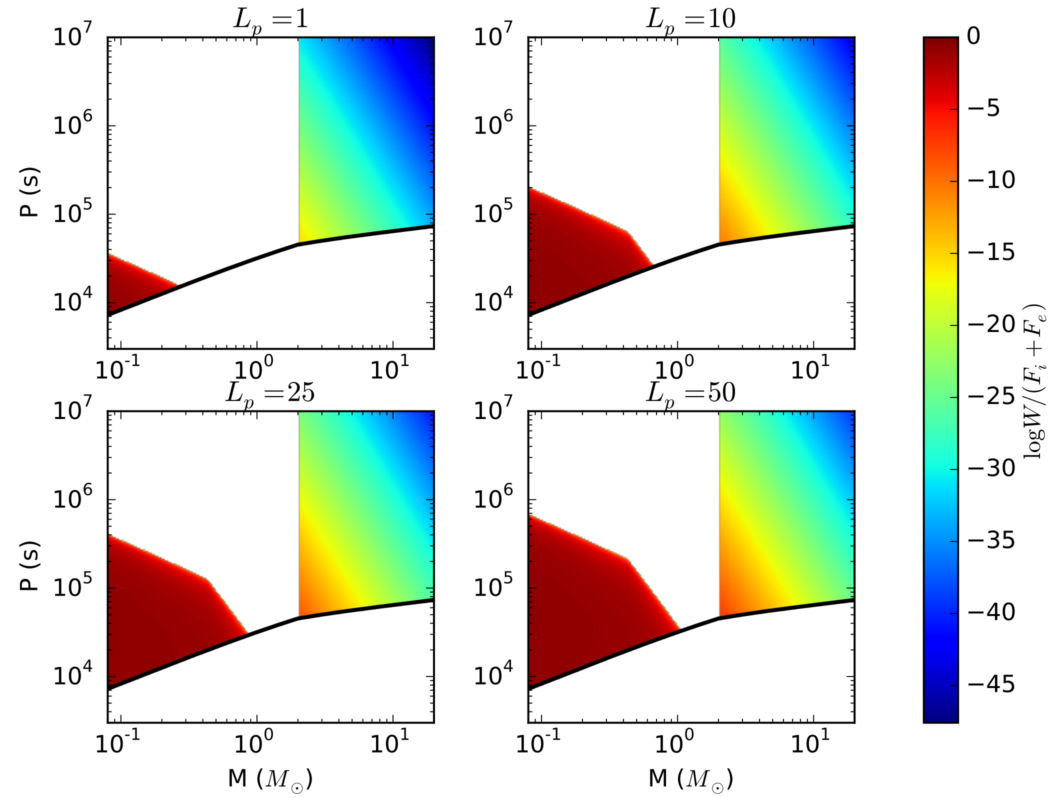

Figure 11.4: The vertical axis is $\mathcal{P}$ in seconds, the horizontal axis is the companion mass in solar masses, with both axes log-scaled. The color represents the log of the day/night flux ratio $\log W/(F_i + F_e)$. The four different plots correspond to four different pulsar luminosities. The black line corresponds to the Roche cutoff. Note that the white region above the Roche cutoff corresponds to the case $W = 0$

see that the winds transport up to $\sim 10\%$ of the flux. Except for the dimmest L_p considered, the transported fraction is not maximized when $\mathcal{P}$ is minimized as one might expect. This is because at low $\mathcal{P}$ the winds are solidly in the hurricane regime, where the transported flux goes as $\mathcal{P}^3$. Thus a balance between maximizing $\Delta F/F$ and maximizing $\mathcal{P}$ is struck. In the case of very low L_p, the optimum does actually occur at the minimum $\mathcal{P}$, but this is because the F_e curve is pushed down in $\mathcal{P}$ until it runs up against the Roche cutoff.

On the night side, the relevant ratio is F_{night}/F_i, as we need not worry about handling bottled flux in the denominator, and this is the directly observable quantity. This ratio is shown in Figure 11.5. Here we see that the winds make a tremendous difference, up to a factor of 30. Here we see the maximum impact made at the lowest $\mathcal{P}$ values. The difference between the day side and the night side in this regard is entirely that the night side's windless flux does not become greater as F_e increases, and so the function being maximized looks like $F_e\mathcal{P}^3(\Delta F/F)^q$ rather than $F_e\mathcal{P}^3(\Delta F/F)^q$.

If this analysis were done on the swollen stars discussed in the X-ray binary context, the key difference would be that R would not match the main sequence. This has the effect of pushing the radiative-convective boundary towards lower M, with the fully-swollen stars being radiative at all M. In that limit, the bottled flux vanishes and the swelling ceases. An interesting extension of this work would be to couple the code which computes swelling to the code which computes anisotropy to determine the difference that wind transport makes to the swelling timescale. This effect is unlikely to change the estimated order of magnitude of the swelling time, so we neglect it here.

11.3 Brown Dwarfs

Brown dwarfs typically have $10^{-2} < M < 0.08$ and so are not nuclear burning. This means that there is no mass-radius or mass-luminosity relation for brown dwarfs, as these properties are history-dependent. Importantly, if heating changes the upper atmospheric boundary condition, the core luminosity adjusts on the convective timescale of a few decades. This, combined with F_i generally being of order 10^{-3}, means that the core luminosity is not a relevant variable. Rather, we ought to view

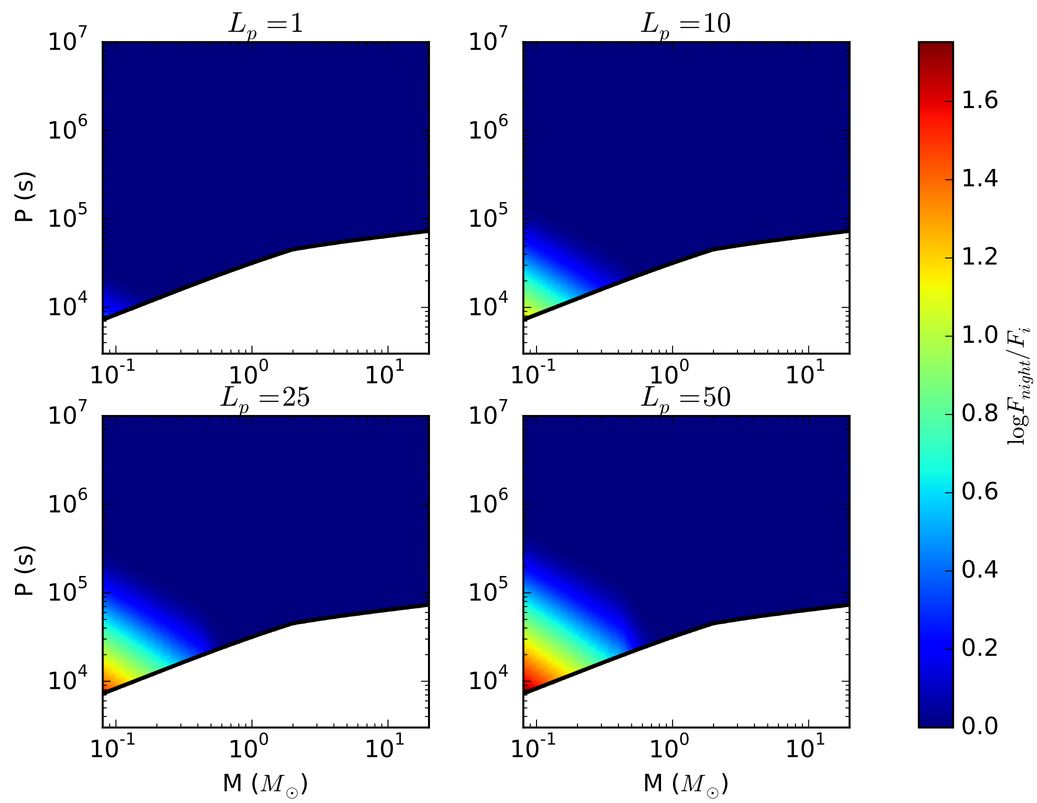

Figure 11.5: The vertical axis is $\mathcal{P}$ in seconds, the horizontal axis is the companion mass in solar masses, with both axes log-scaled. The color represents the log of the day/night flux ratio $\log F_{\mathrm{night}}/F_i$. The four different plots correspond to four different pulsar luminosities. The black line corresponds to the Roche cutoff.

the outer boundary conditions as being set by the illumination. To be quantitative,

$$F_{\text{day}} = F_i + \frac{1}{2}\left(F_e - F_{\text{bottle}} + \Delta F\right) = \frac{1}{2}(F_e + \Delta F), \tag{11.26}$$

$$F_{\text{night}} = F_i + \frac{1}{2}\left(F_e - F_{\text{bottle}} - \Delta F\right) = \frac{1}{2}(F_e - \Delta F). \tag{11.27}$$

Note that we have dropped F_{bottle}, as it is bounded above by F_i. The wind equation may now be written as

$$\Delta F = F_e - 5y' T_4^{3/2} R^{-1} \left(\frac{\Delta T}{T}\right)^q \left(\frac{10^4 l}{2\pi R}\right)^a \mathrm{Ro}_s^b. \tag{11.28}$$

Noting that

$$\mathrm{Ro}_s = \frac{v_s}{2\pi R \Omega} \approx 0.012 T_4^{1/2} \mathcal{P}_4 R^{-1}, \tag{11.29}$$

$$\frac{10^4 l}{2\pi R} = \frac{10^4 v_s^2}{2\pi R g} \approx 2 T_4 R M^{-1}, \tag{11.30}$$

$$\tag{11.31}$$

we find that

$$\Delta F = F_e - 5y' T_4^{3/2} R^{-1} \left(\frac{\Delta T}{T}\right)^q \left(2 T_4 R M^{-1}\right)^a \left(0.012 T_4^{1/2} \mathcal{P}_4 R^{-1}\right)^b. \tag{11.32}$$

This may also be written as

$$F_{\text{day}} = 0.4 y' \left(F_{\text{day}}^{1/4} + F_{\text{night}}^{1/4}\right) R^{-1} \left(2 \frac{F_{\text{day}}^{1/4} - F_{\text{night}}^{1/4}}{F_{\text{day}}^{1/4} + F_{\text{day}}^{1/4}}\right)^q \left(2 T_4 R M^{-1}\right)^a \left(0.012 T_4^{1/2} \mathcal{P}_4 R^{-1}\right)^b. \tag{11.33}$$

If we assume that hurricanes are the dominant transport mechanism, then

$$\Delta F = F_e - \frac{5 T_4^3 \mathcal{P}_4^3}{10^6 R^4} \left(\frac{\Delta T}{T}\right)^5. \tag{11.34}$$

Now note that

$$T_4 \sim 0.6 \left(\frac{F_e}{2}\right)^{1/4}. \tag{11.35}$$

This is true to within 40% in the $F_i \to 0$ limit regardless of ΔF. Thus

$$\Delta F = F_e - \frac{2.5 F_e^{3/4} \mathcal{P}_4^3}{10^6 R^4} \left(\frac{\Delta T}{T}\right)^5 = F_e \left(1 - \frac{4 \mathcal{P}_4^{10/3}}{10^6 L_p^{1/4} R^4} \left(\frac{\Delta T}{T}\right)^5\right). \tag{11.36}$$

This may also be written as

$$\frac{\Delta F}{F_e} = 1 - \chi \left(\frac{\Delta T}{T}\right)^5, \tag{11.37}$$

where

$$\chi = \frac{4\mathcal{P}_4^{10/3}}{10^6 L_p^{1/4} R^4} = \frac{\mathcal{P}_4^{10/3}}{25 L_p^{1/4} R_{-1}^4}. \tag{11.38}$$

There is now only one relevant parameter, χ. The solutions for $\Delta F/F_e$ and $F_{\mathrm{day}}/F_{\mathrm{night}}$ as functions of χ are shown in Figure 11.6. Low values of χ, corresponding to short orbital periods and bright pulsars, exhibit unbounded anisotropies. As χ increases past unity, the anisotropy drops rapidly. Noting that R_{-1} is close to the smallest radius a brown dwarf can achieve[6], we see that for the pulsar luminosities of interest the small-χ regime is characterized by $\mathcal{P} < 3 \times 10^4$s.

It is worth noting that in all cases, the wind speed is comparable to the sound speed, for $\Delta T/T$ is of order unity for these objects so long as $F_e \gg F_i$. As a result, the Rossby number is just the sonic Rossby number to good approximation. This may be written as

$$\mathrm{Ro}_s \sim \frac{L_p}{40 R_{-1} \mathcal{P}_4^{1/3}}. \tag{11.39}$$

Thus the hurricane model holds down to periods of

$$\mathcal{P} \sim 150 \left(\frac{L_p}{10}\right)^3 \mathrm{s}. \tag{11.40}$$

Given that these objects cannot have periods much less than 3×10^3s, we expect any regions where the Rossby number exceeds unity to be small enough that extrapolation from the hurricane regime is appropriate. Note that the condition for Rhines scaling reduces in this case to

$$4 > 25 L_p^{3/4} \left(\frac{\Delta T}{T}\right)^2. \tag{11.41}$$

This is unlikely to be satisfied, given that $\Delta T \sim T$.

In summary, we have computed the anisotropy of flux between the pulsar-facing (day) and night side of both main sequence and brown dwarf stars. These results

[6] Adam Burrows et al. “The theory of brown dwarfs and extrasolar giant planets”. In: *Rev. Mod. Phys.* 73 (3 Sept. 2001), pp. 719–765. DOI: `10.1103/RevModPhys.73.719`. eprint: `http://arxiv.org/pdf/astro-ph/0607583`. URL: `http://link.aps.org/doi/10.1103/RevModPhys.73.719`; Stevenson, op. cit.

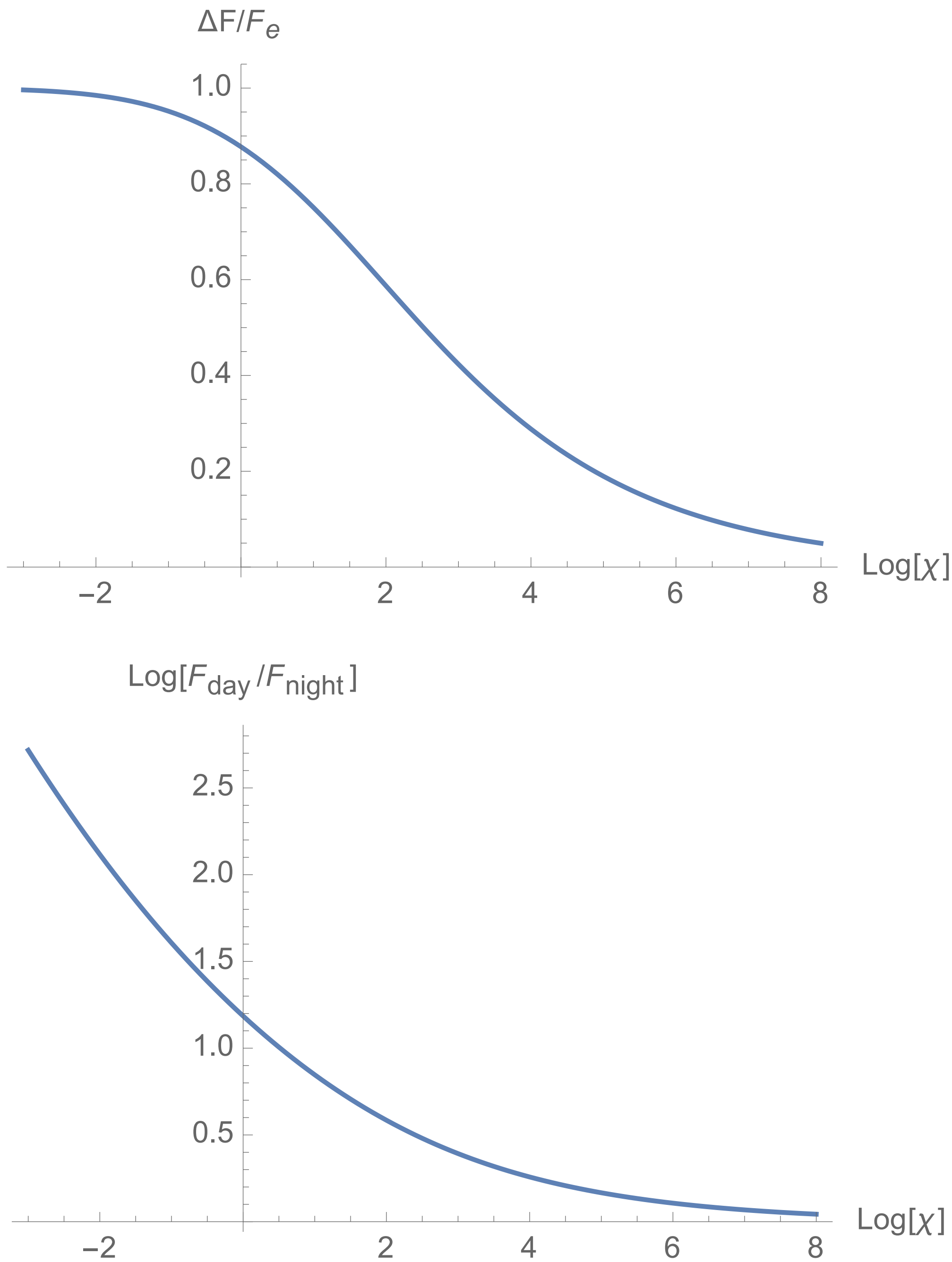

Figure 11.6: Top: $\Delta F/F_e$ is shown as a function of $\log \chi$. Bottom: $\log F_{\rm day}/F_{\rm night}$ is shown as a function of $\log \chi$.

deviate substantially in many cases from the usual predicted black body values. This is a result of our use of a realistic wind transport model. It is worth noting that these results depend on the flux of high energy particles L_p, as well as on their energy, which determines the absorption column density. The former we have carried around as an explicit functional dependence, while the latter we have set to a specific value. These calculations may be redone at any Σ, however. To leading order, the wind flux goes as $\Sigma^{1+3\nabla/2}$, with the dependence on ∇ arising from averaging $T^{3/2} \sim v_s^3$ over the heating depth. As the dependence on L_p is distinct from the dependence on Σ, a series of observations of different systems may reveal Σ, so long as any interdependence between the total power output of the pulsar and the individual particle energies is known. This model, therefore, allows us to place an additional constraint on the pulsar wind, but does not on its own tell us everything that there is to know.

References

Burrows, Adam et al. "The theory of brown dwarfs and extrasolar giant planets". In: *Rev. Mod. Phys.* 73 (3 Sept. 2001), pp. 719–765. DOI: 10.1103/RevModPhys.73.719. eprint: http://arxiv.org/pdf/astro-ph/0607583. URL: http://link.aps.org/doi/10.1103/RevModPhys.73.719 (cit. on p. 193).

Carroll, Bradley W. *An Introduction to Modern Astrophysics*. Vol. 1. Addison-Wesley, 1996, p. 274 (cit. on p. 183).

Demircan, O. and G. Kahraman. "Stellar mass-luminosity and mass-radius relations". In: *Astrophysics and Space Science* 181 (July 1991), pp. 313–322. DOI: 10.1007/BF00639097 (cit. on p. 183).

Eggleton, P. P. "Approximations to the radii of Roche lobes". In: *The Astrophysical Journal* 268 (May 1983), p. 368. DOI: 10.1086/160960 (cit. on p. 184).

Hansen, B. et al. *Day and Night on Hot Jupiters*. Spitzer Proposal. June 2005 (cit. on p. 179).

Kataria, T. et al. "The Atmospheric Circulation of the Hot Jupiter WASP-43b: Comparing Three-Dimensional Models to Spectrophotometric Data". In: *AAS/Division for Planetary Sciences Meeting Abstracts*. Vol. 46. AAS/Division for Planetary Sciences Meeting Abstracts. Nov. 2014, 104.03 (cit. on p. 179).

Paczyński, B. "Evolutionary Processes in Close Binary Systems". In: *Annual Review of Astronomy and Astrophysics* 9 (1971), p. 183. DOI: 10.1146/annurev.aa.09.090171.001151 (cit. on p. 184).

Parmentier, V., A. P. Showman, and Y. Lian. "3D mixing in hot Jupiters atmospheres. I. Application to the day/night cold trap in HD 209458b". In: *Astronomy and Astrophysics* 558, A91 (Oct. 2013), A91. DOI: 10.1051/0004-6361/201321132. arXiv: 1301.4522 [astro-ph.EP] (cit. on p. 179).

Roy, A., J. T. Wright, and S. Sigurð*sson*. "Earthshine on a Young Moon: Explaining the Lunar Farside Highlands". In: *The Astrophysical Journal* 788, L42 (June 2014), p. L42. DOI: 10.1088/2041-8205/788/2/L42. arXiv: 1406.2020 [astro-ph.EP] (cit. on p. 179).

Salaris, Maurizio and Cassisi Santi. *Evolution of stars and stellar populations*. Vol. 1. ISBN: 0-470-09220-3. John Wiley Sons, 2005, pp. 138–140 (cit. on p. 183).

Showman, A. P., K. Menou, and J. Y.-K. Cho. "Atmospheric Circulation of Hot Jupiters: A Review of Current Understanding". In: *Extreme Solar Systems*. Ed. by D. Fischer et al. Vol. 398. Astronomical Society of the Pacific Conference Series. 2008, p. 419. arXiv: 0710.2930 (cit. on p. 179).

Stevenson, D. J. “The search for brown dwarfs”. In: *Annual Review of Astronomy and Astrophysics* 29 (1991), pp. 163–193. DOI: `10.1146/annurev.aa.29.090191.001115` (cit. on pp. 184, 193).

12

Banded Stars

The goal of this chapter is to examine the case where spontaneous atmospheric banding occurs in an axisymmetric star. This effect has been seen in limited circumstances in simulations[1], though analytic understanding has proven elusive. Though this does not relate to the question of pulsar-companion interactions, the possibility is suggested by our analysis in Chapter 6.

To begin, we are interested in lone stars which are axisymmetric and do not experience external heating. Recall that

$$k_{fr} = \sqrt{\frac{\Omega}{Rv_\phi}} = \sqrt{\frac{1}{Rl}}, \tag{12.1}$$

$$k_\beta = \left(\frac{\Omega^3}{R^3\varepsilon}\right)^{1/5} = \left(\frac{\Omega^3}{R^3 v_\phi^2 \tilde{N}}\right)^{1/5} = \left(\frac{\Omega}{R^3 l v_{cr}}\right)^{1/5}. \tag{12.2}$$

The criterion for the Rhines cascade to be in effect is that $k_\beta > k_{fr}$, so

$$\frac{1}{R^5 l^5} < \frac{\Omega^2}{R^6 l^2 v_{cr}^2} \tag{12.3}$$

$$\therefore \frac{v_{cr}^2}{l^3} < \frac{\Omega^2}{R}. \tag{12.4}$$

[1] U. R. Christensen. “Zonal flow driven by strongly supercritical convection in rotating spherical shells”. In: *Journal of Fluid Mechanics* 470 (Nov. 2002), pp. 115–133. DOI: 10.1017/S0022112002002008.

The critical Ω at which the star cannot hold itself together is $\Omega_{crit} \approx \sqrt{g/R}$. Thus

$$\frac{v_{cr}^2}{l^3} < \left(\frac{\Omega}{\Omega_{crit}}\right)^2 \frac{g}{R^2} \tag{12.5}$$

$$\therefore \frac{F^{2/3}}{\rho^{2/3} l^3} < \left(\frac{\Omega}{\Omega_{crit}}\right)^2 \frac{g}{R^2}. \tag{12.6}$$

$$\tag{12.7}$$

The rotation rate is often close to criticality for stars of mass outside the range $[0.5, 2.0]M_\odot$. This is because stars below this range do not have substantial winds with which to spin down, while those above it lack the convectively-driven magnetic field needed to exert a substantial torque[2]. Letting $\Omega = \Omega_{crit}$ then yields

$$F^2 \rho^{-2} l^{-9} R^6 g^{-3} < 1. \tag{12.8}$$

This may also be written ass

$$\frac{F^2 (GM)^6}{R^6 P^4 C} < 1, \tag{12.9}$$

where T_s is the surface temperature and $C \equiv P^5 \rho^{-7}$ is the constant determining the polytrope of interest. We may estimate this using the central density and pressure. The central density is roughly twice the average, and the central pressure is roughly[3]

$$P_c \sim 2\rho_{avg} g_{avg} R = 2\frac{3M}{4\pi R^3}\left(\frac{GM}{R^2}\right) R = \frac{3GM^2}{2\pi R^4}. \tag{12.10}$$

Thus

$$C = P^5 \rho^{-7} = \left(\frac{2\pi R^3}{3M}\right)^7 \left(\frac{3GM^2}{2\pi R^4}\right)^5 = \frac{4\pi^2}{9} G^5 M^3 R. \tag{12.11}$$

Using this, our condition becomes

$$\frac{9F^2 G M^3}{4\pi^2 P^4 R^7} < 1, \tag{12.12}$$

or

$$P > 2 \times 10^9 F^{1/2} M^{3/4} R^{-7/4}, \tag{12.13}$$

---

[2] J. B. Stauffer and L. W. Hartmann. "The rotational velocities of low-mass stars". In: *Astronomical Society of the Pacific, Publications* 98 (Dec. 1986), pp. 1233–1251. DOI: `10.1086/131926`.

[3] E. Böhm-Vitense. *Introduction to Stellar Astrophysics.* Vol. 3. ISBN 0521344042. Cambridge University Press, 1992.

where P is measured in erg/cm^3 and the remaining quantities are all in solar units. Given the scaling of the quantities on the right, we expect most objects exhibiting spontaneous banding near the surface to be low-mass stars. Using the scaling relations for mass and luminosity for this sort of object as well as the fact that $M \propto R$ for $M < M_\odot$ we find[4]

$$P > 3 \times 10^8 M^{-0.85}. \tag{12.14}$$

This may be phrased in terms of Σ in the thin-envelope limit as

$$\Sigma > 10^4 M^{0.15}. \tag{12.15}$$

Note that in this derivation we have assumed that the object remains nuclear burning. From this it is clear that convection alone can drive a banded structure. The number of bands is expected to be

$$n = Rk_\beta = \left(\frac{\Omega R^2}{l v_c}\right)^{1/5}. \tag{12.16}$$

In the low mass stars which exhibit these properties, $\Omega \sim 10^{-4}\mathrm{s}^{-1}$, $v_c \sim 10^4$cm/s, $l \sim 10^8$cm, and $R \sim 10^{10}$cm, so $n \sim 10$.

As a result of all of this, our first prediction regarding these stars is that they will be banded, and that the depth of the bands will be roughly 3×10^3g/cm^2. The number of bands ought to be on the order of 10. In many cases this is close enough to the photosphere that the structure may reasonably be expected to be observable. While it will be difficult to observe this structure using doppler spread measurements, the case is somewhat better if there is a transiting planet. As the planet blocks a different portion of the star at different times, and may be tracked across the star, the *change* in the doppler spread over the course of the transit may be used to determine the presence of bands.

In addition, for Jupiter-type planets the bands will be much more easily visible. With $F \sim 10^{-6} F_\odot$, $M \sim 10^{-3} M_\odot$, and $R \sim 10^{-1} R_\odot$, the lower bound on Σ is just 250g/cm^2. At and near optical frequencies this is well above the photosphere, and so should be observable. The expected number of bands for a cold Jupiter is similar to what we expect for stars[5]. The precise number may be computed via Eq. (12.16). For hot Jupiters, the temperature anisotropy dominates over the spontaneous banding

[4] Maurizio Salaris and Cassisi Santi. *Evolution of stars and stellar populations*. Vol. 1. ISBN: 0-470-09220-3. John Wiley Sons, 2005, pp. 138–140.

[5] Roughly half of the driving force for Jupiter's bands comes from its temperature asymmetry. The remainder comes from convective anisotropy. Thus these objects should have a similar number of bands to Jupiter, with somewhat faster rotation but no temperature anisotropy

effect. Once more transiting objects such as moons provide an easier test than just measuring the doppler spread.

References

Böhm-Vitense, E. *Introduction to Stellar Astrophysics*. Vol. 3. ISBN 0521344042. Cambridge University Press, 1992 (cit. on p. 199).

Christensen, U. R. "Zonal flow driven by strongly supercritical convection in rotating spherical shells". In: *Journal of Fluid Mechanics* 470 (Nov. 2002), pp. 115–133. DOI: 10.1017/S0022112002002008 (cit. on p. 198).

Salaris, Maurizio and Cassisi Santi. *Evolution of stars and stellar populations*. Vol. 1. ISBN: 0-470-09220-3. John Wiley Sons, 2005, pp. 138–140 (cit. on p. 200).

Stauffer, J. B. and L. W. Hartmann. "The rotational velocities of low-mass stars". In: *Astronomical Society of the Pacific, Publications* 98 (Dec. 1986), pp. 1233–1251. DOI: 10.1086/131926 (cit. on p. 199).

Appendices

Appendix A

Viscosity Code

The code used to interpolate the viscosity of a star is shown below. It makes use of tabulated data[1] as well as analytic results[2], choosing between them based on the range of validity of each. Within the range of the tabular data, multilinear interpolation in temperature and log-pressure space is used. Above the maximum temperature covered by this table, which roughly aligns with the bottom edge of validity of the analytic results, the analytic results are used. There are regions at low temperature and very high pressure where neither result is valid, and in these the code returns the IEEE NaN value. Note that this code requires Python, NumPy, and SciPy, and was tested with versions 2.7, 1.9.0, and 0.14.0 respectively.

Viscosity Interpolation Code: viscosity.py

```
import numpy as np
import constants
from scipy.interpolate import RegularGridInterpolator

naan = float('nan')

values = np.array([
    34.1, 34.1, 34.1, 34.1, 34.1, 34.1, 34.1, 34.1, naan, naan, naan, naan,
    38.1, 38.1, 38.1, 38.1, 38.1, 38.1, 38.1, 38.1, naan, naan, naan, naan,
    43.5, 43.5, 43.5, 43.5, 43.5, 43.5, 43.5, 43.5, 43.5, naan, naan, naan,
    51.5, 51.5, 51.5, 51.5, 51.5, 51.5, 51.5, 51.5, 51.5, naan, naan, naan,
    52.7, 62.6, 62.0, 63.2, 63.2, 63.2, 63.2, 63.2, 63.2, naan, naan, naan,
    12.5, 16.2, 22.4, 31.3, 44.5, 56.4, 66.3, 82.2, 82.5, naan, naan, naan,
    3.98, 7.61, 12.2, 15.9, 18.6, 23.6, 32.1, 61.2, 85.8, naan, naan, naan,
    2.84, 3.05, 3.26, 3.56, 4.83, 9.67, 21.5, 27.8, 61.3, 97.1, 117, naan,
    4.74, 6.31, 6.80, 7.29, 7.87, 8.46, 9.24, 13.3, 29.1, 79.6, 109, 159,
    9.76, 10.3, 10.9, 11.6, 12.5, 14.1, 17.3, 26.7, 33.0, 46.1, 100, 163,
    22.0, 23.2, 24.4, 25.8, 27.4, 28.6, 30.7, 37.5, 52.6, 86.6, 119, 185,
    47.9, 50.8, 53.3, 56.1, 59.7, 63.3, 67.3, 77.4, 91.2, 112, 198, 284
])  # dynamic viscosity

theta = np.array(
    [1.4, 1.2, 1.0, 0.8, 0.6, 0.4, 0.3, 0.2, 0.15, 0.1, 0.07, 0.05])
ts = 5040. / theta
tmax = max(ts)
logp = np.array([3, 3.5, 4, 4.5, 5, 5.5, 6, 7, 8, 9, 10, 11])
```

[1]F. N. Edmonds Jr. "The Coefficients of Viscosity and Thermal Conductivity in the Hydrogen Convection Zone." In: *The Astrophysical Journal* 125 (Mar. 1957), p. 535. DOI: 10.1086/146327.

[2]Daniel Kagan and J. Craig Wheeler. "The Role of the Magnetorotational Instability in the Sun". In: *The Astrophysical Journal* 787.1 (2014), p. 21. URL: http://stacks.iop.org/0004-637X/787/i=1/a=21.

```
interp = RegularGridInterpolator((ts,logp),np.reshape(values,(12,12)),bounds_error=False,
    fill_value=np.nan)

def interpolate(t, p, rho):
    return 1e-5*interp(np.transpose([t,np.log10(p)]))/rho

def loglam(t, rho):
    d0 = -17.4 + 1.5 * np.log(t) - 0.5 * np.log(rho)
    d1 = -12.7 + np.log(t) - 0.5 * np.log(rho)
    boolarr = 1.0 * (t < 1.1e5 * np.ones(t.shape))
    return d0 * boolarr + d1 * (1 - boolarr)


def spitzer(t, rho):
    return 5.2e-15 * np.power(t, 5. / 2) / (rho * loglam(t, rho))

def overall(t, p, rho, kappa,anis=1):
    t = np.array(t)
    p = np.array(p)
    rho = np.array(rho)
    # First, produce nu from actual data
    d0 = interpolate(t, p, rho)
    # Next, compute Spitzer values
    d1 = spitzer(t, rho)
    # Replace Spitzer values with NaN if they aren't above the ionization zone
    d1[t<10**4.1] = np.nan
    # Replace data values with Spitzer values if they are NaN
    d0[np.isnan(d0)] = d1[np.isnan(d0)]
    d0*=anis
    return d0

q = 4.80320451e-10
c = 29979245800.
def isotropicB(t,p,rho,mu):
    nu = overall(t,p,rho)
    return 3*p*mu*c/(rho*q*nu)
```

References

Edmonds Jr., F. N. "The Coefficients of Viscosity and Thermal Conductivity in the Hydrogen Convection Zone." In: *The Astrophysical Journal* 125 (Mar. 1957), p. 535. DOI: `10.1086/146327` (cit. on p. 204).

Kagan, Daniel and J. Craig Wheeler. "The Role of the Magnetorotational Instability in the Sun". In: *The Astrophysical Journal* 787.1 (2014), p. 21. URL: `http://stacks.iop.org/0004-637X/787/i=1/a=21` (cit. on p. 204).

Appendix B

Acorn Stellar Integration Code

B.1 Opal and Ferguson Opacity Table Parser

To support the Acorn stellar integration code, modern tables of the Rosseland mean opacity were needed over a wide range of temperatures and densities. In particular, at low temperatures molecular effects become significant, something opacity tables have historically lacked. For this purpose, an interpolation routine was written which uses the OPAL[1] and Ferguson[2] opacity tables. The former is good at high temperature, the latter at low temperature. The OPAL Type 1 and Ferguson 05 tables were used with the GS98 solar composition for this purpose, though other choices are also valid. The code used in this routine is shown below, along with an example of its usage. Note that interpolation proceeds first over stellar composition (X and Y) and then over $\log T$ and the factor $\log R$, defined as $\log\rho - 3\log T_6$, where ρ is in cgs units and T_6 is defined as the temperature measured in units of $10^6 K$. When R exceeds the maximum tabulated R, the maximum tabulated R is used instead. This was found to not matter in most cases, as it only occurred well within highly efficient convection regions where the opacity is largely irrelevant. Multilinear interpolation is used at each step, and the output is the logarithm of the opacity. Note that this code requires Python, NumPy, and SciPy, and was tested with versions 2.7, 1.9.0, and 0.14.0 respectively.

Opacity Interface (opacity.py)

```python
import scipy.interpolate as sin
import numpy as np
import os

def interp(data, x0, y0):
    # Now we're going to assume that rRange and tRange are the same across all tables.
    # First, interpolate the 2D R vs. T grid across the X,Y values of interest.
    x = [i[0] for i in data]
    y = [i[1] for i in data]
    z = [i[4] for i in data]
    table = sin.griddata((x, y), z, (x0, y0))
    return table

def bilinear_interpolator(data,xPts,yPts):
```

[1] C. A. Iglesias and F. J. Rogers. "Updated Opal Opacities". In: *The Astrophysical Journal* 464 (June 1996), p. 943. DOI: 10.1086/177381.

[2] Jason W. Ferguson et al. "Low-Temperature Opacities". In: *The Astrophysical Journal* 623.1 (2005), p. 585. URL: http://stacks.iop.org/0004-637X/623/i=1/a=585.

```
    return sin.RegularGridInterpolator((xPts,yPts),data,bounds_error=False,fill_value=np.nan)

class opac:

    def __init__(self, opalName, fergName, x, y):
        self.a = opacInt(opalName, x, y, "opal")
        self.b = opacInt(fergName, x, y, "ferg")

    def opacity(self, t, rho):
        if not isinstance(t, np.ndarray):
            op = self.b.opacity(t,rho)[0,0]
            if np.isnan(op):
                op = self.a.opacity(t,rho)[0,0]
        else:
            op = self.b.opacity(t,rho)
            whereNan = np.where(np.isnan(op))
            op[whereNan] = self.a.opacity(t[whereNan[0]],rho[whereNan[1]])
        return op

    def dkdT(self,t,rho,eps=1e-3):
        k0 = 10**self.opacity(t*(1-eps),rho)
        k1 = 10**self.opacity(t*(1+eps),rho)
        return (k1-k0)/(2*t*eps)

    def dkdRho(self,t,rho,eps=1e-3):
        k0 = 10**self.opacity(t,rho*(1-eps))
        k1 = 10**self.opacity(t,rho*(1+eps))
        return (k1-k0)/(2*rho*eps)


class opacInt:

    def __init__(self, fname, x, y,opalFerg):
        self.cutoff = 0
        self.data = None
        if opalFerg=="opal":
            self.cutoff = 10
            self.data = readOpalTables(fname)
        elif opalFerg=="ferg":
            self.cutoff = 12
            self.data = readFergTables(fname)
        else:
            raise Exception("No table type specified.")
        self.interpData = interp(self.data, x, y)
        self.interpolator = bilinear_interpolator(self.interpData,self.data[0][3],self.data[0][2])

    def opacityTR(self,t,r):
        tt = np.copy(t)
        tt[tt<600] = 600.
        tt = np.log10(tt)
        r = np.log10(r)
        r = np.array(r)
        r[r>1] = 0.99
        k = self.interpolator(np.dstack((tt,r)))
        k[np.isnan(k)] = 2*self.cutoff
```

```
        k[k>self.cutoff] = np.nan # Each table has a maximum value, so this cuts off interpolation there
        return k

    def opacity(self, t, rho):
        r = rho / (t * 1e-6) ** 3
        return self.opacityTR(t, r)

# Method for reading in non-enriched OPAL tables (i.e. just X,Y,Z are
# nonzero, no dXc or dXo). Tested on latest (as of August 2014)
# GS98 composition tables.


def readOpalTables(fname):
    f = open(fname)
    # checks if we're in the zone where the tables are (as opposed to the
    # header)
    tables = False
    x = 0
    y = 0  # note that z = 1-x-y by definition
    data = []
    for line in f:
        line = line.rstrip('\n')  # remove newlines
        if tables and len(line) > 2:  # eliminates empty lines
            if 'TABLE' in line:  # reads in x,y,z for the table
                s = line.replace('=', '␣').split('␣')
                for i, a in enumerate(s):
                    if a == 'X':
                        x = float(s[i + 1])
                    elif a == 'Y':
                        y = float(s[i + 1])
                data.append([x, y, [], [], []])
            elif 'logT' in line:  # reads in the logR values for the table
                s = line.split('␣')
                rRange = [float(a) for a in s[1:] if len(a) > 0]
                data[-1][2] = rRange
            elif 'R' not in line:  # reads in the table
                s = line.split('␣')
                s = [i for i in s if len(i) > 0]
                t = float(s[0])
                s = s[1:]
                data[-1][3].append(t)
                data[-1][4].append([])
                for i, a in enumerate(s):
                    data[-1][4][-1].append(float(a))
                if len(s) < len(data[-1][2]):
                    for i in range(len(data[-1][2]) - len(s)):
                        data[-1][4][-1].append(1e10)  # absurd value
        if '************************' in line:
            tables = True
    for i in range(len(data)):
        data[i][4] = np.array(data[i][4])
    return data
    # Note that there is some redundancy, as rRange and tRange are expected to
    # be the same for each table. We leave the parser more general, however, as the
    # wasted space is minimal.
```

```
# Method for reading in Ferguson tables. Tested on latest (as of August 2014)
# GS98 composition tables.


def readFergTable(fname, x, y):
    # These tables are pre-split by (X,Z) value, so we can just focus on the
    # reading part.
    f = open(fname)
    # We're intentionally keeping the format the same as the opalParser format.
    data = [x, y, [], [], []]
    for line in f:
        line = line.rstrip('\n')  # remove newlines
        if 'log T' in line:  # reads in the logR values for the table
            s = line.split(' ')
            rRange = [float(a) for a in s[2:] if len(a) > 0]
            data[2] = rRange
        # reads in the table
        elif 'R' not in line and len(line) > 1 and 'Grev' not in line:
            s = line
            t = float(s[:5])
            ss = []
            counter = 6
            while counter < len(s):
                ss.append(s[counter:counter + 7])
                counter += 7
            data[3].append(t)
            data[4].append([])
            # Now we need to filter for columns which merged due to Fortran
            # formatting
            s = ss
            for i, a in enumerate(s):
                data[4][-1].append(float(a))
            if len(s) < len(data[2]):
                for i in range(len(data[2]) - len(s)):
                    data[4][-1].append(1e10)  # absurd value
    data[4] = np.array(data[4])
    data[4] = data[4][::-1]
    data[3] = np.array(data[3])
    data[3] = data[3][::-1]
    return data


def readFergTables(dirName):
    data = []
    for filename in os.listdir(dirName):
        s = filename[4:]  # remove the 'g' from the beginning
        s = s.split('.')
        x = float(s[0]) / 10 ** len(s[0])
        z = float(s[1]) / 10 ** len(s[1])
        y = 1 - x - z
        data.append(readFergTable((dirName + filename), x, y))
    return data
```

Usage Example (opacityTest.py)

```
import numpy as np
import matplotlib.pyplot as plt
```

```
from opacity import *
a = opac('../Opacity Tables/Opal/GS98.txt', '../Opacity Tables/Ferguson/f05.gs98/', 0.7,
    0.28)
tRan = [10 ** (i / 20.) for i in range(60, 180)]
rRan = [10 ** (i / 20.) for i in range(-200, 120)]
t,r = np.meshgrid(tRan,rRan)
z = a.opacity(t,r)
bigR = r/((t/1e6)**3)
z[bigR>10] = np.nan
print t.shape
print r.shape
print z
print z.shape
plt.imshow(z, extent=[3, 9, -10, 6], origin='lower',aspect=0.3)
cb = plt.colorbar()
cb.set_label('log $\kappa$')
plt.ylabel('log $\\rho$')
plt.xlabel('log T')
plt.show()
cs = plt.contourf(np.log10(tRan), np.log10(rRan), z)

cb.set_label('log $\kappa$')
plt.ylabel('log $\\rho$')
plt.xlabel('log T')
plt.show()
```

B.2 Stellar Integration Code

The thermodynamics functions from the Gob stellar integration code[3] were translated into Python, and subsequently into Cython. This is the first file shown below. The next file contains caching routines which precompute the equation of state and perform high-speed vectorized interpolation. These routines have been verified to an accuracy of one part in 10^4, though higher accuracy may be achieved by adjusting the various resolution parameters they accept. The third file simply contains various physical constants. The fourth file contains both a steady-state stellar integrator and a time-dependent stellar code. These provide an interface which accepts as input the macroscopic stellar quantities such as luminosity, external illumination, mass, and radius, and computes the steady-state structure. From there, the time-dependent code may be used to evolve the star, accepting a new external illumination at each time step. The next file provides an example of the usage of the whole package. The next three files provide the addon used to compute self-consistent companion radii as well as the scripts which call it and analyze the resulting output. The final two files provide a caller script and analyzer script for examining accretion induced collapse in red giant systems. Note that this code requires Python, Cython, gcc, NumPy, and SciPy, and was tested with versions 2.7, 0.21, 4.9.0-20130929, 1.9.0, and 0.14.0 respectively.

Thermodynamic Methods (gob.pyx)

```
#cython: cdivision=True
#cython: infer_types=True
import numpy as np
from numpy import exp
from numpy import sqrt
```

[3]B. Paczyński. "Envelopes of Red Supergiants". In: *Acta Astronomica* 19 (1969), p. 1.

```
from scipy.interpolate import griddata

# Useful constants
# ------- set the values of critical densities for pressure ionization:
#                          "rhc1", "rhc2", "rhc3"
# ------- the value of critical second helium ionization: "helim2"
# ------- and the average charge of "metals": "zav" .
cdef double rhcl1 = -1.0
cdef double rhcl2 = -0.5
cdef double rhcl3 = 0.0
cdef double he2lim = 0.99
cdef double zav = 10.0
cdef double rhc1 = 10.0 ** rhcl1
cdef double rhc2 = 10.0 ** rhcl2
cdef double rhc3 = 10.0 ** rhcl3

# p = pressure (cgs)
# ro = density (cgs)
# u = energy density per unit mass (cgs)
# x = hydrogen mass fraction
# y = helium mass fraction
# Returns p,u, as well as
#               xh1             hydrogen ionization fraction
#               xhe1    helium first ionization fraction
#               xhe2    helium second ionization fraction


cdef energ(double ro,double t,double x,double y):
    # rhc1, rhc2, rhc3  are critical densities for "pressure ionization"
    cdef double teta = 5040. / t
    cdef double dm = 2.302585
    cdef double tm = 1 / teta / dm
    cdef double logt = np.log10(t)
    cdef double mue = (1. + x) / 2.
    cdef double h = 1.6734e-24
    cdef double nh = x * ro / h
    cdef double nhe = 0.25 * y * ro / h
    cdef double nmet = 1. / zav / 2. * (1.0 - x - y) * ro / h
    # Assume metals fully ionized
    cdef double nmetel = nmet * zav
    cdef double ne = 0.0
    cdef double nhi = nh
    cdef double nhii = 0.0
    cdef double nhei = nhe
    cdef double nheii = 0.
    cdef double nheiii = 0.
    cdef double xh1 = 0.0
    cdef double xhe1 = 0.0
    cdef double xhe2 = 0.0
    cdef double fac1 = 0.0
    cdef double fac2 = 0.0
    cdef double fac3 = 0.0
    # Hydrogen ionization
    cdef double hi1 = 13.595
    cdef double hi = hi1 * (1 - ro / rhc1 * (1 + tm / hi1))
    cdef double fhl = np.log10(nh)
    cdef double b10 = 15.3828 + 1.5 * logt - hi * teta - fhl
```

```
    if b10 > 10.0:
        b10 = 10.0
    if b10 > -10:
        b = 10.0 ** b10
        c = b
        fac1 = c * nh
        bc = 0.5 * b / c
        xx = 1.0 / (sqrt(bc * bc + 1.0 / c) + bc)
        # xx is the positive root of equation: xx**2 + b*xx - c = 0
        xx1 = 1.0 - xx
        if xx1 < 1.0e-10:
            xx1 = 1.0e-10
        nhii = nh * xx
        ne = nhii
        nhi = nh * xx1
        xh1 = xx
        # Helium ionization
        hi2 = 24.580
        hi = hi2 * (1 - ro / rhc2 * (1 + tm / hi2))
        fhel = np.log10(nhe)
        b10 = 15.9849 + 1.5 * logt - hi * teta - fhel
        if b10 > 10.0:
            b10 = 10.0
        if b10 > -10:
            c = 10.0 ** b10
            b = c + ne / nhe
            fac2 = c * nhe
            bc = 0.5 * b / c
            xx = 1.0 / (sqrt(bc * bc + 1.0 / c) + bc)
            xx1 = 1.0 - xx
            if xx1 < 1e-10:
                xx1 = 1e-10
            nheii = nhe * xx
            ne = ne + nheii
            nhei = nhe * xx1
            xhe1 = xx
            # Second Helium ionization
            hi3 = 54.403
            hi = hi3 * (1 - ro / rhc2 * (1 + tm / hi3))
            fhel = np.log10(nheii)
            b10 = 15.3828 + 1.5 * logt - hi * teta - fhel
            if b10 > 10:
                b10 = 10
            if b10 > -10:
                c = 10.0 ** b10
                b = c + ne / nheii
                fac3 = c * nheii
                bc = 0.5 * b / c
                xx = 1.0 / (sqrt(bc * bc + 1.0 / c) + bc)
                xx1 = 1.0 - xx
                if xx1 < 1e-10:
                    xx1 = 1e-10
                nheiii = nheii * xx
                ne = ne + nheiii
                nheii = nheii * xx1
                xhe2 = xx
            f1 = fac1 / ne
```

```
            f2 = fac2 / ne
            f3 = fac3 / ne
            f4 = nh / ne
            f5 = y / 4 / x
            zz = 1.0
            zz = fzz(zz, f1, f2, f3, f4, f5)
            ne = ne * zz
            xh1 = f1 / (1 + f1)
            xhe1 = f2 / (1 + f2 * (1 + f3))
            xhe2 = xhe1 * f3
            nhi = nh * (1 - xh1)
            nhii = nh * xh1
            nhei = nhe * (1 - xhe1 - xhe2)
            nheii = nhe * xhe1
            nheiii = nhe * xhe2
    nh2 = 0.0
    if nhi > 0.001 * nh and t < 20000:
        fac = 28.0925 - teta * (4.92516 - teta * (0.056191 + teta * 0.0032688)) - logt
        if t < 12000:
            fac = fac + (t - 12000) / 1000.
        fac = exp(dm * fac)
        if fac > 1e-20 * nhi:
            b = fac / nhi
            bc = 0.5
            xx = 1.0 / (sqrt(bc * bc + 1.0 / b) + bc)
            nh2 = 0.5 * nhi * (1 - xx)
            nhi = nhi * xx
        else:
            nh2 = 0.5 * nhi
            nhi = 0.0
    # Correction for slight electron degeneracy
    nedgen = (nmetel + ne) * (1. + 2.19e-2 * (ro / mue) * (t / 1.e6) ** (-1.5))
    nt = nh - nh2 + nhe + nedgen + nmet
    pg = 1.3805e-16 * nt * t
    pr = 2.521922460548802e-15*t**4
    p = pg + pr
    uh2 = t * (2.1 + t * 2.5e-4)
    if t > 3000:
        uh2 = -1890. + t * (3.36 + t * 0.4e-4)
    u = (1.5 * pg + 3. * pr + 1.3805e-16 * nh2 * uh2 + 3.585e-12 * nhi + 25.36e-12 * nhii +
         39.37e-12 * nheii + 126.52e-12 * nheiii) / ro
    return p, u, xh1, xhe1, xhe2

# input:
#    zz = a guess of correcting factor to the electron density (=1.0)
#    f1,f2,f3 = ionization factors divided by electron density
#    f4 = number density of hydrogen ions and atoms / electron number density
#    f5 = ratio of helium to hydrogen nuclei
# output:
#    zz = the iterated value of the correcting factor
#    f1,f2,f3 = ionization factors divided by the corrected electron density
# Helper method for correcting electron density


cdef double fzz(double zz,double f1,double f2,double f3,double f4,double f5,double delta=0.001,double acc=0.00001, int itmax = 30):
```

```
    cdef int iterations = 1
    fz = funzz(zz, f1, f2, f3, f4, f5)
    while abs(fz) > acc and iterations <= itmax:
        zz1 = zz + delta
        fz1 = funzz(zz1, f1, f2, f3, f4, f5)
        dz = delta * fz / (fz - fz1)
        zz = zz + dz
        iterations += 1
        fz = funzz(zz, f1, f2, f3, f4, f5)
    if iterations == itmax:
        print 'Warning: fzz iterations do not converge.'
    return zz


cdef double funzz(double zz,double f1,double f2,double f3,double f4,double f5):  # Helper method
    return f1 / (f1 + zz) + f5 * f2 * (zz + 2 * f3) / (zz * zz + f2 * (zz + f3)) - zz / f4

#   input:
#       ro      density(c.g.s.)
#       t       temp(k)
#       x       hydrogen mass fraction
#       y       helium mass fraction
#       typ     control variable:
#                       > 0 include radiation in ionization region
#                       <=0 neglect radiation in ionization region
#   output:
#       q       -(d ln rho /d ln t)p                            |
#       cp      (du/dt)p   specific heat cap. at const p        |
#       gradad  (d ln t/d ln p)s   adiabatic gradient           |
#       p       pressure (c.g.s.)                               |
#       dpro    (dp/drho)t                                      |--> c.g.s.k.
#       dpt     (dp/dt)rho                                      |
#       u       specific internal energy                        |
#       dut     (du/dt)rho  specific heat cap. at const vol.    |
#       vad     adiabatic sound speed                           |
#       error   log(error)
#       xh1     hydrogen ionization fraction
#       xhe1    helium first ionization fraction
#       xhe2    helium second ionization fraction
#       an adjustment is made to take into account weak electron degen.,
#       here for full ionization, in energ for partial ionization


cpdef termo(double ro,double t,double x,double y):
    p, u, xh1, xhe1, xhe2 = energ(ro, t, x, y)
    z = 1. - x - y
    if xhe2 >= he2lim:
        xh1 = 1.0
        xhe1 = 0.0
        xhe2 = 1.0
        # full ionization
        nelect = (x + y / 2. + z / 2.)
        nnucl = (x + y / 4. + z / zav / 2.)
        mue = (1. + x) / 2.
        ndgen = nelect * (1. + 2.19e-2 * (ro / mue) * (t / 1.e6) ** (-1.5))
```

```
        # p1 is for particles , p2 is for photons
        p1 = 0.825075e8 * (ndgen + nnucl)
        p2 = 2.523e-15 * t ** 3 / ro
        p = (p1 + p2) * ro * t
        u = (1.5 * p1 + 3. * p2) * t + 1.516e13 * x + 1.890e13 * y
        dpro = p1 * t
        dpt = (p1 + 4. * p2) * ro
        duro = -3. * p2 * t / ro
        dut = 1.5 * p1 + 12. * p2
    else:
        # partial ionization of hydrogen and helium
        p1, u1, xh1, xhe1, xhe2 = energ(ro, 0.999 * t, x, y)
        p2, u2, xh1, xhe1, xhe2 = energ(ro, 1.001 * t, x, y)
        p3, u3, xh1, xhe1, xhe2 = energ(0.999 * ro, t, x, y)
        p4, u4, xh1, xhe1, xhe2 = energ(1.001 * ro, t, x, y)
        p = (p1 + p2 + p3 + p4) / 4
        u = (u1 + u2 + u3 + u4) / 4
        dpro = (p4 - p3) * 500 / ro
        dpt = (p2 - p1) * 500 / t
        duro = (u4 - u3) * 500 / ro
        dut = (u2 - u1) * 500 / t
    # evaluation of more complex thermodynamic functions and the error
    q = t / ro * dpt / dpro
    cp = dut + q / ro * dpt
    gradad = p * q / (cp * ro * t)
    vad = sqrt(dpro * cp / dut)
    er1 = np.abs(1 - t / p * dpt - duro * ro ** 2 / p) + 1.0e-10
    error = np.log10(er1)
    return q, cp, gradad, p, dpro, dpt, u, dut, vad, error, xh1, xhe1, xhe2
```

Thermodynamic Caches (thermoCache.py)

```
import numpy as np
import pyximport
pyximport.install()
import gob
from scipy.interpolate import RegularGridInterpolator
from scipy.optimize import newton
from constants import *

class thermCache: # Cache object allowing for precomputation of thermodynamic quantities
	def __init__(self, x, y,minLogRho=-13,maxLogRho=8,minLogT=2.5,maxLogT=8,resRho=500,resT=500):
		rran = 10**np.linspace(minLogRho,maxLogRho,num=resRho)
		tran = 10**np.linspace(minLogT,maxLogT,num=resT)
		data = np.zeros((len(rran),len(tran),13))
		for i in range(len(rran)):
			for j in range(len(tran)):
				data[i,j] = gob.termo(rran[i],tran[j],x,y)
		self.rran = rran
		self.tran = tran
		self.data = data
		self.interp = []
		self.needsLog = [3,4,6,8]
		data[:,:,self.needsLog] = np.log10(data[:,:,self.needsLog])
		self.interp = RegularGridInterpolator((rran,tran),data,bounds_error=False,fill_value=np.nan)
```

```
		self.indDict = {'q':0,'cp':1,'gradad':2,'p':3,'dpro':4,'dpt':5,'u':6,'dut':7,'vad':8,'err':9,\
						'xh1':10,'xhe1':11,'xhe2':12}

	def termo(self,rho,t,name=None):
		# Passing name causes this to just return the specified quantity,
		# otherwise all computed quantities are returned.
		ret = np.transpose(self.interp(np.transpose([rho,t])))
		ret[self.needsLog] = 10**ret[self.needsLog]
		if name==None:
			return ret
		return ret[self.indDict[name]]

	def rhoFromP(self,p,t):
		pg = p-(a*t**4)/3
		if pg<0: # Inconsistent with Eddington limit
			return np.nan
		rho0 = mP*pg/(kB*t)
		f = lambda rho: 1-self.termo(abs(rho),t,name='p')[0]/p
		fp = lambda rho: -(1/p)*self.termo(abs(rho),t,name='dpro')[0]
		ret = np.nan
		try:
			ret = np.abs(newton(f,rho0,fprime=fp,maxiter=50))
		except:
			print 'WARNING: Convergence Failure in Rho-solving! Inputs are log(p),',np.log10(p),'log(t),',np.log10(t)
		return ret


class rhoCache: # Cache object allowing for inversion of the equation of state
	def __init__(self,thermcache,minLogP=-6,maxLogP=16,minLogT=2.5,maxLogT=8,resP=150,resT=150):
		pran = 10**np.linspace(minLogP,maxLogP,num=resP)
		tran = 10**np.linspace(minLogT,maxLogT,num=resT)
		data = np.zeros((len(pran),len(tran)))
		for i in range(len(pran)):
			for j in range(len(tran)):
				data[i,j] = np.log10(thermcache.rhoFromP(pran[i],tran[j]))
		self.pran = pran
		self.tran = tran
		self.data = data
		self.interp = RegularGridInterpolator((pran,tran),data,bounds_error=False,fill_value=np.nan)

	def rho(self,p,t):
		pg = p-(a*t**4)/3
		if not isinstance(t, np.ndarray):
			if pg<0: # Inconsistent with Eddington limit
				return np.nan
		else:
			ret = np.zeros(len(p))
			ret[pg<0] = np.nan # Inconsistent with Eddington limit
		# The above code is necessary because the photosphere sometimes interpolates to NaN values
		# due to proximity to Eddington-violating parameters.
		ret[ret==0] = (10**self.interp(np.transpose([p,t])))[ret==0]
```

```
                return ret

        def drhodT(self,p,t,eps=1e-3): # Scipy's RectBivariateSpline differentiator is broken so I wrote my own
                return (self.rho(p,t*(1+eps))-self.rho(p,t*(1-eps)))/(2*eps*t)

class convGradCache: # Cache object for the root-finding problem of the convective gradient
        def __init__(self,minLogV=-20,maxLogV=20,minLogA=-20,maxLogA=20,resV=100,resA=100):
                vran = 10**np.linspace(minLogV,maxLogV,num=resV)
                aran = 10**np.linspace(minLogA,maxLogA,num=resA)
                data = np.zeros((len(vran),len(aran)))
                for i in range(len(vran)):
                        for j in range(len(aran)):
                                roots = np.roots([2*aran[j],vran[i],vran[i]**2,-vran[i]])
                                data[i,j] = np.max(np.real(roots[np.where(np.isreal(roots))]))
                self.vran = vran
                self.aran = aran
                self.data = data
                self.interp = RegularGridInterpolator((vran,aran),data,bounds_error=False,fill_value=np.nan)

        def convGrad(self,v,a):
                return self.interp(np.transpose([v,a]))
```

Fundamental Constants (constants.py)

```
c        = 2.99792458e10  # cm/s           Speed of light
sigma    = 5.670400e-5    # erg/cm^2/s/K^4 Stephan-Boltzmann
a        = 4*sigma/c      # erg/cm^3/K^4   Photon gas internal energy constant
kB       = 1.3806488e-16  # erg/K          Boltzmann
mP       = 1.672622e-24   # g              Proton mass
newtonG  = 6.67e-8        # erg cm/g^2     G
mSun     = 1.9988435e33   # g              Solar Mass
rSun     = 6.96e10        # cm             Solar Radius
lSun     = 3.846e33       # erg/s          Solar Luminosity
kappaG   = 1000.          # g/cm^2         Gamma ray opacity
```

Steady-state and Time-dependent Integrators (star.py)

```
import opacity
import numpy as np
from thermoCache import *
from scipy.sparse import csr_matrix
from scipy.sparse.linalg import spsolve
from numpy import pi
from constants import *
import plotUtils as pu

def f(tau):
        d = np.array(1-1.5*tau)
        d[d<0] = 0
        return d
```

```python

def s(t,rho,l,r,m):
        return (2./3)*a*t**3*r**0.5*(np.abs(l)/(8*pi*sigma))**0.25/(newtonG*m*rho)

def gradR(kappa,l,m,ff,ss,p,t):
        return 3*p*(kappa*l+ff*ss*4*pi*newtonG*m*c)/(16*pi*newtonG*m*c*a*t**4*(1+ff*ss))

def gradRho(p,dpdt,t,gradd,dpdrho,rho):
        return (p-dpdt*t*gradd)/(dpdrho*rho)

def gradConv(gradRr,gradAd,kappa,rho,hs,alpha,m,r,q,cp,t,convcache):
        lt = hs*alpha
        w = kappa*rho*lt
        g0 = cp*rho*(1+(w**2)/3)/(8*sigma*t**3*w)
        d = newtonG*m*lt**2*q/(8*hs*r**2)
        aa = 9*w**2/(8*(3+w**2))
        v = 1/(g0*d**0.5*(gradRr-gradAd)**0.5)
        y0 = convcache.convGrad(v,aa)
        return gradAd+(gradRr-gradAd)*y0*(y0+v),y0/v,y0/(v*g0)

def gradFull(m,r,tau,l,t,rho,opac,x,y,alpha,thermcache,convcache):
        ff = f(tau)
        ss = s(t,rho,l,r,m)
        q,cp,gradad,p,dpro,dpt,u,dut,vad,error,xh1,xhe1,xhe2 = thermcache.termo(rho,t)
        dlnp = -newtonG*m*(1+ff*ss)/(4*pi*p*r**4)
        kappa = 10**opac.opacity(t,rho)
        gradRr = gradR(kappa,l,m,ff,ss,p,t)
        hs = p*r**2/(rho*newtonG*m)
        gradd = gradR(kappa,l,m,ff,ss,p,t)
        if not isinstance(gradd, np.ndarray):
                if gradRr>gradad:
                        gradd = gradConv(gradRr,gradad,kappa,rho,hs,alpha,m,r,q,cp,t,convcache)[0][0]
        else:
                gradd[gradRr>gradad] = gradConv(gradRr,gradad,kappa,rho,hs,alpha,m,r,q,cp,t,convcache)[0][gradRr>gradad]
                if len(np.where(np.isnan(gradd))[0])>0:
                        print 'Error: Invalid numerics detected in gradient calculation.'
                        print 'Inputs are:'
                        print 't',t
                        print 'rho',rho
                        print 'p',p
                        print 'kappa',kappa
                        print 'l',l
                        print 'Intermediate values are:'
                        print 'Radiative Gradient',gradRr
                        print 'Adiabatic Gradient',gradad
                        exit()
        return gradd

def dgraddT(m,r,p,tau,l,t,opac,x,y,alpha,thermcache,convcache,rhocache,eps=1e-3):
        rho0 = rhocache.rho(p,t*(1-eps))
        rho1 = rhocache.rho(p,t*(1+eps))
        g0 = gradFull(m,r,tau,l,t*(1-eps),rho0,opac,x,y,alpha,thermcache,convcache)
        g1 = gradFull(m,r,tau,l,t*(1+eps),rho1,opac,x,y,alpha,thermcache,convcache)
        return (g1-g0)/(2*t*eps)

```

```
def dgraddL(m,r,p,tau,l,t,opac,x,y,alpha,thermcache,convcache,rhocache,l0,eps=1e-3):
        rho = rhocache.rho(p,t)
        dlp = eps*l0
        g0 = gradFull(m,r,tau,l-dlp,t,rho,opac,x,y,alpha,thermcache,convcache)
        g1 = gradFull(m,r,tau,l+dlp,t,rho,opac,x,y,alpha,thermcache,convcache)
        return (g1-g0)/(2*dlp)

class star:
        def __init__(self,x,y,m0,r0,l0,alpha,thermcache,rhocache,convcache,fnameOpal='../Opacity Tables/Opal/GS98.txt',fnameFerg='../Opacity Tables/Ferguson/f05.gs98/',delM=3e-3,lext=0,minRes=500,caution=500,quiet=False):
                # Store inputs
                self.x = x
                self.y = y
                self.m0 = m0
                self.r0 = r0
                self.t0 = ((l0 + lext)/(8*pi*sigma*self.r0**2))**0.25 # T0 is the surface temp, not the photosphere temp: related by 2^(1/4)
                self.l0 = l0
                self.l = None
                self.lext = lext
                self.alpha = alpha
                self.delM = delM
                self.quiet = quiet

                # Prepare opacity interpolator
                self.opalName = fnameOpal
                self.fergName = fnameFerg
                self.opac = opacity.opac(fnameOpal,fnameFerg,x,y)

                # Caches
                self.thermcache = thermcache
                self.rhocache = rhocache
                self.convcache = convcache

                # Helper for reading out data
                self.indDict = {'t':0,'rho':1,'r':2,'tau':3,'p':4,'cp':5,'gradad':6,'dpro':7,'dpt':8,'u':9,'dut':10,\
                                                'vad':11,'grad':12,'gradRho':13,'gradR':14,'q':15,'mUp':16,'dm':17,'mDown':18,\
                                                'kappa':19,'hs':20,'gamma':21,'vc':22,'mu':23,'sigma':24}

                # Prepare initial star state
                self.steady = self.steadyIntegrate(minRes=minRes,caution=caution)
                sg = np.transpose([self.steady[:,16]/(4*pi*self.r0**2)])
                self.steady = np.concatenate((self.steady,sg),axis=1)
                sel = np.where(self.steady[:,-1]>1e-2)
                self.steady = self.steady[sel] # For plotting convenience
                self.l = self.l[sel]

                # Prepare for time integration
                self.state = np.copy(self.steady)
                sel = np.where(self.state[:,3]>2./3)
                self.state = self.state[sel] # Chop off top of photosphere for time integration
```

```
        self.l = self.l[sel]
        self.l = np.concatenate((self.l,[self.l0]))
        self.tb = self.steady[-1,0]
        # Prepare helper variables for time integration
        self.m = self.state[:,18]
        self.dm = self.state[:-1,17]
        self.mUp = self.state[:,16]
        self.mL = np.concatenate(([self.m[0]],(self.m[1:]+self.m[:-1])/2,[self.m[-1]]))
        self.mLup = np.concatenate(([self.mUp[0]],(self.mUp[1:]+self.mUp[:-1])/2,[self.mUp[-1]]))
        self.dmL = np.concatenate(([self.dm[0]/2],(self.dm[1:]+self.dm[:-1])/2,[self.dm[-1]/2]))
        self.fact = self.l[0]/(4*pi*self.r0**2*sigma*self.state[0,0]**4) # Temp BC correction
        if not self.quiet:
            print self.fact,self.l[0]/(4*pi*self.r0**2*sigma*self.state[0,0]**4)

        # Prepare derivatives matrix
        # L oupies 0 through N, T oupies N+1 through 2N
        n = self.state.shape[0]
        if not self.quiet:
            print n
        ij = np.zeros((4*n-2,2))
        vs = np.zeros(4*n-2)

        # Luminosity derivatives
        ij[:n]            = [[i+1,i] for i in range(n)]
        vs[:n]            = -1/self.dmL
        ij[n:2*n]         = [[i+1,i+1] for i in range(n)]
        vs[n:2*n]         = 1/self.dmL

        # Temperature derivatives
        ij[2*n:3*n-1]     = [[i+n+2,i+n+1] for i in range(n-1)]
        vs[2*n:3*n-1]     = -self.mUp[:-1]/self.dm
        ij[3*n-1:4*n-2]   = [[i+n+2,i+n+2] for i in range(n-1)]
        vs[3*n-1:4*n-2]   = self.mUp[:-1]/self.dm

        # Put it all together
        ij = np.transpose(ij)
        self.diffMat = csr_matrix((vs,ij),shape=(2*n+1,2*n+1))
        self.eps0 = -(self.diffMat*np.concatenate((self.l,self.state[:,0])))[1:1+len(self.state)]

    def plot(self,kind,xVar,yVar,logX,logY,xlab,ylab,axis,endMarker=None,endMarkerSize=None):
        x = self.retrieve(xVar,kind)
        y = self.retrieve(yVar,kind)
        r = self.retrieve('r',kind)

        # Compute marker on the heating depth
        sig = self.retrieve('sigma',kind)
        heatLoc = np.argmin(np.abs(sig-1e3))
        xH = x[heatLoc]
        yH = y[heatLoc]

```

```
            # Compute marker on the photosphere
            tau = self.retrieve('tau',kind)
            pLoc = np.argmin(np.abs(tau-2./3))
            xP = x[pLoc]
            yP = y[pLoc]

            # Continue with plotting
            isConv = (self.retrieve('gradad',kind)>=self.retrieve('gradR',kind))
            if len(x)>500:
                red = len(x)/500
                x = np.copy(x[::red])
                y = np.copy(y[::red])
                r = np.copy(r[::red])
                isConv = isConv[::red]
            if logX:
                x = np.log10(x)
                xH = np.log10(xH)
                xP = np.log10(xP)
            if logY:
                y = np.log10(y)
                yH = np.log10(yH)
                yP = np.log10(yP)
            if yVar!='r':
                thinApproxFilter = np.abs(r-self.r0)<0.5*self.r0
                x = x[thinApproxFilter]
                y = y[thinApproxFilter]
            pu.colorline(axis,x,y,z=0.15+0.7*isConv)
            ranX = np.nanmax(x)-np.nanmin(x)
            ranY = np.nanmax(y)-np.nanmin(y)
            axis.set_xlim([np.nanmin(x)-ranX/10,np.nanmax(x)+ranX/10])
            axis.set_ylim([np.nanmin(y)-ranY/10,np.nanmax(y)+ranY/10])
            axis.set_xlabel(xlab)
            axis.set_ylabel(ylab)
            heatLoc = np.argmin(np.abs(x-1e3))

            # Place markers
            if xVar=='sigma':
                axis.axvspan(xP, xH, alpha=0.3, color='grey')
            if not endMarker is None:
                axis.scatter(x[-1],y[-1],marker=endMarker,s=endMarkerSize,c='k',
                    zorder=100)


        def retrieve(self,name,kind):
            if kind=='steady':
                if name=='l':
                    return self.l0
                return self.steady[:,self.indDict[name]]
            elif kind=='timedep':
                if name=='l':
                    return self.l
                return self.state[:,self.indDict[name]]
            else:
                print 'Error: Invalid kind. Please specify either steady or 
                    timedep.'

        def sigma(self,kind):
```

```
        return self.retrieve('p',kind)*self.r0**2/(newtonG*self.m0)

    def mu(self,kind):
        return self.retrieve('rho',kind)*kB*self.retrieve('t',kind)/self.retrieve('p',kind)

    def steadyIntegrate(self,minRes=500,caution=500):
        z = np.array([np.log(self.t0),np.log(1e-12),self.r0,0]) # rho0 = 1e-12
        i = 0
        data = []
        mUp = 1e-30
        while mUp<self.delM*self.m0:
            # Prepare luminosity
            le = self.lext*np.exp(-mUp/(kappaG*4*pi*self.r0**2))
            l = self.l0 + le
            # Prepare thermodynamics
            t = np.exp(z[0])
            rho = np.exp(z[1])
            tau = z[3]
            r = self.r0
            ff = f(tau)
            ss = s(t,rho,l,r,self.m0)
            kappa = 10**self.opac.opacity(t,rho)
            q,cp,gradad,p,dpro,dpt,u,dut,vad,error,xh1,xhe1,xhe2 = self.thermcache.termo(rho,t)[:,0]
            gradRr = gradR(kappa,l,self.m0,ff,ss,p,t)

            # Compute derivatives
            dlnp = -newtonG*self.m0*(1+ff*ss)/(4*pi*p*r**4)
            dr = 1./(4*pi*r**2*rho)
            dtau = -kappa/(4*pi*r**2)
            dp = p*dlnp

            # Compute other quantities of interest
            hs = p*r**2/(rho*newtonG*self.m0)
            gradC,gam,vc = gradConv(gradRr,gradad,kappa,rho,hs,self.alpha,self.m0,r,q,cp,t,self.convcache)
            gam = gam[0]
            vc = vc[0]
            mu = kB*t*rho/(p-a*(t**4)/3)

            # More derivatives
            gradd = gradRr
            if gradRr>gradad:
                gradd = gradC[0]
            gradRhoo = gradRho(p,dpt,t,gradd,dpro,rho)
            dlnrho = gradRhoo*dlnp
            dlnt = gradd*dlnp

            # Wrap derivatives
            derivs = np.array([dlnt,dlnrho,dr,dtau])

            # Set step size
            h = min(self.m0*self.delM/minRes,(1./caution)*(np.min([1,1,z[2]]/np.abs(derivs[:-1]))))

            # Compute current state
```

```
                nums = np.array([t,rho,r,tau,p,cp,gradad,dpro,dpt,u,dut,vad,gradd,gradRhoo,gradRr,q,0,0,self.m0,kappa,hs,gam,vc,mu])
                nums[self.indDict['r']] = z[2]
                nums[self.indDict['mDown']] = self.m0-mUp
                nums[self.indDict['dm']] = h
                nums[self.indDict['mUp']] = mUp

                # Step forward
                data.append(nums)
                z -= h*derivs
                mUp += h
                i+=1
                # Check for errors
                if not self.quiet:
                    if i%1000==0:
                        print 'Mass Step:',h
                        print 'Net Mass:',mUp/self.m0
                if i>1000000:
                    print 'Warning: Mass step too low!'
                    raise ValueError('Mass step too low!')
        self.l = np.ones(len(data))*self.l0
        return np.array(data)

    def jac(self,vec,tstep):
        # Read in state
        r   =  self.state[:,2]
        tau = self.state[:,3]
        p   =  self.state[:,4]
        cp  =  self.state[:,5]
        n   =  self.state.shape[0]

        # Produce updated quantities
        t = self.state[:,0] + vec[n+1:2*n+1]
        l = self.l + vec[:n+1]*self.l0
        rho = self.rhocache.rho(p,t)

        # Compute helper term
        g   =  newtonG*self.m0/self.r0**2

        # Compute grad
        grad =  gradFull(self.m0,self.r0,tau,l[:-1],t,rho,self.opac,self.x,self.y,self.alpha,self.thermcache,self.convcache)

        # Compute grad derivatives
        dgdt =  dgraddT(self.m0,self.r0,p,tau,l[:-1],t,self.opac,self.x,self.y,self.alpha,self.thermcache,self.convcache,self.rhocache)
        dgdl =  dgraddL(self.m0,self.r0,p,tau,l[:-1],t,self.opac,self.x,self.y,self.alpha,self.thermcache,self.convcache,self.rhocache,self.l0)

        # Prepare sparse matrix
        # L occupies 0 through N, T occupies N+1 through 2N, tau goes 2N+1 to 3N

        ij          =      np.zeros((2+3*n,2))
        vs          =      np.zeros(2+3*n)

        # Boundary condition on T at base
        ij[0]   =      [n+1,2*n]
```

```
        vs[0]   =       1.

        # Boundary condition on L at top
        ij[1]   =       [0,0]
        vs[1]   =       1.
        ij[2]   =       [0,n+1]
        vs[2]   =       -self.fact*16*pi*self.r0**2*sigma*t[0]**3/self.l0

        # Derivatives

        # Output L
        ij[4:4+n]       =       [[i+1,i+n+1] for i in range(n)]
        vs[4:4+n]       =       -cp/tstep/self.l0

        # Output T
        ij[4+n:3+2*n]   =       [[i+n+2,i] for i in range(n-1)]
        vs[4+n:3+2*n]   =       -t[:-1]*dgdl[:-1]*self.l0
        ij[3+2*n:2+3*n] =       [[i+n+2,i+n+1] for i in range(n-1)]
        vs[3+2*n:2+3*n] =       -((t*dgdt+grad)[:-1])

        # Put it all together and solve
        ij = np.transpose(ij)
        mat = csr_matrix((vs,ij),shape=(2*n+1,2*n+1))
        amat = mat + self.diffMat
        return amat

    def func(self,vec,tstep,eps):
        # Read in unchanged things
        r   =  self.state[:,2]
        tau =  self.state[:,3]
        p   =  self.state[:,4]
        cp  =  self.state[:,5]
        n   =  self.state.shape[0]

        # Produce updated quantities
        t1 = self.state[:,0] + vec[n+1:2*n+1]
        l1 = self.l + vec[:n+1]*self.l0
        rho1 = self.rhocache.rho(p,t1)
        grad1 = gradFull(self.m0,self.r0,tau,l1[:-1],t1,rho1,self.opac,self.x,
            self.y,self.alpha,self.thermcache,self.convcache)
        k = self.opac.opacity(t1,rho1)
        # Evaluate derivative conditions
        ders = self.diffMat*np.concatenate((l1,t1))

        # Evaluate left side BC's
        lbcs = np.zeros(len(ders))
        lbcs[0] = l1[0]
        lbcs[n+1] = t1[n-1]

        # Put it together
        left = ders + lbcs

        # Evaluate right side
        rght = np.concatenate(([self.fact*4*pi*self.r0**2*sigma*t1[0]**4]\
                                                        ,(cp*(vec[n+1:2*n+1]/
                                                            tstep))-eps\
```

```
                                                ,[self.tb],(grad1*t1)[:-1]))
        bNew = left-rght
        bNew[:n+2]/=self.l0
        return bNew

    def stepController(self,tstep,eps):
        dt = tstep
        delta = 0
        while delta<tstep:
            backup = np.copy(self.state)
            backupL = np.copy(self.l)
            done = False
            while not done:
                if not self.quiet:
                    print 'dt =',dt
                ret = self.newStep(dt,eps)
                if ret==-1 or np.sum(1.0*(self.state[:,0]<0))>0 or np.sum(1.0*(self.state[:,0]>1e11))>0:
                    self.state = np.copy(backup)
                    self.l = np.copy(backupL)
                    dt /= 2
                else:
                    done = True
            delta += dt

    def newStep(self,tstep,eps,rtol=1e-3,stepSize=0.3):
        n = self.state.shape[0]
        vec = np.zeros(2*self.state.shape[0]+1)
        err = 1.0
        i=0
        while err>rtol:
            j = self.jac(vec,tstep)
            b = self.func(vec,tstep,eps)
            dVec = spsolve(j,-b)
            vec += dVec*stepSize
            if np.sum(1.0*np.isnan(vec))>0:
                return -1
            b[n+2:2*n+1]/=self.state[:-1,0]
            b[1:n+2]*=self.delM*self.m0
            err = np.sum(b**2)**0.5/len(b)
            if not self.quiet:
                print err,stepSize,n,np.argmax(np.abs(b)),np.max(np.abs(vec/np.concatenate((self.l/self.l0,self.state[:,0]))))
            if i>100 and i%200==0:
                stepSize/=2
            if i>1000:
                return -1
            i+=1
        if not self.quiet:
            print 'Step done. Error:',err
            print vec[:n+1:100]
            print vec[n+1::100]
        self.l += self.l0*vec[:n+1]
        self.state[:,0] += vec[n+1:2*n+1]
        self.state[:,1] = self.rhocache.rho(self.state[:,4],self.state[:,0])
```

```
                    kappa = 10**self.opac.opacity(self.state[:,0],self.state[:,1])
                    q,cp,gradad,p,dpro,dpt,u,dut,vad,error,xh1,xhe1,xhe2 = self.thermcache.termo(self.state[:,1],self.state[:,0])[:,0]
                    ff = f(self.state[:,3])
                    ss = s(self.state[:,0],self.state[:,1],self.l[:-1],self.r0,self.m0)
                    self.state[:,5] = cp
                    self.state[:,6] = gradad
                    self.state[:,7] = dpro
                    self.state[:,8] = dpt
                    self.state[:,9] = u
                    self.state[:,10] = dut
                    self.state[:,11] = vad
                    self.state[:,12] = gradFull(self.m0,self.r0,self.state[:,3],self.l[:-1],self.state[:,0],self.state[:,1]\
                                                                ,self.opac,self.x,self.y,self.alpha,self.thermcache,self.convcache)
                    self.state[:,13] = gradRho(self.state[:,4],self.state[:,8],self.state[:,0],self.state[:,12],\
                                                                self.state[:,7],self.state[:,1])
                    self.state[:,14] = gradR(kappa,self.l[:-1],self.m0,ff,ss,self.state[:,4],self.state[:,0])
                    self.state[:,15] = q
                    self.state[:,19] = kappa
                    # TODO: Update r
```

Example Usage (starExample.py)

```
import star
import numpy as np
from numpy import pi
import matplotlib.pyplot as plt
from constants import *
from thermoCache import *

x = 0.7
y = 0.27
thermcache = thermCache(x,y)
rhocache = rhoCache(thermcache)
convcache = convGradCache()

color=plt.cm.rainbow(np.linspace(0,1,200))
st = star.star(x,y,mSun,rSun,100*lSun,1.5,thermcache,rhocache,convcache,lext=0)
eps = 0.5*np.exp((-st.state[:,16])/(4*pi*rSun**2*1000))*st.l0/(4*pi*rSun**2*1000)
t0 = st.state[:,0]
t = 0
tnext = 1e6
for i in range(20):
        tnext = st.stepController(tnext,0)
        t0 = np.copy(st.state[:,0])
for i in range(200): # 501, 1001, 5001
        plt.subplot(211)
        plt.title('$L_{in}=100L_{sun}, \Delta t=2e8s$')
        plt.plot(np.log10(st.state[:,24]),(st.state[:,0]-t0)/t0,color = color[i])
        plt.ylabel('$\Delta T/T$')
        plt.subplot(212)
        plt.plot(np.log10(st.state[:,24]),st.l[:-1]/lSun,color = color[i])
```

```
    plt.ylabel('$L/L_{sun}$')
    plt.xlabel('Log $\Sigma$')
    if i%200==199:
        plt.show()
    t += tnext
    tnext = st.stepController(tnext,i*eps/100)
    if i>100:
        tnext = st.stepController(tnext,eps)
```

Radius Addon (starTracker.py)

```
import star
import numpy as np
from numpy import pi
from constants import *
from thermoCache import *
from scipy.interpolate import interp1d
import os.path
import pickle

q = 4.5 # Kramer's P,T opacity law
gA = 0.4 # Adiabatic gradient in ionized matter
x = 0.7
y = 0.27

if not os.path.exists('cachesLowRes'):
    thermcache = thermCache(x,y,resRho=100,resT=100)
    rhocache = rhoCache(thermcache)
    convcache = convGradCache()
    pickle.dump([thermcache,rhocache,convcache],open('cachesLowRes','w+'))
else:
    thermcache,rhocache,convcache = pickle.load(open('cachesLowRes','rb'))

def lum(m,mc=None):
    if m<0.43 and mc is None:
        return 0.23*m**2.3
    elif mc is None:
        return m**4
    else:
        return (10**5.3)*(mc**6)/(1+10**0.4*mc**4+10**0.5*mc**5)

def r(m,mc=None):
    if mc is None:
        return m**0.9
    else:
        return 3.7*10**3*mc**4/(1+mc**3+1.75*mc**4)

class starT:
    def __init__(self,m,mc=None,sc=1e6):
        # Compute unperturbed equilibrium properties
        self.m = m
        self.mc = mc
        self.sc = sc
        self.l = lum(m,mc=mc)
        self.r0 = r(m,mc=mc)
        self.delMmult = 32702.6*(1e6/sc)
        self.eq = star.star(x,y,mSun*m,rSun*self.r0,lSun*self.l,1.5,\
```

```
                                    thermcache,rhocache,convcache,\
                                    delM=self.r0**2/m/self.delMmult,lext=0,\
                                    minRes=350,caution=50,quiet=True)

            # Compute expansion potential
            sg = self.eq.retrieve('sigma','steady')
            gR = self.eq.retrieve('gradR','steady')
            p = self.eq.retrieve('p','steady')
            t = self.eq.retrieve('t','steady')
            bS = np.argmin(np.abs(sg-self.sc))
            self.pbs = p[bS]
            self.pb0 = p[bS]*(gR[bS]/gA)**(1./(gA*(4+q)-2))
            self.ts = t[bS]
            self.rMax = self.r0*max(1,(self.pb0/self.pbs)**(2./(3*(4+q))))

    def rmax(self,flux):
            print 'Computing self-consistent maximum radius...'
            r = self.r0
            dev = 1
            while abs(dev)>1e-3:
                    st = star.star(x,y,mSun*self.m,rSun*r,lSun*self.l,1.5,\
                                    thermcache,rhocache,convcache,\
                                    delM=r**2/self.m/self.delMmult,lext=flux*lSun*pi*r**2,\
                                    minRes=350,caution=50,quiet=True)
                    sg = st.retrieve('sigma','steady')
                    gR = st.retrieve('gradR','steady')
                    p = st.retrieve('p','steady')
                    bS = np.argmin(np.abs(sg-self.sc))
                    pb = (r**2/self.r0**2)*p[bS]*(gR[bS]/gA)**(1./(gA*(4+q)-2))
                    rNew = self.r0*max(1,(self.pb0/max(pb,self.pbs))**(2./(3*(4+q))))
                    r = (rNew + r)/2
                    dev = rNew - r
            print 'Done!',r
            return r

    def rmaxFromL(self,lum):
            print 'Computing self-consistent maximum period...'
            r = self.r0
            dev = 1
            while abs(dev)>1e-3:
                    rOrbit = (r/0.46)*((2+self.m)/self.m)**(1./3)
                    flux = lum/(4*pi*rOrbit**2)
                    st = star.star(x,y,mSun*self.m,rSun*r,lSun*self.l,1.5,\
                                    thermcache,rhocache,convcache,\
                                    delM=r**2/self.m/self.delMmult,lext=flux*lSun*pi*r**2,\
                                    minRes=350,caution=50,quiet=True)
                    sg = st.retrieve('sigma','steady')
                    gR = st.retrieve('gradR','steady')
                    p = st.retrieve('p','steady')
                    bS = np.argmin(np.abs(sg-self.sc))
                    pb = (r**2/self.r0**2)*p[bS]*(gR[bS]/gA)**(1./(gA*(4+q)-2))
                    rNew = self.r0*max(1,(self.pb0/max(pb,self.pbs))**(2./(3*(4+q))))
                    r = (rNew + r)/2
                    dev = rNew - r
                    print r,dev
```

```
            print 'Done!',r
            return r

    def lIn(self,r,flux,rm=None):
        print 'Computing flux...'
        if rm is None:
            rm = self.rmax(flux)
        print rm
        if r>rm:
            print 'Error: Requested radius greater than possible.'
            return None,None,None,None,None
        elif r<self.r0:
            print 'Error: Requested radius less than possible.'
            return None,None,None,None,None
        pbExp = (self.r0/r)**2*self.pb0*(self.r0/r)**(3.*(4+q)/2)
        l = self.l/2
        lower = 0
        upper = self.l
        dev = 1
        counter = 0
        st = None
        while abs(dev)>3e-3:
            counter += 1
            st = star.star(x,y,mSun*self.m,rSun*r,lSun*l,1.5,\
                        thermcache,rhocache,convcache,\
                        delM=r**2/self.m/self.delMmult,lext=flux*lSun*pi*r**2,\
                        minRes=350,caution=50,quiet=True)
            sg = st.retrieve('sigma','steady')
            gR = st.retrieve('gradR','steady')
            p = st.retrieve('p','steady')
            bS = np.argmin(np.abs(sg-self.sc))
            pb = (r/self.r0)**2*p[bS]*((self.l/l)*gR[bS]/gA)**(1./(gA*(4+q)-2))
            dev = (r-self.r0*max(1,(self.pb0/max(pb,self.pbs))**(2./(3*(4+q)))))/(r-self.r0)
            if dev<0:
                upper = l
            elif dev>0:
                lower = l
            l = (upper + lower)/2
#           print l,dev,self.l,r,self.r0,flux
            if l<1e-4*self.l:
                print 'Need more mass!',self.sc
                s = starT(self.m,sc=self.sc*2)
                return s.lIn(r,flux,rm=None)
            if counter > 100:
                print 'Error: No solution found!'
                return None,None,None,None,None
        print 'Done!',self.m,r,flux

        # Process outputs
        dm = st.retrieve('dm','steady')
        gR = st.retrieve('gradR','steady')
        sg = st.retrieve('sigma','steady')
        t = st.retrieve('t','steady')
        dr = dm/(4*pi*r**2*rSun**2*st.retrieve('rho','steady'))
```

```
        bs = np.argmin(np.abs(sg-self.sc))
        ts = t[bs]
        pbs = p[bs]
        pb0 = (r/self.r0)**2*p[bS]*((self.l/l)*gR[bS]/gA)**(1./(gA*(4+q)-2))
        tau = st.retrieve('tau','steady')
        bt = np.argmin(np.abs(tau-2./3))
        dRpre = np.sum(dr[bt:bs])

        # Compute sudden collapse star
        print 'Computing sudden collapse...'
        stpre = st
        dev = 1
        st = None
        lower = 0
        upper = l + flux*pi*r**2
        lSurf = (lower+upper)/2
        counter = 0
        while abs(dev)>3e-3:
            counter += 1
            st = star.star(x,y,mSun*self.m,rSun*r,lSurf*lSun,1.5,\
                    thermcache,rhocache,convcache,\
                    delM=r**2/self.m/self.delMmult,lext=0,\
                    minRes=350,caution=50,quiet=True)
            sg = st.retrieve('sigma','steady')
            t = st.retrieve('t','steady')
            bS = np.argmin(np.abs(sg-self.sc))
            dev = (t[bS] - ts)/ts
            if dev>0:
                upper = lSurf
            elif dev<0:
                lower = lSurf
            lSurf = (upper+lower)/2
#           print lSurf,dev,self.l,r,self.r0,flux
            if counter > 100:
                print 'Error: No solution found!'
                return None,None,None,None,None
        # Determine change in radius
        sg = st.retrieve('sigma','steady')
        dm = st.retrieve('dm','steady')
        dr = dm/(4*pi*r**2*rSun**2*st.retrieve('rho','steady'))
        bs = np.argmin(np.abs(sg-self.sc))
        tau = st.retrieve('tau','steady')
        bt = np.argmin(np.abs(tau-2./3))
        dR = np.sum(dr[bt:bs])
        print 'Done!!',self.m,r,flux
        return l,ts,pb0,pbs,dRpre-dR
```

Radius Caller (stNew.py)

```
from starTracker import *
import numpy as np
import pickle
from numpy import pi
from multiprocessing import Pool

nM = 80
nR = 80
```

```

lRan = [1.,10.,25.,50.]
nL = len(lRan)
mRan = np.linspace(0.08,1.3,num=nM,endpoint=True)
minR = np.zeros(nM)*float('NaN')
maxR = np.zeros(nM)*float('NaN')
maxRL = np.zeros((nM,nL))*float('NaN')

li = np.zeros((nM,nL,nR))
dR = np.zeros((nM,nL,nR))
pbs = np.zeros((nM,nL,nR))
pb0 = np.zeros((nM,nL,nR))
ts = np.zeros((nM,nL,nR))

for i in range(nM):
    s = starT(mRan[i],sc=1e6)
    minR[i] = s.r0
    maxR[i] = s.rMax

    for j in range(len(lRan)):
        maxRL[i,j] = s.rmaxFromL(lRan[j])
        rRan = np.linspace(minR[i]+1e-2,maxRL[i,j],num=nR,endpoint=True)

        def f(k):
            rOrbit = (rRan[k]/0.46)*((2+mRan[i])/mRan[i])**(1./3)
            flux = lRan[j]/(4*pi*rOrbit**2)
            ret = None
            try:
                ret = s.lIn(rRan[k],flux,rm=maxRL[i,j])
            except ValueError as e:
                ret = (None,None,None,None,None)
            return ret
        p = Pool(16)
        ret = p.map(f,range(nR))
        for k in range(nR):
            li[i,j,k],ts[i,j,k],pb0[i,j,k],pbs[i,j,k],dR[i,j,k] = ret[k]
        p.close()
        print "You are at",i,j,". Percent done:",100.*(i*nL+j+1)/(nM*nL)

pickle.dump([minR,maxR,pbs,pb0,ts,maxRL,li,dR,mRan,nR,lRan],open('dataDump2','w+'))
```

Radius Analyzer (stAnalysisNew.py)

```
import pickle
import numpy as np
from numpy import pi
import matplotlib.pyplot as plt
from scipy.interpolate import interp1d,griddata
from constants import *
import fulltime

def pFromR(r,m):
    return (r/(0.46*0.0021538*m**(1./3)))**(3./2)

def lumm(m):
    return 0.23*m**2.3*(m<0.43)+(m>=0.43)*m**4

```

```
# Read in parameter sweep
minR,maxR,pbs,pb0,ts,maxRL,li,dR,mRan,nR,lRan = pickle.load(open('dataDump2'))

# Set sweep parameters
nM = len(mRan)
nL = len(lRan)

numFigs = 6
figs = []
imm = []
for i in range(numFigs):
    figs.append(plt.figure())
    imm.append([])

# Loop over luminosities
for lIndex in range(nL):

    # Set orbital parameters
    nP = 150
    pRan = 10**np.linspace(3.5,4.8,num=nP,endpoint=True)
    rRoche = 0.46*0.0021538*(np.outer(mRan,pRan**2))**(1./3) # 0.0021538 is (GM_sun/R_sun^3*s^2/(4pi^2))^(1/3)
    rOrbit = (rRoche/0.46)*((mRan[:,np.newaxis]+2)/mRan[:,np.newaxis])**(1./3)
    flux = np.array([lRan[i]/(4*pi*rOrbit**2) for i in range(nL)])

    # Find max/min period as a function of mass
    pMax = np.zeros((nM,nL))
    pMin = np.zeros((nM,nL))
    for i in range(nM):
        for j in range(nL):
            pMax[i,j] = pFromR(maxRL[i,j],mRan[i])
            pMin[i,j] = pFromR(minR[i],mRan[i])

    # Filter pb0
    for i in range(nM):
        rRan = np.linspace(minR[i]+1e-2,maxRL[i,lIndex],num=nR,endpoint=True)
        for j in range(nR):
            if pb0[i,lIndex,j] > newtonG*mSun**2*mRan[i]**2/(4*pi*rRan[j]**4*rSun**4):
                pb0[i,lIndex,j] = newtonG*mSun**2*mRan[i]**2/(4*pi*rRan[j]**4*rSun**4)

    # Interpolate various properties
    lum = np.zeros((nP,nM))
    tss = np.zeros((nP,nM))
    radP = np.zeros((nP,nM))
    netP = np.zeros((nP,nM))
    pb00 = np.zeros((nP,nM))
    pbss = np.zeros((nP,nM))
    dRR = np.zeros((nP,nM))
    for i in range(nM):
        rRan = np.linspace(minR[i]+1e-2,maxR[i],num=nR,endpoint=True)
        interp = interp1d(rRan,li[i,lIndex,:],bounds_error=False)
        lum[:,i] = interp(rRoche[i])
        interp = interp1d(rRan,ts[i,lIndex,:],bounds_error=False)
        tss[:,i] = interp(rRoche[i])
        interp = interp1d(rRan,pb0[i,lIndex,:],bounds_error=False)
```

```
            pb00[:,i] = interp(rRoche[i])
            interp = interp1d(rRan,pbs[i,lIndex,:],bounds_error=False)
            pbss[:,i] = interp(rRoche[i])
            interp = interp1d(rRan,dR[i,lIndex,:],bounds_error=False)
            dRR[:,i] = interp(rRoche[i])

        # Compute Roche scale height
        v0 = rSun*rOrbit*2*pi/pRan[np.newaxis,:]
        hs = rSun*np.transpose(rRoche)*(5*kB/(3*mP))*(((lumm(mRan)[np.newaxis,:]+lum)*
            lSun/(4*pi*rSun**2*np.transpose(rRoche)**2*sigma))**(1./4))/np.transpose(v0)
            **2
        vs = (5*kB*(((lumm(mRan)[np.newaxis,:]+lum)*lSun/(4*pi*rSun**2*np.transpose(
            rRoche)**2*sigma))**(1./4))/(3*mP))**0.5
        for i in range(nM):
            hs[pRan>pMax[i,lIndex],i] = np.nan

        # Compute g
        g = newtonG*mRan[:,np.newaxis]*mSun/(rSun**2*rRoche**2)

        # Compute \dot{R} for expansion
        rdot = 1.4*(mP/2)*lSun*(lumm(mRan)[np.newaxis,:]-lum)*np.transpose(g)/(12*pi*np.
            transpose(rRoche)*rSun*kB*tss*pbss*(pb00/pbss)**1.4)

        # Compute contraction timescale
        time = np.zeros((nP,nM))
        for i in range(nP):
            for j in range(nM):
                rho0 = pbss[i,j]*mP/(2*tss[i,j]*kB)
                time[i,j] = fulltime.f(hs[i,j]*np.log(10),dRR[i,j],rRoche[j,i],
                    mRan[j],lumm(mRan[j])-lum[i,j],lumm(mRan[j]),rho0,pb00[i,j],
                    pbss[i,j])
                lSurf = lum[i,j] + pi*rRoche[j,i]**2*flux[lIndex][j,i]
                time[i,j] += 1e4*(lumm(mRan[j])/(lumm(mRan[j])-lum[i,j]))/(lSurf)
                    **(3./4)
        for i in range(nM):
            time[pRan>pMax[i,lIndex],i] = np.nan
            time[pRan<pMin[i,lIndex],i] = np.nan

        ax = figs[0].add_subplot(2,2,lIndex+1)
        # Plot maximum radius, minimum radius
        ax.plot(mRan,np.log10(pMax[:,lIndex]),c='k',linewidth=2)
        ax.plot(mRan,np.log10(pMin[:,lIndex]),c='k',linewidth=2)
        # Color by expansion timescale
        im = ax.imshow(np.log10(np.abs(hs/rdot)),origin='lower',extent =
            [0.08,1.3,3.5,4.8])
        imm[0].append(im)
        ax.set_xlabel('M')
        ax.set_ylabel('Log P')
        ax.set_title('$L_p='+str(lRan[lIndex])+'L_\odot$')

        ax = figs[1].add_subplot(2,2,lIndex+1)
        # Plot maximum radius, minimum radius
        ax.plot(mRan,np.log10(pMax[:,lIndex]),c='k',linewidth=2)
        ax.plot(mRan,np.log10(pMin[:,lIndex]),c='k',linewidth=2)
        # Color by rapid contraction
        im = ax.imshow(np.log10(np.abs(dRR/hs)),origin='lower',extent =
            [0.08,1.3,3.5,4.8])
```

```
        imm[1].append(im)
        ax.set_xlabel('M')
        ax.set_ylabel('Log P')
        ax.set_title('$L_p='+str(lRan[lIndex])+'L_\odot$')

        ax = figs[2].add_subplot(2,2,lIndex+1)
        # Plot maximum radius, minimum radius
        ax.plot(mRan,np.log10(pMax[:,lIndex]),c='k',linewidth=2)
        ax.plot(mRan,np.log10(pMin[:,lIndex]),c='k',linewidth=2)
        # Color by disk:expansion timescale ratio.
        logTimescaleRat = np.log10(np.abs((3e5*lRan[lIndex]**(-1./8)*np.transpose(rRoche**(5./8)))/(hs/rdot)))
        im = ax.imshow(logTimescaleRat,origin='lower',extent = [0.08,1.3,3.5,4.8])
        imm[2].append(im)
        ax.set_xlabel('M')
        ax.set_ylabel('Log P')
        ax.set_title('$L_p='+str(lRan[lIndex])+'L_\odot$')

        ax = figs[3].add_subplot(2,2,lIndex+1)
        # Plot maximum radius, minimum radius
        ax.plot(mRan,np.log10(pMax[:,lIndex]),c='k',linewidth=2)
        ax.plot(mRan,np.log10(pMin[:,lIndex]),c='k',linewidth=2)
        # Color by contraction timescale.
        im = ax.imshow(np.log10(time),origin='lower',extent = [0.08,1.3,3.5,4.8])
        imm[3].append(im)
        ax.set_xlabel('M')
        ax.set_ylabel('Log P')
        ax.set_title('$L_p='+str(lRan[lIndex])+'L_\odot$')

        ax = figs[4].add_subplot(2,2,lIndex+1)
        # Plot maximum radius, minimum radius
        ax.plot(mRan,np.log10(pMax[:,lIndex]),c='k',linewidth=2)
        ax.plot(mRan,np.log10(pMin[:,lIndex]),c='k',linewidth=2)
        # Color by contraction timescale.
        im = ax.imshow(np.log10((3e5*lRan[lIndex]**(-1./8)*np.transpose(rRoche**(5./8)))/time),origin='lower',extent = [0.08,1.3,3.5,4.8])
        imm[4].append(im)
        ax.set_xlabel('M')
        ax.set_ylabel('Log P')
        ax.set_title('$L_p='+str(lRan[lIndex])+'L_\odot$')

        ax = figs[5].add_subplot(2,2,lIndex+1)
        # Plot maximum radius, minimum radius
        ax.plot(mRan,np.log10(pMax[:,lIndex]),c='k',linewidth=2)
        ax.plot(mRan,np.log10(pMin[:,lIndex]),c='k',linewidth=2)
        # Color by contraction timescale.
        tML = time
        tDisk = 3e5*lRan[lIndex]**(-1./8)*np.transpose(rRoche**(5./8))
        tSpread = (2./5)*((mRan/(mRan+2))*(vs/np.transpose(v0))**2)**(-3./8)*tDisk
        pdata = 1.0*(tML>tDisk)+1.0*(tML>tSpread)
#       pdata = np.log10(np.abs(hs/rdot))
        pdata[np.isnan(np.log10(np.abs(hs/rdot)))] = np.nan
        im = ax.imshow(pdata,origin='lower',extent = [0.08,1.3,3.5,4.8])
        imm[5].append(im)
        ax.set_xlabel('M')
        ax.set_ylabel('Log P')
        ax.set_title('$L_p='+str(lRan[lIndex])+'L_\odot$')
```

```



mins = [1e10 for i in range(numFigs)]
maxs = [-1e10 for i in range(numFigs)]
for i in range(numFigs):
	for j in range(nL):
		ran = imm[i][j].get_clim()
		if ran[0]<mins[i]:
			mins[i] = ran[0]
		if ran[1]>maxs[i]:
			maxs[i] = ran[1]
for i in range(numFigs):
	for j in range(nL):
		imm[i][j].set_clim(mins[i],maxs[i])

cax = figs[0].add_axes([0.85,0.1,0.03,0.8])
cbar = figs[0].colorbar(imm[0][0],cax=cax)
cbar.set_clim(mins[0],maxs[0])
cbar.set_label('Log $h_s/\dot{R}$')
cax = figs[1].add_axes([0.85,0.1,0.03,0.8])
cbar = figs[1].colorbar(imm[1][0],cax=cax)
cbar.set_clim(mins[1],maxs[1])
cbar.set_label('Log $\Delta R/h_s$')
cax = figs[2].add_axes([0.85,0.1,0.03,0.8])
cbar = figs[2].colorbar(imm[2][0],cax=cax)
cbar.set_clim(mins[2],maxs[2])
cbar.set_label('Log $\\tau_\mathrm{disk}/\\tau_\mathrm{exp}$')
cax = figs[3].add_axes([0.85,0.1,0.03,0.8])
cbar = figs[3].colorbar(imm[3][0],cax=cax)
cbar.set_clim(mins[3],maxs[3])
cbar.set_label('Log $\\tau_\mathrm{contraction}$')
cax = figs[4].add_axes([0.85,0.1,0.03,0.8])
cbar = figs[4].colorbar(imm[4][0],cax=cax)
cbar.set_clim(mins[4],maxs[4])
cbar.set_label('Log $\\tau_\mathrm{disk}/\\tau_\mathrm{contraction}$')
#cax = figs[5].add_axes([0.85,0.1,0.03,0.8])
#cbar = figs[5].colorbar(imm[5][0],cax=cax)
#cbar.set_clim(mins[5],maxs[5])
#cbar.set_label('Cycle Type')

for i in range(len(figs)):
	figs[i].tight_layout()
	if i!=5:
		figs[i].subplots_adjust(right=0.8)

figs[0].savefig('Plots/'+'L_expansionTime.pdf',dpi=200)
figs[1].savefig('Plots/'+'L_contraction.pdf',dpi=200)
figs[2].savefig('Plots/'+'L_TimeRatio.pdf',dpi=200)
figs[3].savefig('Plots/'+'L_contractionTime.pdf',dpi=200)
figs[4].savefig('Plots/'+'L_contractionTimeRatio.pdf',dpi=200)
figs[5].savefig('Plots/'+'L_cycleType.pdf',dpi=200)
```

Red Giant Caller (redGiant.py)

```
from starTracker import *
import numpy as np
```

```
import pickle
from numpy import pi
from multiprocessing import Pool

nM = 10
nC = 10
p = 22 # days

lRan = np.array([1.,10.,25.,50.])
nL = len(lRan)
mRan = np.linspace(1.,2.5,num=nM,endpoint=True)
cRan = np.linspace(0.2,0.3,num=nC,endpoint=True)

minR = np.zeros((nM,nC))
maxR = np.zeros((nM,nC))
tKel = np.zeros((nM,nC))
tExp = np.zeros((nM,nC,nL))
li = np.zeros((nM,nC))

for i in range(nM):
        for j in range(nC):
                s = starT(mRan[i],sc=1e6,mc=cRan[j])
                minR[i,j] = s.r0
                maxR[i,j] = s.rMax
                tKel[i,j] = 6*10**14*mRan[i]**2/s.r0/s.l
                li[i,j] = s.l
                r = (216./25)*p**(2./3)
                print i,j
                for k in range(nL):
                        le = (1./4)*lRan[k]*(s.r0**2/r**2)
                        tExp[i,j,k] = tKel[i,j]*s.l/min(le,s.l)

pickle.dump([nM,nC,nL,p,mRan,cRan,lRan,minR,maxR,li,tKel,tExp],open('dataDumpRed','w+'))
```

Red Giant Analysis (redAnalysis.py)

```
import pickle
import numpy as np
from numpy import pi
import matplotlib.pyplot as plt
from constants import *

nM,nC,nL,p,mRan,cRan,lRan,minR,maxR,li,tKel,tExp = pickle.load(open('dataDumpRed'))

plt.imshow(maxR/30,origin='lower',extent=[0.2,0.3,1,2.5],aspect=0.07)
plt.xlabel('$M_c (M_\odot)$')
plt.ylabel('$M (M_\odot)$')
plt.colorbar()
plt.savefig('Plots/redgiants.pdf',dpi=200)
```

References

Ferguson, Jason W. et al. “Low-Temperature Opacities”. In: *The Astrophysical Journal* 623.1 (2005), p. 585. URL: `http://stacks.iop.org/0004-637X/623/i=1/a=585` (cit. on p. 207).

Iglesias, C. A. and F. J. Rogers. “Updated Opal Opacities”. In: *The Astrophysical Journal* 464 (June 1996), p. 943. DOI: `10.1086/177381` (cit. on p. 207).

Paczyński, B. “Envelopes of Red Supergiants”. In: *Acta Astronomica* 19 (1969), p. 1 (cit. on p. 211).

Appendix C

Gob Stellar Integration Code

The unmodified Gob code[1] is shown below. It may be compiled with gfortran version 4.9.0 20140201 via the command

```
gfortran -std=legacy gob84.f
```

Following the original code is the output of the Unix 'diff' command run with the original code and our modified version as its arguments in that order. This may be used in conjunction with the original code to produce the new code[2]. The new version incorporates our modifications to accommodate an input heat at a column density of $1000\frac{\text{g}}{\text{cm}^2}$. In addition, it uses more numerical precision than the previous version, and has a much more extensive output, giving many more atmospheric quantities of interest. It also uses command line arguments rather than interactive input. The code may be compiled with the same version of gfortran using the command

```
gfortran -std=legacy -fdefault-real-8 gobV5.f,
```

where gobV5.f is the filename of the new version. The opacity table used by Gob is shown next. Finally, the first author also wrote a Python script for interfacing with Gob. This is shown at the end of this Appendix. Note that this script is Cython-compatible, and calling it in a Cython context significantly improves performance. Further note that this script requires the new version of Gob, and requires that it be compiled into an executable named 'gob' in the same directory. This script was used to test Acorn, which was ultimately used to generate the figures and data tables in this document.

Gob - Original

```
************************************************************************

************************************************************************
      program gob84
c - "gob84.for" has been tested at Princeton on IBM PC/XT on Sept., 24, 1984
c -----------------------------------------------------------------------
c
c                input:
c
c   unit=1, file='opacity.dat'     opacity data made by caokap.f
c   unit=*, terminal,              control variables
c ------------------------------------------------------------------------
c
c                output:
```

[1] B. Paczyński. "Envelopes of Red Supergiants". In: *Acta Astronomica* 19 (1969), p. 1.

[2] The Unix 'patch' command may be used to do this.

```
c
c    unit=2, file='obc.dat'      outer boundary conditions to be used by
c                                              sch.f and hen.f
c    unit=3, file='print.gob'     results to be printed
c    unit=*, terminal,            condensed output.
c ----------------------------------------------------------------------------
      real m,l,rp,rop,tauf,alfa,x,y,tp,ya,h,dt,vt,vad,fac,tauc,
     *     grad,gradad,gradra,tmax,kap,xx,xp,yy,w,acc,mbol
      integer i,j
      common/fpso/vad,grad,gradad,gradra,rp,tauf,tp,ya,m
      common/kapa/kap(51,31)
      common/dens/rhc1,rhc2,rhc3,xh1,xhe1,xhe2,error
      common/dathe2/he2lim,zav
      dimension xx(6),xp(6),yy(6),w(6),acc(5)

      write(*,*)' program "gob84.f" is running '
      open(1,file='opacity.dat')
      rewind(1)
      open(2,file='obc.dat')
      rewind(2)
      open(3,file='print.gob')
      rewind(3)

c ------------------------ read the opacities ---------------------------
 100  format(2f8.5)
      read (1,100) x,z
      i=0
      k2=0
 300  continue
      i=i+1
      if(i.gt.51)go to 304
 301  format(1x,i5,14f5.2)
      k2=k2+1
      read (1,301) k1,(kap(i,j),j=1,14)
      if(k1.ne.k2)go to 302
      k2=k2+1
      read (1,301) k1,(kap(i,j),j=15,28)
      if(k1.ne.k2)go to 302
      k2=k2+1
      read (1,301) k1,(kap(i,j),j=29,31)
      if(k1.ne.k2)go to 302
      go to 300
 302  continue
 303  format(1x,21hwrong opacity card,k=,i3)
      write(*,303)k2
      call exit
 304  continue
 305  format(7f6.4,3e8.1,i4)

c ------------------------------ setting some control constants ----------
      tauf=2.0/3.0
      alfa=1.0
      rop=1.1e-12
      tmax=1.5e8
      rmin=0.01
      acc(1)=0.2
      acc(2)=0.05
```

```
      acc(3)=0.15
      acc(4)=0.05
      acc(5)=0.1
c ----------------------------  end of constants --------------------------


c ---------------------------- begin a set of envelopes ------------------
  400 continue
      write(*,106)x,z
  106 format(1x,4h x =,f9.6,8h      z =,f9.6,/,
     * 59h  m, fm, flp1 , tp1 , dflp , dtp , nflp , ntp , iprint , alpha = ?)

c ----------------- input the control parameters from the terminal -----

      read(*,*)m,fm,flp1,tp1,dflp,dtp,nflp,ntp,iprint,alfa
      if(m.le.0.) call exit

c ------- set the values of critical densities for pressure ionization:
c                          "rhc1", "rhc2", "rhc3"
c ------- the value of critical second helium ionization: "helim2"
c ------- and the average charge of "metals": "zav" .
      rhcl1=-1.0
      rhcl2=-0.5
      rhcl3=0.0
      he2lim=0.99
      zav=10.0
      rhc1=10.0**rhcl1
      rhc2=10.0**rhcl2
      rhc3=10.0**rhcl3

      y=1.0-x-z
  310 format(1x,2f7.4,2f9.6,5f6.3,2i4)
      if(iprint.le.0)
     *write (*,310) m,fm,x,z,alfa,flp1,tp1,dflp,dtp,nflp,ntp
      write (2,310) m,fm,x,z,alfa,flp1,tp1,dflp,dtp,nflp,ntp
      write (3,199) rhcl1,rhcl2,rhcl3,xxx
  199 format(1x,'␣log␣rhc1,␣log␣rhc2,␣log␣rhc3,␣xxx␣=␣',4f8.4)
      write(3,101)
  101 format(//,30x,'␣printed␣results␣from␣program␣gob84.f␣',/,1x,
     *42h m/msun fm/msun   x      z     alpha   log Lo,
     *33h log To  d logL  d logT nL nT ipr)
  102 format(1x,9f7.4,3i4)
      write (3,102) m,fm,x,z,alfa,flp1,tp1,dflp,dtp,nflp,ntp,iprint
      write (3,199) rhcl1,rhcl2,rhcl3
      ipr=iprint


c ----------------------------------------- envelope integrations begin ----------
      do 311 nfl=1,nflp
      do 311 nt=1,ntp
      xh1=0.0
      xhe1=0.0
      xhe2=0.0
      ermax=-10.0
      iprint=ipr
      fl=flp1+(nfl-1)*dflp
      ft=tp1+(nt-1)*dtp
```

```
      l=10.0**fl
      tp=10.0**ft
      rp=sqrt(5.6e14*l)/tp/tp
      ya=1.0
      dt=0.0
      mbol=4.74-1.0857*alog(l)
      rplog=alog10(rp)
      roplog=alog10(rop)
  105 format(1x,13h log l/lsun =,f6.3,11h    m bol =,f6.3,
     * 16h    log r/rsun =,f6.3,12h    log t0 =,f6.3)
  104 format(1x,35h   l dm    l t   l rho    l r   l tau,
     * 41h   l gr   l ga   l ra  xh1 xhe1 xhe2  err)
  103 format(1x,8f7.2,3f5.2,f6.2)
      if(iprint.le.0)go to 2
      write(*,105)fl,mbol,rplog,ft
      write(*,104)
      write(3,105)fl,mbol,rplog,ft
      write(3,103)
      write(3,104)
      write(3,103)
    2 continue
      xx(1)=1.0e-30
      xx(2)=tp
      xx(3)=rop
      xx(4)=rp
      xx(5)=1.0e-30
      xx(6)=0.0
      k=0

  109 continue
      k=k+1
      if(k.gt.300)go to 115
      do 110 i=1,6
      w(i)=xx(i)
  110 continue
      call pso(xx,x,y,l,alfa,yy,vt,dturb)
      if(error.gt.ermax)ermax=error
      iprint=iprint+1
      if(iprint.lt.0.or.ipr.lt.0)go to 1002
      iprint=-ipr
      dmlog=alog10(xx(1))
      tlog=alog10(xx(2))
      rhlog=alog10(xx(3))
      rlog=alog10(xx(4))
      taulog=alog10(xx(5))
      grl=alog10(grad)
      gal=alog10(gradad)
      gral=alog10(gradra)
      write(*,103)dmlog,tlog,rhlog,rlog,taulog,grl,gal,gral
     * ,xh1,xhe1,xhe2,error
      write(3,103)dmlog,tlog,rhlog,rlog,taulog,grl,gal,gral
     * ,xh1,xhe1,xhe2,error
 1002 continue

c ------------------------------ choose an integration step = h  ---------------
      h=0.0
      if(xx(5).lt.tauf)h=abs(yy(5)/acc(5))
```

```
      if(h.lt.1./acc(1)/(m-xx(1)))h=1./acc(1)/(m-xx(1))
      do 120 i=2,4
      if(h.lt.abs(yy(i)/acc(i)/xx(i)))h=abs(yy(i)/acc(i)/xx(i))
  120 continue
      h=-1./h
c ---------------------------- integration step = h   has been chosen -----------

      iend=-1
      if((xx(1)-h).lt.fm)go to 307
      h=xx(1)-fm
      iend=1
  307 continue
      do 111 i=1,6
      xp(i)=xx(i)+0.5*h*yy(i)
  111 continue
      call pso(xp,x,y,l,alfa,yy,vt,dturb)
      do 112 i=1,6
      xx(i)=xx(i)+h*yy(i)
  112 continue
c ------------------------------- an integration step has been completed ---------
      dt=-6.96e10*h*yy(4)/vad
      if(iend.lt.0)go to 313
      if(ipr.lt.0)go to 1003
      dmlog=alog10(xx(1))
      tlog=alog10(xx(2))
      rhlog=alog10(xx(3))
      rlog=alog10(xx(4))
      taulog=alog10(xx(5))
      grl=alog10(grad)
      gal=alog10(gradad)
      gral=alog10(gradra)
      write(*,103)dmlog,tlog,rhlog,rlog,taulog,grl,gal,gral
     * ,xh1,xhe1,xhe2,error
      write(3,103)dmlog,tlog,rhlog,rlog,taulog,grl,gal,gral
     * ,xh1,xhe1,xhe2,error
 1003 continue
      go to 115
  313 continue
      tauc=-1.0
      if(xx(5).gt.0.05.and.w(5).lt.0.05)tauc=0.05
      if(xx(5).gt.tauf.and.w(5).lt.tauf)tauc=tauf
      if(tauc.lt.0.)go to 113
      fac=(xx(5)-tauc)/(xx(5)-w(5))
      do 114 i=1,6
      w(i)=fac*w(i)+(1.-fac)*xx(i)
  114 continue
      if(ipr.lt.0)go to 1004
c ------------------------ printing at optical depth = 0.05, 0.66667 ------------
      dmlog=alog10(w(1))
      tlog=alog10(w(2))
      rhlog=alog10(w(3))
      rlog=alog10(w(4))
      taulog=alog10(w(5))
      write(*,103)dmlog,tlog,rhlog,rlog,taulog
      write(3,103)dmlog,tlog,rhlog,rlog,taulog
 1004 continue
      if(abs(1.0-tauc/tauf).lt.0.01)tef=alog10(w(2))
```

```
  113 continue
      if(xx(2).gt.tmax)go to 115
      if(xx(1).gt.0.9*m)go to 115
      if(xx(3).gt.1000.)go to 115
      if(xx(3).lt.1.e-12.and.xx(5).gt.tauf)go to 115
      go to 109
c ---------------------------------------------- end of integration ----------

c ------------------------------ preparations of output at the base of envelope
  115 continue
      if(xx(2).lt.tmax)go to 116
      fac=(xx(2)-tmax)/(xx(2)-w(2))
      do 117 i=1,6
      w(i)=fac*w(i)+(1.-fac)*xx(i)
  117 continue
      fac=w(6)/w(1)
  116 continue
      fac=617.*sqrt(abs(fac))*sign(1.,fac)
      ref=7.5246+0.5*fl-2.0*tef
      ti=alog10(xx(2))
      rhoi=alog10(xx(3))
      ri=alog10(xx(4))
  308 format (1x,9f8.4,f6.2)
      write (*,308) m,fm,fl,ft,tef,ref,ti,rhoi,ri,ermax
      write (3,308) m,fm,fl,ft,tef,ref,ti,rhoi,ri,ermax
      write (2,308) m,fm,fl,ft,tef,ref,ti,rhoi,ri
  311 continue
c -------------------------------------- envelope integrations end -----------|


      go to 400
      end
*******************************************************************************

*******************************************************************************
      subroutine pso(xx,x,y,lr,alfa,yy,vt,delt)
      real xx,x,y,lr,alfa,yy,mr,t,ro,r,q,cp,p,dpro,dpt,kp,dpm,g,hp,
     * lt,u,omega,a,gamma,sqc,sqg,v,grop,vad,grad,gradad,gradra,rp,tauf,
     * tp,ya,m,vt,kappa
      dimension xx(6),yy(6)
      common/fpso/vad,grad,gradad,gradra,rp,tauf,tp,ya,m
      mr=m-xx(1)
      t=xx(2)
      ro=xx(3)
      r=xx(4)
      call termo(ro,t,x,y,1.,q,cp,gradad,p,dpro,dpt,u,cv,vad)
      kp=kappa(ro,t)
      dpm=-8.97e14*mr/r**4
      yy(4)=0.470/r**2/ro
      yy(5)=-3.27e10/r**2*kp
      yy(6)=mr/r-5.24e-16*u
      yy(1)=-1.0
      gradra=7.65e9*kp*p/t**4*lr/mr
      if(xx(5).gt.tauf)go to 40
      a=1.285e-26*(lr*r**2)**0.25*(1-xx(5)/tauf)/ro/mr*t**3
      dpm=dpm*(1.+a)
      gradra=gradra*(1+1.296e4*mr/lr/kp*a)/(1+a)
```

```
   40 continue
      if(gradra.gt.gradad)go to 41
      grad=gradra
      vt=0.0
      delt=0.0
      go to 42
   41 continue
      g=2.74e4*mr/r**2
      hp=p/ro/g
      lt=alfa*hp
      omega=kp*ro*lt
      a=1.125*omega**2/(3.+omega**2)
      gamma=826.7*cp*ro/t**3*omega/a
      sqc=lt*sqrt(g*q/8./hp)
      sqg=sqrt(gradra-gradad)
      v=1./gamma/sqc/sqg
      a=2*a/v
   43 continue
      vt=(1.-ya*(v+ya*(1.+ya*a)))/(v+ya*(2.+ya*3.*a))
      ya=ya+vt
      if(abs(vt/ya).gt.0.001)go to 43
      vt=sqc*sqg*ya
      grad=gradad+(gradra-gradad)*ya*(ya+v)
      delt=t*4.0*vt*vt/g/lt/q
   42 continue
      grop=(p-grad*t*dpt)/ro/dpro
      yy(2)=grad*t/p*dpm
      yy(3)=grop*ro/p*dpm
      return
      end
**************************************************************************

**************************************************************************
      real function kappa(ro,te)
      common/kapa/kap(51,31)
      real ro,te,d,t,kapp,kap
      integer di,ti
      d=2.0*alog10(ro)+25.0
      di=int(d)
      d=d-di
      t=20.*alog10(te)-65.
      if(t.gt.35.)t=35.+(t-35.)/4.
      ti=int(t)
      t=t-ti
      if(di.ge.1)go to 30
      di=1
      d=0.
   30 continue
      if(di.le.30)go to 31
      di=30
      d=1.
   31 continue
      if(ti.ge.1)go to 32
      ti=1
      t=0.
   32 continue
      if(ti.le.50)go to 33
```

```
      ti=50
      t=1.
   33 continue
      kapp=(1.-t)*((1.-d)*kap(ti,di)+d*kap(ti,di+1))+
     *     t*((1.-d)*kap(ti+1,di)+d*kap(ti+1,di+1))
      kappa=exp(2.3026*kapp)
      return
      end
************************************************************************

************************************************************************
      subroutine termo(ro,t,x,y,typ,q,cp,gradad,p,dpro,dpt,u,dut,vad)
c --------------------------------------
c   input:
c       ro       density(c.g.s.)
c       t        temp(k)
c       x        hydrogen mass fraction
c       y        helium mass fraction
c       typ      control variable:
c                        > 0 include radiation in ionization region
c                        <=0 neglect radiation in ionization region
c   output:
c       q        -(d ln rho /d ln t)p                          |
c       cp       (du/dt)p   specific heat cap. at const p      |
c       gradad   (d ln t/d ln p)s   adiabatic gradient         |
c       p        pressure (c.g.s.)                             |
c       dpro     (dp/drho)t                                    |--> c.g.s.k.
c       dpt      (dp/dt)rho                                    |
c       u        specific internal energy                      |
c       dut      (du/dt)rho  specific heat cap. at const vol.  |
c       vad      adiabatic sound speed                         |
c
c       an adjustment is made to take into account weak electron degen.,
c       here for full ionization, in energ for partial ionization
c -----------------------------------------------------------------------*
c
      real ro,t,x,y,typ,q,cp,gradad,p,dpro,dpt,u,vad,p1,p2,p3,p4,u1,u2,
     *     u3,u4,duro,dut,z,nelect,nnucl,mue,ndgen
      common/dens/rhc1,rhc2,rhc3,xh1,xhe1,xhe2,error
      common/dathe2/he2lim,zav
c
      z = 1.-x-y
c
      if(xhe2.lt.he2lim)go to 2
c
c -------- full ionization -------------------------------------------------
c
      xh1=1.0
      xhe1=0.0
      xhe2=1.0
c
c  p1 is for particles, p2 is for photons
c
        nelect = (x+y/2.+z/2.)
        nnucl  = (x+y/4.+z/zav/2.)
        mue    = (1.+x)/2.
        ndgen  = nelect*(1. + 2.19e-2*(ro/mue)*(t/1.e6)**(-1.5))
```

```
c     p1=0.825075e8*(0.5+1.5*x+0.25*y)   old less accurate way
      p1=0.825075e8*(ndgen + nnucl)
      p2=2.523e-15*t**3/ro
      p=(p1+p2)*ro*t
      u=(1.5*p1+3.*p2)*t+1.516e13*x+1.890e13*y
c
      dpro=p1*t
      dpt=(p1+4.*p2)*ro
      duro=-3.*p2*t/ro
      dut=1.5*p1+12.*p2
      go to 3
c
    2 continue
c
c -------------- partial ionization of hydrogen and helium ------------------
c
      call energ(ro,0.999*t,x,y,p1,u1,typ)
      call energ(ro,1.001*t,x,y,p2,u2,typ)
      call energ(0.999*ro,t,x,y,p3,u3,typ)
      call energ(1.001*ro,t,x,y,p4,u4,typ)
c
      p=(p1+p2+p3+p4)*0.25
      u=(u1+u2+u3+u4)*0.25
c
      dpro=(p4-p3)/ro*500.
      dpt=(p2-p1)/t*500.
      duro=(u4-u3)/ro*500.
      dut=(u2-u1)/t*500.
c
    3 continue
c
c ----- evaluation of more complex thermodynamic functions and the error
c
      q=t/ro*dpt/dpro
      cp=dut+q/ro*dpt
      gradad=p*q/cp/ro/t
      vad=sqrt(dpro*cp/dut)
c
      er1=abs(1-t/p*dpt-duro*ro**2/p)+1.0e-10
      error=alog10(er1)
c
      return
      end
**********************************************************************

**********************************************************************
      subroutine energ(ro,t,x,y,p,u,typ)
c ----------------------------------------
c   input:
c       ro      density(c.g.s.)
c       t       temp(k)
c       x       hydrogen mass fraction
c       y       helium mass fraction
c       typ     control variable:
c                       > 0 to include radiation
c                       <=0 to neglect radiation
c   output:
```

```
c       p       pressure(c.g.s.)
c       u       specific internal energy
c
c               the gas is assumed non-relativistic.  a first-order
c               electron-degeneracy correction is made.
c               the metals are assumed to be fully ionized (poor assumption)
c----------------------------------------------------------------------*
      real ro,t,x,y,p,u,typ,nt,nh2,nhi,nhii,nhei,nheii,nheiii,ne,pg,pr,
     *     uh2,teta,logt,h,dm,fac,nh,nhe,nmet,mue,nmetel,nedgen
c
      common/dens/rhc1,rhc2,rhc3,xh1,xhe1,xhe2,error
      common/dathe2/he2lim,zav
c
c ------ rhc1, rhc2, rhc3  are critical densities for "pressure ionization"
c
      teta=5040./t
      dm=2.302585
      tm=1/teta/dm
      logt=alog10(t)
      mue = (1.+x)/2.
c
      h=1.6734e-24
      nh=x*ro/h
      nhe=0.25*y*ro/h
      nmet=1./zav/2.*(1.0-x-y)*ro/h
c ----assume metals fully ionized
      nmetel=nmet*zav
      ne=0.0
      nhi=nh
      nhii=0.0
      nhei=nhe
      nheii=0.
      nheiii=0.
c
      xh1=0.0
      xhe1=0.0
      xhe2=0.0
c
      fac1=0.0
      fac2=0.0
      fac3=0.0
c
c ----------------- hydrogen ionization
      hi1=13.595
      hi=hi1*(1-ro/rhc1*(1+tm/hi1))
      fhl=alog10(nh)
      b10=15.3828+1.5*logt-hi*teta-fhl
      if(b10.gt.10.0)b10=10.0
      if(b10.lt.(-10.0))go to 21
      b=10.0**b10
      c=b
      fac1=c*nh
      bc=0.5*b/c
      xx=1.0/(sqrt(bc*bc+1.0/c)+bc)
c
c ------ "xx" is the positive root of equation: " xx**2 + b*xx - c = 0 "
      xx1=1.0-xx
```

```
      if(xx1.lt.1.0e-10)xx1=1.0e-10
      nhii=nh*xx
      ne=nhii
      nhi=nh*xx1
      xh1=xx
c
c ------------------ first helium ionization
      hi2=24.580
      hi=hi2*(1-ro/rhc2*(1+tm/hi2))
      fhel=alog10(nhe)
      b10=15.9849+1.5*logt-hi*teta-fhel
      if(b10.gt.10.0)b10=10.0
      if(b10.lt.(-10.0))go to 21
      c=10.0**b10
      b=c+ne/nhe
      fac2=c*nhe
      bc=0.5*b/c
      xx=1.0/(sqrt(bc*bc+1.0/c)+bc)
      xx1=1.0-xx
c
      if(xx1.lt.1.0e-10)xx1=1.0e-10
      nheii=nhe*xx
      ne=ne+nheii
      nhei=nhe*xx1
      xhe1=xx
c
c ------------------- second helium ionization
      hi3=54.403
      hi=hi3*(1-ro/rhc2*(1+tm/hi3))
      fhel=alog10(nheii)
      b10=15.3828+1.5*logt-hi*teta-fhel
      if(b10.gt.10.0)b10=10.0
      if(b10.lt.(-10.0))go to 20
      c=10.0**b10
      b=c+ne/nheii
      fac3=c*nheii
      bc=0.5*b/c
      xx=1.0/(sqrt(bc*bc+1.0/c)+bc)
      xx1=1.0-xx
c
      if(xx1.lt.1.0e-10)xx1=1.0e-10
      nheiii=nheii*xx
      ne=ne+nheiii
      nheii=nheii*xx1
      xhe2=xx
   20 continue
c
c ----------------- correct the ionization of hydrogen and helium --
      f1=fac1/ne
      f2=fac2/ne
      f3=fac3/ne
      f4=nh/ne
      f5=y/4/x
      zz=1.0
c
      call fzz(zz,f1,f2,f3,f4,f5)
c
```

```
      ne=ne*zz
      xh1=f1/(1+f1)
      xhe1=f2/(1+f2*(1+f3))
      xhe2=xhe1*f3
c
      nhi=nh*(1-xh1)
      nhii=nh*xh1
      nhei=nhe*(1-xhe1-xhe2)
      nheii=nhe*xhe1
      nheiii=nhe*xhe2
c
c ------------------------- molecular hydrogen ----------------------------------
   21 continue
      nh2=0.
      if(nhi.lt.0.001*nh.or.t.gt.20000.)go to 22
      fac=28.0925-teta*(4.92516-teta*(0.056191+teta*0.0032688))-logt
      if(t.gt.12000.)fac=fac+(t-12000.)/1000.
      fac=exp(dm*fac)
      if(fac.lt.(1.0e-20*nhi))go to 23
      b=fac/nhi
      c=b
      bc=0.5*b/c
      xx=1.0/(sqrt(bc*bc+1.0/c)+bc)
      nh2=0.5*nhi*(1-xx)
      nhi=nhi*xx
c
c ---------------------- calculation of energy and pressure
c
   22 continue
c -------corr. for slight electron degeneracy
        nedgen = (nmetel+ne)*(1. + 2.19e-2*(ro/mue)*(t/1.e6)**(-1.5))
      nt=nh-nh2+nhe+nedgen+nmet
      pg=1.3805e-16*nt*t
      pr=0.
      if(typ.gt.0.)pr=2.523e-15*t**4
      p=pg+pr
      uh2=t*(2.1+t*2.5e-4)
      if(t.gt.3000.)uh2=-1890.+t*(3.36+t*0.4e-4)
      u=(1.5*pg+3.*pr+1.3805e-16*nh2*uh2+3.585e-12*nhi+25.36e-12*nhii+
     & 39.37e-12*nheii+126.52e-12*nheiii)/ro
      return
c
   23 continue
      nh2=0.5*nhi
      nhi=0.0
      go to 22
c
      end
**************************************************************************

**************************************************************************
      subroutine fzz(zz,f1,f2,f3,f4,f5)
c-------------------------------------------------------------------------
c input:
c     zz = a guess of correcting factor to the electron density (=1.0)
c     f1,f2,f3 = ionization factors divided by electron density
c     f4 = number density of hydrogen ions and atoms / electron number density
```

```
c     f5 = ratio of helium to hydrogen nuclei
c output:
c     zz = the iterated value of the correcting factor
c     f1,f2,f3 = ionization factors divided by the corrected electron density
c-----------------------------------------------------------------------
      del=0.001
      acc=0.00001
      itmax=30
      iter=0
    1 continue
      iter=iter+1
      if(iter.gt.itmax)go to 2
      call funzz(zz,f1,f2,f3,f4,f5,fz)
      if(abs(fz).lt.acc)go to 3
      zz1=zz+del
      call funzz(zz1,f1,f2,f3,f4,f5,fz1)
      dz=del*fz/(fz-fz1)
      zz=zz+dz
      go to 1
    2 continue
      write(0,*)' fzz iterations do not converge'
      stop
    3 continue
c ------------ iterations converged ---------------------------
      f1=f1/zz
      f2=f2/zz
      f3=f3/zz
      return
      end
************************************************************************

************************************************************************
      subroutine funzz(zz,f1,f2,f3,f4,f5,fz)
c-----------------------------------------------------------------------
      fz=f1/(f1+zz)+f5*f2*(zz+2*f3)/(zz*zz+f2*(zz+f3))-zz/f4
      return
      end
************************************************************************

************************************************************************
```

Gob - Modified, Diff

```
4c4
<       program gob84
---
>       program gobV5
5a6,7
> c -
> c - modified (to gobV5)  by asj to include external heating April 2014
21,22c23,25
<       real m,l,rp,rop,tauf,alfa,x,y,tp,ya,h,dt,vt,vad,fac,tauc,
<      *     grad,gradad,gradra,tmax,kap,xx,xp,yy,w,acc,mbol
---
>       real(8) m,l,rp,rop,tauf,alfa,x,y,tp,ya,h,dt,vt,vad,fac,tauc,
>      *     grad,gradad,gradra,tmax,kap,xx,xp,yy,w,acc,mbol,dlm,le,
>      *     kappaGamma,l0,u,lu,gamma,cp,cv
```

```
23a27
>       CHARACTER(LEN=100) :: arg
85,86c89,116
<
<       read(*,*)m,fm,flp1,tp1,dflp,dtp,nflp,ntp,iprint,alfa
---
> c Note that kappaGamma is in units of M0/R0^2, so 2.43e-15 is equivalent
> c to 1e-3g/cm^2
> c le is the external luminosity being deposited.
> c ---------------------------------------------------------------------
>       CALL getarg(1,arg)
>       read(arg,*) m
>       CALL getarg(2,arg)
>       read(arg,*) fm
>       CALL getarg(3,arg)
>       read(arg,*) flp1
>       CALL getarg(4,arg)
>       read(arg,*) tp1
>       CALL getarg(5,arg)
>       read(arg,*) dflp
>       CALL getarg(6,arg)
>       read(arg,*) dtp
>       CALL getarg(7,arg)
>       read(arg,*) nflp
>       CALL getarg(8,arg)
>       read(arg,*) ntp
>       CALL getarg(9,arg)
>       read(arg,*) iprint
>       CALL getarg(10,arg)
>       read(arg,*) alpha
>       CALL getarg(11,arg)
>       read(arg,*) kappaGamma
>       CALL getarg(12,arg)
>       read(arg,*) fle
121a152
>       dlm=0.0
129a161,163
>       l0=l
>       le=10.0**fle
>       l=le+l
130a165,166
> c 5.6e14=(4pi*R_sun^2*K^4*sigma*2/L_sun)^(-1)
> c The factor of 2 comes from correcting to effective temperature
134,136c170,172
<       mbol=4.74-1.0857*alog(l)
<       rplog=alog10(rp)
<       roplog=alog10(rop)
---
>       mbol=4.74-1.0857*log(l)
>       rplog=log10(rp)
>       roplog=log10(rop)
139,141c175,178
<   104 format(1x,35h   l dm     l t   l rho     l r   l tau,
<        * 41h   l gr    l ga    l ra   xh1 xhe1 xhe2   err)
<   103 format(1x,8f7.2,3f5.2,f6.2)
---
>   104 format(1x,43h   l dm     l t   l rho     l r   l tau     l gr,
```

```
>      * 60h   l ga    l ra   xh1 xhe1 xhe2   err     lpressure   l lu grr grb,
>      * 30h   gr   lu     vad vt gamma cp cv)
>   103 format(1x,23f20.8)
157d193
<
164c200,201
<         call pso(xx,x,y,l,alfa,yy,vt,dturb)
---
> c ---------------------------------------------------------------------------
>         call pso(xx,x,y,l,alfa,yy,vt,dturb,p,u,gamma,cp,cv)
169,176c206,242
<         dmlog=alog10(xx(1))
<         tlog=alog10(xx(2))
<         rhlog=alog10(xx(3))
<         rlog=alog10(xx(4))
<         taulog=alog10(xx(5))
<         grl=alog10(grad)
<         gal=alog10(gradad)
<         gral=alog10(gradra)
---
>         dmlog=log10(xx(1))
>         tlog=log10(xx(2))
>         rhlog=log10(xx(3))
>         rlog=log10(xx(4))
>         taulog=log10(xx(5))
>         grl=log10(grad)
>         gal=log10(gradad)
>         gral=log10(gradra)
>         lu = log10(u)
> c ---------------------------------------------------------------------------
> c dmlog = Log(mass) in solar units
> c tlog = Log(T_surface) in K. Note that T_eff is the surface temperature (i.e.
> c     photosphere), offset from the effective temperature by
> c     T_eff=2^(1/4) T_surf.
> c rhlog = Log(density) in c.g.s.
> c rlog = Log(radius) in solar units
> c taulog = Log(optical depth)
> c grl = log(true gradient)
> c gal = log(adiabatic gradient)
> c gral = log(radiative gradient)
> c xh1 = ?
> c xhe1 = ?
> c xhe2 = ?
> c error = error
> c p = pressure in c.g.s.
> c l = luminosity in solar units
> c gradra = radiative gradient
> c gradad = adiabatic gradient
> c grad = true gradient
> c lu = log(specific energy density) in c.g.s.
> c vad = adiabatic sound speed
> c vt = Convective speed
> c gamma = convection efficiency (in units of 1/vt)
> c cp = heat capacity at constant pressure (per unit mass) in c.g.s.
> c dut = heat capacity at constant volume (per unit mass) in c.g.s.
> c asj 7/10/2014
> c ---------------------------------------------------------------------------
```

```
178c244,245
<      * ,xh1,xhe1,xhe2,error
---
>      * ,xh1,xhe1,xhe2,error,log10(p),log10(l),gradra,gradad,grad,lu
>      * ,vad,vt,gamma,cp,cv
180c247,248
<      * ,xh1,xhe1,xhe2,error
---
>      * ,xh1,xhe1,xhe2,error,log10(p),log10(l),gradra,gradad,grad,lu
>      * ,vad,vt,gamma,cp,cv
201c269,273
<        call pso(xp,x,y,l,alfa,yy,vt,dturb)
---
>        call pso(xp,x,y,l,alfa,yy,vt,dturb,p,u,gamma,cp,cv)
>        l=l0+le*exp(-xx(1)*3.271e10*kappaGamma/(rp*rp))
> c       l=l0+le*exp(-xx(1)*rp*rp*kappaGamma*3.271e10)
> c      write(*,103)xx(1)*3.271e10,l,le,p/(27400),h
> c       write(*,103)xx(1)*2.603e9,rp,p/(27400),l
203a276
>        write(*,103) log10(-h),yy(1),yy(2),yy(3),yy(4),xx(1),xx(2),xx(3),xx(4)
209,216c282,318
<        dmlog=alog10(xx(1))
<        tlog=alog10(xx(2))
<        rhlog=alog10(xx(3))
<        rlog=alog10(xx(4))
<        taulog=alog10(xx(5))
<        grl=alog10(grad)
<        gal=alog10(gradad)
<        gral=alog10(gradra)
---
>        dmlog=log10(xx(1))
>        tlog=log10(xx(2))
>        rhlog=log10(xx(3))
>        rlog=log10(xx(4))
>        taulog=log10(xx(5))
>        grl=log10(grad)
>        gal=log10(gradad)
>        gral=log10(gradra)
>        lu=log10(u)
> c ----------------------------------------------------------------------------
> c dmlog = Log(mass) in solar units
> c tlog = Log(T_surface) in K. Note that T_eff is the surface temperature (i.e.
> c photosphere), offset from the effective temperature by
> c    T_eff=2^(1/4) T_surf.
> c rhlog = Log(density) in c.g.s.
> c rlog = Log(radius) in solar units
> c taulog = Log(optical depth)
> c grl = log(true gradient)
> c gal = log(adiabatic gradient)
> c gral = log(radiative gradient)
> c xh1 = ?
> c xhe1 = ?
> c xhe2 = ?
> c error = error
> c p = pressure in c.g.s.
> c l = luminosity in solar units
> c gradra = radiative gradient
```

```
> c gradad = adiabatic gradient
> c grad = true gradient
> c lu = log(specific energy density) in c.g.s.
> c vad = adiabatic sound speed
> c vt = Convective speed
> c gamma = convection efficiency (in units of 1/vt)
> c cp = heat capacity at constant pressure (per unit mass) in c.g.s.
> c dut = heat capacity at constant volume (per unit mass) in c.g.s.
> c asj 7/10/2014
> c ----------------------------------------------------------------------
218c320,321
<      * ,xh1,xhe1,xhe2,error
---
>      * ,xh1,xhe1,xhe2,error,log10(p),log10(l),gradra,gradad,grad,lu
>      * ,vad,vt,gamma,cp,cv
220c323,324
<      * ,xh1,xhe1,xhe2,error
---
>      * ,xh1,xhe1,xhe2,error,log10(p),log10(l),gradra,gradad,grad,lu
>      * ,vad,vt,gamma,cp,cv
234,240c338,344
<       dmlog=alog10(w(1))
<       tlog=alog10(w(2))
<       rhlog=alog10(w(3))
<       rlog=alog10(w(4))
<       taulog=alog10(w(5))
<       write(*,103)dmlog,tlog,rhlog,rlog,taulog
<       write(3,103)dmlog,tlog,rhlog,rlog,taulog
---
>       dmlog=log10(w(1))
>       tlog=log10(w(2))
>       rhlog=log10(w(3))
>       rlog=log10(w(4))
>       taulog=log10(w(5))
>       write(*,103)dmlog,tlog,rhlog,rlog,taulog,le,l
>       write(3,103)dmlog,tlog,rhlog,rlog,taulog,le,l
242c346
<       if(abs(1.0-tauc/tauf).lt.0.01)tef=alog10(w(2))
---
>       if(abs(1.0-tauc/tauf).lt.0.01)tef=log10(w(2))
262,264c366,368
<       ti=alog10(xx(2))
<       rhoi=alog10(xx(3))
<       ri=alog10(xx(4))
---
>       ti=log10(xx(2))
>       rhoi=log10(xx(3))
>       ri=log10(xx(4))
273d376
<       go to 400
278,279c381,382
<       subroutine pso(xx,x,y,lr,alfa,yy,vt,delt)
<       real xx,x,y,lr,alfa,yy,mr,t,ro,r,q,cp,p,dpro,dpt,kp,dpm,g,hp,
---
>       subroutine pso(xx,x,y,lr,alfa,yy,vt,delt,p,u,gamma,cp,cv)
>       real(8) xx,x,y,lr,alfa,yy,mr,t,ro,r,q,p,dpro,dpt,kp,dpm,g,hp,
299a403
```

```
> c      print *, t,p,xx(5),gradra
333c437
<        real function kappa(ro,te)
---
>        real(8) function kappa(ro,te)
335c439
<        real ro,te,d,t,kapp,kap
---
>        real(8) ro,te,d,t,kapp,kap
337c441
<        d=2.0*alog10(ro)+25.0
---
>        d=2.0*log10(ro)+25.0
340c444
<        t=20.*alog10(te)-65.
---
>        t=20.*log10(te)-65.
393c497
<        real ro,t,x,y,typ,q,cp,gradad,p,dpro,dpt,u,vad,p1,p2,p3,p4,u1,u2,
---
>        real(8) ro,t,x,y,typ,q,cp,gradad,p,dpro,dpt,u,vad,p1,p2,p3,p4,u1,u2,
453c557
<        error=alog10(er1)
---
>        error=log10(er1)
478c582
<        real ro,t,x,y,p,u,typ,nt,nh2,nhi,nhii,nhei,nheii,nheiii,ne,pg,pr,
---
>        real(8) ro,t,x,y,p,u,typ,nt,nh2,nhi,nhii,nhei,nheii,nheiii,ne,pg,pr,
489c593
<        logt=alog10(t)
---
>        logt=log10(t)
516c620
<        fhl=alog10(nh)
---
>        fhl=log10(nh)
537c641
<        fhel=alog10(nhe)
---
>        fhel=log10(nhe)
557c661
<        fhel=alog10(nheii)
---
>        fhel=log10(nheii)
```

Gob Opacity Table

```
  0.70000  0.03000
      1-4.48-3.80-3.20-2.86-2.72-2.67-2.64-2.63-2.63-2.62-2.62-2.62-2.61-2.60
      2-2.60-2.59-2.58-2.56-2.54-2.52-2.49-2.46-2.42-5.65-4.66-4.66-4.66-4.66
      3-4.66-4.66-4.66
      4-4.73-4.71-4.59-4.14-3.52-3.04-2.80-2.69-2.65-2.63-2.61-2.60-2.59-2.57
      5-2.55-2.52-2.49-2.44-2.39-2.33-2.26-2.18-2.09-5.43-4.48-4.48-4.48-4.48
      6-4.48-4.48-4.48
      7-4.53-4.51-4.48-4.41-4.29-4.05-3.60-3.12-2.83-2.69-2.62-2.57-2.53-2.48
      8-2.43-2.36-2.29-2.20-2.09-1.98-1.85-1.72-1.59-5.20-4.30-4.30-4.30-4.30
```

```
  9-4.30-4.30-4.30
 10-4.44-4.41-4.38-4.31-4.21-4.08-3.90-3.64-3.28-2.90-2.60-2.41-2.25-2.13
 11-2.01-1.88-1.73-1.59-1.43-1.28-1.12-0.96-0.81-4.98-4.12-4.12-4.12-4.12
 12-4.12-4.12-4.12
 13-4.31-4.29-4.32-4.24-4.10-3.92-3.68-3.39-3.06-2.72-2.38-2.07-1.82-1.62
 14-1.45-1.27-1.08-0.90-0.71-0.52-0.33-0.15-0.05-4.76-3.94-3.94-3.94-3.94
 15-3.94-3.94-3.94
 16-4.13-4.14-4.23-4.12-3.94-3.68-3.37-3.04-2.69-2.35-2.03-1.72-1.44-1.20
 17-0.98-0.76-0.53-0.30-0.08  0.15  0.38  0.60  0.50-4.54-3.76-3.76-3.76-3.76
 18-3.76-3.76-3.76
 19-3.96-3.99-4.03-3.92-3.71-3.39-3.03-2.69-2.35-2.04-1.73-1.43-1.13-0.86
 20-0.60-0.33-0.06  0.21  0.47  0.74  1.01  1.24  0.79-4.32-3.57-3.57-3.57-3.57
 21-3.57-3.57-3.57
 22-3.31-3.40-3.56-3.52-3.37-3.12-2.82-2.51-2.17-1.82-1.47-1.13-0.80-0.51
 23-0.24  0.05  0.33  0.61  0.89  1.17  1.46  1.67  0.95-4.09-3.39-3.39-3.39-3.39
 24-3.39-3.39-3.39
 25-2.63-2.79-2.95-2.98-2.93-2.78-2.55-2.28-1.96-1.59-1.21-0.84-0.50-0.20
 26  0.08  0.37  0.66  0.96  1.25  1.54  1.83  2.00  1.07-3.87-3.21-3.21-3.21-3.21
 27-3.21-3.21-3.21
 28-1.90-2.06-2.24-2.37-2.39-2.27-2.06-1.81-1.53-1.23-0.91-0.58-0.26  0.05
 29  0.36  0.67  0.98  1.29  1.60  1.91  2.22  2.31  1.19-3.65-3.03-3.03-3.03-3.03
 30-3.03-3.03-3.03
 31-1.27-1.39-1.49-1.61-1.66-1.56-1.39-1.18-0.96-0.72-0.47-0.20  0.09  0.38
 32  0.68  0.97  1.28  1.58  1.88  2.18  2.47  2.48  1.30-3.43-2.85-2.85-2.85-2.85
 33-2.85-2.85-2.85
 34-0.79-0.79-0.77-0.79-0.80-0.73-0.62-0.47-0.30-0.10  0.11  0.33  0.56  0.81
 35  1.06  1.32  1.59  1.85  2.12  2.38  2.64  2.59  1.41-3.21-2.67-2.67-2.67-2.67
 36-2.67-2.67-2.67
 37-0.40-0.32-0.23-0.16-0.08-0.01  0.07  0.19  0.33  0.49  0.67  0.86  1.06  1.29
 38  1.52  1.76  2.01  2.25  2.49  2.73  2.96  2.77  1.52-2.99-2.49-2.49-2.49-2.49
 39-2.49-2.49-2.49
 40-0.44-0.26-0.07  0.18  0.42  0.59  0.74  0.86  0.97  1.10  1.24  1.39  1.56  1.76
 41  1.97  2.18  2.40  2.62  2.83  3.05  3.25  2.91  1.63-2.76-2.31-2.31-2.31-2.31
 42-2.31-2.31-2.31
 43-0.47-0.28-0.08  0.22  0.55  0.89  1.19  1.39  1.54  1.66  1.77  1.90  2.05  2.21
 44  2.38  2.58  2.78  2.97  3.17  3.36  3.52  3.04  1.74-2.54-2.13-2.13-2.13-2.13
 45-2.13-2.13-2.13
 46-0.47-0.40-0.31  0.01  0.43  0.86  1.28  1.62  1.90  2.09  2.24  2.37  2.50  2.63
 47  2.78  2.95  3.12  3.31  3.49  3.67  3.80  3.16  1.85-2.32-1.95-1.95-1.95-1.95
 48-1.95-1.95-1.95
 49-0.47-0.47-0.48-0.18  0.24  0.68  1.14  1.59  2.00  2.31  2.56  2.74  2.88  3.01
 50  3.14  3.28  3.44  3.60  3.78  3.97  4.07  3.27  1.96-2.10-1.77-1.77-1.77-1.77
 51-1.77-1.77-1.77
 52-0.47-0.47-0.49-0.26  0.09  0.49  0.93  1.42  1.90  2.33  2.69  2.96  3.16  3.32
 53  3.45  3.58  3.72  3.87  4.04  4.24  4.30  3.37  2.07-1.88-1.59-1.59-1.59-1.59
 54-1.59-1.59-1.59
 55-0.47-0.47-0.47-0.30-0.04  0.29  0.70  1.19  1.71  2.22  2.68  3.04  3.32  3.54
 56  3.71  3.85  3.98  4.12  4.28  4.44  4.43  3.45  2.18-1.66-1.41-1.41-1.41-1.41
 57-1.41-1.41-1.41
 58-0.47-0.47-0.47-0.35-0.15  0.15  0.53  1.01  1.53  2.07  2.58  3.01  3.37  3.66
 59  3.89  4.07  4.21  4.36  4.50  4.58  4.48  3.53  2.28-1.43-1.23-1.23-1.23-1.23
 60-1.23-1.23-1.23
 61-0.47-0.47-0.47-0.39-0.23  0.03  0.38  0.83  1.34  1.89  2.43  2.91  3.33  3.71
 62  4.02  4.24  4.41  4.58  4.70  4.71  4.53  3.61  2.39-1.21-1.05-1.05-1.05-1.05
 63-1.05-1.05-1.05
 64-0.47-0.47-0.47-0.40-0.26-0.04  0.27  0.69  1.18  1.73  2.28  2.79  3.26  3.69
 65  4.06  4.34  4.57  4.78  4.93  4.95  4.71  3.71  2.50-0.99-0.86-0.86-0.86-0.86
```

```
   66 -0.86 -0.86 -0.86
   67 -0.47 -0.47 -0.47 -0.40 -0.28 -0.10  0.17  0.56  1.04  1.57  2.13  2.66  3.17  3.64
   68  4.06  4.41  4.69  4.94  5.12  5.17  4.87  3.81  2.61 -0.77 -0.68 -0.68 -0.68 -0.68
   69 -0.68 -0.68 -0.68
   70 -0.47 -0.47 -0.47 -0.41 -0.29 -0.14  0.09  0.46  0.91  1.43  1.99  2.53  3.05  3.56
   71  4.02  4.43  4.77  5.06  5.27  5.35  5.00  3.90  2.72 -0.55 -0.50 -0.50 -0.50 -0.50
   72 -0.50 -0.50 -0.50
   73 -0.47 -0.47 -0.47 -0.42 -0.32 -0.18  0.03  0.38  0.82  1.33  1.88  2.42  2.95  3.46
   74  3.95  4.40  4.79  5.11  5.35  5.44  5.07  3.98  2.83 -0.32 -0.32 -0.32 -0.32 -0.32
   75 -0.32 -0.32 -0.32
   76 -0.47 -0.47 -0.47 -0.44 -0.36 -0.23 -0.02  0.32  0.75  1.26  1.80  2.33  2.86  3.38
   77  3.88  4.34  4.76  5.10  5.35  5.42  5.09  4.07  2.93 -0.10 -0.14 -0.14 -0.14 -0.14
   78 -0.14 -0.14 -0.14
   79 -0.47 -0.47 -0.47 -0.46 -0.40 -0.28 -0.07  0.26  0.68  1.18  1.72  2.24  2.76  3.28
   80  3.78  4.26  4.68  5.05  5.30  5.35  5.07  4.14  3.04  0.12  0.04  0.04  0.04  0.04
   81  0.04  0.04  0.04
   82 -0.47 -0.47 -0.47 -0.47 -0.44 -0.32 -0.12  0.20  0.60  1.10  1.63  2.14  2.65  3.16
   83  3.67  4.15  4.58  4.95  5.21  5.23  5.00  4.21  3.15  0.34  0.22  0.22  0.22  0.22
   84  0.22  0.22  0.22
   85 -0.47 -0.47 -0.47 -0.49 -0.47 -0.36 -0.16  0.14  0.52  1.00  1.52  2.02  2.52  3.04
   86  3.54  4.01  4.44  4.82  5.07  5.07  4.88  4.25  3.25  0.56  0.40  0.40  0.40  0.40
   87  0.40  0.40  0.40
   88 -0.47 -0.47 -0.47 -0.49 -0.48 -0.39 -0.23  0.01  0.35  0.80  1.31  1.82  2.34  2.87
   89  3.39  3.87  4.30  4.67  4.92  4.94  4.81  4.30  3.36  0.78  0.58  0.58  0.58  0.58
   90  0.58  0.58  0.58
   91 -0.47 -0.47 -0.47 -0.49 -0.48 -0.42 -0.30 -0.11  0.17  0.60  1.10  1.61  2.15  2.70
   92  3.22  3.71  4.14  4.50  4.76  4.81  4.73  4.34  3.46  1.01  0.76  0.76  0.76  0.76
   93  0.76  0.76  0.76
   94 -0.47 -0.47 -0.47 -0.48 -0.47 -0.44 -0.36 -0.22  0.01  0.39  0.87  1.39  1.94  2.50
   95  3.04  3.54  3.97  4.34  4.59  4.68  4.66  4.37  3.56  1.23  0.94  0.94  0.94  0.94
   96  0.94  0.94  0.94
   97 -0.47 -0.47 -0.47 -0.48 -0.47 -0.46 -0.41 -0.30 -0.09  0.25  0.68  1.18  1.72  2.29
   98  2.85  3.36  3.81  4.19  4.47  4.59  4.59  4.37  3.65  1.45  1.12  1.12  1.12  1.12
   99  1.12  1.12  1.12
  100 -0.47 -0.47 -0.47 -0.47 -0.47 -0.47 -0.44 -0.35 -0.17  0.12  0.51  0.98  1.50  2.07
  101  2.64  3.17  3.65  4.05  4.35  4.49  4.52  4.33  3.72  1.67  1.30  1.30  1.30  1.30
  102  1.30  1.30  1.30
  103 -0.47 -0.47 -0.47 -0.47 -0.47 -0.49 -0.47 -0.39 -0.23  0.01  0.34  0.78  1.29  1.85
  104  2.43  2.98  3.48  3.91  4.23  4.40  4.43  4.27  3.76  1.89  1.48  1.13  0.57 -0.42
  105 -1.40 -2.40 -3.43
  106 -0.47 -0.47 -0.47 -0.47 -0.47 -0.48 -0.49 -0.46 -0.40 -0.30 -0.13  0.16  0.56  1.07
  107  1.63  2.22  2.76  3.21  3.54  3.75  3.82  3.79  3.63  2.73  2.19  1.68  1.07  0.09
  108 -0.88 -1.87 -2.89
  109 -0.47 -0.47 -0.47 -0.47 -0.47 -0.47 -0.47 -0.47 -0.47 -0.44 -0.37 -0.22  0.02  0.38
  110  0.83  1.36  1.91  2.39  2.77  3.01  3.15  3.18  3.18  3.10  2.77  2.21  1.56  0.61
  111 -0.36 -1.34 -2.35
  112 -0.47 -0.47 -0.47 -0.47 -0.47 -0.47 -0.47 -0.48 -0.48 -0.48 -0.46 -0.42 -0.31 -0.14
  113  0.13  0.54  1.02  1.53  1.99  2.31  2.54  2.64  2.71  2.83  2.90  2.63  2.03  1.12
  114  0.16 -0.82 -1.81
  115 -0.47 -0.47 -0.47 -0.47 -0.47 -0.47 -0.47 -0.47 -0.47 -0.47 -0.47 -0.47 -0.45 -0.41
  116 -0.29 -0.06  0.27  0.70  1.17  1.60  1.96  2.19  2.36  2.52  2.70  2.78  2.45  1.62
  117  0.68 -0.30 -1.29
  118 -0.47 -0.47 -0.47 -0.47 -0.47 -0.47 -0.47 -0.47 -0.47 -0.47 -0.47 -0.47 -0.46 -0.46
  119 -0.42 -0.36 -0.22  0.06  0.43  0.92  1.40  1.77  2.06  2.23  2.36  2.52  2.54  2.05
  120  1.19  0.22 -0.77
  121 -0.47 -0.47 -0.47 -0.47 -0.47 -0.47 -0.47 -0.47 -0.47 -0.47 -0.47 -0.47 -0.47 -0.47
  122 -0.47 -0.45 -0.39 -0.26 -0.03  0.34  0.77  1.23  1.64  1.89  2.05  2.16  2.24  2.21
```

```
123 1.65 0.73−0.26
124−0.47−0.47−0.47−0.47−0.47−0.47−0.47−0.47−0.47−0.47−0.47−0.47−0.47−0.47
125−0.47−0.47−0.44−0.40−0.30−0.10 0.19 0.59 1.01 1.31 1.53 1.65 1.74 1.89
126 1.83 1.18 0.23
127−0.47−0.47−0.47−0.47−0.47−0.47−0.47−0.47−0.47−0.47−0.47−0.47−0.47−0.47
128−0.48−0.48−0.47−0.47−0.43−0.37−0.23 0.01 0.30 0.59 0.85 1.01 1.15 1.33
129 1.50 1.42 0.70
130−0.48−0.48−0.48−0.48−0.48−0.48−0.48−0.48−0.48−0.48−0.48−0.48−0.48−0.48
131−0.48−0.48−0.48−0.48−0.48−0.47−0.44−0.35−0.21−0.02 0.20 0.39 0.57 0.74
132 0.93 1.16 1.01
133−0.48−0.48−0.48−0.48−0.48−0.48−0.48−0.48−0.48−0.48−0.48−0.48−0.48−0.48
134−0.48−0.48−0.48−0.48−0.48−0.48−0.47−0.46−0.43−0.35−0.24−0.09 0.07 0.22
135 0.41 0.66 0.87
136−0.49−0.49−0.49−0.49−0.49−0.49−0.49−0.49−0.49−0.49−0.49−0.49−0.49−0.49
137−0.49−0.49−0.49−0.49−0.49−0.49−0.49−0.49−0.49−0.47−0.43−0.35−0.26−0.15
138−0.01 0.20 0.43
139−0.50−0.50−0.50−0.50−0.50−0.50−0.50−0.50−0.50−0.50−0.50−0.50−0.50−0.50
140−0.50−0.50−0.50−0.50−0.50−0.50−0.50−0.50−0.50−0.50−0.49−0.47−0.43−0.37
141−0.28−0.14 0.03
142−0.51−0.51−0.51−0.51−0.51−0.51−0.51−0.51−0.51−0.51−0.51−0.51−0.51−0.51
143−0.51−0.51−0.51−0.51−0.51−0.51−0.51−0.51−0.51−0.52−0.52−0.52−0.50−0.48
144−0.44−0.36−0.26
145−0.53−0.53−0.53−0.53−0.53−0.53−0.53−0.53−0.53−0.53−0.53−0.53−0.53−0.53
146−0.53−0.53−0.53−0.53−0.53−0.53−0.53−0.53−0.53−0.53−0.53−0.53−0.53−0.53
147−0.51−0.49−0.43
148−0.56−0.56−0.56−0.56−0.56−0.56−0.56−0.56−0.56−0.56−0.56−0.56−0.56−0.56
149−0.56−0.56−0.56−0.56−0.56−0.56−0.56−0.56−0.56−0.56−0.56−0.56−0.56−0.56
150−0.56−0.55−0.53
151−0.61−0.61−0.61−0.61−0.61−0.61−0.61−0.61−0.61−0.61−0.61−0.61−0.61−0.61
152−0.61−0.61−0.61−0.61−0.61−0.61−0.61−0.61−0.61−0.61−0.61−0.61−0.61−0.61
153−0.61−0.60−0.60
```

Modified Gob Python Interface: gobPy.pyx

```python
import subprocess
import numpy as np
from numpy import pi
import random
import scipy.optimize as opt
import viscosity as visc

# m - Mass (in solar masses)
# fm - Fraction of the mass in the envelope (in solar masses)
# flp - Log of luminosity/solar luminosity
# tp1 - Log of surface temperature in K (offset by 2^(-1/4) from T__eff)
# alpha - Dimensionless mixing length parameter
# kappaGamma - Opacity in cm^2/g
# le - Log of external luminosity/solar luminosity

def run(m,fm,flp,tp1,alpha,kappaGamma,le,iprint=1):
        # iprint = Number of integration steps per printed line
        dflp = 0.15 # Step (in log space) for sampling luminosity
        dtp = 0.15 # Step (in log space) for sampling temperature
        nflp = 1 # Number of luminosities to consider (log sampled)
        ntp = 1 # Number of temperatures to consider (log sampled)
        p = subprocess.check_output(['../gob/gob',str(m),str(fm*m),str(flp),str(tp1),\
```

```
                                    str(dflp),str(dtp),str(nflp),str(ntp),str(iprint)\
                                    ,str(alpha),str(kappaGamma),str(le)])
        p=p.split('\n')
        data=[]
        counter=-1
        for line in p:
                if 'log' in line:
                        data.append([])
                        counter+=1
                elif counter!=-1 and not 'dm' in line:
                        temp=[]
                        excepted=False
                        for i in line.split():
                                try:
                                        temp.append(float(i))
                                except:
                                        excepted=True
                        if not excepted and len(temp)>14:
                                data[counter].append(temp)
        for i in range(len(data)):
                data[i]=np.array(data[i])
        d=[]
        for i in range(nflp):
                d.append([])
                for j in range(ntp):
                        d[i].append(data[ntp*i+j])
        return d[0][0][1:]
        # We chop off the first datapoint, as it is the boundary condition

# d now holds the data indexed in the same order that Gob output it.
# These are given in that order by:
# dmlog = Log(mass) in solar units
# tlog = Log(T_surface) in K. Note that T_eff is the surface temperature (i.e.
#        photosphere), offset from the effective temperature by
#        T_eff=2^(1/4) T_surf.
# rhlog = Log(density) in c.g.s.
# rlog = Log(radius) in solar units
# taulog = Log(optical depth)
# grl = log(true gradient)
# gal = log(adiabatic gradient)
# gral = log(radiative gradient)
# xh1 = ?
# xhe1 = ?
# xhe2 = ?
# error = error
# p = log(pressure) in c.g.s.
# l = log(luminosity) in solar units
# gradra = radiative gradient
# gradad = adiabatic gradient
# grad = true gradient
# lu = log(specific energy density) in c.g.s.
# vad = adiabatic sound speed
# vc = convective velocity
# gamma = efficiency/vc
# cp = specific heat capacity in c.g.s.
# cv = specific heat capacity in c.g.s.
```

```

# Various helper methods and quantities, all outputs in cgs
# All quantities involving vertical shear assume a scale height for the shear
# r, m when used as inputs are in solar units

mSun = 1.9891e33 # g
rSun = 6.955e10 # cm
c=2.99792458e10 # cm/s
kB = 1.38e-16 # erg/K
newtonG = 6.67259e-8 # cm^3/g/s^2
lSun = 3.846e33 # erg/s
fSun = lSun/(4*np.pi*rSun**2)

def r(d):
        return rSun*(10**d[:,3])

def sigma(d):
        return mSun*10**d[:,0]/(4*np.pi*(r(d))**2)

def p(d):
        return 10**d[:,12]

def radGrad(d):
        return d[:,14]

def adGrad(d):
        return d[:,15]

def cp(d):
        return d[:,21]

def cv(d):
        return d[:,22]

def adiabaticExp(d):
        return cp(d)/cv(d)

def mAbove(d):
        return mSun*(10**d[:,0])

def mBelow(d,m): # m is in solar units
        return mSun*(m-10**d[:,0])

def g(d,m): # m is in solar units
        return newtonG*mBelow(d,m)/r(d)**2

def vs(d):
        return d[:,18]

def vc(d):
        return d[:,19]

def rho(d):
        return 10**d[:,2]

def t(d):
        return 10**d[:,1]
```

```
def hs(d,m): # m is in solar units
        return p(d)/(g(d,m)*rho(d))

def mu(d):
        return rho(d)*kB*t(d)/p(d)

def muGrad(d):
        return np.gradient(np.log10(mu(d)))/np.gradient(d[:,1])

def isConvective(d):
        return 1.0*(d[:,14]>=d[:,15])

def gamma(d):
        return d[:,20]*d[:,19]

def lum(d):
        return lSun*10**(d[:,13])

def flux(d):
        return lum(d)/(4*np.pi*r(d)**2)

def thermalK(d,m):
        return lum(d)*np.gradient(p(d))/(rho(d)*g(d,m)*4*np.pi*r(d)**2*np.gradient(t(d)))

def microViscosity(d):
        return visc.overall(t(d),p(d),rho(d))

def radViscosity(d,m):
        return 3*flux(d)/(4*g(d,m)*(c**2)*radGrad(d))

def richardsonVisc(d,m,alpha,muG,visc,viscR,v):         # Returns the vertical viscosity
    from the Richardson cirterion
                                                        # Note: this is only valid in
                                                            radiative zones.
        richardDenom = g(d,m)*hs(d,m)*((radGrad(d)-adGrad(d))/(alpha+visc)+(1/visc)*muG)
        if v**2/richardDenom<viscR:
                return viscR
        return v**2/richardDenom

def zonalWind(d,omega,m,eps):
        a = (vc(d)/hs(d,m))*(r(d)/(omega*(vc(d)**3/(2*hs(d,m))+eps)))**(1./3)
        b = a*hs(d,m)*(omega/r(d))**(0.5)
        arr = np.array([a,np.zeros(a.shape),-np.ones(a.shape),b])
        q = map(np.roots,np.transpose(arr))
        ret = []
        for k in q:
                if max(np.imag(k))<1e-10:
                        ret.append(np.max(k))
                else:
                        counter=0
                        for kk in k:
                                if np.imag(kk)<1e-10 and counter==0:
                                        ret.append(kk)
                                        counter+=1
        return np.array(ret)
```

```
def coriolisRadius(d,m,omega,theta,v):
    c = omega**2*np.abs(np.sin(theta))*r(d)
    gg = g(d,m)
    return v*np.abs(np.sin(theta))*np.sqrt(gg**2+2*gg*c+2*c*gg*np.sin(theta))/(2*gg*omega*np.abs(np.cos(theta)))

def windDiffusionFlux(d,m,tK,omega,theta,tg,v):
    r = coriolisRadius(d,m,omega,theta,v)
    return hs(d,m)*t(d)*tg*np.minimum(2*cp(d)*v*r,tK)/(3*r)

def radiativeWindDiffusion(dd,m,omega,theta,tg,rec=1e3):
    # Returns the thermal flux along isobars
    # due to wind. theta is the angle from the pole. tg is
    # the typical value of |\nabla_p ln T|.
    visc = microViscosity(dd) + radViscosity(dd,m) # assume non-turbulent
    tK = thermalK(dd,m)
    alpha = tK/(rho(dd)*cp(dd))
    muG = muGrad(dd)
    # solve for v at each point
    vv = np.zeros(len(dd))
    for i,de in enumerate(dd):
        d = np.array([de])
        # First, assume turbulent and k>2cp*v*r/rho
        h = lambda v: rho(d)*richardsonVisc(d,m,alpha[i],muG[i],abs(v)\
            *coriolisRadius(d,m,omega,theta,abs(v)),visc[i],abs(v))*abs(v)*(1/hs(d,m))**2\
            -hs(d,m)*t(d)*tg**2*2*cp(d)/(3*rho(d))
        try:
            vv[i] = opt.brentq(h,1e-5,1e30,maxiter=300)
        except:
            vv[i] = float('NaN')
        if tK[i]<2*cp(d)*vv[i]*coriolisRadius(d,m,omega,theta,vv[i])/rho(d):
            h = lambda v: rho(d)*richardsonVisc(d,m,alpha[i],muG[i],abs(v)\
                *coriolisRadius(d,m,omega,theta,abs(v)),visc[i],v)*(v/hs(d,m))**2\
                -tK[i]*hs(d,m)*t(d)*tg**2/(3*coriolisRadius(d,m,omega,theta,abs(v)))
            try:
                vv[i] = opt.brentq(h,1e-5,1e30,maxiter=300)
            except:
                vv[i] = float('NaN')
        if vv[i]*coriolisRadius(d,m,omega,theta,vv[i])/visc[i] < rec:
            h = lambda v: rho(d)*richardsonVisc(d,m,alpha[i],muG[i],visc[i],visc[i],v)*v*(1/hs(d,m))**2\
                -hs(d,m)*t(d)*tg**2*2*cp(d)/(3*rho(d))
            try:
                vv[i] = opt.brentq(h,1e-5,1e30,maxiter=300)
            except:
                vv[i] = float('NaN')
            if tK[i]<2*cp(d)*vv[i]*coriolisRadius(d,m,omega,theta,vv[i])/rho(d):
                h = lambda v: rho(d)*richardsonVisc(d,m,alpha[i],muG[i],visc[i],visc[i],v)*(v/hs(d,m))**2\
                    -tK[i]*hs(d,m)*t(d)*tg**2/(3*coriolisRadius(d,m,omega,theta,abs(v)))
                try:
                    vv[i] = opt.brentq(h,1e-5,1e30,maxiter=300)
```

```
                                        except:
                                                vv[i] = float('NaN')
        vv = np.abs(vv)
        return windDiffusionFlux(dd,m,tK,omega,theta,tg,vv)

# Assumes eddies are close enough to isotropic
def convectiveViscosity(d,m,aleph=1.5):
        return aleph*vc(d)*hs(d,m)

def overallViscosity(d,m,aleph=1.5):
        return np.maximum(microViscosity(d),convectiveViscosity(d,m,aleph=aleph))\
                +radViscosity(d,m)

def microReynolds(d,m,v,aleph=1.5,x=0,vertical=True): # m is in solar units
        if vertical:
                return v*aleph*hs(d,m)/microViscosity(d)
        else:
                return v*x/microViscosity(d)

def convectiveReynolds(d,m,v,aleph=1.5,x=0,vertical=True): # m is in solar units
        if vertical:
                return v*aleph*hs(d,m)/convectiveViscosity(d,m,aleph=aleph)
        else:
                return (v*x)/(vc(d)*aleph*hs(d,m))

def overallReynolds(d,m,v,aleph=1.5,x=0,vertical=True): # m is in solar units
        if vertical:
                return aleph*hs(d,m)*v/overallViscosity(d,m,aleph=aleph)
        else:
                return x*v/overallViscosity(d,m)

def bruntvaisalasquared(d,m):
        return (g(d,m)**2)*np.gradient(rho(d))/np.gradient(p(d))

def bandSpeed(d,theta,tg,omega):
        return (kB/mu(d))*tg/(2*omega*r(d)*np.cos(theta))

def richardson(d,m,v):
        return bruntvaisalasquared(d,m)*(hs(d,m)**2)/(v**2)

def alpha(d,m):
        return thermalK(d,m)*mu(d)/(adiabaticExp(d)*kB*rho(d))

def peclet(d,m,v,z=0,vertical=True):
        if vertical:
                return v*hs(d,m)/alpha(d,m)
        else:
                return v*z/alpha(d,m)

def richardsonCrit(d,m,v):
        return np.maximum(1,1/peclet(d,m,v,vertical=True))
```

References

Paczyński, B. “Envelopes of Red Supergiants”. In: *Acta Astronomica* 19 (1969), p. 1 (cit. on p. 239).

Appendix D

Anisotropy Code

The code used to compute and plot various quantities relating to the anisotropy in surface flux of pulsar companions may be found below. The equations this code solves are described in Chapter 11. Note that this code requires Python, NumPy, and SciPy, and was tested with versions 2.7, 1.9.0, and 0.14.0 respectively.

Anisotropy Calculator

```
import numpy as np
import matplotlib.pyplot as plt

def lr(m, eps=1e-4): # Implements L,R main sequence relations
        s = m.shape
        m = np.reshape(m,(-1,))
        l = np.zeros(m.shape)
        l[(m>=2) & (m<20+eps)] = 2**(4-3.6)*m[(m>=2) & (m<20+eps)]**3.6
        l[(m>=0.43) & (m<2)] = m[(m>=0.43) & (m<2)]**4
        l[(m>=0.08-eps) & (m<0.43)] = (0.43)**(4-2.3)*m[(m>=0.08-eps) & (m<0.43)]**2.3
        r = np.zeros(m.shape)
        r[(m>=2) & (m<20+eps)] = 2**(0.72-0.57)*m[(m>=2) & (m<20+eps)]**0.57
        r[(m>=0.43) & (m<2)] = m[(m>=0.43) & (m<2)]**0.72
        r[(m>=0.08-eps) & (m<0.43)] = m[(m>=0.08-eps) & (m<0.43)]**0.72
        l = np.reshape(l,s)
        r = np.reshape(r,s)
        m = np.reshape(m,s)
        return l,r

def ut(m,p,lp,df,fe,fi): # Compute T and dT/T
        fn = (fe+fi*(2-df))/2
        fd = (fe+fi*(2+df))/2
        t = 0.6*(fd**(1./4)+fn**(1./4))/2
        u = 2*(fd**(1./4)-fn**(1./4))/(fd**(1./4)+fn**(1./4))
        return u,t

def wind(m,p,lp,df): # Self-consistently compute wind flux/fi
        li,rr = lr(m)
        fi = li/rr**2
        fe = lp/(((2+m)*p**2)**(2./3))/2
        for i in range(5): # Self-consistency loop
                u,t = ut(m,p,lp,df,fe,fi)
                ro = 0.012*t**0.5*p/rr
                rov = ro*u**2/(16*np.pi)
```

```

            a = 0
            b = 3*np.tanh(rov)**2
            q = 5-3*np.tanh(rov)**2
            y = 1+9*np.tanh(rov)**2

            w = 5*y*t**(3./2)*u**q*ro**b*(2*t*rr/m)**a/(fi*rr)

            rho = 2*10**4*m*10**3/rr**2/(10**13*t)
            y = ((4*10**10*10**(-2)*rho/t**(7))*(m/rr**2))**(1./3)
            s = m.shape
            m = np.reshape(m,(-1,))
            p = np.reshape(p,(-1,))
            t = np.reshape(t,(-1,))
            y = np.reshape(y,(-1,))
            u = np.reshape(y,(-1,))
            fe = np.reshape(fe,(-1,))
            fi = np.reshape(fi,(-1,))
            rr = np.reshape(rr,(-1,))
            ro = np.reshape(ro,(-1,))
            w = np.reshape(w,(-1,))
            a = 1./3
            q = 3
            b = 0
            w[1>25*((fe+fi)/2)**(3./4)*u**2*p] = (5*y*t**(3./2)*u**q*ro**b*(2*t*rr/m)
                **a/(fi*rr))[1>25*((fe+fi)/2)**(3./4)*u**2*p]
            t = np.reshape(m,s)
            p = np.reshape(p,s)
            y = np.reshape(y,s)
            u = np.reshape(u,s)
            fe = np.reshape(fe,s)
            fi = np.reshape(fi,s)
            rr = np.reshape(rr,s)
            ro = np.reshape(ro,s)
            w = np.reshape(w,s)
            m = np.reshape(m,s)

            # Calculate bottled area fraction
            ar = (1./2)*(1+w/2)
            ar[ar>1]=1
            ar[np.isnan(ar)]=1./2 # In case a previous iteration messed up

            # Calculate revised fe
            lrat = lp/(((2+m)*p**2)**(2./3))/2/fi
            m = np.reshape(m,(-1,))
            ar = np.reshape(ar,(-1,))
            lrat = np.reshape(lrat,(-1,))
            w = np.reshape(w,(-1,))
            lrat[(m<2) & (lrat<2)] = 0
            lrat[(m<2) & (lrat>2)] -= 4*(ar[(lrat>2) & (m<2)])
            m = np.reshape(m,s)
            w = np.reshape(w,s)
            ar = np.reshape(ar,s)
            lrat = np.reshape(lrat,s)
            df *= lrat*fi/fe
            fe = lrat*fi
        return w,ar,lrat,df,rov
```

```

lpr = [1,10,25,50]
figs = []
imm = []
strs = ['$\log␣F_{day}/F_{night}$','$\log␣F_{day}/(F_e+F_i)$','$\log␣F_{night}/F_i$','$\log␣\Delta␣F/F$','$\log␣W/(F_i+F_e)$']
numFigs = 5
for i in range(numFigs):
	figs.append(plt.figure())
	imm.append([])
for q in range(4):
	lp = lpr[q]
	mr = 10**np.linspace(np.log10(0.08),np.log10(20),num=200,endpoint=True)
	pr = 10**np.linspace(-0.5,3,num=200,endpoint=True)
	dfr = np.concatenate([[0],10**np.linspace(-10,-2,num=150,endpoint=True)\
								,10**np.linspace(-2,0,num=400,endpoint=True)])
	m,pp,df = np.meshgrid(mr,pr,dfr,indexing='ij')
	li,rr = lr(m)
	fi = li/rr**2
	fe = lp/(((2+m)*pp**2)**(2./3))/2
	df *= fe/fi

	w,ar,lra,df,rov = wind(m,pp,lp,df)
	# These locations get NaN'd because we zero-out fe in the
	# convective full-bottling zone, and then update df accordingly.
	# Everywhere that this occurs, df should properly be zero.
	df[np.isnan(df)] = 0
	res = (df - lra + w)
	fN = np.zeros((len(mr),len(pr)))
	fD = np.zeros((len(mr),len(pr)))
	lraa = np.zeros((len(mr),len(pr)))
	lrr = lr(mr)
	for i in range(len(mr)):
		for j in range(len(pr)):
			lraa[i,j] = lra[i,j,np.argmin(res[i,j]**2)]
			fN[i,j] = fi[i,j,0]*(lraa[i,j]+2-df[i,j,np.argmin(res[i,j]**2)])/2
			fD[i,j] = fi[i,j,0]*(lraa[i,j]+2+df[i,j,np.argmin(res[i,j]**2)])/2
			w[i,j,0] = w[i,j,np.argmin(res[i,j]**2)]
			if lrr[1][i]>0.49*((mr[i]+2)**0.5*pr[j]*(mr[i]/2))**(2./3)/(0.6*(mr[i]/2)**(2./3)+np.log(1+(mr[i]/2)**(1./3))):
				fN[i,j] = 0
				fD[i,j] = 0
				w[i,j,0] = 0
	w = w[:,:,0]
	fN = np.transpose(fN)
	fD = np.transpose(fD)
	ax = figs[4].add_subplot(2,2,q+1)
	ax.plot(mr,10**4*(0.49*((mr+2)**0.5*(mr/2))**(2./3)/(0.6*(mr/2)**(2./3)+np.log(1+(mr/2)**(1./3)))/lrr[1])**(-3./2),c='k',linewidth=2)
	im = ax.imshow(np.log10(np.transpose((w*fi[:,:,0])/(fi[:,:,0]+(lp/(((2+m)*pp**2)**(2./3))/2)[:,:,0]))),origin='lower',extent=[0.08,20,3*10**3,10**7],aspect=0.65)
	ax.set_xlim([0.08,20])
	ax.set_ylim([3*10**3,10**7])
```

```
        imm[4].append(im)
        ax.set_title('$L_p='+str(lpr[q])+'$')
        ax.set_xscale('log')
        ax.set_yscale('log')
        if q==2 or q==3:
            ax.set_xlabel('M ($M_\odot$)')
        if q==0 or q==2:
            ax.set_ylabel('P (s)')
        ax = figs[3].add_subplot(2,2,q+1)
        ax.plot(mr,10**4*(0.49*((mr+2)**0.5*(mr/2))**(2./3)/(0.6*(mr/2)**(2./3)+np.log(1+(mr/2)**(1./3)))/lrr[1])**(-3./2),c='k',linewidth=2)
        im = ax.imshow(np.log10(2*(fD-fN)/(fD+fN)),origin='lower',extent=[0.08,20,3*10**3,10**7],aspect=0.65)
        ax.set_xlim([0.08,20])
        ax.set_ylim([3*10**3,10**7])
        imm[3].append(im)
        ax.set_title('$L_p='+str(lpr[q])+'$')
        ax.set_xscale('log')
        ax.set_yscale('log')
        if q==2 or q==3:
            ax.set_xlabel('M ($M_\odot$)')
        if q==0 or q==2:
            ax.set_ylabel('P (s)')
        ax = figs[2].add_subplot(2,2,q+1)
        ax.plot(mr,10**4*(0.49*((mr+2)**0.5*(mr/2))**(2./3)/(0.6*(mr/2)**(2./3)+np.log(1+(mr/2)**(1./3)))/lrr[1])**(-3./2),c='k',linewidth=2)
        im = ax.imshow(np.log10(fN/np.transpose(fi[:,:,0])),origin='lower',extent=[0.08,20,3*10**3,10**7],aspect=0.65)
        ax.set_xlim([0.08,20])
        ax.set_ylim([3*10**3,10**7])
        imm[2].append(im)
        ax.set_title('$L_p='+str(lpr[q])+'$')
        ax.set_xscale('log')
        ax.set_yscale('log')
        if q==2 or q==3:
            ax.set_xlabel('M ($M_\odot$)')
        if q==0 or q==2:
            ax.set_ylabel('P (s)')
        ax = figs[1].add_subplot(2,2,q+1)
        ax.plot(mr,10**4*(0.49*((mr+2)**0.5*(mr/2))**(2./3)/(0.6*(mr/2)**(2./3)+np.log(1+(mr/2)**(1./3)))/lrr[1])**(-3./2),c='k',linewidth=2)
        im = ax.imshow(np.log10(fD/np.transpose(fi[:,:,0]+(lp/(((2+m)*pp**2)**(2./3))/2)[:,:,0])),origin='lower',extent=[0.08,20,3*10**3,10**7],aspect=0.65)
        ax.set_xlim([0.08,20])
        ax.set_ylim([3*10**3,10**7])
        imm[1].append(im)
        ax.set_title('$L_p='+str(lpr[q])+'$')
        ax.set_xscale('log')
        ax.set_yscale('log')
        if q==2 or q==3:
            ax.set_xlabel('M ($M_\odot$)')
        if q==0 or q==2:
            ax.set_ylabel('P (s)')
        ax = figs[0].add_subplot(2,2,q+1)
        ax.plot(mr,10**4*(0.49*((mr+2)**0.5*(mr/2))**(2./3)/(0.6*(mr/2)**(2./3)+np.log(1+(mr/2)**(1./3)))/lrr[1])**(-3./2),c='k',linewidth=2)
```

```
    im = ax.imshow(np.log10(fD/fN),origin='lower',extent=[0.08,20,3*10**3,10**7],
        aspect=0.65)
    ax.set_xlim([0.08,20])
    ax.set_ylim([3*10**3,10**7])
    imm[0].append(im)
    ax.set_title('$L_p='+str(lpr[q])+'$')
    ax.set_xscale('log')
    ax.set_yscale('log')
    if q==2 or q==3:
        ax.set_xlabel('M ($M_\odot$)')
    if q==0 or q==2:
        ax.set_ylabel('P (s)')

for j in range(numFigs):
    minn = 1e10
    maxx = -1e10
    for i in range(4):
        ran = imm[j][i].get_clim()
        if ran[0]<minn:
            minn=ran[0]
        if ran[1]>maxx:
            maxx=ran[1]
    for i in range(4):
        if j!=4:
            imm[j][i].set_clim(minn,maxx)
        else:
            imm[j][i].set_clim(minn,0)

    cax = figs[j].add_axes([0.85,0.1,0.03,0.8])
    cbar = figs[j].colorbar(imm[j][0],cax=cax)
    cbar.set_label(strs[j])
    figs[j].subplots_adjust(right=0.8)
    figs[j].savefig('../Thesis/anisotropy'+str(j+1)+'.pdf',dpi=200)
```

Appendix E

Reference Stellar Models

All quantities other than R and M are given in c.g.s.k., with the former two given in solar units. $M+$ represents the mass above the current integration point, while $M-$ is the mass below. The quantities vs, GradR, GradA, and Grad are v_s, ∇_{rad}, ∇_{ad}, and ∇ respectively. The quantity M represents the total mass above the current integration point. If R is similar to the stellar radius this is related to the column density by $\Sigma = \frac{M}{4\pi R^2}$. The code used to produce these tables is in Appendix B.2.

The Sun: $M = M_\odot$,$L_{in} = L_\odot$,$T_{\text{surface}} = 10^{3.76}K$,$L_e = 0$

Log(Sigma)	Log(M+)	Log(M-)	Log(Rho)	Log(p)	Log(T)	Log(hs)	Log(vs)	Log(vc)
-1.999	20.785	33.301	-8.817	2.443	3.687	6.820	5.675	nan
-1.828	20.956	33.301	-8.643	2.613	3.687	6.816	5.672	nan
-1.657	21.127	33.301	-8.469	2.784	3.687	6.813	5.671	nan
-1.485	21.299	33.301	-8.295	2.955	3.687	6.811	5.669	nan
-1.313	21.471	33.301	-8.122	3.127	3.687	6.809	5.668	nan
-1.141	21.644	33.301	-7.948	3.300	3.687	6.808	5.667	nan
-0.968	21.816	33.301	-7.774	3.472	3.687	6.807	5.667	nan
-0.795	21.990	33.301	-7.601	3.645	3.688	6.806	5.666	nan
-0.621	22.164	33.301	-7.427	3.819	3.689	6.806	5.666	nan
-0.446	22.339	33.301	-7.253	3.994	3.690	6.808	5.667	nan
-0.268	22.516	33.301	-7.079	4.172	3.695	6.811	5.669	nan
-0.086	22.699	33.301	-6.906	4.354	3.703	6.820	5.673	nan
0.107	22.892	33.301	-6.732	4.547	3.722	6.840	5.683	nan
0.329	23.113	33.301	-6.558	4.769	3.764	6.887	5.709	3.923
0.782	23.567	33.301	-6.457	5.223	3.919	7.240	5.950	5.336
1.149	23.933	33.301	-6.286	5.589	4.036	7.435	5.979	5.270
1.396	24.180	33.301	-6.113	5.836	4.086	7.509	6.013	5.198
1.627	24.411	33.301	-5.939	6.067	4.122	7.566	6.042	5.136
1.850	24.635	33.301	-5.765	6.291	4.155	7.616	6.068	5.082
2.071	24.855	33.301	-5.591	6.511	4.185	7.663	6.093	5.036
2.290	25.074	33.301	-5.418	6.730	4.215	7.708	6.118	4.975
2.509	25.293	33.301	-5.244	6.949	4.245	7.753	6.143	4.928
2.729	25.513	33.301	-5.070	7.168	4.276	7.799	6.168	4.874
2.950	25.734	33.301	-4.896	7.390	4.309	7.846	6.195	4.833
3.174	25.958	33.301	-4.723	7.613	4.344	7.896	6.223	4.777
3.400	26.184	33.301	-4.549	7.840	4.383	7.949	6.253	4.733

Log(Sigma)	Log(M+)	Log(M-)	Log(Rho)	Log(p)	Log(T)	Log(hs)	Log(vs)	Log(vc)
3.630	26.414	33.301	-4.375	8.070	4.424	8.006	6.285	4.691
3.864	26.648	33.301	-4.202	8.304	4.470	8.066	6.319	4.639
4.102	26.886	33.301	-4.028	8.542	4.521	8.130	6.355	4.591
4.345	27.129	33.301	-3.854	8.784	4.576	8.199	6.395	4.547
4.594	27.379	33.301	-3.680	9.034	4.640	8.275	6.440	4.508
4.854	27.638	33.301	-3.507	9.294	4.715	8.361	6.492	4.467
5.124	27.909	33.301	-3.333	9.564	4.804	8.458	6.548	4.431
5.401	28.185	33.301	-3.159	9.841	4.900	8.560	6.600	4.370
5.674	28.458	33.301	-2.986	10.114	4.994	8.660	6.646	4.307
5.945	28.729	33.301	-2.812	10.385	5.086	8.757	6.696	4.250
6.221	29.005	33.301	-2.638	10.661	5.183	8.859	6.753	4.202
6.503	29.288	33.301	-2.464	10.943	5.288	8.968	6.811	4.151
6.790	29.574	33.301	-2.291	11.230	5.399	9.081	6.870	4.096
7.079	29.863	33.301	-2.117	11.518	5.513	9.196	6.928	4.040
7.368	30.152	33.300	-1.943	11.808	5.628	9.312	6.987	3.988
7.658	30.442	33.300	-1.770	12.098	5.744	9.428	7.045	3.923
7.947	30.732	33.300	-1.596	12.388	5.859	9.544	7.103	3.866
8.237	31.021	33.298	-1.422	12.677	5.975	9.660	7.161	3.799
8.527	31.311	33.296	-1.248	12.967	6.090	9.775	7.219	3.725
8.817	31.601	33.292	-1.075	13.257	6.206	9.892	7.277	3.621
9.106	31.891	33.284	-0.901	13.546	6.321	10.008	7.335	nan
9.356	32.140	33.270	-0.727	13.796	6.397	10.084	7.373	nan

Log(Sigma)	Log(Gamma)	Log(mu)	Log(Grad)	Log(GradA)	Log(GradR)	Log(Tau)	Log(R)
-1.999	nan	-23.431	-4.145	-0.842	-4.145	-4.417	10.842
-1.828	nan	-23.428	-4.021	-0.831	-4.021	-4.127	10.842
-1.657	nan	-23.425	-3.843	-0.820	-3.843	-3.830	10.842
-1.485	nan	-23.423	-3.611	-0.810	-3.611	-3.527	10.842
-1.313	nan	-23.422	-3.341	-0.801	-3.341	-3.218	10.842
-1.141	nan	-23.420	-3.049	-0.792	-3.049	-2.905	10.842
-0.968	nan	-23.419	-2.744	-0.785	-2.744	-2.590	10.842
-0.795	nan	-23.418	-2.432	-0.779	-2.432	-2.272	10.842
-0.621	nan	-23.417	-2.118	-0.774	-2.118	-1.952	10.842
-0.446	nan	-23.417	-1.806	-0.769	-1.806	-1.630	10.842
-0.268	nan	-23.416	-1.493	-0.767	-1.493	-1.303	10.842
-0.086	nan	-23.417	-1.179	-0.767	-1.179	-0.962	10.842
0.107	nan	-23.418	-0.885	-0.771	-0.885	-0.598	10.842
0.329	-2.061	-23.423	-0.565	-0.790	-0.571	-0.167	10.842
0.782	1.203	-23.621	-0.574	-0.821	0.593	1.377	10.842
1.149	2.288	-23.699	-0.621	-0.878	1.639	2.882	10.842
1.396	3.061	-23.722	-0.764	-0.927	2.108	3.684	10.842
1.627	3.638	-23.743	-0.829	-0.934	2.466	4.270	10.842
1.850	4.147	-23.761	-0.857	-0.928	2.786	4.762	10.842
2.071	4.611	-23.777	-0.865	-0.915	3.074	5.204	10.841
2.290	5.036	-23.793	-0.865	-0.898	3.353	5.621	10.841
2.509	5.460	-23.808	-0.854	-0.877	3.626	6.024	10.841

Log(Sigma)	Log(Gamma)	Log(mu)	Log(Grad)	Log(GradA)	Log(GradR)	Log(Tau)	Log(R)
2.729	5.849	-23.822	-0.838	-0.853	3.881	6.418	10.841
2.950	6.243	-23.837	-0.815	-0.826	4.133	6.807	10.841
3.174	6.606	-23.852	-0.789	-0.796	4.377	7.195	10.840
3.400	6.971	-23.866	-0.758	-0.764	4.614	7.587	10.840
3.630	7.327	-23.881	-0.725	-0.729	4.844	7.984	10.840
3.864	7.644	-23.895	-0.692	-0.694	5.043	8.384	10.839
4.102	7.947	-23.909	-0.658	-0.659	5.220	8.772	10.839
4.345	8.190	-23.922	-0.619	-0.620	5.335	9.151	10.838
4.594	8.321	-23.935	-0.569	-0.570	5.345	9.493	10.838
4.854	8.282	-23.945	-0.510	-0.511	5.189	9.771	10.837
5.124	8.136	-23.954	-0.464	-0.464	4.891	9.978	10.836
5.401	8.019	-23.960	-0.456	-0.456	4.583	10.137	10.835
5.674	8.007	-23.965	-0.471	-0.471	4.344	10.281	10.833
5.945	7.954	-23.971	-0.466	-0.466	4.080	10.420	10.831
6.221	7.765	-23.976	-0.441	-0.441	3.701	10.539	10.828
6.503	7.479	-23.979	-0.419	-0.419	3.220	10.629	10.825
6.790	7.188	-23.981	-0.407	-0.407	2.718	10.695	10.820
7.079	6.933	-23.982	-0.402	-0.402	2.239	10.747	10.814
7.368	6.737	-23.983	-0.400	-0.400	1.812	10.794	10.806
7.658	6.584	-23.983	-0.400	-0.400	1.436	10.843	10.796
7.947	6.445	-23.984	-0.399	-0.399	1.066	10.897	10.781
8.237	6.299	-23.984	-0.399	-0.399	0.698	10.955	10.761
8.527	6.160	-23.984	-0.399	-0.399	0.343	11.019	10.734
8.817	5.966	-23.985	-0.399	-0.399	-0.035	11.088	10.696
9.106	nan	-23.985	-0.420	-0.400	-0.420	11.158	10.641
9.356	nan	-23.985	-0.585	-0.400	-0.585	11.223	10.572

The Sun: $M = M_{\odot}, L_{in} = L_{\odot}, T_{\text{surface}} = 10^{3.76} K, L_e = L_{in}$

Log(Sigma)	Log(M+)	Log(M-)	Log(Rho)	Log(p)	Log(T)	Log(hs)	Log(vs)	Log(vc)
-2.000	20.785	33.301	-8.980	2.445	3.762	6.985	5.784	nan
-1.840	20.944	33.301	-8.806	2.603	3.762	6.970	5.774	nan
-1.679	21.105	33.301	-8.632	2.763	3.762	6.956	5.765	nan
-1.517	21.268	33.301	-8.459	2.925	3.762	6.944	5.756	nan
-1.353	21.432	33.301	-8.285	3.088	3.762	6.934	5.748	nan
-1.188	21.597	33.301	-8.111	3.253	3.762	6.925	5.741	nan
-1.021	21.764	33.301	-7.938	3.419	3.763	6.917	5.735	nan
-0.853	21.932	33.301	-7.764	3.587	3.763	6.912	5.730	nan
-0.682	22.102	33.301	-7.590	3.757	3.765	6.908	5.727	nan
-0.510	22.275	33.301	-7.416	3.930	3.767	6.907	5.725	nan
-0.333	22.452	33.301	-7.243	4.107	3.772	6.910	5.727	nan
-0.146	22.638	33.301	-7.069	4.294	3.783	6.923	5.735	nan
0.091	22.875	33.301	-6.895	4.531	3.821	6.986	5.781	4.276
0.341	23.125	33.301	-7.017	4.780	3.970	7.358	5.942	5.575
0.720	23.504	33.301	-6.914	5.160	4.115	7.635	6.073	5.538
1.038	23.822	33.301	-6.741	5.478	4.187	7.779	6.153	5.520
1.334	24.118	33.301	-6.567	5.774	4.268	7.901	6.229	5.518

Log(Sigma)	Log(M+)	Log(M-)	Log(Rho)	Log(p)	Log(T)	Log(hs)	Log(vs)	Log(vc)
1.620	24.404	33.301	-6.393	6.060	4.361	8.014	6.290	5.476
1.903	24.687	33.301	-6.220	6.343	4.458	8.123	6.372	5.472
2.217	25.002	33.301	-6.046	6.657	4.596	8.263	6.458	5.439
2.503	25.287	33.301	-5.872	6.943	4.705	8.375	6.488	5.321
2.755	25.539	33.301	-5.698	7.195	4.777	8.454	6.521	5.240
3.012	25.796	33.301	-5.525	7.451	4.853	8.536	6.579	5.176
3.290	26.074	33.301	-5.351	7.729	4.955	8.641	6.647	5.081
3.577	26.362	33.301	-5.177	8.018	5.068	8.755	6.708	4.875
3.853	26.638	33.301	-5.004	8.294	5.169	8.858	6.758	nan
4.101	26.885	33.301	-4.830	8.541	5.243	8.931	6.795	nan
4.339	27.123	33.301	-4.656	8.779	5.307	8.995	6.827	nan
4.570	27.355	33.301	-4.482	9.010	5.364	9.053	6.856	nan
4.796	27.581	33.301	-4.309	9.236	5.417	9.105	6.882	nan
5.019	27.804	33.301	-4.135	9.459	5.466	9.155	6.907	nan
5.241	28.026	33.301	-3.961	9.681	5.515	9.203	6.931	nan
5.463	28.247	33.301	-3.788	9.903	5.562	9.251	6.955	nan
5.684	28.469	33.301	-3.614	10.124	5.610	9.299	6.979	nan
5.906	28.690	33.301	-3.440	10.346	5.659	9.346	7.003	nan
6.128	28.912	33.301	-3.266	10.568	5.707	9.394	7.027	nan
6.349	29.134	33.301	-3.093	10.789	5.755	9.442	7.051	nan
6.570	29.354	33.301	-2.919	11.009	5.801	9.489	7.074	nan
6.789	29.573	33.301	-2.745	11.229	5.847	9.534	7.097	nan
7.008	29.792	33.301	-2.572	11.448	5.892	9.580	7.120	nan
7.227	30.011	33.301	-2.398	11.667	5.938	9.625	7.143	nan
7.447	30.231	33.300	-2.224	11.887	5.984	9.671	7.166	nan
7.668	30.452	33.300	-2.050	12.108	6.032	9.719	7.190	nan
7.890	30.674	33.300	-1.877	12.330	6.080	9.767	7.214	nan
8.112	30.897	33.299	-1.703	12.552	6.129	9.815	7.238	nan
8.336	31.120	33.298	-1.529	12.776	6.179	9.865	7.263	nan
8.560	31.344	33.296	-1.356	13.000	6.229	9.916	7.288	nan
8.785	31.569	33.293	-1.182	13.225	6.280	9.967	7.314	nan
9.009	31.794	33.287	-1.008	13.450	6.331	10.018	7.339	nan
9.233	32.017	33.278	-0.834	13.673	6.381	10.068	7.364	nan
9.436	32.221	33.263	-0.675	13.876	6.425	10.112	7.386	nan

Log(Sigma)	Log(Gamma)	Log(mu)	Log(Grad)	Log(GradA)	Log(GradR)	Log(Tau)	Log(R)
-2.000	nan	-23.518	-3.801	-0.921	-3.801	-3.769	10.842
-1.840	nan	-23.504	-3.660	-0.914	-3.660	-3.546	10.842
-1.679	nan	-23.491	-3.484	-0.906	-3.484	-3.316	10.842
-1.517	nan	-23.480	-3.276	-0.896	-3.276	-3.077	10.842
-1.353	nan	-23.470	-3.050	-0.886	-3.050	-2.832	10.842
-1.188	nan	-23.461	-2.806	-0.875	-2.806	-2.582	10.842
-1.021	nan	-23.454	-2.548	-0.864	-2.548	-2.323	10.842
-0.853	nan	-23.447	-2.284	-0.854	-2.284	-2.057	10.842
-0.682	nan	-23.442	-2.003	-0.844	-2.003	-1.783	10.842
-0.510	nan	-23.439	-1.711	-0.836	-1.711	-1.495	10.842

Log(Sigma)	Log(Gamma)	Log(mu)	Log(Grad)	Log(GradA)	Log(GradR)	Log(Tau)	Log(R)
-0.333	nan	-23.437	-1.406	-0.830	-1.406	-1.188	10.842
-0.146	nan	-23.440	-1.068	-0.830	-1.068	-0.844	10.842
0.091	-1.857	-23.465	-0.534	-0.850	-0.561	-0.329	10.842
0.341	0.391	-23.688	-0.044	-0.860	0.583	0.871	10.842
0.720	2.078	-23.819	-0.629	-1.002	1.530	2.908	10.842
1.038	2.424	-23.891	-0.626	-0.900	1.772	3.636	10.841
1.334	2.337	-23.932	-0.495	-0.711	1.758	4.099	10.841
1.620	2.341	-23.952	-0.510	-0.660	1.619	4.426	10.841
1.903	2.268	-23.964	-0.393	-0.489	1.494	4.720	10.840
2.217	2.197	-23.966	-0.361	-0.417	1.222	5.038	10.840
2.503	2.316	-23.969	-0.504	-0.536	0.993	5.301	10.839
2.755	2.424	-23.976	-0.558	-0.577	0.825	5.516	10.838
3.012	2.288	-23.982	-0.480	-0.491	0.546	5.702	10.837
3.290	2.025	-23.984	-0.413	-0.418	0.120	5.858	10.835
3.577	1.754	-23.985	-0.402	-0.404	-0.263	5.998	10.833
3.853	nan	-23.986	-0.499	-0.406	-0.499	6.132	10.830
4.101	nan	-23.985	-0.553	-0.407	-0.553	6.280	10.827
4.339	nan	-23.985	-0.587	-0.407	-0.587	6.448	10.824
4.570	nan	-23.985	-0.622	-0.407	-0.622	6.624	10.820
4.796	nan	-23.985	-0.647	-0.407	-0.647	6.802	10.816
5.019	nan	-23.985	-0.659	-0.406	-0.659	6.980	10.812
5.241	nan	-23.985	-0.665	-0.406	-0.665	7.160	10.806
5.463	nan	-23.985	-0.666	-0.405	-0.666	7.343	10.801
5.684	nan	-23.986	-0.663	-0.405	-0.663	7.529	10.794
5.906	nan	-23.985	-0.663	-0.404	-0.663	7.718	10.786
6.128	nan	-23.985	-0.664	-0.404	-0.664	7.909	10.778
6.349	nan	-23.985	-0.669	-0.403	-0.669	8.098	10.768
6.570	nan	-23.985	-0.677	-0.403	-0.677	8.284	10.757
6.789	nan	-23.985	-0.683	-0.403	-0.683	8.467	10.744
7.008	nan	-23.985	-0.685	-0.402	-0.685	8.648	10.730
7.227	nan	-23.986	-0.683	-0.402	-0.683	8.829	10.713
7.447	nan	-23.986	-0.671	-0.402	-0.671	9.014	10.694
7.668	nan	-23.985	-0.664	-0.401	-0.664	9.204	10.671
7.890	nan	-23.985	-0.661	-0.401	-0.661	9.397	10.644
8.112	nan	-23.985	-0.655	-0.401	-0.655	9.593	10.611
8.336	nan	-23.985	-0.651	-0.401	-0.651	9.792	10.572
8.560	nan	-23.985	-0.646	-0.401	-0.646	9.994	10.522
8.785	nan	-23.985	-0.643	-0.401	-0.643	10.198	10.459
9.009	nan	-23.986	-0.648	-0.400	-0.648	10.401	10.374
9.233	nan	-23.986	-0.657	-0.400	-0.657	10.600	10.255
9.436	nan	-23.986	-0.673	-0.400	-0.673	10.777	10.087

The Sun: $M = M_{\odot}, L_{in} = L_{\odot}, T_{\text{surface}} = 10^{3.76}K, L_e = 10L_{in}$

Log(Sigma)	Log(M+)	Log(M-)	Log(Rho)	Log(p)	Log(T)	Log(hs)	Log(vs)	Log(vc)
-2.000	20.785	33.301	-9.466	2.466	3.953	7.492	5.985	nan
-1.830	20.955	33.301	-9.293	2.628	3.958	7.481	5.981	nan

Log(Sigma)	Log(M+)	Log(M-)	Log(Rho)	Log(p)	Log(T)	Log(hs)	Log(vs)	Log(vc)
-1.648	21.136	33.301	-9.119	2.803	3.966	7.483	5.984	nan
-1.421	21.363	33.301	-8.945	3.025	3.991	7.531	6.011	3.098
-1.032	21.752	33.301	-8.771	3.411	4.096	7.742	6.140	2.313
-0.790	21.995	33.301	-8.598	3.652	4.154	7.810	6.194	nan
-0.561	22.223	33.301	-8.424	3.880	4.204	7.864	6.209	1.391
-0.330	22.455	33.301	-8.250	4.111	4.255	7.922	6.235	2.218
-0.099	22.685	33.301	-8.077	4.342	4.306	7.978	6.282	nan
0.131	22.915	33.301	-7.903	4.571	4.360	8.034	6.332	nan
0.364	23.148	33.301	-7.729	4.804	4.418	8.093	6.371	nan
0.600	23.384	33.301	-7.555	5.040	4.480	8.156	6.404	nan
0.848	23.632	33.301	-7.382	5.288	4.553	8.230	6.431	nan
1.115	23.899	33.301	-7.208	5.555	4.640	8.323	6.446	4.808
1.378	24.162	33.301	-7.034	5.818	4.718	8.412	6.502	nan
1.610	24.394	33.301	-6.861	6.050	4.774	8.471	6.548	nan
1.832	24.617	33.301	-6.687	6.272	4.823	8.520	6.581	nan
2.052	24.836	33.301	-6.513	6.492	4.869	8.565	6.607	nan
2.271	25.055	33.301	-6.339	6.711	4.915	8.611	6.632	nan
2.490	25.275	33.301	-6.166	6.930	4.962	8.656	6.655	nan
2.709	25.494	33.301	-5.992	7.149	5.008	8.701	6.678	nan
2.926	25.711	33.301	-5.818	7.366	5.051	8.745	6.700	nan
3.138	25.922	33.301	-5.645	7.578	5.090	8.783	6.719	nan
3.343	26.127	33.301	-5.471	7.783	5.123	8.814	6.735	nan
3.544	26.329	33.301	-5.297	7.984	5.151	8.842	6.749	nan
3.748	26.532	33.301	-5.123	8.188	5.182	8.871	6.765	nan
3.962	26.747	33.301	-4.950	8.402	5.223	8.912	6.785	nan
4.187	26.971	33.301	-4.776	8.627	5.274	8.963	6.811	nan
4.416	27.200	33.301	-4.602	8.855	5.329	9.018	6.838	nan
4.642	27.427	33.301	-4.429	9.082	5.382	9.071	6.865	nan
4.866	27.651	33.301	-4.255	9.306	5.433	9.121	6.890	nan
5.089	27.873	33.301	-4.081	9.529	5.482	9.170	6.915	nan
5.310	28.095	33.301	-3.907	9.750	5.530	9.218	6.939	nan
5.532	28.316	33.301	-3.734	9.971	5.577	9.265	6.962	nan
5.753	28.538	33.301	-3.560	10.193	5.625	9.313	6.986	nan
5.975	28.759	33.301	-3.386	10.415	5.674	9.361	7.011	nan
6.197	28.981	33.301	-3.212	10.636	5.722	9.409	7.035	nan
6.418	29.202	33.301	-3.039	10.858	5.769	9.457	7.058	nan
6.638	29.422	33.301	-2.865	11.078	5.816	9.503	7.082	nan
6.857	29.641	33.301	-2.691	11.297	5.861	9.549	7.104	nan
7.076	29.860	33.301	-2.518	11.516	5.906	9.594	7.127	nan
7.295	30.079	33.301	-2.344	11.735	5.952	9.639	7.150	nan
7.515	30.300	33.300	-2.170	11.955	5.999	9.685	7.173	nan
7.737	30.521	33.300	-1.996	12.176	6.047	9.733	7.197	nan
7.959	30.743	33.300	-1.823	12.399	6.095	9.782	7.221	nan
8.182	30.966	33.299	-1.649	12.622	6.144	9.831	7.246	nan
8.405	31.190	33.297	-1.475	12.845	6.194	9.881	7.271	nan
8.630	31.414	33.295	-1.302	13.070	6.245	9.932	7.296	nan
8.854	31.639	33.291	-1.128	13.295	6.296	9.983	7.322	nan

Log(Sigma)	Log(M+)	Log(M-)	Log(Rho)	Log(p)	Log(T)	Log(hs)	Log(vs)	Log(vc)
9.079	31.863	33.285	-0.954	13.519	6.347	10.033	7.347	nan
9.300	32.085	33.274	-0.782	13.740	6.396	10.082	7.372	nan
9.463	32.247	33.261	-0.654	13.903	6.431	10.117	7.389	nan

Log(Sigma)	Log(Gamma)	Log(mu)	Log(Grad)	Log(GradA)	Log(GradR)	Log(Tau)	Log(R)
-2.000	nan	-23.814	-1.682	-1.128	-1.682	-1.423	10.841
-1.830	nan	-23.804	-1.453	-1.131	-1.453	-1.174	10.841
-1.648	nan	-23.803	-1.184	-1.130	-1.184	-0.896	10.841
-1.421	-4.740	-23.830	-0.747	-1.114	-0.793	-0.499	10.841
-1.032	-6.165	-23.935	-0.574	-0.770	-0.588	0.259	10.841
-0.790	nan	-23.945	-0.650	-0.606	-0.650	0.563	10.841
-0.561	-6.917	-23.950	-0.666	-0.680	-0.667	0.799	10.840
-0.330	-5.831	-23.958	-0.662	-0.708	-0.669	1.019	10.840
-0.099	nan	-23.964	-0.641	-0.578	-0.641	1.237	10.840
0.131	nan	-23.966	-0.615	-0.468	-0.615	1.462	10.840
0.364	nan	-23.966	-0.590	-0.432	-0.590	1.701	10.839
0.600	nan	-23.967	-0.570	-0.426	-0.570	1.953	10.839
0.848	nan	-23.967	-0.510	-0.462	-0.510	2.247	10.838
1.115	-1.712	-23.972	-0.470	-0.635	-0.493	2.592	10.837
1.378	nan	-23.981	-0.589	-0.566	-0.589	2.905	10.837
1.610	nan	-23.984	-0.646	-0.482	-0.646	3.135	10.836
1.832	nan	-23.985	-0.670	-0.449	-0.670	3.336	10.835
2.052	nan	-23.985	-0.677	-0.435	-0.677	3.531	10.833
2.271	nan	-23.985	-0.675	-0.424	-0.675	3.729	10.832
2.490	nan	-23.985	-0.674	-0.423	-0.674	3.938	10.831
2.709	nan	-23.985	-0.685	-0.421	-0.685	4.160	10.829
2.926	nan	-23.985	-0.710	-0.419	-0.710	4.397	10.828
3.138	nan	-23.985	-0.769	-0.417	-0.769	4.644	10.826
3.343	nan	-23.985	-0.831	-0.414	-0.831	4.900	10.824
3.544	nan	-23.986	-0.855	-0.411	-0.855	5.172	10.822
3.748	nan	-23.985	-0.774	-0.409	-0.774	5.461	10.820
3.962	nan	-23.985	-0.672	-0.408	-0.672	5.764	10.817
4.187	nan	-23.985	-0.625	-0.407	-0.625	6.058	10.814
4.416	nan	-23.985	-0.623	-0.407	-0.623	6.327	10.811
4.642	nan	-23.985	-0.641	-0.407	-0.641	6.567	10.807
4.866	nan	-23.985	-0.655	-0.406	-0.655	6.784	10.802
5.089	nan	-23.985	-0.662	-0.406	-0.662	6.988	10.797
5.310	nan	-23.986	-0.666	-0.405	-0.666	7.186	10.792
5.532	nan	-23.985	-0.665	-0.405	-0.665	7.380	10.785
5.753	nan	-23.985	-0.664	-0.404	-0.664	7.575	10.778
5.975	nan	-23.985	-0.663	-0.404	-0.663	7.769	10.770
6.197	nan	-23.985	-0.666	-0.404	-0.666	7.963	10.761
6.418	nan	-23.985	-0.673	-0.403	-0.673	8.153	10.750
6.638	nan	-23.985	-0.680	-0.403	-0.680	8.339	10.738
6.857	nan	-23.986	-0.684	-0.402	-0.684	8.522	10.725
7.076	nan	-23.986	-0.684	-0.402	-0.684	8.703	10.709

Log(Sigma)	Log(Gamma)	Log(mu)	Log(Grad)	Log(GradA)	Log(GradR)	Log(Tau)	Log(R)
7.295	nan	-23.985	-0.681	-0.402	-0.681	8.885	10.691
7.515	nan	-23.985	-0.669	-0.401	-0.669	9.072	10.670
7.737	nan	-23.985	-0.663	-0.401	-0.663	9.264	10.645
7.959	nan	-23.985	-0.660	-0.401	-0.660	9.458	10.615
8.182	nan	-23.985	-0.653	-0.401	-0.653	9.654	10.579
8.405	nan	-23.985	-0.650	-0.401	-0.650	9.854	10.534
8.630	nan	-23.986	-0.644	-0.401	-0.644	10.057	10.478
8.854	nan	-23.986	-0.643	-0.400	-0.643	10.261	10.404
9.079	nan	-23.985	-0.652	-0.400	-0.652	10.464	10.303
9.300	nan	-23.985	-0.659	-0.400	-0.659	10.660	10.155
9.463	nan	-23.985	-0.676	-0.400	-0.676	10.800	9.981

Low-mass nuclear-burning: $M = 0.3M_{\odot}$,$L_{in} = 0.1L_{\odot}$,$T_{\text{surface}} = 10^{3.3}K$,$L_e = 0$

Log(Sigma)	Log(M+)	Log(M-)	Log(Rho)	Log(p)	Log(T)	Log(hs)	Log(vs)	Log(vc)
-1.999	20.052	32.778	-8.273	2.651	3.370	6.274	5.509	nan
-1.826	20.226	32.778	-8.099	2.824	3.370	6.274	5.509	nan
-1.652	20.399	32.778	-7.925	2.998	3.370	6.274	5.509	nan
-1.478	20.573	32.778	-7.752	3.172	3.370	6.274	5.509	nan
-1.304	20.747	32.778	-7.578	3.346	3.370	6.274	5.509	nan
-1.130	20.921	32.778	-7.404	3.520	3.370	6.274	5.509	nan
-0.957	21.095	32.778	-7.231	3.694	3.370	6.274	5.509	nan
-0.783	21.269	32.778	-7.057	3.867	3.371	6.274	5.509	nan
-0.608	21.443	32.778	-6.883	4.041	3.371	6.275	5.509	nan
-0.434	21.617	32.778	-6.709	4.216	3.372	6.275	5.510	nan
-0.260	21.792	32.778	-6.536	4.390	3.372	6.276	5.510	nan
-0.085	21.967	32.778	-6.362	4.565	3.374	6.277	5.511	nan
0.091	22.142	32.778	-6.188	4.741	3.376	6.280	5.512	nan
0.268	22.319	32.778	-6.015	4.918	3.379	6.283	5.513	nan
0.446	22.497	32.778	-5.841	5.096	3.383	6.287	5.515	nan
0.626	22.678	32.778	-5.667	5.276	3.390	6.294	5.518	nan
0.811	22.862	32.778	-5.493	5.460	3.400	6.304	5.523	nan
1.001	23.052	32.778	-5.320	5.651	3.417	6.321	5.531	nan
1.204	23.255	32.778	-5.146	5.853	3.446	6.349	5.545	nan
1.420	23.471	32.778	-4.972	6.070	3.488	6.392	5.565	4.282
1.636	23.688	32.778	-4.799	6.286	3.531	6.435	5.587	4.287
1.852	23.903	32.778	-4.625	6.502	3.573	6.477	5.608	4.281
2.067	24.119	32.778	-4.451	6.717	3.615	6.519	5.628	4.260
2.282	24.333	32.778	-4.277	6.932	3.655	6.559	5.648	4.220
2.495	24.546	32.778	-4.104	7.145	3.695	6.599	5.668	4.165
2.708	24.759	32.778	-3.930	7.358	3.734	6.638	5.687	4.105
2.921	24.972	32.778	-3.756	7.571	3.773	6.677	5.707	4.057
3.133	25.184	32.778	-3.583	7.783	3.810	6.715	5.726	3.990
3.345	25.397	32.778	-3.409	7.995	3.848	6.754	5.746	3.930
3.559	25.610	32.778	-3.235	8.209	3.885	6.794	5.769	3.876
3.777	25.829	32.778	-3.061	8.427	3.923	6.839	5.798	3.814
4.009	26.061	32.778	-2.888	8.659	3.963	6.897	5.850	3.762

Log(Sigma)	Log(M+)	Log(M-)	Log(Rho)	Log(p)	Log(T)	Log(hs)	Log(vs)	Log(vc)
4.291	26.342	32.778	-2.714	8.941	4.011	7.005	5.969	3.692
4.678	26.729	32.778	-2.540	9.327	4.079	7.217	6.081	3.683
4.948	27.000	32.778	-2.366	9.597	4.165	7.313	6.072	3.669
5.207	27.258	32.778	-2.193	9.856	4.244	7.399	6.109	3.604
5.463	27.514	32.778	-2.019	10.126	4.316	7.495	6.155	3.533
5.723	27.774	32.778	-1.845	10.381	4.383	7.576	6.197	3.468
5.985	28.036	32.778	-1.672	10.639	4.447	7.661	6.245	3.405
6.255	28.306	32.778	-1.498	10.907	4.511	7.755	6.303	3.336
6.541	28.593	32.778	-1.324	11.193	4.578	7.867	6.375	3.275
6.851	28.902	32.778	-1.150	11.502	4.649	8.002	6.460	3.223
7.180	29.231	32.778	-0.977	11.830	4.733	8.157	6.543	3.187
7.502	29.553	32.778	-0.803	12.153	4.832	8.306	6.605	3.161
7.806	29.857	32.777	-0.629	12.456	4.936	8.436	6.660	3.110
8.106	30.158	32.777	-0.456	12.757	5.040	8.562	6.726	3.056
8.402	30.453	32.776	-0.282	13.052	5.156	8.684	6.779	3.014
8.692	30.743	32.774	-0.108	13.342	5.272	8.800	6.836	2.949
8.982	31.033	32.770	0.066	13.632	5.388	8.916	6.894	2.891
9.267	31.318	32.763	0.236	13.917	5.502	9.030	6.951	2.836

Log(Sigma)	Log(Gamma)	Log(mu)	Log(Grad)	Log(GradA)	Log(GradR)	Log(Tau)	Log(R)
-1.999	nan	-23.413	-3.903	-0.711	-3.903	-3.685	10.476
-1.826	nan	-23.413	-3.755	-0.711	-3.755	-3.480	10.476
-1.652	nan	-23.413	-3.596	-0.711	-3.596	-3.280	10.476
-1.478	nan	-23.413	-3.432	-0.711	-3.432	-3.086	10.476
-1.304	nan	-23.414	-3.263	-0.711	-3.263	-2.896	10.476
-1.130	nan	-23.414	-3.090	-0.711	-3.090	-2.709	10.476
-0.957	nan	-23.414	-2.916	-0.711	-2.916	-2.524	10.476
-0.783	nan	-23.413	-2.740	-0.711	-2.740	-2.340	10.476
-0.608	nan	-23.413	-2.563	-0.711	-2.563	-2.157	10.476
-0.434	nan	-23.413	-2.391	-0.711	-2.391	-1.976	10.476
-0.260	nan	-23.413	-2.218	-0.711	-2.218	-1.796	10.476
-0.085	nan	-23.413	-2.044	-0.712	-2.044	-1.616	10.476
0.091	nan	-23.414	-1.870	-0.712	-1.870	-1.435	10.476
0.268	nan	-23.414	-1.695	-0.712	-1.695	-1.252	10.476
0.446	nan	-23.414	-1.519	-0.713	-1.519	-1.065	10.476
0.626	nan	-23.413	-1.340	-0.715	-1.340	-0.871	10.476
0.811	nan	-23.413	-1.155	-0.717	-1.155	-0.666	10.476
1.001	nan	-23.413	-0.960	-0.720	-0.960	-0.439	10.476
1.204	nan	-23.413	-0.744	-0.726	-0.744	-0.170	10.476
1.420	0.628	-23.413	-0.700	-0.733	-0.547	0.159	10.476
1.636	0.878	-23.414	-0.706	-0.735	-0.452	0.479	10.476
1.852	1.269	-23.414	-0.713	-0.737	-0.247	0.785	10.476
2.067	1.807	-23.414	-0.720	-0.739	0.101	1.178	10.476
2.282	2.406	-23.414	-0.727	-0.741	0.523	1.688	10.476
2.495	2.933	-23.414	-0.733	-0.744	0.888	2.221	10.476
2.708	3.373	-23.414	-0.739	-0.747	1.172	2.716	10.475

Log(Sigma)	Log(Gamma)	Log(mu)	Log(Grad)	Log(GradA)	Log(GradR)	Log(Tau)	Log(R)
2.921	3.810	-23.414	-0.745	-0.750	1.439	3.164	10.475
3.133	4.256	-23.415	-0.751	-0.754	1.729	3.595	10.475
3.345	4.789	-23.416	-0.757	-0.759	2.090	4.066	10.475
3.559	5.391	-23.419	-0.761	-0.762	2.497	4.583	10.475
3.777	6.030	-23.426	-0.761	-0.762	2.911	5.139	10.475
4.009	6.790	-23.444	-0.760	-0.760	3.345	5.737	10.475
4.291	7.790	-23.503	-0.786	-0.786	3.846	6.447	10.475
4.678	8.473	-23.648	-0.605	-0.605	4.490	7.368	10.475
4.948	8.835	-23.658	-0.501	-0.501	5.004	8.134	10.475
5.207	9.489	-23.665	-0.535	-0.535	5.419	8.893	10.475
5.463	10.056	-23.689	-0.565	-0.565	5.778	9.573	10.474
5.723	10.576	-23.703	-0.593	-0.593	6.060	10.191	10.474
5.985	11.048	-23.723	-0.614	-0.614	6.304	10.734	10.474
6.255	11.440	-23.754	-0.630	-0.630	6.489	11.223	10.473
6.541	11.765	-23.799	-0.638	-0.638	6.622	11.699	10.473
6.851	11.957	-23.863	-0.623	-0.623	6.654	12.118	10.472
7.180	11.962	-23.934	-0.556	-0.556	6.524	12.457	10.470
7.502	11.908	-23.984	-0.479	-0.479	6.272	12.707	10.469
7.806	11.892	-24.010	-0.466	-0.466	6.004	12.903	10.466
8.106	11.797	-24.032	-0.430	-0.430	5.718	13.081	10.463
8.402	11.596	-24.038	-0.399	-0.399	5.276	13.225	10.458
8.692	11.455	-24.038	-0.398	-0.398	4.777	13.328	10.453
8.982	11.205	-24.038	-0.398	-0.398	4.295	13.407	10.445
9.267	10.998	-24.038	-0.398	-0.398	3.857	13.472	10.436

Low-mass nuclear-burning: $M = 0.3M_\odot$,$L_{in} = 0.1L_\odot$,$T_{\mathrm{surface}} = 10^{3.3}K$,$L_e = L_{in}$

Log(Sigma)	Log(M+)	Log(M-)	Log(Rho)	Log(p)	Log(T)	Log(hs)	Log(vs)	Log(vc)
-2.000	20.051	32.778	-8.612	2.652	3.692	6.613	5.677	nan
-1.829	20.222	32.778	-8.438	2.822	3.693	6.610	5.675	nan
-1.657	20.394	32.778	-8.264	2.993	3.693	6.608	5.673	nan
-1.485	20.566	32.778	-8.090	3.165	3.693	6.606	5.672	nan
-1.313	20.738	32.778	-7.917	3.337	3.693	6.604	5.671	nan
-1.141	20.911	32.778	-7.743	3.510	3.693	6.603	5.670	nan
-0.968	21.084	32.778	-7.569	3.683	3.693	6.602	5.670	nan
-0.794	21.257	32.778	-7.396	3.856	3.694	6.602	5.669	nan
-0.619	21.432	32.778	-7.222	4.030	3.695	6.603	5.670	nan
-0.443	21.608	32.778	-7.048	4.207	3.698	6.605	5.671	nan
-0.263	21.788	32.778	-6.874	4.387	3.705	6.611	5.674	nan
-0.076	21.975	32.778	-6.701	4.574	3.718	6.625	5.681	nan
0.128	22.180	32.778	-6.527	4.779	3.746	6.656	5.697	3.270
0.438	22.489	32.778	-6.381	5.088	3.852	6.819	5.813	5.246
0.948	22.999	32.778	-6.225	5.598	4.000	7.174	5.963	5.289
1.209	23.260	32.778	-6.052	5.859	4.065	7.261	5.996	5.201
1.442	23.494	32.778	-5.878	6.093	4.106	7.321	6.026	5.126
1.667	23.719	32.778	-5.704	6.317	4.139	7.372	6.052	5.065
1.888	23.939	32.778	-5.531	6.538	4.170	7.418	6.076	5.007

Log(Sigma)	Log(M+)	Log(M-)	Log(Rho)	Log(p)	Log(T)	Log(hs)	Log(vs)	Log(vc)
2.106	24.158	32.778	-5.357	6.756	4.200	7.463	6.100	4.953
2.324	24.376	32.778	-5.183	6.974	4.230	7.508	6.124	4.881
2.543	24.594	32.778	-5.009	7.193	4.261	7.553	6.149	4.820
2.762	24.814	32.778	-4.836	7.413	4.293	7.599	6.174	4.731
2.984	25.035	32.778	-4.662	7.634	4.327	7.646	6.201	4.632
3.208	25.259	32.778	-4.488	7.858	4.363	7.696	6.229	4.507
3.435	25.486	32.778	-4.315	8.085	4.401	7.749	6.259	4.351
3.665	25.717	32.778	-4.141	8.315	4.444	7.806	6.291	4.212
3.900	25.951	32.778	-3.967	8.550	4.490	7.867	6.325	4.143
4.138	26.190	32.778	-3.793	8.788	4.541	7.932	6.362	4.099
4.382	26.433	32.778	-3.620	9.032	4.597	8.002	6.402	4.049
4.632	26.684	32.778	-3.446	9.283	4.660	8.079	6.447	4.009
4.891	26.943	32.778	-3.272	9.542	4.734	8.164	6.498	3.973
5.161	27.212	32.778	-3.099	9.811	4.820	8.259	6.553	3.920
5.436	27.487	32.778	-2.925	10.086	4.915	8.361	6.606	3.875
5.711	27.762	32.778	-2.751	10.361	5.010	8.462	6.654	3.815
5.984	28.035	32.778	-2.577	10.634	5.104	8.561	6.705	3.751
6.260	28.312	32.778	-2.404	10.910	5.201	8.664	6.760	3.706
6.542	28.594	32.778	-2.230	11.193	5.305	8.773	6.819	3.651
6.829	28.880	32.778	-2.056	11.479	5.416	8.886	6.877	3.595
7.117	29.169	32.778	-1.883	11.768	5.529	9.000	6.936	3.536
7.407	29.458	32.778	-1.709	12.057	5.644	9.116	6.994	3.475
7.696	29.748	32.777	-1.535	12.347	5.759	9.232	7.052	3.382
7.986	30.038	32.777	-1.361	12.636	5.874	9.348	7.110	3.244
8.271	30.322	32.776	-1.188	12.921	5.984	9.458	7.166	nan
8.515	30.566	32.775	-1.014	13.165	6.054	9.529	7.201	nan
8.746	30.797	32.773	-0.840	13.396	6.112	9.587	7.230	nan
8.973	31.025	32.770	-0.666	13.624	6.164	9.640	7.256	nan
9.198	31.250	32.765	-0.493	13.848	6.215	9.691	7.282	nan
9.410	31.462	32.756	-0.327	14.061	6.261	9.738	7.305	nan

Log(Sigma)	Log(Gamma)	Log(mu)	Log(Grad)	Log(GradA)	Log(GradR)	Log(Tau)	Log(R)
-2.000	nan	-23.429	-3.985	-0.835	-3.985	-4.262	10.476
-1.829	nan	-23.426	-3.861	-0.824	-3.861	-3.969	10.476
-1.657	nan	-23.424	-3.676	-0.814	-3.676	-3.668	10.475
-1.485	nan	-23.422	-3.441	-0.804	-3.441	-3.360	10.475
-1.313	nan	-23.421	-3.170	-0.796	-3.170	-3.048	10.475
-1.141	nan	-23.420	-2.873	-0.788	-2.873	-2.732	10.475
-0.968	nan	-23.419	-2.565	-0.781	-2.565	-2.413	10.475
-0.794	nan	-23.418	-2.251	-0.776	-2.251	-2.092	10.475
-0.619	nan	-23.417	-1.939	-0.771	-1.939	-1.769	10.475
-0.443	nan	-23.416	-1.624	-0.768	-1.624	-1.443	10.475
-0.263	nan	-23.416	-1.312	-0.767	-1.312	-1.108	10.475
-0.076	nan	-23.417	-1.013	-0.769	-1.013	-0.758	10.475
0.128	-2.668	-23.419	-0.718	-0.778	-0.725	-0.370	10.475
0.438	0.241	-23.477	-0.430	-0.845	-0.057	0.429	10.475

Log(Sigma)	Log(Gamma)	Log(mu)	Log(Grad)	Log(GradA)	Log(GradR)	Log(Tau)	Log(R)
0.948	1.812	-23.684	-0.499	-0.778	1.311	2.345	10.475
1.209	2.751	-23.706	-0.705	-0.888	1.886	3.309	10.475
1.442	3.394	-23.725	-0.799	-0.913	2.282	3.966	10.475
1.667	3.927	-23.742	-0.842	-0.916	2.606	4.494	10.475
1.888	4.409	-23.758	-0.860	-0.909	2.897	4.961	10.474
2.106	4.868	-23.773	-0.863	-0.897	3.171	5.394	10.474
2.324	5.274	-23.787	-0.859	-0.880	3.408	5.805	10.474
2.543	5.682	-23.801	-0.846	-0.860	3.622	6.207	10.474
2.762	6.048	-23.815	-0.830	-0.837	3.793	6.601	10.473
2.984	6.389	-23.829	-0.808	-0.812	3.897	6.996	10.473
3.208	6.699	-23.844	-0.782	-0.784	3.914	7.392	10.473
3.435	6.970	-23.858	-0.752	-0.753	3.840	7.795	10.472
3.665	7.238	-23.872	-0.721	-0.721	3.797	8.202	10.472
3.900	7.512	-23.887	-0.688	-0.689	3.894	8.595	10.471
4.138	7.825	-23.901	-0.655	-0.656	4.070	8.980	10.471
4.382	8.046	-23.915	-0.618	-0.618	4.164	9.346	10.470
4.632	8.149	-23.928	-0.573	-0.573	4.139	9.668	10.469
4.891	8.111	-23.939	-0.520	-0.520	3.973	9.926	10.468
5.161	7.967	-23.949	-0.474	-0.474	3.695	10.123	10.466
5.436	7.866	-23.955	-0.458	-0.458	3.400	10.281	10.464
5.711	7.826	-23.961	-0.465	-0.465	3.141	10.424	10.462
5.984	7.745	-23.967	-0.463	-0.463	2.853	10.557	10.459
6.260	7.548	-23.973	-0.443	-0.443	2.456	10.668	10.455
6.542	7.246	-23.977	-0.422	-0.422	1.961	10.749	10.450
6.829	6.954	-23.980	-0.410	-0.410	1.462	10.809	10.443
7.117	6.702	-23.981	-0.404	-0.404	0.992	10.858	10.434
7.407	6.500	-23.982	-0.401	-0.401	0.568	10.902	10.421
7.696	6.323	-23.983	-0.400	-0.400	0.197	10.949	10.404
7.986	6.117	-23.983	-0.400	-0.400	-0.157	11.002	10.381
8.271	nan	-23.984	-0.483	-0.399	-0.483	11.060	10.350
8.515	nan	-23.984	-0.586	-0.399	-0.586	11.121	10.315
8.746	nan	-23.985	-0.623	-0.399	-0.623	11.197	10.272
8.973	nan	-23.985	-0.641	-0.399	-0.641	11.292	10.219
9.198	nan	-23.986	-0.654	-0.399	-0.654	11.408	10.151
9.410	nan	-23.987	-0.668	-0.398	-0.668	11.533	10.065

Low-mass nuclear-burning: $M = 0.3M_{\odot}$,$L_{in} = 0.1L_{\odot}$,$T_{\text{surface}} = 10^{3.3}K$,$L_e = 10L_{in}$

Log(Sigma)	Log(M+)	Log(M-)	Log(Rho)	Log(p)	Log(T)	Log(hs)	Log(vs)	Log(vc)
-1.999	20.052	32.778	-9.204	2.665	3.944	7.219	5.957	nan
-1.829	20.223	32.778	-9.030	2.831	3.948	7.212	5.954	nan
-1.648	20.404	32.778	-8.857	3.009	3.956	7.215	5.958	nan
-1.434	20.617	32.778	-8.683	3.220	3.977	7.253	5.977	3.099
-1.027	21.024	32.778	-8.565	3.624	4.108	7.540	6.144	2.770
-0.777	21.274	32.778	-8.391	3.874	4.173	7.615	6.200	nan
-0.546	21.505	32.778	-8.218	4.104	4.224	7.672	6.217	2.167
-0.313	21.739	32.778	-8.044	4.338	4.276	7.732	6.249	2.358

Log(Sigma)	Log(M+)	Log(M-)	Log(Rho)	Log(p)	Log(T)	Log(hs)	Log(vs)	Log(vc)
-0.081	21.971	32.778	-7.870	4.570	4.329	7.790	6.300	nan
0.151	22.203	32.778	-7.696	4.802	4.386	7.848	6.348	nan
0.386	22.437	32.778	-7.523	5.036	4.446	7.909	6.385	nan
0.626	22.678	32.778	-7.349	5.276	4.512	7.975	6.418	nan
0.880	22.932	32.778	-7.175	5.530	4.590	8.056	6.439	3.176
1.151	23.202	32.778	-7.001	5.801	4.678	8.152	6.465	4.907
1.398	23.450	32.778	-6.828	6.048	4.745	8.226	6.520	nan
1.626	23.677	32.778	-6.654	6.276	4.797	8.280	6.561	nan
1.847	23.898	32.778	-6.480	6.497	4.844	8.327	6.591	nan
2.066	24.117	32.778	-6.307	6.716	4.890	8.373	6.617	nan
2.286	24.337	32.778	-6.133	6.936	4.936	8.419	6.642	nan
2.506	24.557	32.778	-5.959	7.156	4.984	8.466	6.666	nan
2.725	24.777	32.778	-5.785	7.375	5.030	8.511	6.689	nan
2.941	24.992	32.778	-5.612	7.591	5.072	8.553	6.710	nan
3.149	25.200	32.778	-5.438	7.799	5.107	8.587	6.727	nan
3.348	25.399	32.778	-5.264	7.998	5.133	8.612	6.740	nan
3.537	25.588	32.778	-5.091	8.187	5.149	8.628	6.748	nan
3.718	25.769	32.778	-4.917	8.368	5.158	8.635	6.753	nan
3.897	25.949	32.778	-4.743	8.547	5.164	8.641	6.756	nan
4.080	26.132	32.778	-4.569	8.730	5.173	8.650	6.760	nan
4.271	26.323	32.778	-4.396	8.921	5.191	8.667	6.769	nan
4.475	26.526	32.778	-4.222	9.125	5.221	8.697	6.784	nan
4.689	26.741	32.778	-4.048	9.339	5.262	8.738	6.805	nan
4.910	26.961	32.778	-3.875	9.560	5.309	8.785	6.828	nan
5.131	27.183	32.778	-3.701	9.781	5.356	8.832	6.852	nan
5.351	27.403	32.778	-3.527	10.002	5.403	8.879	6.875	nan
5.571	27.622	32.778	-3.353	10.221	5.448	8.924	6.898	nan
5.789	27.840	32.778	-3.180	10.439	5.493	8.969	6.920	nan
6.007	28.059	32.778	-3.006	10.657	5.538	9.013	6.943	nan
6.226	28.277	32.778	-2.832	10.876	5.583	9.058	6.965	nan
6.445	28.496	32.778	-2.659	11.095	5.628	9.104	6.988	nan
6.664	28.716	32.778	-2.485	11.314	5.673	9.149	7.011	nan
6.884	28.935	32.778	-2.311	11.534	5.720	9.196	7.034	nan
7.104	29.155	32.778	-2.137	11.754	5.766	9.242	7.057	nan
7.323	29.375	32.778	-1.964	11.973	5.812	9.287	7.079	nan
7.542	29.594	32.778	-1.790	12.192	5.857	9.332	7.102	nan
7.761	29.813	32.777	-1.616	12.411	5.903	9.377	7.125	nan
7.981	30.033	32.777	-1.443	12.631	5.949	9.424	7.148	nan
8.202	30.253	32.777	-1.269	12.852	5.997	9.471	7.172	nan
8.424	30.476	32.776	-1.095	13.074	6.045	9.520	7.196	nan
8.647	30.699	32.774	-0.921	13.298	6.094	9.569	7.221	nan
8.871	30.923	32.772	-0.748	13.521	6.144	9.619	7.246	nan
9.095	31.146	32.768	-0.574	13.745	6.193	9.669	7.271	nan
9.302	31.353	32.761	-0.413	13.953	6.239	9.715	7.294	nan

Log(Sigma)	Log(Gamma)	Log(mu)	Log(Grad)	Log(GradA)	Log(GradR)	Log(Tau)	Log(R)
-1.999	nan	-23.771	-1.718	-1.132	-1.718	-1.439	10.474
-1.829	nan	-23.763	-1.477	-1.127	-1.477	-1.192	10.474
-1.648	nan	-23.762	-1.209	-1.121	-1.209	-0.915	10.474
-1.434	-4.492	-23.780	-0.825	-1.118	-0.834	-0.546	10.474
-1.027	-5.430	-23.934	-0.507	-0.778	-0.534	0.365	10.474
-0.777	nan	-23.945	-0.638	-0.614	-0.638	0.688	10.473
-0.546	-5.861	-23.951	-0.654	-0.698	-0.660	0.925	10.473
-0.313	-5.452	-23.959	-0.647	-0.682	-0.652	1.147	10.473
-0.081	nan	-23.964	-0.626	-0.538	-0.626	1.373	10.472
0.151	nan	-23.966	-0.601	-0.449	-0.601	1.606	10.472
0.386	nan	-23.967	-0.579	-0.424	-0.579	1.853	10.471
0.626	nan	-23.967	-0.521	-0.425	-0.521	2.120	10.470
0.880	-3.518	-23.968	-0.498	-0.505	-0.499	2.437	10.469
1.151	-1.362	-23.975	-0.523	-0.638	-0.531	2.782	10.468
1.398	nan	-23.982	-0.614	-0.534	-0.614	3.053	10.467
1.626	nan	-23.984	-0.661	-0.467	-0.661	3.267	10.466
1.847	nan	-23.985	-0.677	-0.439	-0.677	3.463	10.464
2.066	nan	-23.985	-0.678	-0.428	-0.678	3.657	10.462
2.286	nan	-23.985	-0.671	-0.418	-0.671	3.859	10.460
2.506	nan	-23.985	-0.672	-0.416	-0.672	4.074	10.458
2.725	nan	-23.985	-0.686	-0.415	-0.686	4.303	10.456
2.941	nan	-23.985	-0.734	-0.413	-0.734	4.545	10.453
3.149	nan	-23.985	-0.823	-0.411	-0.823	4.793	10.451
3.348	nan	-23.985	-0.968	-0.409	-0.968	5.053	10.448
3.537	nan	-23.986	-1.201	-0.406	-1.201	5.324	10.445
3.718	nan	-23.986	-1.449	-0.404	-1.449	5.610	10.442
3.897	nan	-23.985	-1.416	-0.402	-1.416	5.915	10.439
4.080	nan	-23.985	-1.160	-0.401	-1.160	6.236	10.436
4.271	nan	-23.985	-0.925	-0.400	-0.925	6.564	10.433
4.475	nan	-23.985	-0.767	-0.400	-0.767	6.887	10.430
4.689	nan	-23.985	-0.688	-0.400	-0.688	7.189	10.425
4.910	nan	-23.985	-0.665	-0.399	-0.665	7.458	10.421
5.131	nan	-23.986	-0.670	-0.399	-0.670	7.696	10.415
5.351	nan	-23.985	-0.679	-0.399	-0.679	7.909	10.409
5.571	nan	-23.985	-0.687	-0.399	-0.687	8.107	10.402
5.789	nan	-23.985	-0.690	-0.399	-0.690	8.297	10.394
6.007	nan	-23.985	-0.690	-0.399	-0.690	8.482	10.386
6.226	nan	-23.985	-0.687	-0.399	-0.687	8.666	10.376
6.445	nan	-23.985	-0.683	-0.399	-0.683	8.850	10.365
6.664	nan	-23.985	-0.679	-0.399	-0.679	9.035	10.352
6.884	nan	-23.986	-0.678	-0.399	-0.678	9.220	10.337
7.104	nan	-23.985	-0.679	-0.399	-0.679	9.406	10.320
7.323	nan	-23.985	-0.680	-0.399	-0.680	9.590	10.300
7.542	nan	-23.984	-0.681	-0.399	-0.681	9.773	10.277
7.761	nan	-23.984	-0.680	-0.399	-0.680	9.957	10.250
7.981	nan	-23.984	-0.676	-0.399	-0.676	10.142	10.218

Log(Sigma)	Log(Gamma)	Log(mu)	Log(Grad)	Log(GradA)	Log(GradR)	Log(Tau)	Log(R)
8.202	nan	-23.984	-0.667	-0.399	-0.667	10.331	10.178
8.424	nan	-23.984	-0.659	-0.399	-0.659	10.524	10.130
8.647	nan	-23.985	-0.654	-0.399	-0.654	10.721	10.067
8.871	nan	-23.985	-0.655	-0.399	-0.655	10.920	9.984
9.095	nan	-23.985	-0.655	-0.399	-0.655	11.118	9.868
9.302	nan	-23.986	-0.666	-0.398	-0.666	11.299	9.701

Brown Dwarf: $M = 0.02M_{\odot}$,$L_{in} = 0.01L_{\odot}$,$T_{\text{surface}} = 10^3K$,$L_e = 0$

Log(Sigma)	Log(M+)	Log(M-)	Log(Rho)	Log(p)	Log(T)	Log(hs)	Log(vs)	Log(vc)
-1.999	19.078	31.602	-8.220	2.449	3.116	6.221	5.387	nan
-1.824	19.253	31.602	-8.046	2.624	3.117	6.222	5.387	nan
-1.648	19.428	31.602	-7.872	2.800	3.119	6.224	5.388	nan
-1.472	19.605	31.602	-7.699	2.977	3.122	6.228	5.390	nan
-1.293	19.783	31.602	-7.525	3.156	3.127	6.232	5.392	nan
-1.113	19.964	31.602	-7.351	3.336	3.133	6.238	5.395	nan
-0.931	20.146	31.602	-7.178	3.518	3.142	6.247	5.399	nan
-0.747	20.330	31.602	-7.004	3.702	3.152	6.257	5.404	nan
-0.562	20.514	31.602	-6.830	3.886	3.163	6.268	5.409	nan
-0.379	20.697	31.602	-6.656	4.069	3.172	6.277	5.414	nan
-0.200	20.876	31.602	-6.483	4.248	3.177	6.283	5.416	nan
-0.023	21.054	31.602	-6.309	4.426	3.181	6.286	5.418	nan
0.155	21.232	31.602	-6.135	4.604	3.185	6.291	5.420	nan
0.335	21.412	31.602	-5.962	4.784	3.192	6.297	5.423	nan
0.519	21.596	31.602	-5.788	4.968	3.202	6.307	5.428	nan
0.709	21.785	31.602	-5.614	5.157	3.218	6.323	5.436	nan
0.906	21.982	31.602	-5.440	5.354	3.241	6.346	5.447	nan
1.101	22.178	31.602	-5.267	5.550	3.263	6.368	5.458	nan
1.282	22.358	31.602	-5.093	5.730	3.270	6.375	5.461	nan
1.461	22.537	31.602	-4.919	5.910	3.275	6.380	5.463	nan
1.643	22.719	31.602	-4.746	6.091	3.283	6.388	5.467	nan
1.829	22.905	31.602	-4.572	6.277	3.295	6.401	5.473	nan
2.022	23.098	31.602	-4.398	6.470	3.315	6.420	5.483	nan
2.226	23.303	31.602	-4.224	6.674	3.345	6.450	5.497	nan
2.442	23.518	31.602	-4.051	6.890	3.387	6.492	5.517	3.649
2.657	23.734	31.602	-3.877	7.105	3.429	6.534	5.537	3.689
2.871	23.948	31.602	-3.703	7.320	3.469	6.575	5.556	3.656
3.085	24.161	31.602	-3.530	7.533	3.508	6.614	5.576	3.613
3.298	24.374	31.602	-3.356	7.747	3.548	6.654	5.596	3.558
3.511	24.588	31.602	-3.182	7.959	3.587	6.693	5.615	3.508
3.724	24.801	31.602	-3.008	8.172	3.626	6.732	5.635	3.456
3.937	25.013	31.602	-2.835	8.385	3.665	6.771	5.654	3.400
4.149	25.226	31.602	-2.661	8.598	3.703	6.810	5.673	3.343
4.362	25.439	31.602	-2.487	8.811	3.741	6.849	5.693	3.290
4.575	25.651	31.602	-2.313	9.023	3.779	6.888	5.712	3.224
4.787	25.864	31.602	-2.140	9.236	3.817	6.927	5.732	3.169
5.000	26.077	31.602	-1.966	9.449	3.854	6.966	5.752	3.111

Log(Sigma)	Log(M+)	Log(M-)	Log(Rho)	Log(p)	Log(T)	Log(hs)	Log(vs)	Log(vc)
5.213	26.290	31.602	-1.792	9.662	3.890	7.006	5.772	3.048
5.428	26.505	31.602	-1.619	9.877	3.927	7.047	5.795	2.986
5.648	26.724	31.602	-1.445	10.096	3.963	7.093	5.827	2.924
5.889	26.966	31.602	-1.271	10.338	4.001	7.161	5.902	2.847
6.264	27.341	31.602	-1.100	10.715	4.041	7.366	6.166	2.700
6.570	27.647	31.602	-1.024	11.022	4.061	7.598	6.359	2.659

Log(Sigma)	Log(Gamma)	Log(mu)	Log(Grad)	Log(GradA)	Log(GradR)	Log(Tau)	Log(R)
-1.999	nan	-23.413	-2.220	-0.674	-2.220	-1.889	9.988
-1.824	nan	-23.413	-2.031	-0.674	-2.031	-1.674	9.988
-1.648	nan	-23.414	-1.851	-0.674	-1.851	-1.467	9.988
-1.472	nan	-23.414	-1.674	-0.675	-1.674	-1.266	9.988
-1.293	nan	-23.414	-1.516	-0.675	-1.516	-1.069	9.988
-1.113	nan	-23.413	-1.383	-0.676	-1.383	-0.881	9.988
-0.931	nan	-23.413	-1.280	-0.677	-1.280	-0.705	9.988
-0.747	nan	-23.413	-1.233	-0.678	-1.233	-0.546	9.988
-0.562	nan	-23.413	-1.254	-0.679	-1.254	-0.417	9.988
-0.379	nan	-23.413	-1.420	-0.681	-1.420	-0.322	9.988
-0.200	nan	-23.414	-1.651	-0.681	-1.651	-0.275	9.988
-0.023	nan	-23.414	-1.691	-0.682	-1.691	-0.243	9.988
0.155	nan	-23.414	-1.519	-0.682	-1.519	-0.205	9.988
0.335	nan	-23.413	-1.346	-0.683	-1.346	-0.152	9.988
0.519	nan	-23.413	-1.170	-0.684	-1.170	-0.075	9.988
0.709	nan	-23.413	-0.996	-0.687	-0.996	0.031	9.988
0.906	nan	-23.413	-0.888	-0.690	-0.888	0.173	9.988
1.101	nan	-23.413	-1.211	-0.693	-1.211	0.294	9.987
1.282	nan	-23.414	-1.582	-0.694	-1.582	0.330	9.987
1.461	nan	-23.414	-1.441	-0.695	-1.441	0.358	9.987
1.643	nan	-23.414	-1.266	-0.696	-1.266	0.400	9.987
1.829	nan	-23.414	-1.092	-0.698	-1.092	0.462	9.987
2.022	nan	-23.414	-0.917	-0.701	-0.917	0.555	9.987
2.226	nan	-23.414	-0.741	-0.707	-0.741	0.696	9.987
2.442	1.725	-23.414	-0.712	-0.714	-0.549	0.909	9.987
2.657	2.207	-23.414	-0.720	-0.723	-0.324	1.193	9.987
2.871	2.620	-23.414	-0.730	-0.731	-0.101	1.531	9.987
3.085	2.935	-23.414	-0.733	-0.734	0.042	1.872	9.987
3.298	3.186	-23.414	-0.735	-0.736	0.132	2.171	9.987
3.511	3.632	-23.414	-0.737	-0.738	0.414	2.497	9.987
3.724	4.172	-23.415	-0.740	-0.740	0.792	2.914	9.987
3.937	4.726	-23.415	-0.742	-0.743	1.189	3.428	9.986
4.149	5.236	-23.416	-0.745	-0.745	1.540	3.946	9.986
4.362	5.668	-23.417	-0.748	-0.748	1.811	4.420	9.986
4.575	6.081	-23.418	-0.752	-0.752	2.076	4.859	9.986
4.787	6.547	-23.419	-0.756	-0.756	2.382	5.290	9.986
5.000	7.071	-23.421	-0.761	-0.761	2.747	5.766	9.986
5.213	7.637	-23.424	-0.767	-0.767	3.153	6.286	9.985

Log(Sigma)	Log(Gamma)	Log(mu)	Log(Grad)	Log(GradA)	Log(GradR)	Log(Tau)	Log(R)
5.428	8.213	-23.428	-0.774	-0.774	3.556	6.830	9.985
5.648	8.823	-23.438	-0.788	-0.788	3.958	7.386	9.985
5.889	9.520	-23.468	-0.851	-0.851	4.376	7.976	9.985
6.264	10.356	-23.634	-1.117	-1.117	4.918	8.774	9.984
6.570	10.813	-23.845	-1.207	-1.207	5.301	9.305	9.983

Brown Dwarf: $M = 0.02M_{\odot}$,$L_{in} = 0.01L_{\odot}$,$T_{\text{surface}} = 10^3K$,$L_e = L_{in}$

Log(Sigma)	Log(M+)	Log(M-)	Log(Rho)	Log(p)	Log(T)	Log(hs)	Log(vs)	Log(vc)
-2.000	19.077	31.602	-8.811	2.451	3.688	6.813	5.676	nan
-1.829	19.248	31.602	-8.637	2.621	3.688	6.810	5.674	nan
-1.658	19.419	31.602	-8.463	2.792	3.688	6.807	5.672	nan
-1.486	19.591	31.602	-8.289	2.964	3.688	6.805	5.670	nan
-1.314	19.763	31.602	-8.116	3.135	3.689	6.803	5.669	nan
-1.141	19.935	31.602	-7.942	3.308	3.689	6.801	5.668	nan
-0.969	20.108	31.602	-7.768	3.480	3.689	6.800	5.668	nan
-0.795	20.281	31.602	-7.595	3.653	3.690	6.799	5.667	nan
-0.621	20.455	31.602	-7.421	3.827	3.691	6.800	5.668	nan
-0.446	20.631	31.602	-7.247	4.002	3.693	6.801	5.668	nan
-0.269	20.808	31.602	-7.073	4.180	3.697	6.805	5.670	nan
-0.086	20.991	31.602	-6.900	4.363	3.705	6.814	5.675	nan
0.107	21.184	31.602	-6.726	4.556	3.724	6.833	5.685	nan
0.329	21.406	31.602	-6.552	4.778	3.767	6.882	5.712	3.952
0.795	21.872	31.602	-6.451	5.244	3.924	7.246	5.955	5.339
1.150	22.226	31.602	-6.279	5.599	4.038	7.429	5.980	5.265
1.396	22.472	31.602	-6.105	5.845	4.087	7.501	6.014	5.193
1.626	22.702	31.602	-5.931	6.075	4.123	7.558	6.042	5.129
1.849	22.926	31.602	-5.758	6.298	4.155	7.607	6.068	5.071
2.069	23.145	31.602	-5.584	6.517	4.185	7.653	6.093	5.016
2.287	23.364	31.602	-5.410	6.736	4.214	7.697	6.117	4.945
2.505	23.582	31.602	-5.237	6.954	4.244	7.742	6.141	4.886
2.724	23.801	31.602	-5.063	7.172	4.275	7.787	6.166	4.796
2.944	24.021	31.602	-4.889	7.393	4.307	7.833	6.192	4.697
3.166	24.243	31.602	-4.715	7.615	4.342	7.882	6.220	4.566
3.392	24.468	31.602	-4.542	7.840	4.379	7.934	6.249	4.378
3.620	24.697	31.602	-4.368	8.069	4.420	7.988	6.280	4.125
3.853	24.929	31.602	-4.194	8.301	4.464	8.047	6.313	3.890
4.089	25.166	31.602	-4.020	8.538	4.514	8.110	6.349	3.823
4.331	25.408	31.602	-3.847	8.779	4.568	8.178	6.387	3.777
4.579	25.655	31.602	-3.673	9.027	4.629	8.252	6.431	3.738
4.836	25.912	31.602	-3.499	9.284	4.701	8.335	6.481	3.699
5.104	26.180	31.602	-3.326	9.552	4.787	8.430	6.537	3.656
5.379	26.456	31.602	-3.152	9.828	4.882	8.531	6.590	3.606
5.653	26.730	31.602	-2.978	10.102	4.977	8.632	6.638	3.548
5.925	27.001	31.602	-2.804	10.373	5.069	8.729	6.686	3.491
6.199	27.276	31.602	-2.631	10.648	5.164	8.830	6.741	3.431
6.480	27.556	31.602	-2.457	10.928	5.268	8.937	6.800	3.378

Log(Sigma)	Log(Gamma)	Log(mu)	Log(Grad)	Log(GradA)	Log(GradR)	Log(Tau)	Log(R)
-2.000	nan	-23.431	-3.447	-0.843	-3.447	-4.409	9.986
-1.829	nan	-23.428	-3.422	-0.832	-3.422	-4.119	9.986
-1.658	nan	-23.426	-3.372	-0.821	-3.372	-3.823	9.986
-1.486	nan	-23.424	-3.280	-0.811	-3.280	-3.521	9.986
-1.314	nan	-23.422	-3.134	-0.802	-3.134	-3.212	9.986
-1.141	nan	-23.420	-2.932	-0.794	-2.932	-2.900	9.986
-0.969	nan	-23.419	-2.681	-0.786	-2.681	-2.584	9.986
-0.795	nan	-23.418	-2.400	-0.780	-2.400	-2.266	9.986
-0.621	nan	-23.417	-2.101	-0.774	-2.101	-1.945	9.985
-0.446	nan	-23.417	-1.796	-0.770	-1.796	-1.622	9.985
-0.269	nan	-23.417	-1.486	-0.768	-1.486	-1.294	9.985
-0.086	nan	-23.417	-1.176	-0.768	-1.176	-0.953	9.985
0.107	nan	-23.418	-0.883	-0.772	-0.883	-0.589	9.985
0.329	-2.023	-23.423	-0.562	-0.792	-0.562	-0.153	9.985
0.795	1.229	-23.631	-0.558	-0.807	0.639	1.444	9.984
1.150	2.309	-23.699	-0.628	-0.880	1.646	2.904	9.983
1.396	3.068	-23.723	-0.768	-0.927	2.104	3.694	9.983
1.626	3.640	-23.743	-0.832	-0.934	2.452	4.276	9.982
1.849	4.142	-23.761	-0.860	-0.928	2.758	4.765	9.981
2.069	4.596	-23.777	-0.869	-0.915	3.025	5.204	9.980
2.287	5.011	-23.792	-0.869	-0.897	3.272	5.620	9.979
2.505	5.421	-23.806	-0.858	-0.877	3.490	6.021	9.978
2.724	5.777	-23.820	-0.843	-0.854	3.655	6.413	9.976
2.944	6.114	-23.834	-0.822	-0.828	3.759	6.801	9.975
3.166	6.405	-23.849	-0.796	-0.799	3.752	7.187	9.973
3.392	6.630	-23.863	-0.766	-0.767	3.576	7.577	9.971
3.620	6.782	-23.877	-0.734	-0.734	3.167	7.974	9.969
3.853	6.925	-23.891	-0.700	-0.700	2.833	8.374	9.966
4.089	7.212	-23.905	-0.666	-0.666	2.950	8.762	9.963
4.331	7.468	-23.918	-0.629	-0.629	3.078	9.144	9.960
4.579	7.623	-23.931	-0.582	-0.582	3.108	9.492	9.955
4.836	7.625	-23.942	-0.525	-0.525	2.991	9.782	9.949
5.104	7.484	-23.951	-0.474	-0.474	2.715	10.000	9.942
5.379	7.356	-23.958	-0.455	-0.455	2.403	10.166	9.932
5.653	7.327	-23.963	-0.467	-0.467	2.146	10.310	9.920
5.925	7.300	-23.969	-0.469	-0.469	1.900	10.451	9.904
6.199	7.125	-23.974	-0.448	-0.448	1.542	10.575	9.883
6.480	6.846	-23.978	-0.424	-0.424	1.074	10.669	9.854

Brown Dwarf: $M = 0.02M_{\odot}$,$L_{in} = 0.01L_{\odot}$,$T_{\text{surface}} = 10^3K$,$L_e = 10L_{in}$

Log(Sigma)	Log(M+)	Log(M-)	Log(Rho)	Log(p)	Log(T)	Log(hs)	Log(vs)	Log(vc)
-2.000	19.077	31.602	-9.432	2.472	3.946	7.456	5.971	nan
-1.830	19.246	31.602	-9.258	2.634	3.950	7.444	5.968	nan
-1.652	19.425	31.602	-9.084	2.808	3.957	7.443	5.969	nan
-1.448	19.629	31.602	-8.910	3.008	3.974	7.470	5.984	2.900
-1.042	20.035	31.602	-8.748	3.410	4.081	7.709	6.120	2.864

Log(Sigma)	Log(M+)	Log(M-)	Log(Rho)	Log(p)	Log(T)	Log(hs)	Log(vs)	Log(vc)
-0.780	20.297	31.602	-8.575	3.671	4.151	7.797	6.191	nan
-0.549	20.527	31.602	-8.401	3.900	4.202	7.852	6.209	1.233
-0.318	20.759	31.602	-8.227	4.131	4.253	7.910	6.233	2.336
-0.086	20.990	31.602	-8.053	4.362	4.305	7.967	6.280	nan
0.144	21.221	31.602	-7.880	4.593	4.359	8.024	6.331	nan
0.377	21.453	31.602	-7.706	4.826	4.417	8.083	6.370	nan
0.613	21.690	31.602	-7.532	5.062	4.479	8.146	6.403	nan
0.860	21.937	31.602	-7.358	5.309	4.552	8.219	6.431	nan
1.126	22.203	31.602	-7.185	5.575	4.638	8.311	6.445	4.836
1.390	22.467	31.602	-7.011	5.839	4.717	8.401	6.500	nan
1.622	22.699	31.602	-6.837	6.071	4.773	8.460	6.547	nan
1.845	22.922	31.602	-6.664	6.293	4.822	8.509	6.579	nan
2.064	23.141	31.602	-6.490	6.513	4.868	8.554	6.606	nan
2.283	23.359	31.602	-6.316	6.732	4.913	8.599	6.631	nan
2.501	23.578	31.602	-6.142	6.951	4.959	8.645	6.654	nan
2.719	23.796	31.602	-5.969	7.168	5.003	8.688	6.676	nan
2.934	24.010	31.602	-5.795	7.382	5.045	8.729	6.697	nan
3.141	24.218	31.602	-5.621	7.590	5.080	8.763	6.714	nan
3.339	24.416	31.602	-5.448	7.788	5.106	8.787	6.727	nan
3.527	24.604	31.602	-5.274	7.976	5.121	8.801	6.734	nan
3.707	24.784	31.602	-5.100	8.156	5.128	8.807	6.738	nan
3.882	24.959	31.602	-4.926	8.331	5.130	8.809	6.739	nan
4.057	25.133	31.602	-4.753	8.506	5.131	8.810	6.740	nan
4.232	25.309	31.602	-4.579	8.681	5.134	8.811	6.740	nan
4.410	25.486	31.602	-4.405	8.858	5.138	8.815	6.742	nan
4.592	25.669	31.602	-4.232	9.040	5.147	8.824	6.746	nan
4.783	25.859	31.602	-4.058	9.231	5.164	8.840	6.754	nan
4.985	26.062	31.602	-3.884	9.433	5.193	8.869	6.769	nan
5.197	26.274	31.602	-3.710	9.646	5.231	8.908	6.788	nan
5.415	26.492	31.602	-3.537	9.864	5.276	8.952	6.811	nan
5.634	26.711	31.602	-3.363	10.083	5.321	8.998	6.833	nan
5.852	26.929	31.602	-3.189	10.301	5.365	9.041	6.856	nan
6.068	27.145	31.602	-3.016	10.517	5.408	9.084	6.877	nan
6.279	27.356	31.602	-2.846	10.728	5.449	9.125	6.898	nan
6.427	27.503	31.602	-2.727	10.875	5.478	9.154	6.912	nan
6.520	27.597	31.602	-2.651	10.969	5.496	9.172	6.921	nan
6.581	27.658	31.602	-2.602	11.030	5.507	9.183	6.927	nan
6.621	27.697	31.602	-2.570	11.069	5.515	9.191	6.931	nan
6.647	27.724	31.602	-2.549	11.095	5.520	9.196	6.933	nan
6.664	27.741	31.602	-2.535	11.113	5.523	9.199	6.935	nan

Log(Sigma)	Log(Gamma)	Log(mu)	Log(Grad)	Log(GradA)	Log(GradR)	Log(Tau)	Log(R)
-2.000	nan	-23.795	-1.731	-1.132	-1.731	-1.486	9.980
-1.830	nan	-23.786	-1.503	-1.133	-1.503	-1.237	9.980
-1.652	nan	-23.783	-1.256	-1.131	-1.256	-0.963	9.979
-1.448	-4.780	-23.796	-0.897	-1.125	-0.931	-0.624	9.979

Log(Sigma)	Log(Gamma)	Log(mu)	Log(Grad)	Log(GradA)	Log(GradR)	Log(Tau)	Log(R)
-1.042	-5.368	-23.928	-0.499	-0.863	-0.524	0.233	9.977
-0.780	nan	-23.944	-0.634	-0.612	-0.634	0.595	9.976
-0.549	-7.026	-23.949	-0.663	-0.672	-0.664	0.835	9.974
-0.318	-5.649	-23.957	-0.660	-0.713	-0.669	1.055	9.972
-0.086	nan	-23.963	-0.641	-0.586	-0.641	1.274	9.970
0.144	nan	-23.966	-0.615	-0.471	-0.615	1.500	9.967
0.377	nan	-23.966	-0.590	-0.432	-0.590	1.739	9.965
0.613	nan	-23.967	-0.570	-0.425	-0.570	1.991	9.961
0.860	nan	-23.967	-0.511	-0.457	-0.511	2.284	9.957
1.126	-1.633	-23.972	-0.470	-0.628	-0.493	2.626	9.952
1.390	nan	-23.981	-0.587	-0.572	-0.587	2.942	9.945
1.622	nan	-23.984	-0.646	-0.484	-0.646	3.173	9.938
1.845	nan	-23.984	-0.672	-0.449	-0.672	3.375	9.930
2.064	nan	-23.985	-0.680	-0.434	-0.680	3.570	9.921
2.283	nan	-23.985	-0.681	-0.423	-0.681	3.768	9.911
2.501	nan	-23.986	-0.682	-0.421	-0.682	3.977	9.899
2.719	nan	-23.986	-0.698	-0.419	-0.698	4.199	9.887
2.934	nan	-23.985	-0.735	-0.417	-0.735	4.436	9.872
3.141	nan	-23.985	-0.824	-0.415	-0.824	4.684	9.856
3.339	nan	-23.985	-0.977	-0.411	-0.977	4.940	9.839
3.527	nan	-23.985	-1.233	-0.408	-1.233	5.209	9.822
3.707	nan	-23.985	-1.656	-0.405	-1.656	5.494	9.804
3.882	nan	-23.985	-2.151	-0.403	-2.151	5.797	9.786
4.057	nan	-23.986	-2.099	-0.401	-2.099	6.117	9.768
4.232	nan	-23.985	-1.779	-0.403	-1.779	6.448	9.748
4.410	nan	-23.985	-1.463	-0.403	-1.463	6.785	9.727
4.592	nan	-23.985	-1.175	-0.404	-1.175	7.124	9.703
4.783	nan	-23.984	-0.939	-0.404	-0.939	7.460	9.677
4.985	nan	-23.984	-0.782	-0.403	-0.782	7.784	9.645
5.197	nan	-23.985	-0.708	-0.403	-0.708	8.080	9.607
5.415	nan	-23.985	-0.686	-0.402	-0.686	8.342	9.558
5.634	nan	-23.985	-0.689	-0.401	-0.689	8.571	9.497
5.852	nan	-23.985	-0.698	-0.401	-0.698	8.777	9.417
6.068	nan	-23.984	-0.707	-0.400	-0.707	8.967	9.309
6.279	nan	-23.984	-0.713	-0.400	-0.713	9.142	9.152
6.427	nan	-23.984	-0.714	-0.400	-0.714	9.262	8.978
6.520	nan	-23.984	-0.715	-0.400	-0.715	9.337	8.804
6.581	nan	-23.984	-0.714	-0.400	-0.714	9.386	8.630
6.621	nan	-23.984	-0.714	-0.400	-0.714	9.417	8.456
6.647	nan	-23.984	-0.714	-0.400	-0.714	9.438	8.283
6.664	nan	-23.984	-0.714	-0.400	-0.714	9.452	8.109

Bibliography

A. Maeder. “Stellar rotation: Evidence for a large horizontal turbulence and its effects on evolution”. In: *Astronomy and Astrophysics* 399.1 (2003), pp. 263–269. DOI: 10.1051/0004-6361:20021731. eprint: http://arxiv.org/abs/astro-ph/0301258. URL: http://dx.doi.org/10.1051/0004-6361:20021731.

Adzhemyan, L. Ts. et al. “Renormalization-group approach to the stochastic Navier Stokes equation: Two-loop approximation”. In: *International Journal of Modern Physics B* 17.10 (2003), pp. 2137–2170. DOI: 10.1142/S0217979203018193. eprint: http://www.worldscientific.com/doi/pdf/10.1142/S0217979203018193. URL: http://www.worldscientific.com/doi/abs/10.1142/S0217979203018193.

Anderhub, H. et al. “Search for Very High Energy Gamma-ray Emission from Pulsar-Pulsar Wind Nebula Systems with the MAGIC Telescope”. In: *The Astrophysical Journal* 710.1 (2010), p. 828. URL: http://stacks.iop.org/0004-637X/710/i=1/a=828.

Atkinson, D. H., J. B. Pollack, and A. Seiff. “The Galileo probe Doppler wind experiment: Measurement of the deep zonal winds on Jupiter”. In: *Journal of Geophysical Research* 103 (Sept. 1998), pp. 22911–22928. DOI: 10.1029/98JE00060.

Balbus, S. A. “A simple model for solar isorotational contours”. In: *Monthly Notices of the Royal Astronomical Society* 395 (June 2009), pp. 2056–2064. DOI: 10.1111/j.1365-2966.2009.14469.x. arXiv: 0809.2883.

Balbus, S. A. and H. N. Latter. “The tachocline and differential rotation in the Sun”. In: *Monthly Notices of the Royal Astronomical Society* 407 (Oct. 2010), pp. 2565–2574. DOI: 10.1111/j.1365-2966.2010.17086.x. arXiv: 1005.5100 [astro-ph.SR].

Balbus, S. A., H. Latter, and N. Weiss. “Global model of differential rotation in the Sun”. In: *Monthly Notices of the Royal Astronomical Society* 420 (Mar. 2012), pp. 2457–2466. DOI: 10.1111/j.1365-2966.2011.20217.x. arXiv: 1111.3809 [astro-ph.SR].

Balbus, S. A. and E. Schaan. “The stability of stratified, rotating systems and the generation of vorticity in the Sun”. In: *Monthly Notices of the Royal Astronomical Society* 426 (Oct. 2012), pp. 1546–1557. DOI: 10.1111/j.1365-2966.2012.21729.x. arXiv: 1207.3810 [astro-ph.SR].

Balbus, S. A. and N. O. Weiss. “Differential rotation in fully convective stars”. In: *Monthly Notices of the Royal Astronomical Society* 404 (May 2010), pp. 1263–1271. DOI: 10.1111/j.1365-2966.2010.16380.x. arXiv: 1001.3542 [astro-ph.SR].

Balbus, S. A. et al. “Differential rotation and convection in the Sun”. In: *Monthly Notices of the Royal Astronomical Society* 400 (Nov. 2009), pp. 176–182. DOI: 10.1111/j.1365-2966.2009.15464.x. arXiv: 0907.5075 [astro-ph.SR].

Barbi, Dirk and Gernot Munster. *Renormalization Group Analysis of Turbulent Hydrodynamics*. May 2013. URL: http://arxiv.org/abs/1012.0461.

Beringer, J. et al. “Particle Data Group”. In: *Phys. Rev. D* 86 (2012), p. 010001.

Beuermann, K. et al. “The eclipsing post-common envelope binary CSS21055: a white dwarf with a probable brown-dwarf companion”. In: *Astronomy and Astrophysics* 558, A96 (Oct. 2013), A96. DOI: 10.1051/0004-6361/201322241. arXiv: 1312.5088 [astro-ph.SR].

Bhattacharya, Dipankar. “The Evolution of the Magnetic Fields of Neutron Stars”. In: *J. Astrophys. Astr.* 16 (Mar. 1994), pp. 217–232. URL: http://www.ias.ac.in/jarch/jaa/16/217-232.pdf.

Bhattacharyya, B. et al. “GMRT Discovery of PSR J1544+4937: An Eclipsing Black-widow Pulsar Identified with a Fermi-LAT Source”. In: *The Astrophysical Journal Letters* 773.1 (2013), p. L12. eprint: http://arxiv.org/abs/1304.7101. URL: http://stacks.iop.org/2041-8205/773/i=1/a=L12.

Boffetta, G et al. *Kolmogorov and Bolgiano scaling in thermal convection: the case of Rayleigh-Taylor turbulence*. Tech. rep. arXiv:1101.5917. Comments: 4 pages, 5 figures. Feb. 2011. URL: http://arxiv.org/pdf/1101.5917.pdf.

Böhm-Vitense, E. *Introduction to Stellar Astrophysics*. Vol. 3. ISBN 0521344042. Cambridge University Press, 1992.

Breton, R. P. et al. “Discovery of the Optical Counterparts to Four Energetic Fermi Millisecond Pulsars”. In: *The Astrophysical Journal* 769 (2013), p. 108. URL: http://arxiv.org/abs/1302.1790.

Brickhill, A. J. “The pulsations of ZZ Ceti stars. III - The driving mechanism”. In: *Monthly Notices of the Royal Astronomical Society* 251 (Aug. 1991), pp. 673–680.

Brown, J. C. and C. B. Boyle. “An exploratory eccentric orbit ’Roche lobe’ overflow model for recurrent X-ray transients”. In: *Astronomy and Astrophysics* 141 (Dec. 1984), pp. 369–375.

Brown, R. A. "Longitudinal instabilities and secondary flows in the planetary boundary layer: A review". In: *Reviews of Geophysics* 18.3 (1980), pp. 683–697. ISSN: 1944-9208. DOI: 10.1029/RG018i003p00683. URL: http://dx.doi.org/10.1029/RG018i003p00683.

Burrows, Adam et al. "The theory of brown dwarfs and extrasolar giant planets". In: *Rev. Mod. Phys.* 73 (3 Sept. 2001), pp. 719–765. DOI: 10.1103/RevModPhys.73.719. eprint: http://arxiv.org/pdf/astro-ph/0607583. URL: http://link.aps.org/doi/10.1103/RevModPhys.73.719.

Canuto, V. M. "Turbulence in Stars. II. Shear, Stable Stratification, and Radiative Losses". In: *The Astrophysical Journal* 508.2 (1998), p. 767. URL: http://stacks.iop.org/0004-637X/508/i=2/a=767.

Carroll, Bradley W. *An Introduction to Modern Astrophysics*. Vol. 1. Addison-Wesley, 1996, p. 274.

Chen, Hai-Liang et al. "Formation of Black Widows and Redbacks—Two Distinct Populations of Eclipsing Binary Millisecond Pulsars". In: *The Astrophysical Journal* 775.1 (2013), p. 27. eprint: http://arxiv.org/abs/1308.4107. URL: http://stacks.iop.org/0004-637X/775/i=1/a=27.

Ching, Emily S. C. et al. "Scaling behavior in turbulent Rayleigh-Bénard convection revealed by conditional structure functions". In: *Phys. Rev. E* 87 (1 Jan. 2013), p. 013005. DOI: 10.1103/PhysRevE.87.013005. URL: http://link.aps.org/doi/10.1103/PhysRevE.87.013005.

Christensen, U. R. "Zonal flow driven by strongly supercritical convection in rotating spherical shells". In: *Journal of Fluid Mechanics* 470 (Nov. 2002), pp. 115–133. DOI: 10.1017/S0022112002002008.

Clayton, Donald D. *Principles of Stellar Evolution and Nucleosynthesis*. Vol. 1. ISBN: 978-0521566315. University of Chicago Press, 1968.

Danilov, S. and D. Gurarie. "Scaling, spectra and zonal jets in beta-plane turbulence". In: *Physics of Fluids* 16 (July 2004), pp. 2592–2603. DOI: 10.1063/1.1752928.

Danilov, Sergey and David Gurarie. "Rhines scale and spectra of the β-plane turbulence with bottom drag". In: *Phys. Rev. E* 65 (6 June 2002), p. 067301. DOI: 10.1103/PhysRevE.65.067301. URL: http://link.aps.org/doi/10.1103/PhysRevE.65.067301.

Demircan, O. and G. Kahraman. "Stellar mass-luminosity and mass-radius relations". In: *Astrophysics and Space Science* 181 (July 1991), pp. 313–322. DOI: 10.1007/BF00639097.

Edmonds Jr., F. N. "The Coefficients of Viscosity and Thermal Conductivity in the Hydrogen Convection Zone." In: *The Astrophysical Journal* 125 (Mar. 1957), p. 535. DOI: 10.1086/146327.

Eggleton, P. P. "Approximations to the radii of Roche lobes". In: *The Astrophysical Journal* 268 (May 1983), p. 368. DOI: 10.1086/160960.

Ferguson, Jason W. et al. "Low-Temperature Opacities". In: *The Astrophysical Journal* 623.1 (2005), p. 585. URL: http://stacks.iop.org/0004-637X/623/i=1/a=585.

Feynman, Richard P. *Los Alamos From Below*. https://www.youtube.com/watch?v=0ogSC6JKkrY. Feb. 6, 1975. URL: http://calteches.library.caltech.edu/34/3/FeynmanLosAlamos.htm.

Freire, P. C. C. and T. M. Tauris. "Direct formation of millisecond pulsars from rotationally delayed accretion-induced collapse of massive white dwarfs". In: *Monthly Notices of the Royal Astronomical Society* 438 (Feb. 2014), pp. L86–L90. DOI: 10.1093/mnrasl/slt164. arXiv: 1311.3478 [astro-ph.SR].

Galperin, Boris, Semion Sukoriansky, and Huei-Ping Huang. "Universal n-5 spectrum of zonal flows on giant planets". In: *Physics of Fluids (1994-present)* 13.6 (2001), pp. 1545–1548. DOI: http://dx.doi.org/10.1063/1.1373684. URL: http://scitation.aip.org/content/aip/journal/pof2/13/6/10.1063/1.1373684.

Garaud, P. et al. "A model of the entropy flux and Reynolds stress in turbulent convection". In: *Monthly Notices of the Royal Astronomical Society* 407 (Oct. 2010), pp. 2451–2467. DOI: 10.1111/j.1365-2966.2010.17066.x. arXiv: 1004.3239 [astro-ph.SR].

Hansen, B. et al. *Day and Night on Hot Jupiters*. Spitzer Proposal. June 2005.

Hathaway, D. H., L. Upton, and O. Colegrove. "Giant Convection Cells Found on the Sun". In: *ArXiv e-prints* (Jan. 2014). arXiv: 1401.0551 [astro-ph.SR].

Hessels, J. "M28I and J1023+0038: The Missing Links Go Missing, but Provide a New Link". In: NS Workshop. Dec. 2013. URL: http://www.astro.uni-bonn.de/NS2013-2/Hessel_M28i.pdf.

Icdem, B. and Baykal, A. "Viscous timescale in high mass X-ray binaries". In: *Astronomy and Astrophysics* 529 (2011), A7. DOI: 10.1051/0004-6361/201015810. eprint: http://arxiv.org/abs/1102.4203. URL: http://dx.doi.org/10.1051/0004-6361/201015810.

Iglesias, C. A. and F. J. Rogers. "Updated Opal Opacities". In: *The Astrophysical Journal* 464 (June 1996), p. 943. DOI: 10.1086/177381.

Itsweire, E. C., K. N. Helland, and C. W. Van Atta. "The evolution of grid-generated turbulence in a stably stratified fluid". In: *Journal of Fluid Mechanics* 162 (Jan. 1986), pp. 299–338. ISSN: 1469-7645. DOI: 10.1017/S0022112086002069. URL: http://journals.cambridge.org/article_S0022112086002069.

Joss, P. C., S. Rappaport, and W. Lewis. "The core mass-radius relation for giants - A new test of stellar evolution theory". In: *The Astrophysical Journal* 319 (Aug. 1987), pp. 180–187. DOI: 10.1086/165443.

Kagan, Daniel and J. Craig Wheeler. "The Role of the Magnetorotational Instability in the Sun". In: *The Astrophysical Journal* 787.1 (2014), p. 21. URL: http://stacks.iop.org/0004-637X/787/i=1/a=21.

Kaltenegger, L. and W. A. Traub. "Transits of Earth-like Planets". In: *The Astrophysical Journal* 698 (June 2009), pp. 519–527. DOI: 10.1088/0004-637X/698/1/519. arXiv: 0903.3371 [astro-ph.IM].

Kataria, T. et al. "The Atmospheric Circulation of the Hot Jupiter WASP-43b: Comparing Three-Dimensional Models to Spectrophotometric Data". In: *AAS/Division for Planetary Sciences Meeting Abstracts*. Vol. 46. AAS/Division for Planetary Sciences Meeting Abstracts. Nov. 2014, 104.03.

Kerkwijk, M. H. van, R. P. Breton, and S. R. Kulkarni. "Evidence for a Massive Neutron Star from a Radial-velocity Study of the Companion to the Black-widow Pulsar PSR B1957+20". In: *The Astrophysical Journal* 728.2 (2011), p. 95. eprint: http://arxiv.org/abs/1009.5427. URL: http://stacks.iop.org/0004-637X/728/i=2/a=95.

King, A. R. et al. "Mass Transfer Cycles in Close Binaries with Evolved Companions". In: *The Astrophysical Journal* 482 (June 1997), pp. 919–928. eprint: astro-ph/9701206.

Kippenhahn, Rudolf, Alfred Weigert, and Achim Weiss. *Stellar Structure and Evolution*. Springer, 2012. ISBN: 978-3-642-30304-3.

Knispel, B. et al. "Einstein@Home Discovery of a PALFA Millisecond Pulsar in an Eccentric Binary Orbit". In: *ArXiv e-prints* (Apr. 2015). arXiv: 1504.03684 [astro-ph.HE].

Köhler, H. "Differential Rotation Caused by Anisotropic Turbulent Viscosity". In: *Solar Physics* 13 (July 1970), pp. 3–18. DOI: 10.1007/BF00963937.

Lattimer, J. M. and M. Prakash. "Neutron Star Structure and the Equation of State". In: *The Astrophysical Journal* 550.1 (2001), p. 426. eprint: http://arxiv.org/abs/astro-ph/0002232. URL: http://stacks.iop.org/0004-637X/550/i=1/a=426.

Lesaffre, Pierre et al. "A two-dimensional mixing length theory of convective transport". In: *Monthly Notices of the Royal Astronomical Society* (2013). DOI: 10.1093/mnras/stt317. eprint: http://mnras.oxfordjournals.org/content/early/2013/03/20/mnras.stt317.full.pdf+html. URL: http://mnras.oxfordjournals.org/content/early/2013/03/20/mnras.stt317.abstract.

Linares, M. "X-Ray States of Redback Millisecond Pulsars". In: *The Astrophysical Journal* 795, 72 (Nov. 2014), p. 72. DOI: 10.1088/0004-637X/795/1/72. arXiv: 1406.2384 [astro-ph.HE].

Littlefair, S. P. et al. *The substellar companion in the eclipsing white dwarf binary SDSS J141126.20+200911.1*. 2014. eprint: arXiv:1409.3125.

Lohse, Detlef and Ke-Qing Xia. "Small-Scale Properties of Turbulent Rayleigh-Benard Convection". English. In: *Annual Review Of Fluid Mechanics*. Annual Review of Fluid Mechanics 42 (2010), pp. 335–364. ISSN: 0066-4189. DOI: 10.1146/annurev.fluid.010908.165152.

Lommen, Andrea N and Paul Demorest. "Pulsar timing techniques". In: *Classical and Quantum Gravity* 30.22 (2013), p. 224001. eprint: http://arxiv.org/abs/1309.1767. URL: http://stacks.iop.org/0264-9381/30/i=22/a=224001.

Lyman Spitzer, Jr. *Physics of Fully Ionized Gases*. Vol. 1. ISBN 978-0-486-44982-1. Dover, 2006.

Lynden-Bell, D. and J. E. Pringle. "The evolution of viscous discs and the origin of the nebular variables." In: *Monthly Notices of the Royal Astronomical Society* 168 (Sept. 1974), pp. 603–637.

Lyons, Richard, A. H. Panopsky, and Sarah Wollaston. "The Critical Richardson Number and Its Implications for Forecast Problems". In: *Journal of Applied Meteorology* 3 (Jan. 1964), pp. 136–142. URL: http://journals.ametsoc.org/doi/pdf/10.1175/1520-0450(1964)003%3C0136:TCRNAI%3E2.0.CO;2.

Mei, C. C. and T. Y.-t. Wu. "Gravity Waves due to a Point Disturbance in a Plane Free Surface Flow of Stratified Fluids". In: *Physics of Fluids* 7 (Aug. 1964), pp. 1117–1133. DOI: 10.1063/1.1711351.

Mergui, S., X. Nicolas, and S. Hirata. "Sidewall and thermal boundary condition effects on the evolution of longitudinal rolls in Rayleigh-Bénard-Poiseuille convection". In: *Physics of Fluids (1994-present)* 23.8, 084101 (2011), pages. DOI: http://dx.doi.org/10.1063/1.3605698. URL: http://scitation.aip.org/content/aip/journal/pof2/23/8/10.1063/1.3605698.

Mestel, L. and D. L. Moss. "On mixing the Eddington-Sweet circulation". In: *Monthly Notices of the Royal Astronomical Society* 221 (July 1986), pp. 25–51.

Nguyen Duc, J.M., Ph. Caperan, and J. Sommeria. "An Experimental Study of the Inverse Cascade of Energy in Two-Dimensional Turbulence". English. In: *Advances in Turbulence*. Ed. by Geneviève Comte-Bellot and Jean Mathieu. Springer Berlin Heidelberg, 1987, pp. 265–268. ISBN: 978-3-642-83047-1. DOI: 10.1007/978-3-642-83045-7_30. URL: http://dx.doi.org/10.1007/978-3-642-83045-7_30.

Paczyński, B. "Envelopes of Red Supergiants". In: *Acta Astronomica* 19 (1969), p. 1.

— "Evolutionary Processes in Close Binary Systems". In: *Annual Review of Astronomy and Astrophysics* 9 (1971), p. 183. DOI: 10.1146/annurev.aa.09.090171.001151.

Padmanabhan, T. *Theoretical Astrophysics*. Vol. 2. ISBN: 978-0521566315. Cambridge University Press, 2001. Chap. 6.

Parmentier, V., A. P. Showman, and Y. Lian. “3D mixing in hot Jupiters atmospheres. I. Application to the day/night cold trap in HD 209458b”. In: *Astronomy and Astrophysics* 558, A91 (Oct. 2013), A91. DOI: 10.1051/0004-6361/201321132. arXiv: 1301.4522 [astro-ph.EP].

Paxton, Bill et al. “Modules for Experiments in Stellar Astrophysics (MESA): Planets, Oscillations, Rotation, and Massive Stars”. In: *The Astrophysical Journal Supplement Series* 208.1 (2013), p. 4. URL: http://stacks.iop.org/0067-0049/208/i=1/a=4.

Phinney, E. S. “Pulsars as Probes of Newtonian Dynamical Systems”. In: *Royal Society of London Philosophical Transactions Series A* 341 (Oct. 1992), pp. 39–75. DOI: 10.1098/rsta.1992.0084.

Podsiadlowski, P. “Irradiation-driven mass transfer low-mass X-ray binaries”. In: *Nature* 350 (Mar. 1991), pp. 136–138. DOI: 10.1038/350136a0.

Podsiadlowski, P., S. Rappaport, and E. D. Pfahl. “Evolutionary Sequences for Low- and Intermediate-Mass X-Ray Binaries”. In: *The Astrophysical Journal* 565 (Feb. 2002), pp. 1107–1133. DOI: 10.1086/324686. eprint: astro-ph/0107261.

Pons, José A. et al. “Evidence for Heating of Neutron Stars by Magnetic-Field Decay”. In: *Phys. Rev. Lett.* 98 (7 Feb. 2007), p. 071101. DOI: 10.1103/PhysRevLett.98.071101. eprint: http://arxiv.org/pdf/astro-ph/0607583.pdf?origin=publication_detail. URL: http://link.aps.org/doi/10.1103/PhysRevLett.98.071101.

Prat, V. and Lignières, F. “Turbulent transport in radiative zones of stars”. In: *Astronomy and Astrophysics* 551 (2013), p. L3. DOI: 10.1051/0004-6361/201220577. eprint: http://arxiv.org/abs/1301.4151. URL: http://dx.doi.org/10.1051/0004-6361/201220577.

Refsdal, S. and A. Weigert. “Shell Source Burning Stars with Highly Condensed Cores”. In: *Astronomy and Astrophysics* 6 (July 1970), p. 426.

Reynolds, M. T. et al. “The light curve of the companion to PSR B1957+20”. In: *Monthly Notices of the Royal Astronomical Society* 379.3 (2007), pp. 1117–1122. DOI: 10.1111/j.1365-2966.2007.11991.x. eprint: http://arxiv.org/abs/0705.2514. URL: http://mnras.oxfordjournals.org/content/379/3/1117.abstract.

Rhines, Peter B. “Waves and turbulence on a beta-plane”. In: *Journal of Fluid Mechanics* 69 (03 June 1975), pp. 417–443. ISSN: 1469-7645. DOI: 10.1017/S0022112075001504. URL: http://journals.cambridge.org/article_S0022112075001504.

Rincon, F. *Theories of convection and the spectrum of turbulence in the solar photosphere*. Tech. rep. astro-ph/0611842. Contribution to the proceedings : 239 Convection in Astrophysics, International Astronomical Union., held 21-25 August, 2006 in Prague, Czech Republic. Nov. 2006. eprint: `http://arxiv.org/pdf/astro-ph/0611842.pdf`. URL: `http://cds.cern.ch/record/1001690/files/0611842.pdf`.

Ritter, H., Z.-Y. Zhang, and U. Kolb. "Irradiation and mass transfer in low-mass compact binaries". In: *Astronomy and Astrophysics* 360 (Aug. 2000), p. 969. eprint: `astro-ph/0005480`.

Roberts, Mallory S. E. *Surrounded by Spiders! New Black Widows and Redbacks in the Galactic Field*. 2012. eprint: `arXiv:1210.6903`. URL: `http://arxiv.org/abs/1210.6903`.

Romani, Roger W. et al. "PSR J1311–3430: A Heavyweight Neutron Star with a Flyweight Helium Companion". In: *The Astrophysical Journal Letters* 760.2 (2012), p. L36. eprint: `http://arxiv.org/abs/1210.6884`. URL: `http://stacks.iop.org/2041-8205/760/i=2/a=L36`.

Roy, A., J. T. Wright, and S. Sigurð*sson*. "Earthshine on a Young Moon: Explaining the Lunar Farside Highlands". In: *The Astrophysical Journal* 788, L42 (June 2014), p. L42. DOI: `10.1088/2041-8205/788/2/L42`. arXiv: `1406.2020 [astro-ph.EP]`.

S. Mathis, A. Palacios, and J.-P. Zahn. "On shear-induced turbulence in rotating stars". In: *Astronomy and Astrophysics* 425.1 (2004), pp. 243–247. DOI: `10.1051/0004-6361:20040279`. eprint: `http://arxiv.org/abs/astro-ph/0403580`. URL: `http://dx.doi.org/10.1051/0004-6361:20040279`.

Salaris, Maurizio and Cassisi Santi. *Evolution of stars and stellar populations*. Vol. 1. ISBN: 0-470-09220-3. John Wiley Sons, 2005, pp. 138–140.

Schatzman, E., J.P. Zahn, and P. Morel. "Shear turbulence beneath the solar tachocline". In: *Astronomy and Astrophysics* (Oct. 2000). eprint: `http://arxiv.org/pdf/astro-ph/0010543v1.pdf`.

Shiode, J. H. et al. "The observational signatures of convectively excited gravity modes in main-sequence stars". In: *Monthly Notices of the Royal Astronomical Society* 430 (Apr. 2013), pp. 1736–1745. DOI: `10.1093/mnras/sts719`. arXiv: `1210.5525 [astro-ph.SR]`.

Showman, A. P., K. Menou, and J. Y.-K. Cho. "Atmospheric Circulation of Hot Jupiters: A Review of Current Understanding". In: *Extreme Solar Systems*. Ed. by D. Fischer et al. Vol. 398. Astronomical Society of the Pacific Conference Series. 2008, p. 419. arXiv: `0710.2930`.

Škandera, Dan, Angela Busse, and Wolf-Christian Müller. *Scaling Properties of Convective Turbulence*. English. Ed. by Siegfried Wagner et al. Springer Berlin

Heidelberg, 2009, pp. 387–396. ISBN: 978-3-540-69181-5. DOI: 10.1007/978-3-540-69182-2_31. URL: http://dx.doi.org/10.1007/978-3-540-69182-2_31.

Smith David, A. "Gamma Ray Pulsars with the Fermi LAT". In: 3rd Fermi Symposium. May 2011. URL: http://fermi.gsfc.nasa.gov/science/mtgs/symposia/2011/program/session14/Smith_FermiPSRs.pdf.

Stauffer, J. B. and L. W. Hartmann. "The rotational velocities of low-mass stars". In: *Astronomical Society of the Pacific, Publications* 98 (Dec. 1986), pp. 1233–1251. DOI: 10.1086/131926.

Stevens, Richard J.A.M., Herman J.H. Clercx, and Detlef Lohse. "Heat transport and flow structure in rotating RayleighâBÃ©nard convection". In: *European Journal of Mechanics - B/Fluids* 40 (2013). Fascinating Fluid Mechanics: 100-Year Anniversary of the Institute of Aerodynamics, {RWTH} Aachen University, pp. 41–49. ISSN: 0997-7546. DOI: http://dx.doi.org/10.1016/j.euromechflu.2013.01.004. URL: http://www.sciencedirect.com/science/article/pii/S0997754613000058.

Stevenson, D. J. "The search for brown dwarfs". In: *Annual Review of Astronomy and Astrophysics* 29 (1991), pp. 163–193. DOI: 10.1146/annurev.aa.29.090191.001115.

Sukoriansky, Seimion, Nadejda Dikovskaya, and Boris Galperin. "On the Arrest of Inverse Energy Cascade and the Rhines Scale". In: *Journal of the Atmospheric Sciences* 64 (2006). URL: http://journals.ametsoc.org/doi/abs/10.1175/JAS4013.1.

Sukoriansky, Semion, Boris Galperin, and Nadejda Dikovskaya. "Universal Spectrum of Two-Dimensional Turbulence on a Rotating Sphere and Some Basic Features of Atmospheric Circulation on Giant Planets". In: *Phys. Rev. Lett.* 89 (12 Aug. 2002), p. 124501. DOI: 10.1103/PhysRevLett.89.124501. URL: http://link.aps.org/doi/10.1103/PhysRevLett.89.124501.

Tombrello, Thomas A. *Caltech Oral History*. Dec. 2012. URL: http://resolver.caltech.edu/CaltechOH:OH_Tombrello_T.

Unal Ertan. "Inner disk radius, accretion and the propeller effect in the spin-down phase of neutron stars". In: (). eprint: http://arxiv.org/pdf/1504.03996v1.pdf.

Verhoeven, J. and S. Stellmach. "The compressional beta effect: A source of zonal winds in planets?" In: *Icarus* 237 (July 2014), pp. 143–158. DOI: 10.1016/j.icarus.2014.04.019. arXiv: 1404.6940 [astro-ph.EP].

Wu, Y. and P. Goldreich. "Gravity Modes in ZZ Ceti Stars. IV. Amplitude Saturation by Parametric Instability". In: *The Astrophysical Journal* 546 (Jan. 2001), pp. 469–483. DOI: 10.1086/318234. eprint: astro-ph/0003163.

Yakhot, Victor and StevenA. Orszag. “Renormalization group analysis of turbulence. I. Basic theory”. English. In: *Journal of Scientific Computing* 1.1 (1986), pp. 3–51. ISSN: 0885-7474. DOI: 10.1007/BF01061452. URL: http://dx.doi.org/10.1007/BF01061452.

Zhou, Ye, David W. McComb, and George Vahala. “Renormalization Group (RG) in Turbulence: Historical and Comparative Perspective”. In: (Aug. 1997). URL: http://ntrs.nasa.gov/archive/nasa/casi.ntrs.nasa.gov/19970028852.pdf.